Computational Methods in Engineering & the Sciences

Anders Eriksson
Arne Nordmark

Structural Stability and Its Computational Modelling

Springer

Computational Methods in Engineering & the Sciences

This Series publishes books on all aspects of computational methods used in engineering and the sciences. With emphasis on simulation through mathematical modelling, the Series accepts high quality content books across different domains of engineering, materials, and other applied sciences. The Series publishes monographs, contributed volumes, professional books, and handbooks, spanning across cutting edge research as well as basics of professional practice. The topics of interest include the development and applications of computational simulations in the broad fields of Solid & Structural Mechanics, Fluid Dynamics, Heat Transfer, Electromagnetics, Multiphysics, Optimization, Stochastics with simulations in and for Structural Health Monitoring, Energy Systems, Aerospace Systems, Machines and Turbines. Climate Prediction, Effects of Earthquakes, Geotechnical Systems, Chemical and Biomolecular Systems, Molecular Biology, Nano and Microfluidics, Materials Science, Nanotechnology, Manufacturing and 3D printing, Artificial Intelligence, Internet-of-Things.

Anders Eriksson · Arne Nordmark

Structural Stability and Its Computational Modelling

Springer

Anders Eriksson
Department of Engineering Mechanics
KTH Royal Institute of Technology
Stockholm, Sweden

Arne Nordmark
Department of Engineering Mechanics
KTH Royal Institute of Technology
Stockholm, Sweden

ISSN 2662-4869 ISSN 2662-4877 (electronic)
Computational Methods in Engineering & the Sciences
ISBN 978-3-031-36071-8 ISBN 978-3-031-36072-5 (eBook)
https://doi.org/10.1007/978-3-031-36072-5

This Springer imprint is published by the registered company Springer Nature Switzerland AG
The registered company address is: Gewerbestrasse 11, 6330 Cham, Switzerland

Preface

Stability of a structure exposed to acting forces is a key concept in engineering design and has been extensively studied for a long time. The studies have focussed on the single components, from which the structure is composed, and given engineering formulae and charts for the stability limits for, e.g., beam and plate objects.

The methods for most stability investigations have been semi-analytical approaches, where, e.g., series solutions are used to describe a potential equilibrium state characterizing an instability. Based on an assumed deflection, picturesque terms like 'lateral-torsional buckling' of beams are introduced and handled by a safety factor philosophy. In structural engineering, design codes more or less explicitly define which situations need be considered, but with limited applicability for more complex structures.

The traditional views on component stability do not always fit well into the modern design process, where large-scale numerical simulation tools, such as finite element software, are used in the design analyses. Neither the deflected equilibrium view nor the classification of instabilities is easily introduced in this context. The numerical simulations, however, give new possibilities to find, evaluate and interpret instability situations even for cases where they are not expected.

The present treatise has the aim to discuss structural stability in terms suited for computational modelling and analysis. The text is based on an extensive set of previous research publications on topics within the general scope of the book. The focus is set on the 'ab initio' treatment of the stability of static equilibrium for a numerical structural model. With a primary focus on conservative situations, a discussion is given on different classes of exterior forcing and their effects on the stability conclusions.

Throughout the text, an energy viewpoint is applied, where the kinetic and strain energies within a loaded structure are related to the potential of acting external forces, with some comments also on non-conservative situations. In particular, incremental and virtual changes to the energy and potential are formulated. The key motivation for this approach is that a consistent view can be established and applied to several situations. Without introduction of completely new terms, the treatment sets the equilibrium and stability issues in a new context, suited for systematic computations.

After a review in Chap. 1 of common situations of stability investigations in engineering design, a brief account of relevant solid mechanics is given in Chap. 2, where energy, potential and mechanical work are the main aspects. The approximations and interpolations in finite element-based structural modelling are discussed in Chap. 3. Based on these tools, Chap. 4 gives a rather extensive discussion on the numerical solution methods needed to handle the equilibrium systems formulated. Finally, Chap. 5 discusses a number of more complex stability investigations, where previous research has shown that a deep problem understanding is needed for the formulation and correct interpretation of computational results; these show the potential of computational stability modelling for complex structures, but are also a memento against unreflected trust in computational results.

The reader of this book is expected to have some familiarity with engineering problems and at least the basic concepts of numerical techniques. The presentation also assumes that the reader has some experience from at least linear finite element simulations and access to some general commercial software for structural analysis.

Although not primarily conceived as a textbook for course usage, a small set of exercises, or rather projects, are related to each of the chapters in the book. These can serve as check-out questions to the reader, or as a basis for academic exercises in a text book context.

As noted above, this book is based on a long period of research on the subtopics considered. Many parts of the underlying work have been performed by a long row of Ph.D. students at the Royal Institute of Technology, KTH. While all of our students have made important contributions to engineering science, the present book in particular relies on the work by Costin Pacoste, Torbjörn Lidström, Tomomi Yagi, Karin Forsell, Aleksandar Filipovski, Jean-Marc Battini, Gunnar Tibert, Nasseradeen Ashwear, Amit Patil, and Yang Zhou, and we are most grateful for their efforts. The first author also expresses the gratitude to the memory of Per-Olof Thomasson, supervisor and mentor, who initiated the interest in structural stability.

Stockholm, Sweden
March 2023

Anders Eriksson
Arne Nordmark

Contents

About the Authors

Anders Eriksson, Ph.D. is a professor (retired) of Structural mechanics at KTH Royal Institute of Technology, Stockholm. Born in 1953 and with an M.Sc. in Civil engineering, he got his degree in 1981 within the subject of Steel structures; he became professor in 1991. Initiated already in the thesis work, a major research interest has been focused on the numerical treatment, primarily by FEM techniques, of non-linear and stability issues in structural equilibrium. While the thesis work dealt with thin shells, also other classes of problems, such as tensegrities, have been treated. Element formulations for these, but even more the solution techniques for the resulting non-linear systems are frequent topics in the scientific publications. Not least, settings and methods for parametric equilibrium problems have been developed and published. A secondary research interest has been directed towards bio-mechanical simulations, and in particular on aspects of the human musculo-skeletal system. The research efforts have resulted in over 100 journal publications, and a similar number of conference papers. Eriksson has a very large experience from teaching in undergraduate and graduate courses, but also from supervision of M.Sc. and Ph.D. thesis work. He also has several years of experience from university leadership and management roles.

Arne Nordmark, Ph.D. is part-time senior lecturer at KTH Royal Institute of Technology, Stockholm and part-time development engineer at Comsol AB, Stockholm. Born in 1964 and with an M.Sc. in Engineering physics, he got his degree within the subject of Impacting dynamical systems. A major research interest has been the study of bifurcations in mechanical system with discontinuities in the governing equations, which arise for example in models of impact and friction. He has developed the general method of using discontinuity mappings to study such systems. Recent research interests include the study of instabilities of pressurized wrinkled membranes, and utilizing symmetry and group representation theory when analysing structures. The research has resulted in more than 50 journal publications. Nordmark also has experience from teaching at the undergraduate and graduate levels, and from

co-supervising Ph.D. thesis work. At Comsol AB, he has been involved in developing the Partial Differential Equation Toolbox for MATLAB, and COMSOL Multiphysics simulation software, and is co-inventor of several patents.

Chapter 1
Engineering Stability Evaluations

This Chapter discusses some common engineering approaches to stability problems, of which at least a few should be well-known to a reader. The objectives are to set the basis for the following treatment, and to add aspects to the common methods, where more general approaches can provide further information. The demonstration examples primarily give expressions for limit and buckling states, often interpreted as maximum forcing levels for the considered structure, even if secondary equilibrium states may exist. As the present book will promote a view on stability, which differs from many common approaches, the engineering examples will be accompanied by analyses where dynamic aspects of stability are in focus. An energy view on structural equilibrium will thereby allow the unification of common static and dynamic stability criteria. The present treatise will also emphasize that stability is parameter dependent property of one particular state, and not just a limit for a certain qualitative response of the structure. This view is introduced in loose terms already in this Chapter, and will be a theme for coming Chapters, where more comprehensive settings are introduced.

Brief Objective of this Chapter

This Chapter demonstrates common engineering views on structural stability, introduces and discusses important concepts, and prepares for the coming more general and detailed treatment of parametric structural stability.

A. Eriksson and A. Nordmark, *Structural Stability and Its Computational Modelling*, Computational Methods in Engineering & the Sciences,
https://doi.org/10.1007/978-3-031-36072-5_1

1.1 Stability and Instability

Stability is a fundamental requirement on any kind of structure subjected to exterior forcing.[1] Even if this statement seems obvious to anyone, the concept is often mis-interpreted as the necessity for integrity of the structure, i.e., the avoidance of any kind of failure. In more precise terms, stability is a qualified concept, relating to specific kinds of failures, and demanding the structure to keep qualitatively its intended method of action. Stability implies that small disturbances to an equilibrium configuration will not lead to other equilibrium states or to vibrations of increasing amplitude. For the typical engineering context, with some forcing level parameter, stability is typically interpreted as a demand for a unique and monotonously increasing response to increased forcing, limited deformations, and no increasing or persisting unintended vibrations. Instability is thereby, as a general term, the opposite to this situation, but is commonly used rather for the critical situations, where stability is lost, and a transition between stable and unstable solutions appears.

In engineering, lack of stability has often been considered as a problem and a failure mechanism, but the phenomena are now increasingly studied from other viewpoints. Better analysis methods have made it possible to design structures which will use post-critical modes of response for improved structural efficiency. According to Reis (2015), 'bucklifobia', the fear of buckling, has in many contexts been modified into new possibilities. Champneys et al. (2019) formulate this as "…buckling instabilities, rather than to be avoided at all costs, can, in principle, be beneficial happy catastrophes". As one example, airplane wings can be allowed to buckle locally under at least extreme operational conditions. Non-unique solutions can also lead to new engineering solutions, for instance in so-called morphing structures, for which the existence of multi-stable equilibrium solutions is the main advantage, and buckling is rather an asset than a problem. As other examples, architected cellular materials can be used for creating auxetic materials, for controlling the propagation of elastic waves, and for creating efficient energy absorbers, cf. Bertoldi (2017). All the mentioned applications are related to sophisticated analyses of large configuration-changing displacements, instabilities and post-critical responses of structures.

The notion of stability investigations is frequently used in engineering analyses, for a broad spectrum of situations, but it has been noted that "the precise notion of stability, always tacitly assumed essentially static in nature, is in fact, left undefined", cf. Como and Grimaldi (1995, p. 5). Studies of structural stability commonly take their starting points in treatments of its opposite, i.e., the critical situation, when a structure loses the intended function. This Chapter discusses to some depth a set of examples and their possible instabilities, where typically the structure responds to forcing in an unintended direction, or loses its monotonic response to increased forcing.

[1] This treatise will use this term as a generic term for any kind of exterior action on the structure. It is thereby used as a rather loose term, with a set of force combinations as, perhaps, the most typical situation.

The following Chapters of this treatise will take as their fundamental basis that stability is a dynamic concept. For a structure under forcing, stability thereby is a capacity to remain close to an equilibrium situation after a minor disturbance. This view is related to the stability criterion criterion by Liapunov (1966), where a dynamic process starting near an equilibrium state stays close to it. In practice, this means that any damping existing in the system will eventually bring the structure back to the static equilibrium. The criteria and implications will be further discussed in Sects. 2.9 and 3.7.

The concept of stability thereby refers to one particular equilibrium state, with geometry, forces and other parameters fixed, and is a property of this frozen parameter state. Quantities defining stability can thereby be fully evaluated from this. In this presentation, energy-based criteria will be the main tools for such evaluations.

Even if stability is a property of one equilibrium state, the typical engineering viewpoint focuses interest on how and when stability is lost (or in some cases established) when tracing a parametric forcing regime. Common methods thereby study critical states, by seeking the forcing magnitude at which the corresponding equilibrium state changes between stable and unstable. The procedures, more or less explicitly, rely on solutions to the equilibrium states for a parametric forcing, and an evaluation of the stability for these states. Commonly, in both analytical and software-based methods, the stability judgement is based on a 'static stability' criterion, demanding for stability a minimum potential energy at the equilibrium state, even if classical works like the treatise by Timoshenko and Gere (1961) do not formulate this explicitly. In the dynamic setting employed in this treatise, this view implicitly uses a simplified formulation of kinetic energy and inertia. The axiomatic definition of stability from the potential energy is discussed by Godoy (2000), who notes that this has been in many cases an issue of "faith", but that the definition has been "of great value to improve our understanding of the buckling and postbuckling of structures". As further discussed in coming Chapters, the static and dynamic views on stability are not as different as they might initially seem.

As this Chapter describes a set of examples, common in engineering practice, the descriptions uses the notation common in the field, whereas coming Chapters adopt a more formal notation for the quantities involved in the theories, e.g., full $3D$ formulations for geometry and displacement and tensor-based interior quantities.

1.2 Spring-Supported Rigid Link

A simple model problem serves as a first introduction to stability investigations. Although of limited practical importance in itself, it demonstrates several important terms for the sequel of this book. The problem is a compressed ideal rigid link,

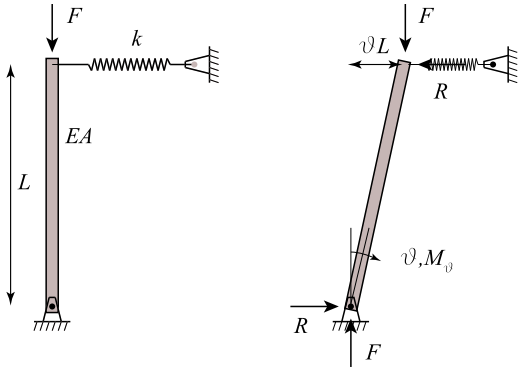

Fig. 1.1 Spring-supported compressed rigid link: model and assumed deflection

where the rigidity refers to bending.[2] The link is attached to a hinge at one end, and supported by an elastic spring at the other, according to Fig. 1.1. The parameters of the problem are the length of the link L, the acting vertical force F, the axial stiffness of the link EA, and the spring stiffness k. The problem is here described by three successively more accurate and complex models.

A basic equilibrium solution is that force F just acts straight through the link, without any sideways movement. This thereby implies a length change of the link

$$\mathrm{d}L = -\frac{FL}{EA} \tag{1.1}$$

as the only result from the force. For the further work in this treatise, it also noted that the stored elastic strain energy in the link at force F is

$$\Pi_p = \frac{1}{2}\sigma\varepsilon V = \frac{1}{2}\frac{F^2 L}{EA}, \tag{1.2}$$

with common notation (ε, σ) for strain and stress, and V the volume of the link.

Within linear theory, the above expressions are valid for any value of F. The stability question is whether this solution is unique, and investigates an assumed tilted configuration, described by one degree of freedom, the angle ϑ. Whether this deflected equilibrium configuration can exist is the question.

By a moment equilibrium equation, or by simple visual inspection, it is obvious that the reactive force R from the spring[3] and the force F must give a resulting force directed along the link, through the hinge.

---

[2] the idealizations being that the link is not bending, that the hinge is frictionless, that the force is perfectly vertical, and that the spring is always horizontal, and acting linearly for all lengths, with its slack length when the link is perfectly vertical

[3] The force is directed as in the figure, for the assumed positive angle ϑ, which gives a compressed spring.

The simplest model for this case is that the link is axially very stiff, and also that the angle ϑ is small. Then, the top end only moves horizontally, a distance $L \sin\vartheta \approx L\vartheta$. The spring force is then expressed as $R = k \cdot L\vartheta$, and this can be related through geometry to F as

$$k \cdot L\vartheta = \frac{\vartheta L}{L} F. \tag{1.3}$$

A deflected equilibrium, within this model, thus exists for a critical force

$$F_{\text{cr}} = k\, L \tag{1.4}$$

for any angle ϑ. It is easy to verify that the same expression holds for negative ϑ. The conclusion is that for an exact critical equilibrium with the acting force $F = F_{\text{cr}}$, the link will stay in an introduced disturbed position. The vertical force has created a mechanism, without horizontal stiffness. The vertical position is thereby not the only possible solution for this force. As the configuration for this force is arbitrary, the common engineering interpretation is that—given a high EA, and fixed L and k—there exists a maximum force F_{cr}, which the structure can carry.

As this model is only valid for small angles ϑ, it can be improved. Keeping the axial rigidity of the link, but introducing more correct trigonometric expressions leads to a vertical position of the top end $L \cos\vartheta$, and a horizontal movement $L \sin\vartheta$, giving the compression of the spring. If the spring is so long that it can be assumed to be horizontal for any ϑ, the relation between acting forces is then

$$k \cdot L \sin\vartheta = F \tan\vartheta, \tag{1.5}$$

or

$$F(\vartheta) = k\, L \cos\vartheta. \tag{1.6}$$

This expression agrees with the critical force in Eq. (1.4) for $\vartheta = 0$, but allows deflected equilibrium at other force values, lower than F_{cr}.

The results above can be interpreted graphically, and show two classes of possible equilibrium states, Fig. 1.2. As long as no material capacity is introduced, the vertical primary equilibrium branch can exist for any value of the force F. The deflected secondary equilibrium[4] states follow either Eq. (1.4) or Eq. (1.6), depending on the assumed model.

The possible equilibria are just the indicated lines, not the regions between them. The crossing of primary and secondary equilibrium branches is a critical equilibrium state, where structural response qualitatively changes. In particular, it is a bifurcation state, where the 'bi' is related to a lacking uniqueness: two or more branches cross in one point. A brief discussion of this concept and its relation to the mathematical bifurcation analysis is given in Sect. 3.7.5.

[4] or post-critical equilibrium

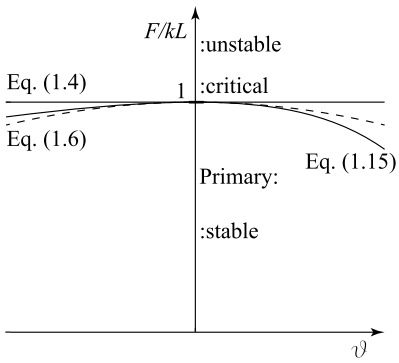

Fig. 1.2 Primary and secondary response for compressed rigid link in Fig. 1.1, with secondary response evaluated for three different structural models

This problem was trivially solved through a visual equilibrium. In order to introduce a more general setting, the energy in the system is formulated. In a deflected static equilibrium, this consists of one term related to the shortening of the link, one term related to the length change of the spring and one term describing the loss of potential energy for the force. Based on Eq. (1.2), the first can be neglected if EA is assumed as large. The total potential, cf. Sect. 2.6.5, considered is thereby

$$\Pi(\vartheta) = \Pi_p + \Pi_t = \frac{1}{2}k\,(L\sin\vartheta)^2 + FL\cos\vartheta \approx \frac{1}{2}kL^2\vartheta^2 + FL\left(1 - \frac{\vartheta^2}{2}\right), \tag{1.7}$$

identifying the shortening of the spring and the vertical level of the acting force, and introducing low order approximations for the trigonometric functions. Equilibrium demands stationarity of the first derivative; for the first expression this gives

$$\frac{\mathrm{d}\Pi}{\mathrm{d}\vartheta} = kL^2\sin\vartheta\cos\vartheta - FL\sin\vartheta = L\sin\vartheta\,(kL\cos\vartheta - F) = 0, \tag{1.8}$$

which gives as solutions both $\vartheta = 0$ (for any F), and $F = kL\cos\vartheta$ (for any ϑ). The latter expression agrees with Eq. (1.6), while a differentiation of the truncated form in Eq. (1.7) similarly gives Eq. (1.4).

Turning from possible equilibrium to stability of the studied system, a naive view on the stability of the equilibrium solutions is based on Fig. 1.1. With an assumed deflected configuration ϑ, giving a reactive force R, and an arbitrary force F, it is qualitatively obvious that a too large force F will dominate R; the angle will tend to increase. A small F will be dominated by R, and the angle will tend to decrease. In loose terms, this defines stability as a tendency for an introduced deflection to disappear, while an unstable state will lead to a growing deflection; critical equilibrium is the borderline case.

The stability analysis can be formalized. One more differentiation of the total potential energy Π gives

$$\frac{\mathrm{d}^2\Pi}{\mathrm{d}\vartheta^2} = kL^2\left(\cos^2\vartheta - \sin^2\vartheta\right) - FL\cos\vartheta = \{\vartheta \to 0\} = kL^2 - FL, \qquad (1.9)$$

where the final member evaluates the second differential at $\vartheta = 0$.

When this quantity is positive for a solution to Eq. (1.8), the energy is at a minimum, which can be interpreted as a stable equilibrium. With further discussion in Sect. 2.9, the criterion implies that more energy must be introduced into the system in order to deflect it from this equilibrium. A stability coefficient[5] for the primary equilibrium solution is

$$\Sigma(L, k, F) = kL^2 - FL, \qquad (1.10)$$

where Σ is a function of the relevant parameters in the model. The coefficient is positive for zero force, but decreases with increasing F, becomes zero at the critical force F_{cr}, and is negative above this, where the structure is unstable. The stability properties regarding the primary equilibrium states are introduced in Fig. 1.2. The concept of stable, unstable and critical (or neutral) equilibrium are further discussed in Sect. 3.7.

The stability coefficient for equilibria on the secondary, deflected, branch are similarly derived from Eq. (1.9), when introducing the force relation $F = kL\cos\vartheta$ obtained from Eq. (1.8) for $\vartheta \neq 0$. This gives

$$\Sigma(L, k, \vartheta) = -kL^2\sin^2\vartheta \equiv -\frac{1}{k}(kL - F)(kL + F) \qquad (1.11)$$

which is always negative for $\vartheta \neq 0$, and such equilibria are unstable. This corresponds, in this case, to the decreasing force values with increasing magnitude of the angle ϑ.

The stability coefficient in Eq. (1.10) is a stiffness relating to the rotation angle. One interpretation is that—for fixed L and F—a sufficiently high spring constant k is needed to avoid loss of stability. Lack of stability does not necessarily come from an excessive forcing; it may also come from a too flexible spring!

Still another viewpoint can be applied, if the problem is described in a context of dynamics. At an assumed deflected configuration described by ϑ, the two forces give a moment around the hinge, parallel to the angle ϑ

$$M_\vartheta = FL\sin\vartheta - RL\cos\vartheta = \left(FL - kL^2\cos\vartheta\right)\sin\vartheta. \qquad (1.12)$$

This moment gives an angular acceleration, which, for small ϑ, is

$$I_\vartheta\,\ddot{\vartheta} = M_\vartheta \quad \Rightarrow \quad I_\vartheta\,\ddot{\vartheta} + \left(kL^2 - FL\right)\vartheta = 0, \qquad (1.13)$$

[5] which, in this case of one degree of freedom, is the second derivative of the potential energy with respect to the single displacement component, but in general is an eigenvalue

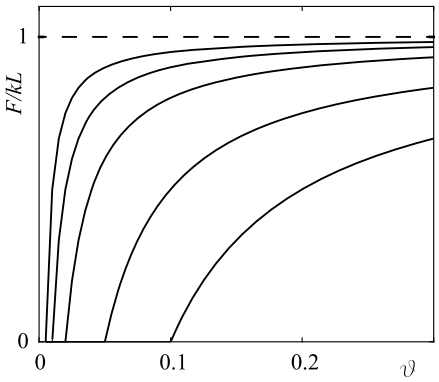

Fig. 1.3 Effects of imperfect spring in rigid link example. The imperfection x_0 is seen as the crossing with the horizontal axis

where a superposed dot denotes time differentiation, and I_ϑ is the rotational inertia of the link around the hinge.[6] The solution to this differential equation is a harmonic vibration[7] with calculable frequency for a positive $\Sigma(L, k, F)$, with the stability coefficient in Eq. (1.10); otherwise, exponential divergent movement will appear. The exact vibrations are described by initial conditions for position and velocity, which constitute perturbations from the vertical position. It is noted that this conclusion is not dependent on an exact value for the inertia, as long as it is positive. This is an important observation for the discussion on different stability criteria in Sect. 2.9.

Both the two models employed above are idealized views on the structure, and practical modelling must also consider possible imperfections—in the structure itself or in its representation. This can, for instance, be related to a spring of incorrect length. Considering the first formulation above, and assuming that the spring is unstrained when the link top is horizontally deflected by $x = x_0$, gives a spring force $R = k(\vartheta L - x_0)$. Similar calculations as above then give

$$F = kL\left(1 - \frac{x_0}{L}\frac{1}{\vartheta}\right), \tag{1.14}$$

which is identical to Eq. (1.4) when $x_0 = 0$. This shows that equilibrium exists for $F = 0$ at $\vartheta = \vartheta_0 = \frac{x_0}{L}$. For $x_0 > 0$ and larger angles ϑ, the force F will yield a graph with a horizontal asymptote at $F = kL$. The result is strongly dependent on the imperfection magnitude $\frac{x_0}{L}$, cf. Fig. 1.3. The expressions also shows that the result is no longer symmetric in the angle ϑ, as a case with $x_0 > 0$ and $\vartheta < \frac{x_0}{L}$ gives very different results.[8]

[6] which is $I_\vartheta = \frac{mL^3}{3}$ for a link with uniform mass distribution m

[7] which, in a real situation, will be damped out with time

[8] $\vartheta = 0$ is obviously no longer a solution

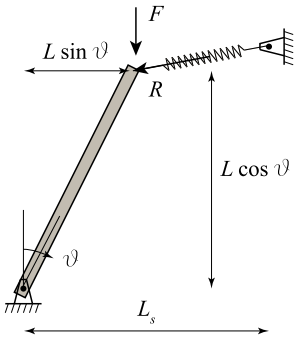

Fig. 1.4 More accurate description of displacement of compressed rigid link in Fig. 1.1

If the spring is given a limited length L_s, the spring is no longer acting horizontally, cf. Fig. 1.4. An assumption of $L_s = L$, still assuming an axially rigid link, gives—after some not trivial algebra—the force F in a deflected equilibrium ϑ as

$$F = kL\frac{1-\sqrt{3-2\cos\vartheta-2\sin\vartheta}}{\sqrt{3-2\cos\vartheta-2\sin\vartheta}}\left(\frac{\cos\vartheta}{\sin\vartheta}-1\right). \tag{1.15}$$

The primary equilibrium and the critical F are the same as above, but the force expression is not symmetric in ϑ, as the recruited horizontal spring force component is accompanied by a downwards force for $\vartheta > 0$ but an upwards one for $\vartheta < 0$. The secondary equilibrium branch is shown in Fig. 1.2.

Considering also the shortening of the link gives a more intricate geometry, but qualitatively similar results, even if the bifurcation state disappears, and is replaced by relations asymptotic to the graphs in the figure. The clear-cut situation comes from the idealization. The main lesson from this is that stability conclusions are related to a particular model of a structure.

1.3 Plane 2-Bar Truss

A second simple example can show another form of lacking stability. The plane truss in Fig. 1.5 shows two identical bars of length L, modelled as ideal springs of axial stiffness EA,[9] symmetrically connected as a structure of height H and attached to two supports by ideal hinges; it is affected by the downwards force F. The bars are assumed to be always straight, but otherwise freely deformable. The problem

[9] with a linear relation between force and strain, and unlimited stretch capacity

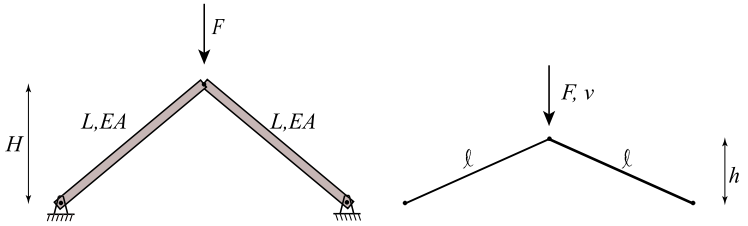

Fig. 1.5 Geometry and schematic deflected shape for plane truss

is defined by the parameters (L, H, EA, F), and is discussed in many treatises of structural non-linearity; it is treated numerically by Eriksson and Nordmark (2019), with the same assumptions but with another notation for geometry parameters and another strain measure.[10]

A symmetric deformation under F is described by only the current height h, which is the vertical coordinate for the top joint. Geometry and algebra together with common assumptions gives the current length of each bar $\ell = \sqrt{L^2 - H^2 + h^2}$, with normal forces $N = EA\frac{\ell - L}{L}$, and the acting force

$$F = -2\,N\frac{h}{L} = 2EA\frac{h}{L}\left(\frac{L}{\sqrt{h^2 - H^2 + L^2}} - 1\right), \tag{1.16}$$

which allows an interpretation $F = F(v)$ after introduction of the downwards depression $v = H - h$. This relates downwards force to downwards depression, and gives a force-displacement graph expression. Evaluation of Eq. (1.16) shows that $F = 0$ for $h = H$, but also for $h = 0$ and $h = -H$, the latter being the truss inverted, with what was the top joint now below the supports.

For consistency with the main theme of this treatise, a total potential of the formulated model is

$$\Pi = 2 \cdot \frac{1}{2}\frac{EA}{L}(\ell - L)^2 - Fv, \tag{1.17}$$

from which expression all results can be obtained, after some non-trivial algebra.

The shape of the relation $F = F(v)$ is shown in Fig. 1.6 for a case where $EA = 1$, $H = 1.5$ and $L = \sqrt{\frac{13}{4}}$ in consistent units. For small depressions v, the force monotonously increases with the deflection, but around $v \approx 0.53H$, a maximum F is reached. After this state, the force can be reduced while depression still increases.[11] At $v = H$, the normal forces N are very high, due to he severely shortened bars, but the forces are completely horizontal, and thereby $F = 0$. For depressions $H < v < 2H$,

[10] Green-Lagrange deformation, cf. Eqs. (2.16)–(2.18) and the accompanying discussion

[11] due to the more shallowly acting—but increasing—normal forces in the bars. This would clearly demand a very special setting to allow physical experimental verification

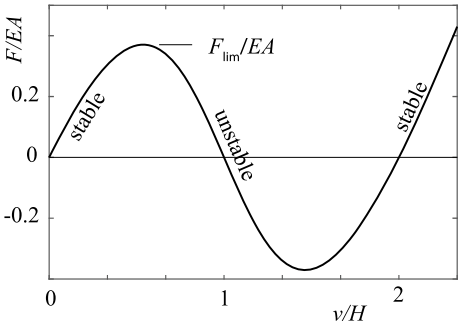

Fig. 1.6 Force-depression graph for plane truss

the force F must be negative, i.e., upwards to keep a certain depression. A new extreme (negative) F is passed on the branch. At the inverted shape $v = 2H$, $F = 0$ as initial bar lengths are restored. When $v > 2H$, F must increase to overcome tensile forces in the bars in the inverted shape. The equilibrium is unstable between the maximum and minimum states for F, but stable otherwise.

The critical force for the maximum force state above is

$$F_{\text{lim}} = \frac{2EA}{L} \frac{\left(\left(L^3 - H^2 L \right)^{2/3} + H^2 - L^2 \right)^{3/2}}{L^2 - H^2}, \tag{1.18}$$

while the force at the minimum force point is $-F_{\text{lim}}$. The extremum force points are limit states, i.e., states with—at least locally—extreme forcing F, and are the most common situations where a structure loses, or re-gains, stability.

The example is somewhat confusing to anyone used to think about common engineering structures, where deformations need be kept small, and force is proportional to deflection, with the relation derived from the initial geometry. Similar situations as in the snap-through behaviour of this example are sometimes technically utilized, for instance in toggle-type switches.

The behaviour of this structure is, however, even richer if the structure is high enough. If the assumption of symmetry in response is disregarded, a sequence of deformed shapes can exist, when the exterior forcing is carried by one compressive and one tensile normal force in the bars, as indicated in Fig. 1.7.[12] Analysis of such equilibria must include two degrees of freedom: the v from above, and a quantity u for the horizontal movement of the top joint. More extensive algebra shows that this situation can only exist if $H > \sqrt{\frac{23}{27}} L \approx 0.923L$.

The critical force for this bifurcation state, very similar to the example in Sect. 1.2, is evaluated as the analytical expression

[12] or by its mirror image

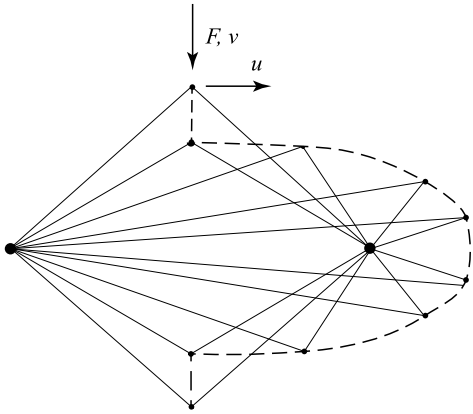

Fig. 1.7 Snapshots of secondary solutions for plane truss. Dashed graph connects positions of top joint

$$F_{\text{bif}} = \frac{2EA}{L}\sqrt{\frac{\ell_3 + 6\,H^2 - 4\,L^2}{\ell_3 + 2\,L^2}}\left(L - \frac{\sqrt{\ell_3 + 2\,L^2}}{\sqrt{6}}\right), \tag{1.19}$$

after introduction of the short hand notations

$$\begin{aligned}
\ell_1 =& \sqrt{L^4\left(L^2 - H^2\right)^3\left(23\,L^2 - 27\,H^2\right)},\\
\ell_2 =& \sqrt[3]{-36\,H^2\,L^4 + 27\,H^4\,L^2 + 3\sqrt{3}\ell_1 + 11\,L^6},\\
\ell_3 =& 2^{2/3}\ell_2 + \frac{2\sqrt[3]{2}\left(6\,H^2\,L^2 - 5\,L^4\right)}{\ell_2},
\end{aligned} \tag{1.20}$$

which all are different powers of lengths.

Two stability coefficients for the primary equilibrium solutions are now described as

$$\begin{aligned}
\Sigma_{\text{lim}}(L, H, EA, v) =& \frac{2EA}{L}\left(\frac{H^2\,L - L^3}{\ell_4} + 1\right),\\
\Sigma_{\text{bif}}(L, H, EA, v) =& \frac{2EA}{L}\;\frac{-H^2 L + \ell_4 + 2\,HLv - Lv^2}{\ell_4},
\end{aligned} \tag{1.21}$$

with an auxiliary variable involving the deflection, as

$$\ell_4 = \left(v(v - 2H) + L^2\right)^{3/2}. \tag{1.22}$$

These are essentially of the same form as in the previous example, but there are two of them and these are more complex. One of the stability coefficients will become zero for the critical states expressed by Eqs. (1.18) or (1.19). It is noted

that the stability coefficient expressions are not explicitly dependent on the acting force F, as was the case in Sect. 1.2, but are evaluated for the state variables and parameters; the acting force is also directly calculable from these.[13] If a practical situation were considered, the lower of the critical forces, obtained for vanishing Σ_{lim} or Σ_{bif}, dependent on geometry H/L, is the maximum capacity of the structure.

A main restriction introduced in the analyses is that the problem is considered as plane. Compared to Sect. 1.2, the bars now deform axially—but not in bending, and are assumed to carry any normal forces. When H is rather large, these are very high, which demands that the material has a high elasticity limit, so that forces are always directly related to strain. It is also assumed that the bars do not buckle under the acting compressive forces. The treatment of buckling in compressed members will be the topic of the next section.

1.4 Compressed Beam

Beams in the structural context are slender mechanical components carrying forces primarily through bending. The forcing is typically acting transversally to the beam length direction. In $2D$ or $3D$ frames, combinations of axial and bending forces are used to transmit exterior forcing to the supports.

The combinations of axial force and bending in a plane beam is probably the most common stability problem studied. The typical cases are those of Euler buckling, differing in their boundary conditions. The fundamental case is a simply supported beam, acted upon by a compressive force, as in Fig. 1.8.[14,15]

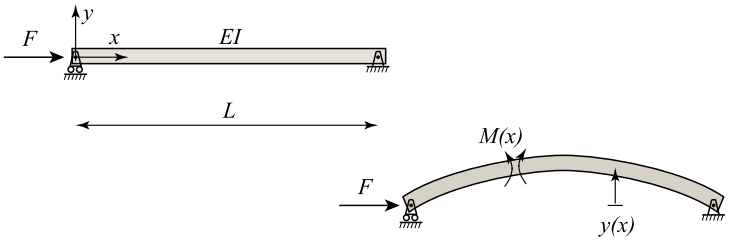

Fig. 1.8 Model and assumed deflected equilibrium configuration for compressed simply supported plane beam. $M(x)$ is interior moment in a fictitious section cut at x

[13] The force F could be introduced as parameter, but then any of the others could be eliminated, as they are connected through Eq. (1.16)

[14] Compared to the bending case for a transversal forcing, one support must allow a horizontal movement; this would be of no importance for the transversal forcing.

[15] The beam is here, uncommonly, drawn as horizontal, which is of no importance since self-weight is anyhow neglected.

The analysis uses the equation of the elastica—or the beam equation—for an assumed deflected equilibrium, roughly similar to the drawn shape between the supports. On the part to the left of a virtual section at coordinate x, a driving interior moment

$$M_f(x) = F\, y(x), \tag{1.23}$$

is acting, the magnitude varying along the beam length. The expression respects that the transversal deflection is no longer assumed as infinitesimally small.

The resisting interior moment M_r is

$$M_r(x) = E I\, y''(x), \tag{1.24}$$

from the elastica equation, and with $E I$ the bending rigidity of the beam.[16] The primes here denote derivatives with respect to the x coordinate.

Equating the moments as $M_r + M_f = 0$ for the existence of a deflected equilibrium, gives a homogeneous differential equation

$$E I\, y'' + F\, y = 0. \tag{1.25}$$

With the essential boundary conditions $y(0) = y(L) = 0$ for the case considered in Fig. 1.8, the equation has solutions of the form

$$y(x) = d_n \sin \frac{n\pi x}{L} \tag{1.26}$$

for any positive integer n, with arbitrary amplitudes d_n, and for a critical force

$$F_{\mathrm{cr},n} = \frac{n^2\, \pi^2}{L^2} E I. \tag{1.27}$$

The same result is obtained from the first differential with respect to d_n of the total potential, which is

$$\Pi = \frac{E I}{2} \int_0^L (y'')^2 \mathrm{d}x + F \left(L - \int_0^L \left(1 + \frac{1}{2} (y')^2 \right) \mathrm{d}x \right), \tag{1.28}$$

as an alternative to Eq. (1.25), when $y''(0) = y''(L) = 0$. The first part here comes from bending strains, and the second from an approximation to the horizontal shortening of the bent inextensible beam due to bowing.[17]

[16] Note that both y'' and $M(x)$ are negative in the figure

[17] The integrand in the last integral of Eq. (1.28) is an approximation to $\sqrt{1 + (y')^2} > 1$.

The result in Eq. (1.27) exists for one specific compressive force, exactly as for the rigid link in Sect. 1.2. Here, many deflected shapes are possible, but the n^2 factor in the critical force $F_{\mathrm{cr},n}$ shows that only $n = 1$ is normally of any practical relevance. The higher critical forcing levels are practically impossible to reach without very special measures. Compared to Fig. 1.2, several critical states and several secondary equilibrium graphs could be drawn, but all primary states for forces above $F_{\mathrm{cr},1}$ are unstable.

Similarly as in the previous section, stability coefficients are introduced for the compressed simply supported beam. In this case, one stability coefficient can be defined for each mode, i.e., integer numbers of sinusoidal half-waves. Some algebra on the results above shows that the stability coefficient for the n half-wave mode is

$$\Sigma_n(EI, L, F) = \frac{\mathrm{d}^2\Pi}{\mathrm{d}\, d_n^2} = \left(\frac{n^2\pi^2 EI}{L^2} - F\right), \tag{1.29}$$

showing that stability coefficients for higher n vanish for much higher compressive forces. Like in Sect. 1.2, but contrary to Sect. 1.3, the acting force F can not be eliminated as parameter, as it does not act directly on the critical mode direction.

Euler buckling for beams is typically presented as four (or five) clear-cut situations of boundary conditions. As the homogeneous Eq. (1.25) is always the basis, the solutions will be similar to Eq. (1.26), which is one sinusoidal half-wave over a representative beam length. The buckling length for a particular case is dependent on the support conditions, and can be both longer and shorter than the physical beam.[18] A visual inspection of the possible buckling shapes can often give a sufficiently accurate guess for less clear-cut cases. The main idea is thereby to introduce an estimated buckling length L^* in the denominator of Eq. (1.27)—and, of course, $n = 1$. Solved cases and general methods to decide the buckling length in different situations are available in engineering handbooks.

When no tabulated solutions can be found, an iterative method is available through the Vianello method, also often named Stodola-Vianello method. This method, which is an instance of power iterations for a matrix eigenvalue problem, is intuitive and easily implemented also in spreadsheet software. A brief example, dealing with a compressed cantilever of variable bending stiffness, is given in Fig. 1.9 showing a systematic tabular calculation for a deflected equilibrium, i.e., a critical equilibrium state, where columns are successively built from left to right.

A deflected shape for the cantilever is represented by a number of discrete deflection values, at points 0–8 in the example, i.e., the beam length is divided into 8 parts. A rough assumed deflected equilibrium shape is guessed,[19] and introduced in the second column[20] y_i. From the assumed deflections, the corresponding inte-

[18] e.g., twice the physical length for a compressed cantilever, half the physical length for a double-sided clamped beam

[19] which here does not even fulfil the clamped condition at $i = 0$

[20] Everything is scalable, so the deflections are represented as fractions of L to see the dimensions of each column.

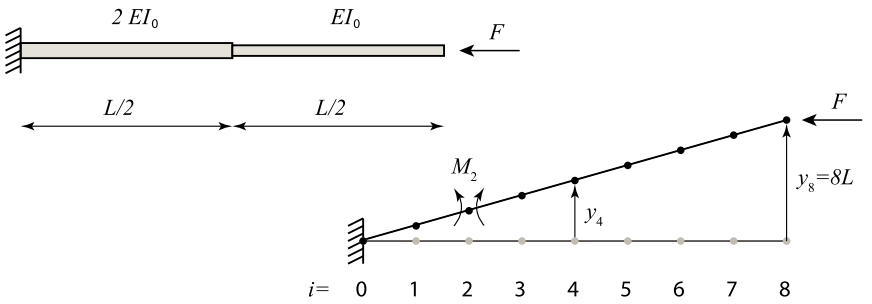

i	y(guess)	M	EI	y''	y'	y(res)	y(res)*y(gue)	y(gue)*y(gue)
0	0.00	8.00	2.00	4.00	0.00	0.00	0.00	0.00
					2.00			
1	1.00	7.00	2.00	3.50		2.00	2.00	1.00
					5.50			
2	2.00	6.00	2.00	3.00		7.50	15.00	4.00
					8.50			
3	3.00	5.00	2.00	2.50		16.00	48.00	9.00
					11.00			
4	4.00	4.00	1.50	2.67		27.00	108.00	16.00
					13.67			
5	5.00	3.00	1.00	3.00		40.67	203.33	25.00
					16.67			
6	6.00	2.00	1.00	2.00		57.33	344.00	36.00
					18.67			
7	7.00	1.00	1.00	1.00		76.00	532.00	49.00
					19.67			
8	8.00	0.00	1.00	0.00		95.67	765.33	64.00
	L	FL	EI_0	FL/EI_0	$FL^2/8EI_0$	$FL^3/64EI_0$	$FL^4/64EI_0$	L^2
							2017.67	204.00
						F=	6.47	EI_0/L^2

Fig. 1.9 Evaluation of critical forcing magnitude for variable-section cantilever beam, by Vianello's method

rior moments are calculated, as $M_i = F(y_8 - y_i)$, and then—through the point-wise bending stiffnesses—the curvatures y_i''. By introducing half-way points $i + \frac{1}{2}$, these are integrated first to slopes y_i' and then to deflections y_i(res) by forward stepping, through successive additions of the table values. For simplicity, the step length $L/8$ is considered in the multipliers below each column.

The condition for a deflected equilibrium is that the resulting column shape agrees with the assumed. This means that for a perfect guess, there should be an equality, e.g., $8L \equiv 95.67 \frac{FL^3}{64\,EI_0}$ for $i = 8$. To consider all points, the best fit comes from an evaluation from the average ratio

$$F_{\rm cr} = \frac{\sum_i (y_{{\rm guess},i}\ y_{{\rm guess},i})}{\sum_i (y_{{\rm guess},i}\ y_{{\rm res},i})} \frac{64\,EI_0}{L^2}, \tag{1.30}$$

where the sums use the numerical values in the table, and the final factor takes care of the column multipliers. In this case, the very crude guess gives the ratio of sums as 204/2017.67, and the critical $F_{\text{cr}} = 6.47\frac{EI_0}{L^2}$. Feeding the numbers from the resulting y column into the column for guessed y, a much better approximation is obtained, with the leading multiplier as 4.39. With more iterations, a convergent value with multiplier 4.18 is reached. This is very close to an analytical value, even if the discretization of the beam through nine discrete values gives a small approximation error.[21]

The same approach can be used for many classes of beam buckling problems, if no more sophisticated software is available. For some boundary conditions, the table will need two similar schemes, where an extra scheme considers an unknown reactive force. The resulting two columns are matched to fulfil a specific boundary condition.

For many structures, combinations of axial and transversal forces affect the beams. The situation shown in Fig. 1.10 is a typical case. This is commonly analysed by what is known as a second order,[22] a beam-column, or a $P-\Delta$ method. The terms are not uniquely defined, but always indicate that axial forces give bending deformations through a considered finite transversal deflection. The homogeneous differential equation (1.25) for compressed beam deflection is thereby complemented by a right hand side according to

$$EI\, y'' + F\, y = -M_{f,q}(x), \tag{1.31}$$

where $M_{f,q}(x)$ describes the forcing moment from the transversal forces at section x. The potential loss under the transversal force intensity is also easily added to the total potential in Eq. (1.28), allowing an energy-based treatment.

For the uniformly distributed force intensity q in Fig. 1.10, $M_{f,q} = \frac{q}{2}x(L-x)$ and some non-trivial algebra is needed to reach the solution. This solution is, with increasing values of the compressive force F, dominated by a term which includes a factor $1/\cos(\frac{L}{2}\sqrt{\frac{F}{EI}})$, which goes towards infinity when F approaches the critical force for $n = 1$ in Eq. (1.27).

A clearer view on the effect from the compressive force is obtained by introducing the sinusoidal force intensity distribution in Fig. 1.10. Without going into details, this is the dominating term in a series expansion of the uniform force intensity q in trigonometric functions if $q_1 = \frac{4}{\pi}q$. With the corresponding forcing moment $M_{f,q} = \frac{q_1 L^2}{\pi^2}\sin\frac{\pi x}{L}$ in Eq. (1.31), the solution for the deflection y is

[21] An analytical solution gives the critical $F_{\text{cr}} = 4.135\frac{EI_0}{L^2}$, which lies between the values $\frac{\pi^2}{4}\frac{EI_0}{L^2}$ and $\frac{\pi^2}{4}\frac{2{\cdot}EI_0}{L^2}$ valid for constant bending stiffnesses; the result is closer to the higher one, as an increase of bending stiffness is more 'useful' at the clamped end.

[22] The 'second order' term has no mathematical meaning; it seems to just reflect that this approach is somewhat improved from a linear first-order approach.

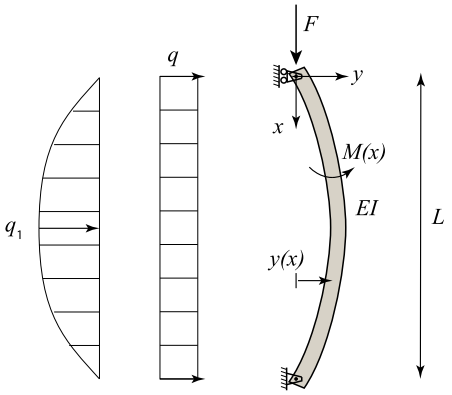

Fig. 1.10 Deflected equilibrium configuration for column with compressive force and uniform distributed forcing q. Left: first term q_1 of trigonometric series expansion of q

$$y(x) = \frac{q_1 L^4}{\pi^4 E I} \sin \frac{\pi x}{L} \cdot \frac{1}{1 - F/F_{\text{cr}}}. \tag{1.32}$$

The first part in the expression is the deflection without the axial force, while the final ratio is a magnification factor expressing the nearness to the critical compressive force.[23]

The intention of the second order methods is to introduce the coupling between axial and bending behaviour in the beam, where an axial force magnifies or reduces both deflection and interior bending moment from transversal forces. The method is commonly available in specialized design software for structural analysis, and is recommended or demanded in design codes.

The second order methods, as described here, are similar—but not identical—to the linear pre-buckling (LPB) approaches to be further discussed in Sect. 4.1.3.

The approach, however, has limitations, and must be used with care. The main drawback is that the coupling is uni-directional in the sense that axial forces affect calculated bending response, but not the opposite; the axial stiffness is not at all affected by the extensive bending.[24] This can be a major drawback, for instance, in statically indeterminate frame structures where the force distribution is decided by the relative stiffnesses of the members. Better models for beam and frame analyses are discussed in Chap. 3, the main ingredient being a correct and more complete coupling between axial and bending responses. The second order methods can only be considered as reasonably valid as long as axial forces are well below the critical.

[23] The derivation is equally valid for a tensile force, here denoted $F < 0$, in which case the final factor is a reduction < 1.

[24] It is easily shown by experiments that a compressed beam of length a few meters can be calculated to have deflections of several meters, with a shortening of just a few millimeters, if the compressive force is close to the buckling force.

Further discussion on assumed plane conditions, and on imperfections could be motivated by this example, but such comments are made already in previous examples.

1.5 System Stability

Building structures are large and complex systems, normally with a rather clear differentiation of mechanical components for different aspects of forcing. Even if the main challenge for most building structures is to carry vertical gravity effects, also horizontal forces can be of considerable magnitudes.

A typical multi-storey building is schematically shown in Fig. 1.11, where a few stiff components in shear walls and staircases are the main contributors to the carrying of horizontal forces, while a set of more slender hinged columns just carry vertical forces. The floor slabs are typically built as—and are assumed to be—rigid in both bending and in-plane senses, so that they are not deformed to any appreciable measure during any mechanical action considered on them. The stiff vertical components are typically continuous from the ground upwards, and must be arranged with a clear strategy, in order to give stiffness in the $3D$ space. The columns act only between two floors.

The term stabilization of a building is commonly referring to the case of horizontal forces, i.e., the existence of force transmission pathways from the points of attack to the ground supports. This gives primarily a need for sufficient capacity of the affected components to resist the magnitudes of the design forcing cases; the building becoming a mechanism[25] is avoided, cf. Sect. 3.7. By considering also acting vertical forces, the problem comes closer to the main topics in this treatise.

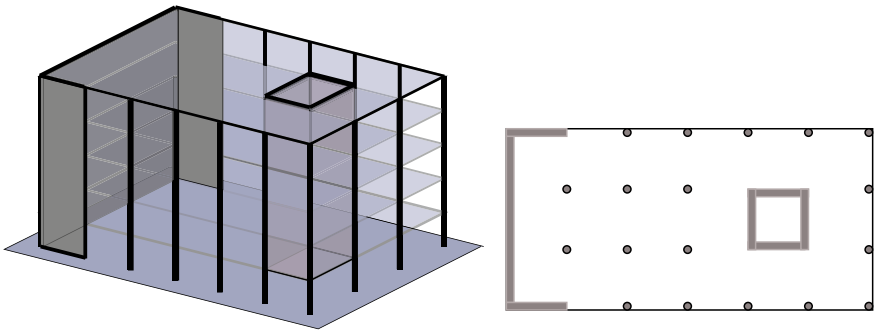

Fig. 1.11 Schematic view on multi-storey building system

[25] which lacks stiffness in, at least, some particular movement direction

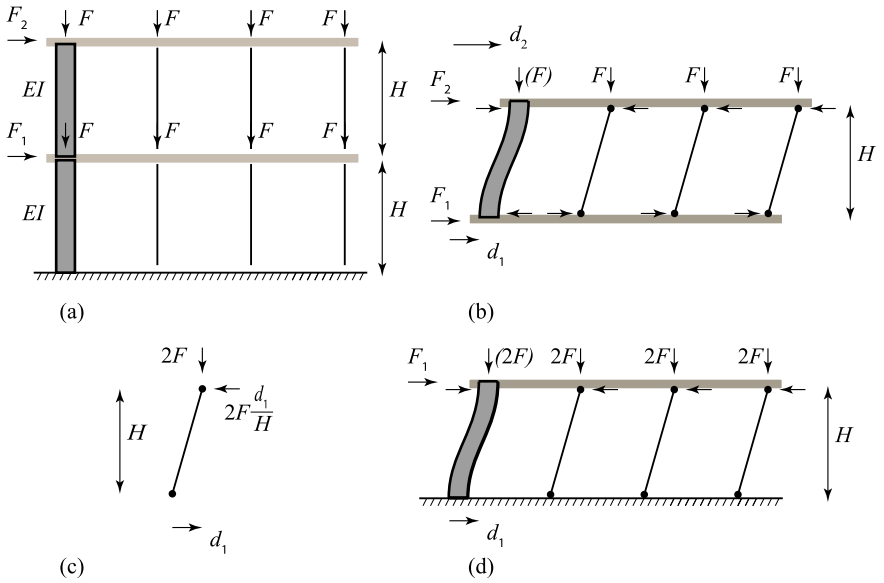

Fig. 1.12 Simplified example of structural system stability involving several components. **a** Model. **c** Hinged column analysis. **d** First level analysis model. **b** Second level model

A simple two-storey structure of total height $2 \cdot H$ is shown in Fig. 1.12a. It consists of two infinitely rigid floors, which are vertically supported by beam-like components of relevant bending stiffness EI and a number of hinged column elements, without any particular properties.[26] For the calculations, the order of the components is arbitrary, and their horizontal spacing is of no importance.

The forcing of the structure is represented by equal floor force resultants F on the beam and columns, and two horizontal forces F_1 and F_2 on the floor levels. The requirement is that the effects from the horizontal forcing on the vertical beam are well within bending capacity. A stability investigation then considers how the vertical forces affect the response through a deflected equilibrium view, cf. Sect. 1.2.

Figure 1.12d shows how floor number 1 is assumed to be horizontally moved the distance d_1 from its original position. With the assumption that the beam is rigidly connected to ground and the floor, the force needed to move the top is $\frac{12\,EI}{H^3} d_1$. The contributions from the columns are then given by Fig. 1.12c. Equilibrium for one link of height H affected by a compressive force of $2F$ demands a horizontal force of magnitude $2F \frac{d_1}{H}$. The force components active in the horizontal displacement are shown symbolically in Fig. 1.12d.

[26] The floors are rigid with respect to both bending and axial behaviour, the columns have sufficient compressive capacity to resist the vertical forcing, the floors are assumed as rigidly connected to the vertical beam, while the hinged connections are perfectly friction-free.

Further, assuming that the second floor just follows in a rigid translation, such that its horizontal displacement is $d_2 = d_1$, the horizontal force to create this displacement can be expressed as

$$F_1(d_1, d_2 = d_1) = 12\frac{EI}{H^3}d_1 - 3 \cdot 2F\frac{d_1}{H} = \left(12\frac{EI}{H^3} - 6\frac{F}{H}\right)d_1, \tag{1.33}$$

where vertical forces tend to reduce the bending stiffness.

Figure 1.12b studies the second level of components. As this figure focusses on the difference in horizontal displacement $(d_2 - d_1)$, the horizontal forces are

$$F_2(d_1, d_2) = \left(12\frac{EI}{H^3} - 3\frac{F}{H}\right)(d_2 - d_1) = -F_1(d_1, d_2), \tag{1.34}$$

when the first floor must give a reaction.

Summing the two cases, for an arbitrary horizontal deflection configuration (d_1, d_2) gives

$$\begin{aligned} F_1 &= \left(24\frac{EI}{H^3} - 9\frac{F}{H}\right)d_1 + \left(-12\frac{EI}{H^3} + 3\frac{F}{H}\right)d_2, \\ F_2 &= \left(-12\frac{EI}{H^3} + 3\frac{F}{H}\right)d_1 + \left(12\frac{EI}{H^3} - 3\frac{F}{H}\right)d_2. \end{aligned} \tag{1.35}$$

In matrix form, this is a stiffness relation for the deflected configuration

$$\begin{pmatrix} F_1 \\ F_2 \end{pmatrix} = \left(\frac{EI}{H^3}\begin{pmatrix} 24 & -12 \\ -12 & 12 \end{pmatrix} - \frac{F}{H}\begin{pmatrix} 9 & -3 \\ -3 & 3 \end{pmatrix}\right)\begin{pmatrix} d_1 \\ d_2 \end{pmatrix}, \tag{1.36}$$

where the first matrix is recognized as the linear stiffness of the beam, while the second term shows the geometric stiffness from compressed columns.[27]

Solving Eq. (1.35) with known parameters and known forces F, F_1, F_2 gives the horizontal displacements of the two floors (d_1, d_2), and then all relevant interior forces. The result quantities are magnified by the vertical forces, as in Sect. 1.4.

With respect to stability, the expressions define an eigenvalue problem, the results of which can be shown by simple demonstration. Assuming—seemingly without particular reason—that $d_1 = 0$, Eq. $(1.35)_2$ give

$$F_2 = \left(12\frac{EI}{H^3} - 3\frac{F}{H}\right)d_2 = -F_1. \tag{1.37}$$

This implies that a horizontal displacement $d_2 \neq 0$ can exist with zero horizontal forces[28] if the vertical forces are

[27] which is here negative, i.e., de-stabilizing

[28] and, thereby, any horizontal force will create infinite movement

$$F = F_{\text{cr},2} = 4\frac{EI}{H^2}. \tag{1.38}$$

Similarly, a horizontal displacement described by $d_2 = d_1 \neq 0$ exists without horizontal forces, according to Eq. (1.33), for

$$F = F_{\text{cr},1} = 2\frac{EI}{H^2}, \tag{1.39}$$

with $F_2 = 0$. This critical force is lower than the one from Eq. (1.38), and thereby the deciding one.

The results obtained can be expressed through two stability coefficients

$$\begin{aligned} \Sigma_1(EI, H, F) &= 12\frac{EI}{H^3} - 6\frac{F}{H}, \\ \Sigma_2(EI, H, F) &= 12\frac{EI}{H^3} - 3\frac{F}{H}. \end{aligned} \tag{1.40}$$

where, the force F can not be eliminated, as it is orthogonal to the critical deflection. Being initially positive, both Σ values will decrease with increasing value of F, and a critical state is reached when either of them becomes zero,[29] and the stability is lost.

It is obvious from the above treatment that the stability is only dependent on the vertical forces in this case, not on any particular horizontal force. In reality, the modelled structure would, before reaching the critical vertical force, have lost its integrity due to some material failure when the response to any existing horizontal force was magnified by the nearness to the critical force.

The treatment above considered a very simple plane system, where each floor was described by just its horizontal displacement, i.e., a discretization by one degree of freedom per storey. A full $3D$ building structure can be modelled, if three degrees of freedom are introduced for each storey: two in-plane translations and a floor rotation. As the manual work to create the stiffness expressions for all degrees of freedom is overwhelming, and thereby extremely error-prone, a systematic algorithm is needed for this analysis.

In a systematic investigation, the stability coefficients can be used to evaluate a safety factor against loss of stability of the system,[30] related to a chosen design level of F. As the loss of stability is a catastrophic failure, this safety margin must be very high. Such a safety factor is immediately obtained from a linear pre-buckling setting in Sect. 4.1.3, but the shortcomings of such approaches must be noted.

The analysis here is another example of a second order formulation, when effects from finite deformations are included in a bending formulation. Compared to the compressed beam analysis in Sect. 1.4, the present example leads to a case of system

[29] as any, however small, horizontal force would meet no resisting force stiffness

[30] but note the difference between the safety factor and the stability coefficients

stability in the sense that several components are acting together, with some of them stabilizing and some de-stabilizing the considered structure.

This example uses several simplifications in the modelling, in particular that the floor slabs are supposed to be infinitely stiff in bending as well as in in-plane action. This over-estimated stiffness in the system will lead to an over-estimation of the critical forcing for the structure.[31] This gives further arguments for aiming at very high safety factors in this simplified modelling, or for using more elaborate analyses.

1.6 Plate Buckling

In the engineering terminology, a plate is a thin flat structure, often but not always horizontally arranged. Plates exist in pure form as floor slabs in buildings, but are otherwise most often components in more complex structures, for instance in welded beams, cf. Sects. 1.7 and 5.2. The fact that plates are thin implies that they have a thickness which is significantly smaller than the in-plane measures. They are also often of rather simple in-plane shape. Depending on the situation and context, the plates can have a wide variety of support conditions along their circumferential edges.

Only ideally elastic response of the thin plate is considered here. The basic analysis further assumes that the plate is situated in the $x - y$-plane, with a thickness attribute parameter h, and a force intensity $q(x, y)$ in the z direction, cf. Fig. 1.13.

According to the Kirchhoff plate theory, the response to the transversal force intensity q is just a vertical deflection $w(x, y)$ of the plate midplane. The assumptions are similar to the common Euler-Bernoulli beam theory, as further discussed in Sect. 3.4.2.

Under these assumptions, the differential plate equation for a thin, transversally forced isotropic and ideally elastic plate is obtained as

$$D\left(\frac{\partial^4 w}{\partial x^4} + 2\frac{\partial^4 w}{\partial x^2 \partial y^2} + \frac{\partial^4 w}{\partial y^4}\right) = q, \tag{1.41}$$

with the so called plate stiffness quantity (at a point)

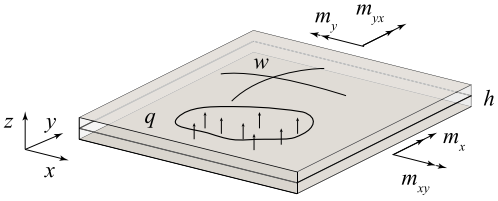

Fig. 1.13 Basic figure for plate carrying transversal force intensity, showing section moment resultants

[31] As an illustration, the terms $12\frac{EI}{H^3}$ in the expressions will have a lower numerical factor, if the end conditions are not completely rigid.

$$D = \frac{Eh^3}{12(1-\nu^2)}, \tag{1.42}$$

resembling a beam section of height h and width 1 unit, and involving the elastic parameters (E, ν) for the plate material. Compared to the equation of the elastica, the resistance to forcing is split between the two directions. The interior force resultants are three moment intensities,[32] obtained as

$$\begin{aligned} m_x &= -D\left(\frac{\partial^2 w}{\partial x^2} + \nu\frac{\partial^2 w}{\partial y^2}\right), \quad m_y = -D\left(\nu\frac{\partial^2 w}{\partial x^2} + \frac{\partial^2 w}{\partial y^2}\right), \\ m_{xy} &= m_{yx} = D(1-\nu)\frac{\partial^2 w}{\partial x \partial y}, \end{aligned} \tag{1.43}$$

when it is noted that the indices commonly refer to the corresponding stress component, and do not reflect the axis around which the moment acts. The moments are converted to the corresponding stress components $(\sigma_x, \sigma_y, \tau_{xy})$ by handling them as in a beam section of unit width. Some care must be taken in evaluating the signs of the stresses in relation to the general form in Chap. 2.

The most difficult part of plate analysis is often to decide and describe the support conditions for the considered region. Common situations are free edges, with all edge forces zero, clamped edges with zero deflection and no rotation around the edge, or simply supported edges with no deflection and no moment around a vector along the edge.[33] These issues are discussed, for a numerical solution method by Ghali et al. (2003). Largely independent of these conditions, the solution for the plate under any distributed downwards force intensity is more or less in the form of a hanging mat.

Although not within the most generic definition of a plate, a thin region can also be affected by forces within its plane.[34] Constant stresses in the $x-y$-directions are integrated over the thickness at a point (x, y) to normal force intensities, cf. Fig. 1.14[35]

$$\begin{aligned} n_x(x,y) &= \sigma_x h; \quad n_y(x,y) = \sigma_y h; \\ n_{xy}(x,y) &= n_{yx} = \tau_{xy} h, \end{aligned} \tag{1.44}$$

where $(\sigma_x, \sigma_y, \tau_{xy} = \tau_{yx})$ are the common linear stress components in the plane.

Equilibrium without body forces gives two equations as, cf. Sect. 2.5.1,

$$\begin{aligned} \frac{\partial n_x}{\partial x} + \frac{\partial n_{xy}}{\partial y} &= 0, \\ \frac{\partial n_y}{\partial y} + \frac{\partial n_{yx}}{\partial x} &= 0. \end{aligned} \tag{1.45}$$

[32] typically of the dimension Nm/m

[33] which is somewhat complicated by the Poisson effect

[34] Formally, the problem should then be analyzed as a 'membrane' or a 'plane-stress' structure. If both in-plane and transversal force are present, the problem is really a 'shell'

[35] Note the somewhat unusual indexing of shear stress and shear stress resultant used here.

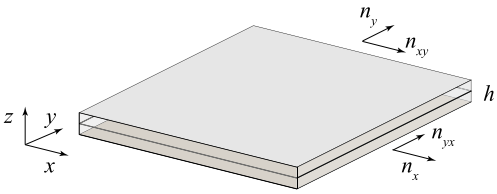

Fig. 1.14 In-plane force components in plate

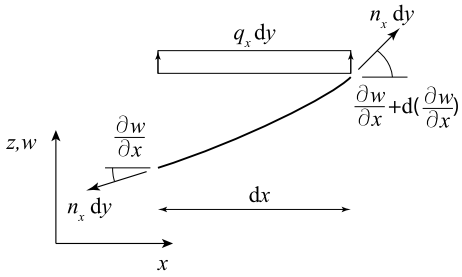

Fig. 1.15 In-plane force creating transversal plate force intensity. The quantity $\mathrm{d}y$ is the measure normal to the figure, which is just a multiplier for 'unit width'

Like the beam in Sect. 1.4, a plate compressed in its plane can deflect in the transversal direction, but general solutions to the plate buckling problem are very complex. Assuming a finite, but small, deflection $w(x, y)$ of the plate, and the in-plane force intensities in Eq. (1.45), Fig. 1.15 can be used to visualize that the force intensity n_x will give a transversal component of force

$$Q_x \equiv q_x \cdot \mathrm{d}x\mathrm{d}y = n_x\,\mathrm{d}\left(\frac{\partial w}{\partial x}\right)\mathrm{d}y = n_x\frac{\partial^2 w}{\partial x^2}\cdot \mathrm{d}x\mathrm{d}y \tag{1.46}$$

to a $\mathrm{d}x\,\mathrm{d}y$ element of the midplane surface, when $\mathrm{d}y$ is a (small) width perpendicular to the figure plane.

With similar figures, the total transversal force intensity component from the in-plane force intensities is

$$q = n_x\frac{\partial^2 w}{\partial x^2} + n_y\frac{\partial^2 w}{\partial y^2} + 2n_{xy}\frac{\partial^2 w}{\partial x\partial y}, \tag{1.47}$$

which can be introduced in Eq. (1.41). A deflected equilibrium situation can be solved for, where boundary conditions for both the combined cases must be fulfilled.

The only reasonably simple cases to handle analytically are constant levels for any of the in-plane resultants. For $n_y = n_{xy} = n_{yx} = 0$, and n_x a constant resultant force intensity[36,37] in a rectangular region ab in the (x, y) plane, Eq. (1.41) becomes

[36] assuming that the in-plane boundary conditions allow this uniform and uni-axial stress state

[37] Many treatises of this case define the in-plane force intensity as positive for compression, the only interesting case. This just gives a change of sign in Eq. (1.48).

$$D\left(\frac{\partial^4 w}{\partial x^4}+2\frac{\partial^4 w}{\partial x^2\partial y^2}+\frac{\partial^4 w}{\partial y^4}\right)-n_x\frac{\partial^2 w}{\partial x^2}=0, \tag{1.48}$$

which can be compared to a twice differentiated Eq. (1.25).

With simply supported edges with respect to transversal deflection, the boundary value problem lends itself to solutions of the form

$$w(x,y)=w_{mn}\sin\frac{m\pi x}{a}\sin\frac{n\pi y}{b} \tag{1.49}$$

for any positive m and n. Introducing an arbitrary term in Eq. (1.48) gives

$$\left[D\left(\frac{m^4\pi^4}{a^4}+2\frac{m^2n^2\pi^4}{a^2b^2}+\frac{n^4\pi^4}{b^4}\right)+n_x\frac{m^2\pi^2}{a^2}\right]\sin\frac{m\pi x}{a}\sin\frac{n\pi y}{b}=0. \tag{1.50}$$

The solution to this equation gives an expression for the intensity n_x in relation to D and as functions of m and n, with given a and b. The solution is often given as

$$n_{x,\mathrm{cr}}=-\frac{\pi^2 D}{b^2}\cdot k, \tag{1.51}$$

where $k=\left(\frac{mb}{a}+\frac{a}{mb}\right)^2$, when it is observed that $n=1$ always gives the smallest value. The minimum value $k=4$ appears for $m=1$ and a square plate $a=b$. For other ratios (a/b), higher m might give the lowest values for k. In general, minimum buckling force intensity occurs when a/m and b give an approximate square, as in Fig. 1.16. With $a/b=2.8$ in the figure, $k=4.02$ for $m=3$ and $k=4.47$ for $m=2$.

Another interpretation of the results, closer to the beam case in Sect. 1.4, is to evaluate the total compressive force in the deflected equilibrium state

$$-(n_x b)_{\mathrm{cr}}=\frac{\pi^2 D\,b}{a^2}\left(m+\frac{1}{m}\left(\frac{a}{b}\right)^2\right)^2, \tag{1.52}$$

where the product $D\,b$ is resembling $E\,I$ for a beam. The parenthesis approaches unity for $m=1$, and a wide plate $b\gg a$, when the transverse bending effects disappear. For narrow plate strips with $b<a$, $m>1$ might give the lowest critical force.

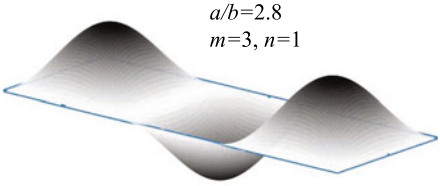

Fig. 1.16 Buckling pattern for long plate

Plate buckling under compressive forces differs from beam buckling in its higher degree of parameter dependence, for instance the aspect ratio of the edges. The lowest critical buckling force can therefore be related to different buckling modes, and two different modes can give the same critical intensity; $a/b = \sqrt{2}$ in Eq. (1.51) gives $k = 4.5$ for both $m = 1$ and $m = 2$. In the vicinity of this aspect ratio, the two m values will give almost equal buckling forces, but for two different modes. Cases where two critical situations (almost) coincide are always more problematic from several viewpoints.[38]

As opposed to the beam case, the plate also gives a significant secondary capacity in a buckled configuration, with a stiffness to further forcing after buckling about 40% of the initial stiffness. Post-critical capacity is often calculated through 'effective width' or 'effective thickness' approaches. In addition, the secondary solutions are strongly dependent on the transversal and in-plane boundary conditions.

1.7 Thin-Walled Column

One application of the plate buckling analysis above is in the design of thin-walled beams. An example is the compressed thin-walled hollow square section column in Fig. 1.17. The section has a thickness h, and a mid-surface width b; the length of the column is L. An elastic material described by (E, ν) is assumed.

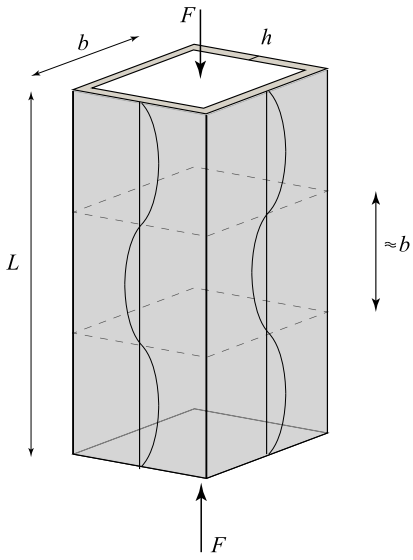

Fig. 1.17 Compressed thin-walled hollow square section column

[38] This will, for instance, happen when a structure is mathematically optimized for a maximal lowest critical magnitude, which often means that the two lowest magnitudes will tend to coincide.

Assuming first that $L \gg b$, the sides of the column will buckle synchronously, with buckles of approximate length b.[39] Using Eq. (1.51) for the circumference length $4b$ gives a total compressive force at buckling

$$F_{\text{loc}} = 4b \cdot 4\pi^2 \frac{D}{b^2} \approx 14.5 Ebh \left(\frac{h}{b}\right)^2 \tag{1.53}$$

with $\nu = 0.3$ introduced in the final member. At this compressive force, the column will undergo local buckling in a repetitive pattern on all sides, as sketchily indicated by the figure.

Recalling Sect. 1.4, a compressed column can also be affected by Euler buckling over the whole column length. Assuming end conditions which can be represented by hinged supports, so that L will be the buckling length,[40] global buckling will result. As the area moment of inertia of the section can be approximated as

$$I \approx \frac{2}{3} b^3 h, \tag{1.54}$$

the Euler buckling force for the column is, according to Eq. (1.27) with $n = 1$,

$$F_{\text{glob}} \approx 6.58 Ebh \left(\frac{b}{L}\right)^2. \tag{1.55}$$

As the two expressions contain different parameters, it can not be stated generally which critical force is the lowest, i.e., the deciding force. For a thin-walled section with

$$h < 0.67 \frac{b^2}{L} \tag{1.56}$$

the local buckling will be the first to appear; otherwise, the Euler buckling will come first. For parametric cases where the two members of Eq. (1.56) are approximately equal, the stability conclusions are often very complex, as the two critical responses interact: a mode interaction situation, which is further discussed in Sect. 5.2. Such designs will also be extremely sensitive to imperfections in the structure. Similar to this example, a compressed thin-walled cylinder is a well-known case of very complex stability behaviour.

As a final comment on this example, the symmetry of the square beam section will make the column susceptible to global buckling in any direction, unless the support condition restraints are asymmetric.

[39] or, to be precise, the L divided by an integer number, close to b

[40] which would not be practically trivial for the $3D$ beam in uniform compression

1.8 Pressurized Sphere

Sofar, all examples in this Chapter have dealt with stability related to geometric non-linearities, assuming a linear elastic material description. The present case deals with a non-linear material model.

A thin spherical membrane, of unstretched radius R and thickness h, is subjected to an interior over-pressure p, Fig. 1.18. The material follows a two-parameter incompressible Mooney-Rivlin material model, with two constitutive parameters (c_1, c_2), and defining $k = \frac{c_2}{c_1}$. It is formulated from the two first invariants of the Green deformation tensor C, cf. Sects. 2.3 and 2.4.2.

The problem is one-dimensional in the sense that the primary response is a uniform spherical expansion, described by the current radius r. This will give an equi-biaxial strain state, where $C_{11} = C_{22} = \left(\frac{r}{R}\right)^2$, and $C_{33} = \left(\frac{R}{r}\right)^4$ from the incompressibility; all shear strains vanish. From this, and the (local) plane stress condition, the components of the relevant 2nd Piola-Kirchhoff stress tensor S are

$$S_{11} = S_{22} = 2c_1 \left(1 - \frac{1}{C_{11}^3}\right)(1 + kC_{11})\,; \tag{1.57}$$

The stress approaches an asymptote $S_{11} = 2c_1(1 + kC_{11})$ for increasing C_{11} and can therefore even reach a maximum value, if $k < 0$.

The stress is related to interior over-pressure through

$$\pi r^2 p = 2\pi r h S_{11} \tag{1.58}$$

where it is noted that the used stress tensor is related to initial geometry, when the over-pressure p is a conservative but not displacement-independent forcing, cf. Sect. 2.6.3. Some algebra shows that the over-pressure is related to the radius by

$$\frac{p}{c_1}\frac{R}{h} = 4\frac{\left(1 + k\lambda^2\right)\left(\lambda^6 - 1\right)}{\lambda^7} \tag{1.59}$$

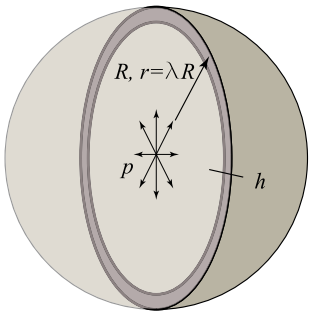

Fig. 1.18 Pressurized spherical membrane. R and r refer to mid-surface

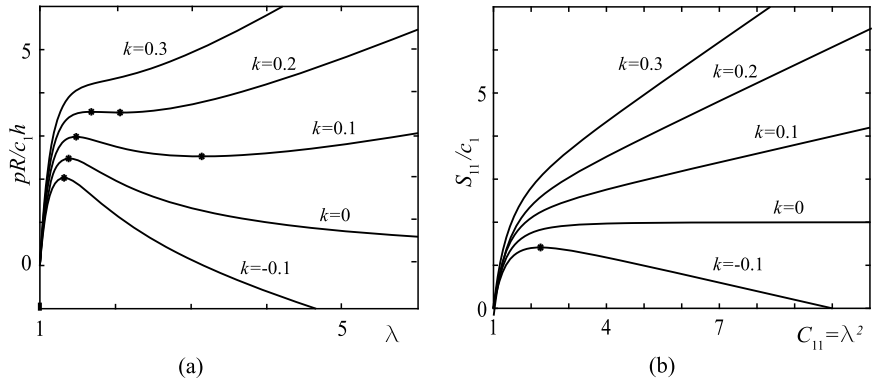

Fig. 1.19 Radial expansion of pressurized spherical membrane. **a** Over-pressure p. **b** Stress S_{11}, normalized to geometry and material parameters. Note the different horizontal axis labels

where the circumferential stretch $\lambda = \frac{r}{R}$ is introduced.[41]

Results from the above expressions are shown by Fig. 1.19 for a few different values of the ratio parameter k. Subfigure (a) shows that, depending on the value for k, zero, one or two limit pressure states can exist in the response, as marked in the figure. The situation of a maximum pressure being passed in the process is easily identified from the inflation of toy balloons.[42] More sophisticated analysis methods can reveal at exactly which value of k the limit state disappears, cf. the treatise by Eriksson and Nordmark (2020). Further analyses also show that a bifurcation into a non-spherical mode can exist for this problem.

Figure 1.19b shows that the stress approaches the asymptotic linear relation following from Eq. (1.57), with, e.g., $S_{11} = 2c_1$ for $k = 0$. The stress also eventually becomes negative when $k < 0$, which is a failure of the sphere. The marked maximum value for stress does obviously not correspond to the maximum pressure state shown in subfigure (a).

1.9 Spinning Rigid Object

The examples above have all referred to the stability of static equilibrium cases, but stability can also be of importance for dynamically moving structures. A simple example will be given, even if the treatment of such problems is not the main topic of the present treatise.

[41] The pressure-stretch relation is most easily derived from a formulation of the total potential for the system, cf. Sect. 2.6.5.

[42] Even if more air must be introduced, the resistance is reduced after a while.

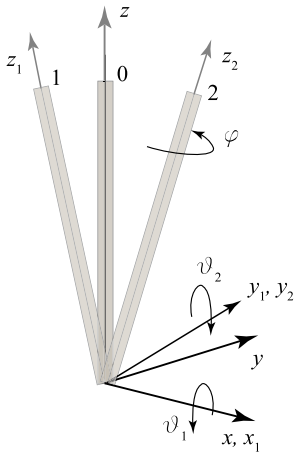

Fig. 1.20 Rigid spinning link, with successive configurations from rotation description

The example has some similarities to the problem in Sect. 1.2, and consists of a rigid link spinning freely around a ball joint at the lower end, Fig. 1.20. The link has an axi-symmetrically distributed mass, which is represented by a summed mass m at a distance L from the hinge, and gives mass moments of inertia quantified by J_1 and J_3 around any arbitrary axis in the horizontal plane, and the link axis, respectively.

The position of the free end is described by two Euler angles describing the orientation of the link, compared to the vertical: first an angle ϑ_1 around the x axis and then ϑ_2 around the new orientation $\mathbf{y}_1$ of the original y axis; the figure schematically shows the successive configurations 0, 1, 2 and the axes appearing after the rotation steps. An angle φ then describes the spinning motion of the link around its own inclined axis. The fundamental stability question is if the link can balance in an essentially vertical position, stabilized by its rotation.

From the position of the end point

$$x = L \sin \vartheta_2, \quad y = -L \sin \vartheta_1 \cos \vartheta_2, \quad z = L \cos \vartheta_1 \cos \vartheta_2, \tag{1.60}$$

a Lagrangian[43] is formulated from the difference between kinetic and potential energy, as

$$L = \frac{J_1}{2} \left(\cos^2 \vartheta_2 \dot{\vartheta}_1^2 + \dot{\vartheta}_2^2 \right) + \frac{J_3}{2} \left(\sin \vartheta_2 \dot{\vartheta}_1 + \dot{\varphi} \right)^2 - mgL \cos \vartheta_1 \cos \vartheta_2 \tag{1.61}$$

where the superposed dot represents a time differentiation of the quantity.

As the rotation variable φ is a cyclic variable, it is possible to introduce a constant for the angular momentum

[43] which can be used to derive the dynamic response

$$p_\varphi = \frac{\partial L}{\partial \dot{\varphi}} = J_3 \left(\sin \vartheta_2 \dot{\vartheta}_1 + \dot{\varphi} \right). \tag{1.62}$$

By removing the spinning velocity $\dot{\varphi}$, the constant is introduced to reduce the Lagrangian to

$$L_1 = L - p_\varphi \dot{\varphi} = \frac{J_1}{2} \left(\cos^2 \vartheta_2 \dot{\vartheta}_1^2 + \dot{\vartheta}_2^2 \right) + p_\varphi \sin \vartheta_2 \dot{\vartheta}_1 - \frac{p_\varphi^2}{2J_3} - mgL \cos \vartheta_1 \cos \vartheta_2. \tag{1.63}$$

From this function, the dynamic response is decided by the Lagrange equations for the two position variables

$$\begin{aligned} \frac{\mathrm{d}}{\mathrm{d}t} \left(\frac{\partial L_1}{\partial \dot{\vartheta}_1} \right) - \frac{\partial L_1}{\partial \vartheta_1} &= J_1 \cos^2 \vartheta_2 \ddot{\vartheta}_1 - 2J_1 \sin \vartheta_2 \cos \vartheta_2 \dot{\vartheta}_1 \dot{\vartheta}_2 \\ &\quad + p_\varphi \cos \vartheta_2 \dot{\vartheta}_2 - mgL \sin \vartheta_1 \cos \vartheta_2 = 0, \\ \frac{\mathrm{d}}{\mathrm{d}t} \left(\frac{\partial L_1}{\partial \dot{\vartheta}_2} \right) - \frac{\partial L_1}{\partial \vartheta_2} &= J_1 \ddot{\vartheta}_2 + J_1 \sin \vartheta_2 \cos \vartheta_2 \dot{\vartheta}_1^2 \\ &\quad - p_\varphi \cos \vartheta_2 \dot{\vartheta}_1 - mgL \cos \vartheta_1 \sin \vartheta_2 = 0, \end{aligned} \tag{1.64}$$

which is a basis for tracing a movement from an assumed initial state.

The stability question posed is answered by a linearization of the equations of motion around the relative equilibrium with

$$\vartheta_1(t) = 0, \quad \vartheta_2(t) = 0, \quad p_\varphi = J_3 \, \omega. \tag{1.65}$$

This gives the equations of motion, in matrix form, as

$$J_1 \begin{pmatrix} 1 & 0 \\ 0 & 1 \end{pmatrix} \begin{pmatrix} \ddot{\vartheta}_1 \\ \ddot{\vartheta}_2 \end{pmatrix} + p_\varphi \begin{pmatrix} 0 & 1 \\ -1 & 0 \end{pmatrix} \begin{pmatrix} \dot{\vartheta}_1 \\ \dot{\vartheta}_2 \end{pmatrix} - mgL \begin{pmatrix} 1 & 0 \\ 0 & 1 \end{pmatrix} \begin{pmatrix} \vartheta_1 \\ \vartheta_2 \end{pmatrix} = \begin{pmatrix} 0 \\ 0 \end{pmatrix}, \tag{1.66}$$

or in common notation for discretized structural dynamics

$$\underline{\underline{M}} \, \underline{\ddot{d}} + \underline{\underline{C}} \, \underline{\dot{d}} + \underline{\underline{K}} \, \underline{d} = \underline{0}, \quad \underline{d} = \begin{pmatrix} \vartheta_1 \\ \vartheta_2 \end{pmatrix} \tag{1.67}$$

with mass and stiffness matrices $\underline{\underline{M}}$ and $\underline{\underline{K}}$ symmetric, but with an antisymmetric matrix $\underline{\underline{C}}$ replacing the damping matrix. Although the mass matrix still represents inertia, the matrix resembling stiffness is here notably negative definite, as it reflects the gravity force trying to make the link fall; it is thereby de-stabilizing. The matrix $\underline{\underline{C}}$ also deviates from the common situation, as it is not dissipating energy, due to its antisymmetry[44]; it is in this case potentially stabilizing.

[44] with zeroes on the main diagonal

An ansatz is made for the dynamic motion from a configuration $\underline{d}_0$, which is a deviation from the vertical equilibrium, as

$$\underline{d}(t) = e^{\lambda t}\underline{d}_0, \tag{1.68}$$

whence stability in the movement then demands that all four eigenvalues, which are evaluated from the fourth order polynomial of the characteristic equation

$$\det\left(\lambda^2\underline{\underline{M}} + \lambda\underline{\underline{C}} + \underline{\underline{K}}\right) = 0, \tag{1.69}$$

have non-positive real parts, so that the initial deviation is non-increasing with time. Solving the eigenvalue problem shows that this demands that the magnitude of the angular velocity ω fulfils

$$|\omega| > 2\frac{\sqrt{J_1 mgL}}{J_3}. \tag{1.70}$$

The conclusion from the analysis is that the spinning link is stable in a vertical configuration—where the potential energy is now a maximum—if it is spinning with a high enough angular velocity around its axis.

It should be obvious from this very simple example that stability of dynamic motions can lead to many types of responses and analyses. As these problems are outside the main scope of the present treatise, they will only be briefly mentioned in Sect. 2.9.2.

Conclusions from this Chapter

One conclusion from this Chapter is that stability issues are common in many engineering branches, and that they are often fundamentally important for the response of the structure in its operational context. Another conclusion is that the used viewpoints on structural stability evaluations are manifold, and based on very different approaches and contexts. All of these approaches, more or less clearly, see the existence of unstable equilibria as unexpected deviations from the intended primary function of the structure or component. This can mean that a structure loses its carrying capacity at a limit state, from which forcing must be reduced in order to avoid failure. The stability can also be lost in connection with a bifurcation state, where the response mode changes, and alternative equilibrium sequences appear.

Even if loss of stability is often considered as catastrophic for the structure, the secondary response aspects demand more complex[45] analysis models than the commonly used ones. These aspects often include some form of non-linearity in the description of structural response, and in the analysis models. With this increased

[45] where the word is used to denote wider, not necessarily more difficult

complexity in the formulation, secondary equilibrium configurations may exist and be fully functional, albeit often at the expense of rather large deformations.

The methods described in this Chapter are based on three different viewpoints on stability. These are related to the existence of a deflected equilibrium, the minimum of the potential or the existence of vibration frequencies. These viewpoints will in the following Chapters be brought together, and will be shown to be different views on the same fundamental situation. The understanding of the relation between these viewpoints is of major importance for more systematic analyses of the stability of structural response.

An important conclusion from this Chapter is related to the parametric view on the considered structural model. Common engineering approaches always tend to consider the magnitude of forcing as the only parameter, and see loss of stability as a critical value for this. A more expanded view on stability in a parameter space will be further utilized in coming Chapters, and give further information on stability and its sensitivity to assumptions and parameters, which is. for instance, necessary when structural optimization is attempted.

Tasks for this Chapter

1. Study the same problem as in Sect. 1.2, but with the translational stiffness k in Fig. 1.1 replaced by a rotational spring of stiffness c (with typical unit Nm/rad.) resisting the inclination angle at the lower end. Evaluate the critical force F_{cr}, and the secondary response. Consider whether there are several models also here.
2. Each of the columns number 3–7 in the example in Fig. 1.9 can be expressed as a matrix operating on the previous column, and thereby the whole transformation of y_{guess} to y_{res} as a matrix product. First, find all these matrices and their product. Second, use this matrix to perform several iterations to improve the estimate for the buckling force. Third, re-formulate the matrices to the case with the length divided into $L/16$, using the systematic contents. Fourth, formulate another beam buckling problem along the same ideas.
3. In a software which offers 'second order' beam analysis: study a vertical beam of chosen section—as a plane case—when subjected to a transversal force intensity of fixed, rather small, magnitude and a variable compressive force. Test a number of cases and study the shortening and some measure of transversal deflection as functions of the compressive force. It may be a good start to first evaluate the Euler buckling force for the column, in order to get some feeling for the magnitude of interesting compressive forces.
4. Evaluate the critical buckling stress for an ideally elastic thin plate affected by pure shear along the same lines as for the normal stress in Sect. 1.4. Neglect the difficulties in practically arranging this, and assume that the shear stress resultants $n_{xy} = n_{yx}$ are constant over a rectangle with side lengths a and $b = 2a$.

5. Formulate the problem in Sect. 1.2 with consideration of the changing length of the link, i.e., by adding the term from Eq. (1.2) into Eq. (1.7). Pick a few different ratios for (EA/kL), and evaluate the response. Note that this model must be described by two displacement components. Show what happens to the bifurcation if $EA \neq \infty$.

References

Bertoldi K (2017) Harnessing instabilities to design tunable architected cellular materials. Ann Rev Mater Rese 47

Champneys AR, Dodwell TJ, Groh RMJ, Hunt GW, Neville RM, Pirrera A, Sakhaei AH, Schenk M, Wadee MA (2019) Happy catastrophe: recent progress in analysis and exploitation of elastic instability. Frontiers Appl Math Stat 5

Como M, Grimaldi A (1995) Theory of stability of continuous elastic structures. CRC Press, Boca Raton, FL

Eriksson A, Nordmark A (2019) Constrained stability of conservative static equilibrium. Comput Mech 64(4):1199–1219

Eriksson A, Nordmark A (2020) Computational stability investigations for a highly symmetric system: the pressurized spherical membrane. Comput Mech 66(2):405–430

Ghali A, Neville A, Brown T (2003) Structural analysis. A unified classical and matrix approach, 5th edn. Spon Press, London, New York

Godoy L (2000) Theory of elastic stability: analysis and sensitivity. Taylor & Francis

Liapunov AM (1966) Stability of motion. (Mathematics in science and engineering, Volume 30). Academic Press, New York/London (translated from Russian Doctoral dissertation, Univ. Kharkov 1892)

Reis PM (2015) A perspective on the revival of structural (in)stability with novel opportunities for function: from Buckliphobia to Buckliphilia. J Appl Mech Trans ASME 82:11

Timoshenko SP, Gere JM (1961) Theory of elastic stability, 2nd edn. McGraw-Hill, New York

Chapter 2
Underlying Theories

This Chapter discusses the necessary theoretical background for more systematic treatment of structural stability, and has a focus on the relations between kinematics, kinetics and energy. These aspects are considered in a sufficiently wide context for the subsequent computations, and are consistently based on a displacement form. The treatment is primarily aimed at the approach common in commercial software for structural analysis, i.e., a Lagrangian reference frame, the Green-Lagrange strain and the 2nd Piola-Kirchhoff stress, which give a consistent view when used with the initial structural volume. Full continuum formulation is used in this Chapter, but the presentation is aimed at the discretized formulations in the next Chapter. The setting of an engineering problem in relation to a general continuum is discussed. As stability issues are most relevant for thin structures, the dimensional reduction from the $3D$ continuum to $1D$ and $2D$ analysis models is considered. For systematic stability investigations based on the Liapunov criterion, the formulation of a strain energy density in the structural model is a key quantity, together with an almost trivial kinetic energy; these constitute the basis for the stability criteria used, and the effects from exterior forcing.

Brief objective of this Chapter

The Chapter discusses kinematic, kinetic and energy concepts needed for the definition of stability in a $3D$ continuum setting, aiming at discretized numerical models for systematic stability investigations in engineering structures.

A. Eriksson and A. Nordmark, *Structural Stability and Its Computational Modelling*, Computational Methods in Engineering & the Sciences,
https://doi.org/10.1007/978-3-031-36072-5_2

2.1 Reference Frame

The previous Chapter describes several cases of engineering stability investigations. These show that the stability evaluations need more complex formulations than the linear analyses, as new aspects come into action. These are always, more or less clearly, connected to displacement in the structure, and very often to secondary directions of movement. Rather than following the basic engineering approach where exterior forcing is the source of all response, with stress in the components as main result, systematic stability investigations demand descriptions of the displacement field in the model used.

This Chapter begins with a brief discussion of continuum mechanics. The assumption for this is that a sufficiently macroscopic view can be used for the mechanics of a structure, in essence averaging the microscopic, atomic events to a scale relevant for the structural model. The presentation is also aiming at the discretized settings used in the next Chapter. For wider and deeper descriptions of other aspects of continuum mechanics, the reader is referred to the vast literature available, e.g., the books by Malvern (1969) or Gurtin (1982). The notation from the excellent book by Holzapfel (2000) is almost completely adopted here.

The presentation in this Chapter uses a Lagrangian formulation, as this is almost exclusively used in structural mechanics software. The implementation of this term is not absolutely unique,[1] but is always based on a material reference state: an unstrained geometry of the structure. All quantities are referred to this reference configuration, implying for instance that integrated quantities are evaluated over the defined geometry, not the deformed one. This also has effects on, e.g., the stress quantities calculated, which are expressed as force per initial area. This form is also the most tractable one, when a complex structure is to be defined.

The term unstrained geometry needs some discussion, as this is not necessarily the same as an unloaded configuration. A counter-example is a balloon, which might be unstrained for a spherical shape of some radius, but takes another shape when not pressurized.[2] The continuum macroscopic approach also assumes a continuity of material within the defined reference configuration.

The time dimension is a key aspect in all treatments of mechanics. In the present treatise, the symbol t always refers to a physical time, with time $t = 0$ connected to the reference state, and increasing time to a changing configuration. All problems can thereby be treated as dynamic, and a time-dependent motion sought for a prescribed time variation of exterior forcing, given the initial conditions for the model. A special case is when the forcing is constant over time, and the structure is assumed to be stationary for this forcing. If the structure is resting at this state, no dynamic effects are present and the structural model is defined to be in an equilibrium state, which can be solved. Equilibrium may also be an asymptotic state, in which a constantly forced structure eventually comes to rest, due to the always present damping. As

[1] as it allows both so called Total Lagrangian and Co-rotational discretized forms

[2] as the small self-weight introduces some small strain in an equilibrium before the forcing is introduced

further elaborated below, the distinction between motion and equilibrium refers to the physical model considered, but solution methods can also be classified as belonging to either class.

With assumptions and solution methods clearly defined for the two situations, a term quasi-static equilibrium is sometimes used, but with different meanings. One interpretation of the term is a dynamic solution for a time-dependent forcing, but found through neglecting the dynamic terms of the governing equations.[3] The time is then just a parametric description of the forcing, and the solution a sequence of equilibrium configurations. Here, a pseudo-time τ is introduced for this parametric equilibrium setting, where τ is just a measure for the progress along a result graph. This setting is generalized, and used as the basis for the treatment of solution methods in Chap. 4.

The expressions formulated below are always referred to a Euclidean system, i.e., a time-independent Cartesian coordinate system, where the mutually orthogonal unit vectors $(\mathbf{e}_1, \mathbf{e}_2, \mathbf{e}_3)$ form a right-hand system at a fixed origin. This means that the distinction between covariant and contravariant components is of no interest, and the metric trivial. A physical vector is in this Chapter always of dimension 3-by-1, containing the components in the Cartesian coordinate directions. This also implies that the second-order tensor quantities below are always represented by 3-by-3 matrices. Physical vectors are here denoted by bold letters, $\mathbf{x}$, while matrices representing tensors are denoted by a sans serif font, E.

While Chap. 1 uses a common simplified engineering notation, a systematic and more formalized notation for all mechanical quantities is used from this Chapter onwards.

2.2 Kinematics

In order to obtain the necessary quantities in a continuum formulation of a structure, a description of kinematics is needed for the movement of each point.[4] For the present applications—without cracking or other discontinuities—a point can be uniquely labelled by its coordinates in the reference configuration, which implies that functional descriptions are intended with point $\mathbf{X}$ as argument.

Figure 2.1 shows that an arbitrary point of coordinate $\mathbf{X}$ in the reference configuration $t = 0$ appears at the point $\mathbf{x}(t)$ in the current configuration, at time t. Similar drawings could be made for any point $\mathbf{X}$. For fixed t, this description gives information on the current configuration, and the complete movement up to this configuration is described as a function of t. The displacement field describes similarly the displacement of every point $\mathbf{X}$ within a region Ω, and thereby defines the whole situation also at time t, when referred to its reference configuration.

[3] This may be a more or less realistic assumption of 'slow' time scales in the forcing

[4] where a point denotes a differential amount of material, suitably averaged from the microscopic scale

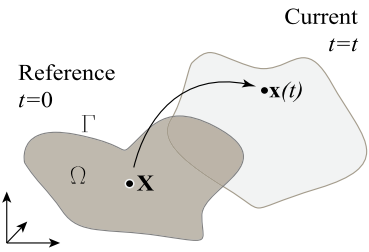

Fig. 2.1 Displacement of one material point **X** in reference configuration to its position $\mathbf{x}(t)$ in the current. Ω is the considered region, with Γ its boundary

The current position of the point—in the same coordinate system—is thereby a function of its reference coordinates, according to

$$\mathbf{x} = \mathbf{x}(\mathbf{X}, t), \tag{2.1}$$

where the definition implies that $\mathbf{x}(\mathbf{X}, 0) = \mathbf{X}$.

As comments to Fig. 2.1 and the expressions, it is noted that upper-case symbols are consistently used to denote quantities related to the reference configuration, and lower-case ones for the current. It is also noted that the coordinates are position vectors with $\mathbf{X} = (X_1, X_2, X_3)^{\mathrm{T}}$ (or, very commonly, $\mathbf{X} = (X, Y, Z)^{\mathrm{T}}$), and $\mathbf{x} = (x_1, x_2, x_3)^{\mathrm{T}}$ (or $\mathbf{x} = (x, y, z)^{\mathrm{T}}$). The index notation is used in the sequel.

The mechanics developed below can be formulated in terms of current positions **x**, but for compatibility with small displacement theory, it is natural to define the displacement. From Fig. 2.1, this is the movement a point has undergone up to time t, as the difference between its current and reference positions. A point-wise displacement vector

$$\mathbf{U}(\mathbf{X}, t) = \mathbf{x}(\mathbf{X}, t) - \mathbf{X} \tag{2.2}$$

is written as a function of the reference position **X**, with $\mathbf{U} = (U_1, U_2, U_3)^{\mathrm{T}}$ (or $\mathbf{U} = (U, V, W)^{\mathrm{T}}$, or $\mathbf{U} = (u, v, w)^{\mathrm{T}}$). Without argument, **U** is used to describe the whole displacement field over the considered region. At a specific t, it does not say anything about the route taken, but the notion of **U** as a function of time t implies that the movement path from the reference to the current position of any point **X** is traced, and the current velocity $\dot{\mathbf{x}}$ of the point calculable as

$$\dot{\mathbf{x}} = \frac{\partial \mathbf{x}}{\partial t} \tag{2.3}$$

for fixed material point **X**. For the considered region, the velocity field gives the velocities of all points **X**. Similarly, the acceleration field can be obtained from one further time differentiation.

2.3 Deformation and Strain

Even if the displacement field **U**, including all points **X** in the reference configuration, can collectively be denoted a deformation of the considered structure, this term is here specialized to refer to the change of shape. In particular, deformation refers to the change of a differential volume element around the point **X**, i.e., a local quantity.

Figure 2.2 schematically shows how the neighbourhood of a point **X** in the reference configuration is changed into its shape around the point **x** in the current configuration. The arbitrary differential vector d**X** emanating at **X** is thereby mapped to d**x** at **x** valid at time t. The figure indicates that the region around the point **X** in general is subjected to stretching, shearing, translation and rotation.

Based on the continuity, the local relation between the two vectors can be written

$$\mathrm{d}\mathbf{x} = \mathsf{F}\,\mathrm{d}\mathbf{X}, \tag{2.4}$$

where the components of F are

$$F_{ij} = \frac{\partial x_i}{\partial X_j}, \tag{2.5}$$

and vary with **X**.

The operator F is the deformation gradient tensor, from $\mathsf{F} = \mathrm{grad}_X\,\mathbf{x}$, with respect to reference coordinates **X**, and defines the relation between the vectors d**x** and d**X**. This matrix is obviously of dimension 3-by-3, and is, in general, unsymmetric. Using Eq. (2.2) to obtain $\mathsf{F} = \mathrm{grad}_X(\mathbf{X} + \mathbf{U})$, the components of F are also obtained as

$$F_{ij} = \frac{\partial U_i}{\partial X_j} + \delta_{ij}, \tag{2.6}$$

with δ_{ij} the Kronecker delta operator.[5]

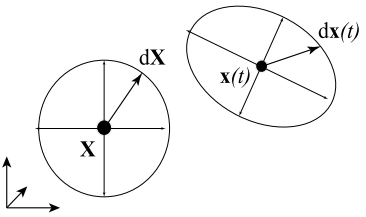

Fig. 2.2 Deformation of surroundings to point in the reference configuration to the current, cf. Fig. 2.1

[5] which is $= 1$ for $i = j$, zero otherwise. Here, it just adds a $+1$ to the diagonal components of $\mathrm{grad}_X\,\mathbf{U}$

From the, at least in principle, measurable displacement quantities within the structure, the continued treatment demands quantifiable measures for the interior effects. Several measures for the deformation are introduced in different contexts.

The perhaps most obvious effect from the vector $\mathrm{d}\mathbf{X}$ being mapped to $\mathrm{d}\mathbf{x}$ in Fig. 2.2 is that it may change its length. With the Euclidean norm as length measure in the used coordinate system, the local stretch of a vector $\mathrm{d}\mathbf{X}$ at point $\mathbf{X}$ is written as

$$\Lambda(\mathrm{d}\mathbf{X}) = \frac{\| \mathrm{d}\mathbf{x} \|}{\| \mathrm{d}\mathbf{X} \|} \approx \frac{\| \mathsf{F}\, \mathrm{d}\mathbf{X} \|}{\| \mathrm{d}\mathbf{X} \|}, \tag{2.7}$$

where a first-order approximation to the change of length is the commonly used expression for stretch; it is dependent on the choice of a particular $\mathrm{d}\mathbf{X}$.

The deformation gradient F has a major role in describing transformations between the reference and current states. One particular aspect of this is described by the Jacobian determinant of the deformation gradient

$$J = \det(\mathsf{F}) \tag{2.8}$$

which describes how a differential volume in the reference state $\mathrm{d}V = \mathrm{d}X_1\, \mathrm{d}X_2\, \mathrm{d}X_3$ at point $\mathbf{X}$ is magnified into its current volume $\mathrm{d}v = \mathrm{d}x_1\, \mathrm{d}x_2\, \mathrm{d}x_3$. The Jacobian determinant thereby becomes a scaling factor in several integrated quantities.[6]

Mechanical effects of the deformation gradient are shown by a polar decomposition

$$\mathsf{F} = \boldsymbol{\Theta} \mathsf{F}' \tag{2.9}$$

where $\boldsymbol{\Theta}$ is a local orthogonal rotation matrix, F' is a symmetric positive definite matrix, and the latter describes the change of shape of a small volume around a point $\mathbf{X}$. The simple example in Fig. 2.3 shows how a deformation gradient tensor

$$\mathsf{F} = \begin{pmatrix} 0.78 & -0.24 & 0 \\ 0.96 & 0.82 & 0 \\ 0 & 0 & 1 \end{pmatrix} = \begin{pmatrix} 0.8 & -0.6 & 0 \\ 0.6 & 0.8 & 0 \\ 0 & 0 & 1 \end{pmatrix} \begin{pmatrix} 1.2 & 0.3 & 0 \\ 0.3 & 0.8 & 0 \\ 0 & 0 & 1 \end{pmatrix}, \tag{2.10}$$

operating on the initial unit square, is split into a re-scaling and shearing, followed by a rigid rotation in the plane.[7]

The tensor $\mathbf{F}'$ contains all the essential information on the deformation of the material at the considered point, and would give a very convenient strain measure as

$$\mathsf{E}' = \mathsf{F}' - \mathsf{1}, \tag{2.11}$$

[6] This Jacobian term should not be confused with the Jacobian matrix appearing in the treatment of non-linear sets of equations in Chap. 4

[7] as a second transformation, i.e., written in front of the shape-changing operation

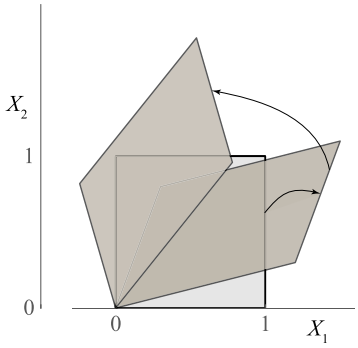

Fig. 2.3 Polar decomposition of deformation gradient tensor into deformation (re-scaling and shearing) and rotation. Arrows indicate the successive steps as in Eq. (2.9)

with $\mathsf{1}$ the identity tensor, which compares the deformed configuration to the undeformed.[8] Even if F' is formally obtained as $\mathsf{F}' = \sqrt{\mathsf{F}^{\mathrm{T}}\mathsf{F}}$, the evaluation is demanding the solution of a high order polynomial equation, or a non-linear set of equations.

When used as measure for the deformation at a point, the principal stretches $(\Lambda_1, \Lambda_2, \Lambda_3)$, which are the eigenvalues of $\mathbf{F}'$, are most commonly used. As physical lengths are the basis, stretch must always be strictly positive, $\Lambda_i > 0$. The Λ values, however, say nothing about the direction of the stretches.

Not least for computational convenience, other measures of deformation are more common. The deformation of any small line element $\mathrm{d}\mathbf{X}$ emanating at the point $\mathbf{X}$ can also be quantified by the square of the stretches, according to

$$\Lambda^2(\mathrm{d}\mathbf{X}) = \frac{\| \mathrm{d}\mathbf{x} \|^2}{\| \mathrm{d}\mathbf{X} \|^2} = \frac{\mathrm{d}\mathbf{X}^{\mathrm{T}} \, (\mathsf{F}^{\mathrm{T}}\mathsf{F}) \, \mathrm{d}\mathbf{X}}{\| \mathrm{d}\mathbf{X} \|^2} \tag{2.12}$$

where the tensor product in the numerator is the Green deformation tensor

$$\mathsf{C} = \mathsf{F}^{\mathrm{T}}\mathsf{F} \tag{2.13}$$

at a specific point and time. The components of C are derived from the components of F as, with the summation convention for repeated indices,

$$C_{ij} = F_{ki} \, F_{kj}, \tag{2.14}$$

This matrix is symmetric, and can always be expressed from the equations above through Eq. (2.6). It has eigenvalues being the squares of those of F', i.e., it is always positive definite. For any rigid translation of the object,[9] F, F' and C give unit

[8] with zero representing no deformation

[9] with no translation as a special case

matrices, while for a rigid rotation—or an arbitrary combination of rigid rotations and translations—F is represented by an orthogonal matrix, while F' and C remain unit matrices. The choice of C as deformation measure is a compromise between the accurate strain measure in F' and the algebraic convenience of C.

The above deformation descriptions through F' or C express the deformation through scaling measures, where identity represents no deformation. Due to the orthogonality of $\boldsymbol{\Theta}$, Eqs. (2.9) and (2.13) show that the Green deformation can also be written[10] $\mathsf{C} = \mathsf{F}'\,\mathsf{F}'$. Equation (2.11) then gives, noting the symmetry of F' and E', that

$$\mathsf{C} = (\mathsf{E}' + \mathsf{1})(\mathsf{E}' + \mathsf{1}) = \mathsf{1} + 2\mathsf{E}' + \mathsf{E}'\,\mathsf{E}'. \tag{2.15}$$

The commonly used Green-Lagrange deformation

$$\mathsf{E} = \frac{1}{2}\left(\mathsf{F}^{\mathrm{T}}\mathsf{F} - \mathsf{1}\right) = \frac{1}{2}\left(\mathsf{C} - \mathsf{1}\right) \tag{2.16}$$

agrees to first order with the E' tensor above. It is thereby a relevant measure for the local deformation, with the interpretation that a zero tensor is no deformation.

The components of E are obtained from Eq. (2.14) as

$$E_{ij} = \frac{1}{2}\left(F_{ki}\,F_{kj} - \delta_{ij}\right), \tag{2.17}$$

from which two sample components are

$$\begin{aligned} E_{11} &= \frac{1}{2}\left(2\frac{\partial U_1}{\partial X_1} + \left(\frac{\partial U_1}{\partial X_1}\right)^2 + \left(\frac{\partial U_2}{\partial X_1}\right)^2 + \left(\frac{\partial U_3}{\partial X_1}\right)^2\right), \\ E_{12} = E_{21} &= \frac{1}{2}\left(\frac{\partial U_1}{\partial X_2} + \frac{\partial U_2}{\partial X_1} + \frac{\partial U_1}{\partial X_1}\frac{\partial U_1}{\partial X_2} + \frac{\partial U_2}{\partial X_1}\frac{\partial U_2}{\partial X_2} + \frac{\partial U_3}{\partial X_1}\frac{\partial U_3}{\partial X_2}\right). \end{aligned} \tag{2.18}$$

The first and the two first terms, respectively, are the common linear strain expressions.[11] The shallow beam bending[12] expressions are also recognized in E_{11}, which in common engineering notation is $\varepsilon_x = \frac{\mathrm{d}u}{\mathrm{d}x} + \frac{1}{2}\left(\frac{\mathrm{d}w}{\mathrm{d}x}\right)^2$, with some disregarded quadratic terms. Selective inclusion of terms from the full tensor has effects on the resulting expressions, like the missing coupling in Sect. 1.4.

From Eq. (2.16), it is obvious that E shares principal directions, i.e., eigenvectors with C. The eigenvalues of E are, however, not necessarily positive. The tensor is easily evaluated, as the discretized setting discussed in Chap. 3 is normally based on a description of the point-wise displacement. Using Eq. (2.17), the components

[10] as F' is symmetric

[11] noting that both the equal E_{12} and E_{21} are parts of the shear deformation, often denoted γ_{12} in the $(\mathbf{e}_1, \mathbf{e}_2)$ plane

[12] or the theory of moderate deflection beam bending

of E are then immediately evaluated. If requested, the components of C follow. The principal values of C, and the corresponding directions, are obtained from a small eigenvalue problem.

2.4 Strain Energy

The deformation measures discussed above can serve as main quantities in mechanical formulations. In order for them to do so, the defining descriptions of the constituent material must be based on experiments, where the same measures are used as parameters. The connection between experimental setups and simulations is often the strain energy stored in a structure, as this can be equated to the mechanical work performed by exterior forcing in the clear-cut testing situation.

The strain energy in the deformed structure is thereby a key quantity in analyses. The total strain energy Π_p in the current configuration of a structure is evaluated as an integral over the whole structural reference volume Ω, as

$$\Pi_p = \int_\Omega \pi_p \, \mathrm{d}V \tag{2.19}$$

where the energy density π_p is a point-wise scalar quantity. With the above deformation quantities, strain energy density can (with a slight abuse of notation) be expressed as

$$\pi_p \equiv \pi_C(\mathsf{C}) \equiv \pi_E(\mathsf{E}), \tag{2.20}$$

where arguments emphasize that either of the deformation measures are used. One requirement on the strain energy density is that it is non-negative, with zero value only when the point and its surrounding is at the reference state or any rigidly displaced version of this. A set of constitutive constants is implicitly considered in the forms; these are denoted $\underline{\Xi}$ below. These parameters, and even the strain density function itself, may vary with $\mathbf{X}$. Often this is related to subregions of the whole structure, cf. Sect. 2.5.

A few different constitutive equations for hyper-elastic materials are discussed below, but many more are used in literature. No complete review is given here, but an interesting approach to material modelling is given by Crespo et al. (2017). Models for biological materials are given by Fung (1993) and Holzapfel et al. (2000).

2.4.1 Stress

A strain energy density for the strained material is here the defining constitutive relation. When defining the strain energy density, a stress measure follows automatically from the requirement that stress, i.e., an expression for interior force must be a conjugated quantity to the used deformation measure.

Of particular interest in the present applications to stability of elastic structures—where continuity in the material deformation is assumed—is to express the stress as a 2nd Piola-Kirchhoff stress, described by the tensor or matrix S. This stress can be obtained in a straight-forward manner from the strain energy density expressions as either of the two forms

$$\mathsf{S} = 2\frac{\mathrm{d}\pi_C(\mathsf{C})}{\mathrm{d}\mathsf{C}} \quad \text{or} \quad \mathsf{S} = \frac{\mathrm{d}\pi_E(\mathsf{E})}{\mathrm{d}\mathsf{E}}. \tag{2.21}$$

The derivatives of the strain energy density expressions are evaluated formally with respect to the components of the respective deformation tensor.

The main argument for using the 2nd Piola-Kirchhoff stress tensor as local force intensity measure in computations is that this stress is energy conjugate to the deformation tensors C and E, which were in Sect. 2.3 argued to be convenient in computations; this defines a natural connection between these tensors. The symmetry properties of C and E, as well as of S, are also favorable for the numerical treatment.

From the viewpoint introduced, stress comes out as a consequence of the constitutive material description, rather than as the quantities causing the interior behaviour of the material. In several formulations of the mechanical problem, the stress under forcing is not even interesting except in the introduction of boundary traction on the structure, cf. Sect. 2.5.2. Whichever view is adopted, the 2nd Piola-Kirchhoff stress components are measured as force per unit of reference configuration area. The force intensities are also given in relation to initial coordinate directions, even if the geometry is extensively deformed by the forcing. For many—but, definitely not all—common engineering settings, this stress measure is also easily related to the methods used for description of exterior forcing, one reason being the relation to initial, undeformed geometry.

With the approach in Eq. (2.21), the stress components have another notation than in large parts of engineering literature. According to Fig. 2.4, the stress components have as their first index the direction of force, and as second the plane they are acting on[13]; other conventions are used in many engineering treatises. The figure shows the stress components acting on an $(\mathbf{e}_1, \mathbf{e}_2)$ plane section of the continuum, and the stress components are represented as arrows at the mid-sides of the area. It is well-known that shear stress components must be pair-wise equal, e.g., $S_{21} = S_{12}$, or the volume is not in moment equilibrium; S is therefore symmetric. This also implies a need for a certain symmetry of π_p.

Other stress measures, like the Cauchy stress tensor σ—by definition given as force per unit of deformed area[14]—are related to other measures of strain, but can always be evaluated from a transformation of the components of S, as the two stress tensors at a point are related by

$$\mathsf{S} = J\,\mathsf{F}^{-1}\sigma\,\mathsf{F}^{-\mathrm{T}}. \tag{2.22}$$

[13] with the plane defined by its normal direction

[14] Cauchy stress is by Nguyen (2000) described as a generalized pressure, in the sense that it can give the interior force intensity for any plane through the considered point

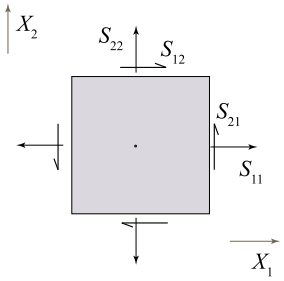

Fig. 2.4 Positive stress components on plane projection of continuum, with component indexing according to Holzapfel (2000), deviating from common engineering notation

Incremental stress relation

For the further development, Eq. (2.21) implies that increments in strain energy density during a small increment in strain is

$$\mathrm{d}\pi_C = \frac{1}{2}\mathsf{S}{:}\mathrm{d}\mathsf{C} \quad \text{or} \quad \mathrm{d}\pi_E = \mathsf{S}{:}\mathrm{d}\mathsf{E} \tag{2.23}$$

where the double contraction symbol : for the two tensors is used to denote an addition of all products of the corresponding components. In the further development, an important quantity is also the differential constitutive tensor in, e.g.,

$$\mathrm{d}\mathsf{S} = \mathcal{K}\,\mathrm{d}\mathsf{E}, \tag{2.24}$$

which is derived from the strain energy, and where $\mathcal{K}$ is a fourth order tensor, relating increments in stress and strain. Except for linearly elastic materials, the tensor is dependent on the current strain state.

Isotropic stress formulation

With respect to the intended applications below, an assumption of—not only a continuous, but also—an isotropic material reflects the primary interest. That the material has the same properties in all directions gives implications on the strain energy density π_p, which must be possible to formulate from the three invariants of the deformation. These are the polynomial coefficients of κ in the determinant of the tensor $(\mathsf{E} - \kappa\mathsf{1})$ for the Green-Lagrange strain E. The invariants are expanded as

$$\begin{aligned} I_1(\mathsf{E}) &= E_{11} + E_{22} + E_{33} \\ I_2(\mathsf{E}) &= E_{11}E_{22} + E_{22}E_{33} + E_{33}E_{11} - E_{12}E_{21} - E_{23}E_{32} - E_{31}E_{13} \\ I_3(\mathsf{E}) &= E_{11}(E_{22}E_{33} - E_{23}E_{32}) + E_{12}(E_{23}E_{31} - E_{21}E_{33}) \\ &\quad + E_{13}(E_{21}E_{32} - E_{22}E_{31}). \end{aligned} \tag{2.25}$$

With an assumption of isotropy, it is also possible to define the strain energy as a function of the stretches, i.e.,

$$\pi_p \equiv \pi_\Lambda(\Lambda_1, \Lambda_2, \Lambda_3), \tag{2.26}$$

in addition to the two forms in Eq. (2.20).

The conclusion from this section is that stress at any point of the considered region can always be expressed from the displacement. The stress is evaluated through the chosen strain measure and a (matching) constitutive strain energy density function.

2.4.2 Hyper-Elastic Materials

Many different classes of material descriptions are used in engineering. The present treatise consistently uses a strain energy density as the constitutive material model, i.e., deals with hyper-elastic materials.[15] The definition through a strain energy density implies that the materials are history-independent, as the energy is completely defined by current strains.

Linearly elastic material

A St Venant-Kirchhoff material is a linearly elastic model, with strain energy density stated from the Green-Lagrange deformation as

$$\pi_E(\mathsf{E}) = \frac{\lambda}{2}\left(I_1(\mathsf{E})\right)^2 - \mu\left(2I_2(\mathsf{E}) - \left(I_1(\mathsf{E})\right)^2\right) \tag{2.27}$$

The two constitutive parameters are the Lamé constants (λ, μ), which are connected to the common elastic parameters (E_m, ν_m) through

$$\lambda = \frac{E_m \nu_m}{(1+\nu_m)(1-2\nu_m)}, \quad \mu = \frac{E_m}{2(1+\nu_m)}. \tag{2.28}$$

Formal differentiation of $\pi_E(\mathsf{E})$ with respect to the components of E gives 2nd Piola-Kirchhoff stress in S, with the examples

$$\begin{aligned} S_{11} &= \lambda(E_{11} + E_{22} + E_{33}) + 2\mu E_{11}, \\ S_{12} &= 2\mu E_{12}, \end{aligned} \tag{2.29}$$

[15] albeit not necessarily linearly elastic

noting that[16] $E_{21} = E_{12}$. The expressions for the other seven components are obviously similar in form, due to the isotropic and symmetric assumptions.

Introducing a simple free $1D$ stress state,[17] for which $S_{22} = S_{33} = 0$, and all shear components of E zero, gives

$$S_{11} = E_m \, E_{11}, \quad \frac{\mathrm{d}S_{11}}{\mathrm{d}E_{11}}|_{E_{11}=0} = E_m. \tag{2.30}$$

One also finds from Eq. $(2.29)_2$ that

$$\frac{\mathrm{d}S_{12}}{\mathrm{d}E_{12}}|_{E_{12}=0} = 2\mu \tag{2.31}$$

agreeing with common expressions for initial (linear) strain. The expressions in Eq. (2.29) are valid for any level of strain, even if the strain is no longer necessarily linear in the physical elongations, due to the quadratic terms in Eq. (2.18).

Incompressible Mooney-Rivlin material

A common Mooney-Rivlin material model uses two constitutive constants and the invariants of the Green deformation C in a strain energy density

$$\pi_C(\mathsf{C}) = c_1 \, (I_1(\mathsf{C}) - 3) + c_2 \, (I_2(\mathsf{C}) - 3) \tag{2.32}$$

with two constitutive parameters (c_1, c_2). An incompressibility assumption is often enforced through a Lagrange multiplier p, which is interpreted as a hydrostatic pressure, to be conjugated to I_3. The augmented strain energy expression to differentiate is

$$L_C(\mathsf{C}) = \pi_C(\mathsf{C}) - \frac{p}{2}(I_3 - 1). \tag{2.33}$$

A formal differentiation of this L_C with respect to the components of C and p, and a specialization to the same one-component cases as above gives, for instance,

$$S_{11} = 2\frac{\left(C_{11}^{3/2} - 1\right)\left(c_1\sqrt{C_{11}} + c_2\right)}{C_{11}^2} \tag{2.34}$$

where $S_{22} = S_{33} = 0$ have been introduced as restrictions to the general expressions, and all shear strain components equal zero. The expression is non-linear, i.e., stress

[16] and that common engineering views relate the shear stress to the shear angle, which is $\gamma_{12} = E_{12} + E_{21}$, through the shear modulus $G = \mu$

[17] which gives the orthogonal normal strain components $E_{22} = E_{33} = -\nu E_{11}$

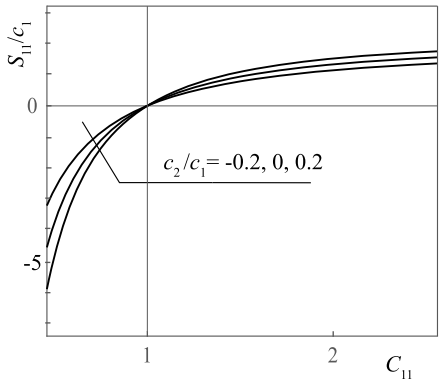

Fig. 2.5 Examples of $1D$ stress, evaluated for incompressible Mooney-Rivlin material model

is not proportional to strain. Figure 2.5 gives examples of evaluations of the stress component S_{11} as function of the strain component C_{11} for three parametric cases (c_1, c_2). The effects of the non-linearity is also obvious from, e.g., the example in Sect. 1.8, where an equi-biaxial situation $C_{11} = C_{22}$, $S_{33} = 0$ is analysed.

Differentiation of Eq. (2.34) leads to an initial stiffness for $1D$ strain as

$$\frac{\mathrm{d}S_{11}}{\mathrm{d}C_{11}}|_{C_{11}=1} = 3(c_1 + c_2), \tag{2.35}$$

or, noting that $\mathrm{d}C_{11} = 2\mathrm{d}E_{11}$, and that $C_{11} = 1$ corresponds to $E_{11} = 0$,

$$\frac{\mathrm{d}S_{11}}{\mathrm{d}E_{11}}|_{E_{11}=0} = 6(c_1 + c_2). \tag{2.36}$$

Similar treatment of the shear component C_{12}, with the restrictions $C_{21} = C_{12}$, and $C_{ii} = 1$ for all i, gives, around $C_{12} = 0$,

$$\frac{\mathrm{d}S_{12}}{\mathrm{d}E_{12}}|_{E_{12}=0} = 2\frac{\mathrm{d}S_{12}}{\mathrm{d}C_{12}}|_{C_{12}=0} = 4(c_1 + c_2), \tag{2.37}$$

identifying the initial shear stiffness of the material model as $\mu = 2(c_1 + c_2)$.

The expressions for axial and shear stress in the two material models above are not completely comparable, as they are based on different assumptions. The expressions for initial stiffness, however, show that the incompressibility condition in Eqs. (2.35)–(2.37) corresponds to $\nu_m = \frac{1}{2}$ in Eqs. (2.29)–(2.31). This is, however, not a general relation between the two formulations.

Compared to the St Venant-Kirchhoff material, the Mooney-Rivlin material model can, at least with some choices of the constitutive parameters, give an asymptotic relation between the stress and strain, discussed in relation to Eq. (1.57). The model

can also give unexpected and non-intuitive results for special strain situations, as shown by Eriksson and Nordmark (2014).

Other material models

A more limited version of the Mooney-Rivlin model is the one-parameter neo-Hookean material model, which contains only the first term of Eq. (2.32), and thus uses $c_1 = \frac{\mu}{2}$, with μ the linearized shear modulus at small strain; the model is not identical to a linearly elastic model when strain is not small.

Many other hyper-elastic material models have also been developed for more or less particular applications. A highly general model is the Ogden material model, which can be adjusted by a large number of parameters. The model uses the principal stretches, and is thereby only useful within isotropic assumptions. Comparisons between different models in different contexts are frequent in literature.

2.5 Continuum Mechanics Problems

The continuum mechanical problem setting is commonly shown by the simplified schematic Fig. 2.6, where the arbitrary shape is indicating the generality of the formulation. This section discusses how general problems can be formulated in terms of interior force residual and boundary conditions. How the general forms can be specialized to structural problems is further elaborated in the context of discretized settings in Chap. 3.

Figure 2.6 shows in its top part a region Ω in its reference configuration, with the boundary Γ. The interior of the region is affected by a body force field $\mathbf{B}$. The boundary is divided into two distinct, but not necessarily continuous, parts, where

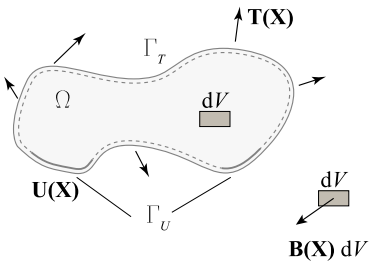

Fig. 2.6 Continuum equilibrium, with region and boundary parts, body force, traction and displacement boundary conditions. Differential volume for residual force expressions

the displacement $\mathbf{U}$ is known on part Γ_U, and the traction $\mathbf{T}$ is known on part Γ_T.[18] Together they form the whole of Γ. The important conclusion is that traction is unknown in Γ_U where displacement is prescribed, while the displacement is unknown on Γ_T, where traction is prescribed.[19] The boundary conditions are further discussed in Sect. 2.5.2.

It is noted that, although drawn in Fig. 2.6 as a plane arbitrary figure, the region is always a region of $3D$ space, and the boundary—shown as a circumferential line—consists of a surface. In general, the setting needs an adaptation to the structure considered in an engineering problem. This is the topic of Sect. 2.5.5.

2.5.1 Interior Forces

Within the region Ω, there exists a body force[20] with an intensity vector field $\mathbf{B}$, as shown by the bottom part of Fig. 2.6. This is expressed as dependent on the reference coordinates, and can come from different sources. A common case in engineering problems is related to gravity, in which case the material density ρ_X[21] and the gravity acceleration define the body force intensity and direction.

Formally, this is a very general setting of the forcing within the region, the limitation being that no point couple intensities are considered. The interior of the boundary value problem studies the differential volume $\mathrm{d}V$, where stress components around it must relate to the body force intensity.

Even if the problem setting from Fig. 2.6 is the desired final form, the fundamental basis for the mechanical formulations is more easily described in the current configuration. All appearing quantities are then transformed into their forms in the reference configuration, essentially by using the gradient F and the Jacobian determinant J.

The conservation of mass leads to the conditions that a density ρ_x in the current configuration must fulfil

$$\rho_x \, \mathrm{d}v = \rho_X \, \mathrm{d}V \quad \text{or} \quad \rho_x = \frac{1}{J} \rho_X \tag{2.38}$$

in relation to the reference density ρ_X and the corresponding volume $\mathrm{d}V$, when J is the Jacobian determinant from Eq. (2.8).

For interior force, i.e., stress, an (x_1, x_2) plane projection of the volume $\mathrm{d}v = \mathrm{d}x_1 \mathrm{d}x_2 \mathrm{d}x_3$ is shown in Fig. 2.7, with the visible Cauchy stress components, marked as representative arrows, and the stress component indices from Fig. 2.4. With the

[18] The term 'traction' is here only used for the situations at the boundary of the region, i.e., 'boundary traction'.

[19] with zero boundary traction, a free boundary, as a very common special case

[20] which is, as stated above, seen as an exterior forcing, although it acts within the region

[21] Subindex $\mathbf{X}$ is used to denote a quantity related to the reference configuration.

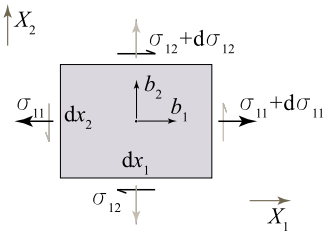

Fig. 2.7 Current view of continuum equilibrium. The rectangle has an out-of-drawing thickness dx_3. Arrows represent stress value at side midpoint and body force intensity at area midpoint

body force[22] represented by the mid-point intensity,[23] this figure fully defines the interior mechanical situation.

No direct coupling exists between the indicated volume elements dV and dv in Figs. 2.6 and 2.7, respectively. Both are regular hexahedra in their respective configurations, and they contain, respectively, a material point $\mathbf{X}$ and its current position $\mathbf{x}$, but otherwise the volumes are not related. Careful transformations of all relevant quantities must therefore be introduced between the views, cf. Eq. (2.22).

The conservation of linear momentum introduces the interior forces for the considered volume dv, and relates this to the velocity of the point currently at the position $\mathbf{x}$. Consideration of the $\mathbf{e}_1$ components of force, which are the only ones denoted in Fig. 2.7, shows that contributions come from the body force intensity, but also the differences in stress on opposite sides of the area. Considering the area on which the stress components act, the total force in the x_1 direction come from $d\sigma_{11} \cdot dx_2 dx_3$ and $d\sigma_{12} \cdot dx_1 dx_3$, but also similarly from the out-of-plane component as $d\sigma_{13} \cdot dx_1 dx_2$. The body force contribution to the x_1 component of force is $b_1 \cdot dx_1 dx_2 dx_3$.

When introducing for the stress differentials the derivatives

$$d\sigma_{11} = \frac{\partial \sigma_{11}}{\partial x_1} \cdot dx_1, \quad d\sigma_{12} = \frac{\partial \sigma_{12}}{\partial x_2} \cdot dx_2, \quad d\sigma_{13} = \frac{\partial \sigma_{13}}{\partial x_3} \cdot dx_3, \tag{2.39}$$

which are correct to first order, the summed force component in the x_1 direction acting in and on the volume dv can be written as a residual force intensity

$$r_1 = dv \left(b_1 + \frac{\partial \sigma_{11}}{\partial x_1} + \frac{\partial \sigma_{12}}{\partial x_2} + \frac{\partial \sigma_{13}}{\partial x_3} \right). \tag{2.40}$$

The $\mathbf{e}_2$ and $\mathbf{e}_3$ components of resultant force on dv are obtained similarly. The three component equations, together given as

$$\mathbf{r} = (\mathbf{b} + \mathrm{div}_x \sigma)\, dv, \tag{2.41}$$

[22] considered as an exterior forcing, but part of the interior force residual

[23] correct to first order for a continuously variable intensity

describe the full mechanical situation in the differential current volume, and give a general basis for equilibrium or motion in Sect. 2.8 below. The divergence is here related to the spatial coordinates **x**.

The same plane figure is used to study the shear stress relation. With origin in the area midpoint, the linear body force variations

$$b_x = b_{x0} + b_{x1}x + b_{x2}y \quad \text{and} \quad b_y = b_{y0} + b_{y1}x + b_{y2}y \tag{2.42}$$

give an equation for moment equilibrium of the area element as

$$\left(\int \int \left(b_y x - b_x y \right) \cdot \mathrm{d}x_1 \mathrm{d}x_2 - \sigma_{12} \mathrm{d}x_1 \cdot \mathrm{d}x_2 + \sigma_{21} \mathrm{d}x_2 \cdot \mathrm{d}x_1 \right) \cdot \mathrm{d}x_3 = 0. \tag{2.43}$$

As the contribution from the body force is one order lower in the differential measures, the symmetry in shear stress $\sigma_{21} = \sigma_{12}$ must be valid also in this case.

Although most easily visualized in the current configuration as in Fig. 2.7, it is for the present purpose favourable to express the point-wise interior forces in quantities referring to the initial reference configuration. Transformation of the quantities in Eq. (2.41) verifies that a residual force field is defined by

$$\mathbf{R} = \left(\mathbf{B} + \mathrm{div}_X \left(\mathsf{FS} \right) \right) \mathrm{d}V, \tag{2.44}$$

where the body force **B** and the 2nd Piola-Kirchhoff stress tensor S at a point **X** are related to a differential volume $\mathrm{d}V$ at point **X** and time t. In Eq. (2.44), the subindex on the divergence operator refers to the reference coordinate components. The expression in Eq. (2.44) is used in the further treatment.

In the transformation, F transforms the stress in S to the global coordinate directions,[24] in which the body force is defined, while the body force intensities in reference and current configurations are related by

$$\mathbf{b} = \frac{1}{J} \mathbf{B}. \tag{2.45}$$

2.5.2 Boundary Traction

At the boundary of the considered region, the interior stress state becomes a boundary traction. At each point of the boundary, the traction intensity is a general $3D$ vector, which can be resolved into one component normal to the boundary, and two orthogonal tangential components.

[24] The tensor product FS is the 1st Piola-Kirchhoff stress tensor P, often used in formulations but not trivial to work with, as it does not match any attractive conjugate strain measure.

A boundary traction vector is obtained from the Cauchy stress as

$$\mathbf{t}(\mathbf{n}) = \sigma\, \mathbf{n} \tag{2.46}$$

giving $\mathbf{t}$ as a vector connected to the boundary point $\mathbf{x}$, when $\mathbf{n}$ is the outwards unit normal vector, defining the current boundary. For the 2nd Piola-Kirchhoff stress tensor S, a similar transformation gives

$$\mathbf{T}(\mathbf{N}) = (\mathsf{FS})\mathbf{N} \tag{2.47}$$

where $\mathbf{N}$ is the outwards unit normal vector to the boundary point $\mathbf{X}$. As the normals are variable along the boundary, traction is a function of positions $\mathbf{x}$ and $\mathbf{X}$, or symbolically

$$\mathbf{t} \equiv \mathbf{t}(\mathbf{x}), \quad \mathbf{T} \equiv \mathbf{T}(\mathbf{X}), \tag{2.48}$$

with the implicit definition of $\mathbf{n} = \mathbf{n}(\mathbf{x})$ and $\mathbf{N} = \mathbf{N}(\mathbf{X})$.

The traction in $\mathbf{T}$ is measured in the global axis directions, and related to one unit of initial area. The traction vectors $\mathbf{t}$ and $\mathbf{T}$ share the same direction, but are differently scaled, with the condition $\mathrm{d}a\, \mathbf{t} = \mathrm{d}A\, \mathbf{T}$, where

$$\mathrm{d}a = J \parallel \mathsf{F}^{-\mathrm{T}}\mathbf{N} \parallel \mathrm{d}A \tag{2.49}$$

with $\mathrm{d}a$ or $\mathrm{d}A$ used in any boundary integral.

Two examples

The example in Fig. 2.8a uses the deformation gradient F from Eq. (2.10) to operate on a unit square; the Jacobian determinant is evaluated as $J = 0.87$. For any point on the edge with normal $\mathbf{N} = (1, 0, 0)^{\mathrm{T}}$, the single stress component $S_{11} = 2$ corresponds to a force intensity vector $\mathbf{f}_1 = \mathsf{S}\mathbf{N} = (2, 0, 0)^{\mathrm{T}}$ in relation to the undeformed configuration, and a traction vector $\mathbf{T}_1 = \mathsf{F}\,\mathbf{f}_1 = (1.56, 1.92, 0)^{\mathrm{T}}$ on the corresponding deformed edge. This traction vector is not normal to the edge. A single stress component $S_{21} = 1$ at the same point corresponds to a vector $\mathbf{f}_2$ in relation to the material configuration, and a traction vector $\mathbf{T}_2 = (-0.24, 0.82, 0)^{\mathrm{T}}$, which acts along the deformed edge. The resulting traction vectors from the two stress components are no longer orthogonal (as $\mathbf{f}_1$ and $\mathbf{f}_2$ are), due to the shearing involved in F. If the stress components are constant on the whole edge, their resultant forces are obtained through a multiplication by the area of the edge in the reference configuration. One also calculates that the relation between initial and deformed areas for this edge are $\mathrm{d}a = 0.8544\, \mathrm{d}A$, which can be used to evaluate the traction in deformed coordinates.

Figure 2.8b similarly shows how a stress component S_{11} represents a horizontal force intensity vector $\mathbf{f}_3$ in an initially horizontal bar, but also can give a vertical component in the traction vector $\mathbf{T}_3$, when the bar undergoes a finite vertical deflection. With the quantities

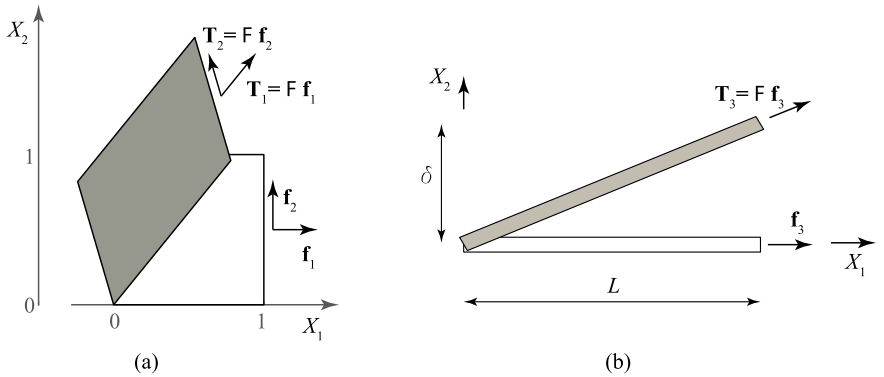

Fig. 2.8 Traction component from 2nd Piola-Kirchhoff stress components. **a** Two stress components in example from Fig. 2.3. **b** Axial stress in finite deflection of bar

$$\mathsf{S} = \begin{pmatrix} S_{11} & 0 & 0 \\ 0 & 0 & 0 \\ 0 & 0 & 0 \end{pmatrix}, \quad \mathsf{F} = \begin{pmatrix} 1 & 0 & 0 \\ \delta/L & 1 & 0 \\ 0 & 0 & 1 \end{pmatrix}, \quad \mathbf{N} = \begin{pmatrix} 1 \\ 0 \\ 0 \end{pmatrix}, \tag{2.50}$$

the traction vector at the right end is

$$\mathbf{T}_3 = (S_{11}\ ,\ S_{11}\delta/L\ ,\ 0)^{\mathrm{T}}\,, \tag{2.51}$$

which is to be multiplied by the reference area to yield the axial force resultant. With the axial strain component[25] $E_{11} = \frac{1}{2}\,(\delta/L)^2$, the vertical force component at the right end is related to $\approx (\delta/L)^3$, if the constitutive relation is approximately linear.

2.5.3 Boundary Conditions

While the above expressions define the interior behaviour of the region, the problem setting also needs boundary conditions. Primarily, the stress has to be matched to the traction boundary conditions on the boundary part Γ_T in Fig. 2.6. These prescribe either of the traction vectors to

$$\mathbf{t} - \bar{\mathbf{t}} = \mathbf{0}, \quad \text{or} \quad \mathbf{T} - \overline{\mathbf{T}} = \mathbf{0}, \tag{2.52}$$

where $\bar{\mathbf{t}}$ or $\overline{\mathbf{T}}$ defines the condition, expressed point-wise in relation to current or initial configurations. The over-bar is here used to denote a prescribed quantity. A zero prescribed traction on parts of Γ_T, i.e., a stress-free boundary part is a common

[25] immediately calculable from F through Eq. (2.16)

special case. Through Eq. (2.52), the traction boundary conditions can be interpreted as indirect boundary conditions for $\mathbf{U}$ on the boundary part Γ_T.

An example

An initially horizontal bar in Fig. 2.9a, with reference length L and transversal width w, is affected by forcing, and deformed to a current configuration described by δ, cf. Fig. 2.8b. Dependent on the origin of the forcing, the representation as body force and boundary traction in relation to the reference configuration needs consideration. Key aspects are whether the forcing is constant in direction, or follows the displacement of the component, and whether it is measured in relation to the reference or deformed geometry. The subfigures show typical cases of forcing to the left, and their representations in the reference configuration to the right.

If the body force comes from gravity effects (downwards), as in subfigure (a), the total vertical force at all times is given by the intensity multiplied by the volume of the bar, as the forcing direction is well-defined. The body force intensity, constant over the region is

$$\mathbf{B} = (0, -\rho_X g, 0)^{\mathrm{T}}, \tag{2.53}$$

based on material density ρ_X measured in the reference volume,[26] and the gravity acceleration. The total vertical force is obtained by multiplication by reference volume. If the body force has another origin, this may lead to other relations.

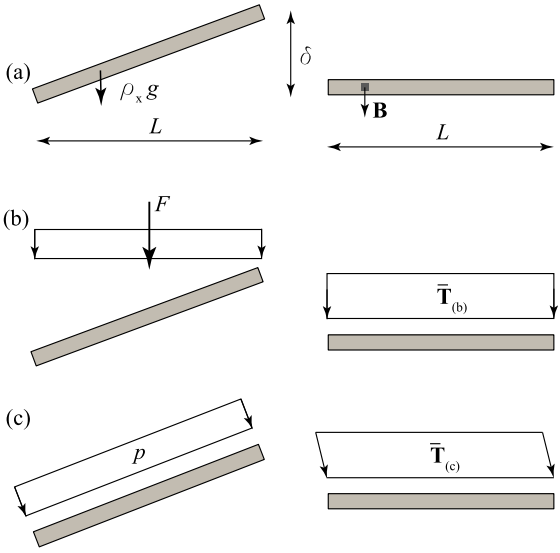

Fig. 2.9 Schematic example of exterior forcing for $2D$ model, and its representation in relation to reference volume. **a** Body force intensity from gravity. **b** Traction prescribed in reference configuration. **c** Pressure prescribed in current configuration

[26] but denoted to the left as the density ρ_x, in relation to current volume

The forcing in subfigure (b) implies that the forcing on the top surface is always acting downwards, and is rather measured as a total force F; this typically corresponds to the case when the structure carries gravity forces from some supported objects. The total force is distributed as a traction[27] for this case

$$\overline{\mathbf{T}}_{(b)} = (0, -\frac{F}{wL}, 0)^{\mathrm{T}}, \tag{2.54}$$

It is obvious that the total traction force, after integration over the reference top surface area becomes the expected F.

Subfigure (c) shows a prescribed pressure p acting on the bar. The pressure is normal to the bar direction, and acting on the deformed length. Acting on a boundary surface with reference normal direction $\mathbf{N} = \mathbf{e}_2$, the corresponding traction vector can be described as

$$\overline{\mathbf{T}}_{(c)} = -pJ\mathsf{F}^{-\mathrm{T}}\mathbf{N}, \tag{2.55}$$

where J measures the overall deformation, and $\mathsf{F}^{-\mathrm{T}}\mathbf{N}$ is the vector to which the reference configuration unit vector $\mathbf{e}_2$ is deformed; it is no longer a unit vector. The transformation in the second component can be re-written as

$$J\mathsf{F}^{-\mathrm{T}}\mathbf{N} = \left(\frac{\partial \mathbf{x}}{\partial X_3} \times \frac{\partial \mathbf{x}}{\partial X_1}\right). \tag{2.56}$$

For the case in Fig. 2.8b, this implies that the pressure forcing is represented as a prescribed traction with

$$\overline{\mathbf{T}}_{(c)} = p\left(\frac{\delta}{L}, -1, 0\right)^{\mathrm{T}}. \tag{2.57}$$

The total force is also here obtained from a multiplication with the initial upper surface area Lw. In numbers, with $L = 3\,\mathrm{m}$, $\delta = 0.2\,\mathrm{m}$, $p = 4\,\mathrm{kPa}$, the results become $J = 1, \mathsf{F}^{-\mathrm{T}}\mathbf{e}_2 = (-0.067, 1, 0)^{\mathrm{T}}, \overline{\mathbf{T}}_{(c)} = (0.267, -4, 0)^{\mathrm{T}}\,\mathrm{kPa}$. Multiplied by the initial top surface area Lw, the total force acting is $w \cdot (0.8, -12, 0)^{\mathrm{T}}\,\mathrm{kN/m}$, with components obtained from the pressure multiplied by the exposed areas in the three coordinate planes, respectively.

A final comment on subfigure (c) is that the deflection δ is assumed as known, and not a response to the pressure. This implies that some form of iteration is commonly needed for pressure forcing.

[27] It is assumed that the top surface width does not change from deformation

2.5.4 Displacement Basis

The discussion sofar has only considered interior stress and boundary traction. For instance, a static equilibrium state is identified from Eq. (2.44) with $\mathbf{R} = \mathbf{0}$ for any point in the region. Even if this problem might seem solvable from interior equilibrium and boundary traction, a coupling always exists between the two fields displacement and stress. The displacement field $\mathbf{U}$ is therefore also part of a solution.

The stress is always possible to express from the displacement, through a deformation measure and the form of the strain energy density. This implies that the stress tensor S can be evaluated for any point $\mathbf{X}$ within the region, from E, which is dependent on $\mathbf{U}$, and a set of constitutive parameters $\underline{\Xi}$, which are inherently connected to the strain energy density form. The opposite is not necessarily true, due to the possibility for rigid body motions under identical stress. It is also obvious that boundary traction can be evaluated from Eq. (2.47), with F and S coming from the displacement field $\mathbf{U}$, the constitutive parameters $\underline{\Xi}$ and the normal direction $\mathbf{N}$ for all points $\mathbf{X}$ on the boundary of the region.

This implies that it is possible to build a problem definition on the displacement field only. This is the sole method promoted here, although other, e.g., mixed formulations are sometimes used to advantage.

2.5.5 Structural Regions

In relation to any engineering problem, the above setting needs some comments and clarifications. The more practical setting can be described by Fig. 2.10, which is a still schematic but elaborated version of Fig. 2.6. The figure must again be interpreted as a general $3D$ region, but it is drawn to emphasize that a considered structure[28] is normally composed of several distinct parts Ω_e, each with an intended function and a specific shape. The figure also aims to emphasize that the subregions of the whole may—or might not—consist of different materials, with their respective descriptions. Holes in the structure lead to new segments of boundary, which contribute to Γ_T or Γ_U. For each differential volume $\mathrm{d}V$, the expressions above are fully valid.

The composition of several subregions Ω_e to one whole focusses additional interest on the boundaries between the subregions. As the discussion above has assumed that the region is continuous, without cracks, overlaps or other localized effects, the displacement field must be continuous across the subregion boundaries. This is a foundation for the discretized structural models discussed in Chap. 3. Regarding the stress, the traction must also be continuous over these subregion boundaries, but stress components in their tangential plane may be discontinuous.

[28] "A structure is an arrangement and organization of interrelated elements in a material object or system, or the object or system so organized", https://en.wikipedia.org/wiki/Structure as of 2021-08-02 (Giving a quote to OED)

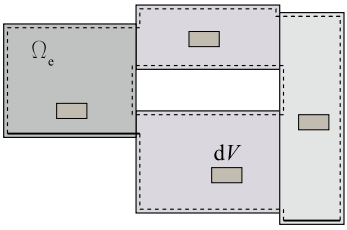

Fig. 2.10 Structural equilibrium

2.5.6 Dimensional Reduction

From the general descriptions of a $3D$ solid region, structural problems are often modelled through a dimensional reduction, where the geometry of the region or the considered forcing allow simplified forms. Typically, this means that the geometry is of lower dimension: the models are approximations of the real region with one or two material dimensions approaching zero. This is further discussed in Sect. 3.4, in relation to discretized analysis models, where an important distinction is whether the dimensions are small but finite—in shells and beams, when interior force has a simple variation over the small dimension(s)—or can be assumed to be vanishing—in membranes and bars, when interior force is constant over the small dimensions.

When using these reduced views, like bar, beam or plate models, quantities are evaluated in integral form over omitted spatial dimensions. From this follows that the models use resultants of the interior stress, e.g., as normal force resultants or moment resultants as main problem variables.[29] For a straight beam, where two size parameters are significantly smaller than the length direction, the stress on a fictitious section of the beam can be integrated to three force and three moment resultants.[30]

Also, boundary traction is affected when the problem is reduced by one or two dimensions. The distribution of the traction component over the integrated directions is thereby based on some assumptions. For instance, a downwards pressure on a horizontal beam is implicitly integrated over the top surface width—and the gravity intensity over the beam section area—to a force intensity per length unit.

The integral forms of the fundamental equations for the general $3D$ solid also affect the defining equations for the problem setting. In particular, this means that point forces and point supports can be introduced in the simplified models, even if such conditions can not exist in the analytical continuum descriptions; only force intensities and boundary segments of finite areas with prescribed displacement are legal in the full form. This also has implications in the interpretation of traction boundary conditions, evaluated from single or double integrals over the reduced dimensions.

[29] corresponding to translations and rotations

[30] for the $3D$ case; in $2D$, there are two force and one moment components

2.6 Energy, Work and Power

Section 2.4 gives a rather broad discussion on the strain energy, which describes the interior response to forcing. This is defined as a density for small volume elements, and utilizes the local deformation and a constitutive expression, which implicitly defines the interior stress from the strain. The strain energy is a potential in the sense that it represents energy stored in the structure. The present section discusses other forms of energy, potential, work and power in and on the structure. These are necessary to consider in the equilibrium and stability analyses in coming sections. For these, the identification of the problem region in Sect. 2.5 is a pre-requisite, in particular the meanings of the region and its boundary.

2.6.1 Kinetic Energy

When movements occur in the structure, not only the strain energy but also the kinetic energy must be considered. This is formulated from each differential volume element $\mathrm{d}V$ of the region, cf. Fig. 2.6, and uses the current velocity of the element. Based on the reference configuration, the velocity at a point is $\dot{\mathbf{U}} = \frac{\mathrm{d}\mathbf{U}}{\mathrm{d}t}$, i.e., a vector in Cartesian space, with the superposed dot denoting a time differentiation.[31] The velocity field is dependent on $\mathbf{X}$ and t.

Corresponding to the kinetic energy in a particle of mass m, i.e., $\Pi_k = \frac{1}{2}mv^2$, with v the speed[32] of the particle, the general expression for the kinetic energy density in a unit volume at point $\mathbf{X}$ is

$$\pi_k = \frac{1}{2}\rho_X \dot{\mathbf{U}} \bullet \dot{\mathbf{U}}, \tag{2.58}$$

where the current velocity field $\dot{\mathbf{U}}$ and the density ρ_X are related to the initial reference configuration. The full dot denotes a scalar product of the two vectors. The total kinetic energy is integrated over the whole reference region

$$\Pi_k = \int_\Omega \pi_k \,\mathrm{d}V, \tag{2.59}$$

and is obviously non-negative.

[31] It could equally well be stated in $\dot{\mathbf{x}} = \dot{\mathbf{U}}$, due to the constant $\mathbf{X}$ in Eq. (2.2).

[32] Speed is here used to denote the magnitude, or norm, of the velocity vector.

Mechanical energy

In motion problems, the mechanical energy is the sum of kinetic and strain energies, or

$$\Pi_m = \Pi_k + \Pi_p, \tag{2.60}$$

and is considered a fundament in many analysis models. The energy may—as in the oscillation of a linear springed mass without exterior forcing—change between kinetic and strain energy, but the sum

$$\Pi_m = \text{const.} \quad \text{or} \quad \frac{\mathrm{d}}{\mathrm{d}t}\left(\Pi_k + \Pi_p\right) = 0. \tag{2.61}$$

The latter part of Eq. (2.61) can be re-organized, using Eqs. (2.58)–(2.59), as

$$\frac{\mathrm{d}}{\mathrm{d}t}\Pi_k = \int_\Omega \rho_X \dot{\mathbf{U}} \bullet \ddot{\mathbf{U}}\, \mathrm{d}V = -\frac{\mathrm{d}}{\mathrm{d}t}\Pi_p = P_p, \tag{2.62}$$

relating the time rate of kinetic energy to the interior strain power P_p, which is also the time derivative of released strain energy.

For a small time increment $\mathrm{d}t$, this gives the increment in kinetic energy as

$$\mathrm{d}\Pi_k = \int_\Omega \rho_X \ddot{\mathbf{U}} \bullet \mathrm{d}\mathbf{U}\, \mathrm{d}V = P_p\, \mathrm{d}t = \mathrm{d}W_p = -\mathrm{d}\Pi_p, \tag{2.63}$$

when $\mathrm{d}\mathbf{U} = \mathrm{d}t\, \dot{\mathbf{U}}$ for the small increment, and shows that incremental positive strain work $\mathrm{d}W_p$ gives an increment to Π_k at the cost of a decreasing Π_p. This statement is based on the assumption that no exterior force affects the system.[33]

2.6.2 Strain Energy

In Eq. (2.62), the strain power P_p is the negative of the time rate of strain energy, which, according to Eqs. (2.19) and (2.23), can be written

$$P_p = -\frac{\mathrm{d}}{\mathrm{d}t}\Pi_p = -\int_\Omega \mathsf{S} : \dot{\mathsf{E}}\, \mathrm{d}V, \tag{2.64}$$

when a strain energy Π_p is defined, $\dot{\mathsf{E}}$ is the strain rate, i.e., the time differential of the Green-Lagrange deformation tensor, and S the current 2nd Piola-Kirchhoff

[33] noting carefully that the mass appearing in the oscillation equation is the inertia, not related to a gravity force; thus, no exterior force affects the system.

stress tensor.[34] The strain rate is here related to the velocity field $\dot{\mathbf{U}}$, but also the displacement field $\mathbf{U}$.

The strain work during a small incremental displacement $\mathrm{d}\mathbf{U}$,[35] which creates strain increments $\mathrm{d}\mathsf{E}$ in time $\mathrm{d}t$ is

$$\mathrm{d}W_p = -\int_\Omega \mathsf{S}{:}\mathrm{d}\mathsf{E}\,\mathrm{d}V. \tag{2.65}$$

Even if the basis for this expression was taken in the strain energy in Eq. (2.64), the expression in Eq. (2.65) is always valid as long as current stress tensor S can be evaluated, with or without history dependence, i.e., also for non-elastic situations.

From strain energy density π_p, which makes S derivable from the strain E, a positive work done by the stress corresponds to a loss of strain energy, according to

$$\mathrm{d}W_p = -\mathrm{d}\Pi_p = -\int_\Omega \mathrm{grad}_U \pi_p \bullet \mathrm{d}\mathbf{U}\,\mathrm{d}V, \tag{2.66}$$

where grad_U differentiates point-wise with respect to the displacement.

2.6.3 *Exterior Forcing*

A simplistic view on a structure identifies the interior stress and velocity fields in the region as effects of the exterior forcing through body force intensity and boundary traction. A fundamental aspect of forcing is whether it can be considered as conservative, in which case it can be described through an exterior potential.[36] This is here handled as a contribution to the total energy, even if the potential terms are somewhat debatable in a thermomechanics setting. The discussion below also treats non-conservative forcing, which is not possible to represent by a potential expression.

An example

The basic expressions are demonstrated by a special case of conservative forcing: the potential[37] of a mass m lifted a distance $\mathrm{d}y = h$ in a gravitational field of acceleration g, well-known as

[34] Equation (2.64) could equally well have been written with any other energy-conjugated pair of strain rate and stress

[35] and at a current configuration $\mathbf{U}$, this distinction only being necessary when the strain measure is not linear in displacement

[36] even if this might not be the preferable way for describing it

[37] This treatise uses the term potential for energy terms related to exterior forcing, even if the term potential energy is frequently used.

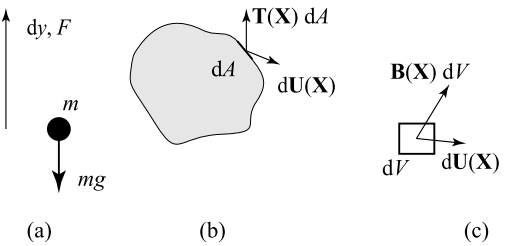

Fig. 2.11 Force potential and work. **a** Mass particle in a gravitational field. **b** Area boundary element affected by boundary traction. **c** Volume element with body force

$$\Pi_{\text{con}} = -Fy \quad \text{and} \quad \mathrm{d}\Pi_{\text{con}} = -F\,\mathrm{d}y = mgh. \tag{2.67}$$

where the subindex emphasizes the conservative case. The gravity forcing is here measured in the direction of positive y, cf. Fig. 2.11a. With an arbitrary zero level, the expression is given as an increment of potential

$$\mathrm{d}W_{\text{con}} = F\,\mathrm{d}y = -\mathrm{d}\Pi_{\text{con}}. \tag{2.68}$$

with the work positive when a movement follows the acting force, corresponding to a loss of potential. Although suggesting a small additional displacement, the expression is valid for any dy in this particular case.

The exterior power from the forcing is the time derivative of work, or

$$P_{\text{con}} = F\dot{y} = -\frac{\mathrm{d}}{\mathrm{d}t}\Pi_{\text{con}}, \tag{2.69}$$

The close relationship between power, work and potential is based on the conservative force system and displacement-independent gravity force. The relations shown by the simple example have wide generality for conservative problems.

General forcing

When acting force can not be assumed as conservative, the incremental work and power from forcing can still be formulated for small displacement increments $\mathrm{d}\mathbf{U} = \mathrm{d}t\,\dot{\mathbf{U}}$. Then, work is performed by the exterior boundary traction acting on the region, according to Fig. 2.11b.[38] A differential area dA at point $\mathbf{X}$ on the boundary part Γ_T is affected by a traction $\overline{\mathbf{T}}$, implicitly using that the normal $\mathbf{N}$ is unique at a boundary point $\mathbf{X}$,[39] cf. Eq. (2.47). At a displacement $\mathbf{U}$, the incremental work done by the traction during an increment d$\mathbf{U}$ gives the total traction work increment

[38] where it is again noted that the plane figure represents a volume, and the circumference thereby denotes a surface

[39] but possibly discontinuous at a corner point

$$\mathrm{d}W_t = \int_{\Gamma_T} \overline{\mathbf{T}} \bullet \mathrm{d}\mathbf{U}\, \mathrm{d}A, \tag{2.70}$$

effectively considering the part of the boundary where neither $\mathrm{d}\mathbf{U}$ nor $\overline{\mathbf{T}}$ is zero.

Exterior forcing in the form of body force intensity is shown by Fig. 2.11c. With a differential volume $\mathrm{d}V$ around point $\mathbf{X}$ affected by a body force intensity $\mathbf{B}$, the work during a small displacement $\mathrm{d}\mathbf{U}$ is

$$\mathrm{d}W_b = \int_{\Omega} \mathbf{B} \bullet \mathrm{d}\mathbf{U}\, \mathrm{d}V. \tag{2.71}$$

The total exterior work affecting the considered region during a small incremental displacement field $\mathrm{d}\mathbf{U}$ from a configuration with $\mathbf{U}$ is the sum of the two contributions

$$\mathrm{d}W_{\text{ext}} = \mathrm{d}W_t + \mathrm{d}W_b. \tag{2.72}$$

Consequently, the exterior power is

$$P_{\text{ext}} = P_t + P_b = \int_{\Gamma_T} \overline{\mathbf{T}} \bullet \dot{\mathbf{U}}\, \mathrm{d}A + \int_{\Omega} \mathbf{B} \bullet \dot{\mathbf{U}}\, \mathrm{d}V, \tag{2.73}$$

which is an instantaneous expression, valid at time t.

The expressions in Eqs. (2.72) and (2.73) are valid for any exterior forcing, but can sometimes be more easily handled for conservative forcing.[40] The work and power terms are then split into two parts

$$\mathrm{d}W_{\text{ext}} = \mathrm{d}W_{\text{con}} + \mathrm{d}W_{\text{non}} \quad \text{and} \quad P_{\text{ext}} = P_{\text{con}} + P_{\text{non}} \tag{2.74}$$

With both conservative and non-conservative forcing in a structural model, boundary traction and body force are expressed as

$$\overline{\mathbf{T}} = \overline{\mathbf{T}}_{\text{con}} + \overline{\mathbf{T}}_{\text{non}}; \quad \mathbf{B} = \mathbf{B}_{\text{con}} + \mathbf{B}_{\text{non}}, \tag{2.75}$$

and incremental work and power are expressed as

$$\begin{aligned} P_{\text{ext}} &= P_{\text{con}} + \int_{\Gamma_T} \overline{\mathbf{T}}_{\text{non}} \bullet \dot{\mathbf{U}}\, \mathrm{d}A + \int_{\Omega} \mathbf{B}_{\text{non}} \bullet \dot{\mathbf{U}}\, \mathrm{d}V \\ \mathrm{d}W_{\text{ext}} &= \mathrm{d}W_{\text{con}} + \int_{\Gamma_T} \overline{\mathbf{T}}_{\text{non}} \bullet \mathrm{d}\mathbf{U}\, \mathrm{d}A + \int_{\Omega} \mathbf{B}_{\text{non}} \bullet \mathrm{d}\mathbf{U}\, \mathrm{d}V. \end{aligned} \tag{2.76}$$

[40] which is a very common situation in structural analyses

Conservative forcing

Systems affected by conservative forcing are important special cases of structural mechanics, for which forcing is[41] expressed by a potential. This implies that the work done by a force during a movement is only dependent on its initial and final positions. The corresponding displacement of the acting force is measured by the displacement field **U**.

A potential for the conservative exterior forcing is often described as

$$\Pi_{\text{con}} = \int_{\Gamma_T} \pi_t \mathrm{d}A + \int_{\Omega} \pi_b \mathrm{d}V, \tag{2.77}$$

where the densities represent the contributions to the potential at relevant points **X**. The exterior potential contributions on $\mathrm{d}A$ and $\mathrm{d}V$ allow arbitrary expressions, but these are often rather simple forms involving **U**, $\overline{\mathbf{T}}$ and **B**. A potential also sometimes gives a convenient method to express more global forcing classes. As an example, an interiorly pressurized object gives a potential according to

$$\Pi_{\text{con}} = pV, \tag{2.78}$$

with p the over-pressure and V the current volume.

The exterior work from conservative forcing is

$$\mathrm{d}W_{\text{con}} = -\mathrm{d}\Pi_{\text{con}} = -\int_{\Gamma_T} \mathrm{grad}_U \pi_t \bullet \mathrm{d}\mathbf{U}\, \mathrm{d}A - \int_{\Omega} \mathrm{grad}_U \pi_b \bullet \mathrm{d}\mathbf{U}\, \mathrm{d}V \tag{2.79}$$

during a small incremental displacement $\mathrm{d}\mathbf{U}$, while the exterior power is

$$P_{\text{con}} = -\frac{\mathrm{d}}{\mathrm{d}t}\Pi_{\text{con}} = -\int_{\Gamma_T} \mathrm{grad}_U \pi_t \bullet \dot{\mathbf{U}}\, \mathrm{d}A - \int_{\Omega} \mathrm{grad}_U \pi_b \bullet \dot{\mathbf{U}}\, \mathrm{d}V \tag{2.80}$$

—special cases of the general Eqs. (2.72) and (2.73).

Displacement-independent forcing

A further, very common, specialization of the conservative system is when the acting forcing is displacement-independent, i.e., when the potential Π_{con} of exterior force is linear in the displacement. This appears for forcing which is fixed in orientation and material region of action. The typical case is when a mechanical structure is

[41] or, can be

designed to be essentially geometrically unchanged under forcing. The assumption is not valid for, e.g., pressure acting on the spatial configuration of a deformed object.

In this special case, the exterior potential of the boundary traction in Fig. 2.11b and the body force intensity in Fig. 2.11c is thereby, with a generalization of Eq. (2.67),

$$\Pi_{\text{con}} = -\int_{\Gamma_T} \overline{\mathbf{T}} \bullet \mathbf{U}\, \mathrm{d}A - \int_{\Omega} \mathbf{B} \bullet \mathbf{U}\, \mathrm{d}V, \tag{2.81}$$

where $\mathrm{d}A$ is a differential area on the boundary, $\mathrm{d}V$ a differential volume, $\overline{\mathbf{T}}$ the prescribed boundary traction, and $\mathbf{B}$ the body force intensity, with the forcing quantities independent of displacement $\mathbf{U}$.

The incremental work and power during a differential displacement $\mathrm{d}\mathbf{U} = \mathrm{d}t\dot{\mathbf{U}}$ are

$$\mathrm{d}W_{\text{con}} = \int_{\Gamma_T} \overline{\mathbf{T}} \bullet \mathrm{d}\mathbf{U}\, \mathrm{d}A + \int_{\Omega} \mathbf{B} \bullet \mathrm{d}\mathbf{U}\, \mathrm{d}V. \quad \text{and} \quad P_{\text{con}} = \int_{\Gamma_T} \overline{\mathbf{T}} \bullet \dot{\mathbf{U}}\, \mathrm{d}A + \int_{\Omega} \mathbf{B} \bullet \dot{\mathbf{U}} \mathrm{d}V \tag{2.82}$$

—special cases of Eqs. (2.79)–(2.80), and thereby of Eqs. (2.72)–(2.73).

Considerations

The three situations treated in Sect. 2.6.3 formulate the incremental work during a differential displacement, with or without energy and potential as the basis. This is a common, idealized description of a structure from several viewpoints. The simplifications involved are related to assumptions for the forcing and to neglecting dissipative material effects from, e.g., material damping, plasticity or visco-elasticity.

Aspects of dissipation can occur in a structure due to several reasons, but normally implies a loss of mechanical energy in the model, and typically giving heat. One example is when the stress at a point is not obtained from a strain energy density function π_p as above, but other contributions appear. Formally, this means that a stress tensor S_{non} need be added to the expressions in Eq. (2.21). As has been noted in connection with Eq. (2.65), the incremental strain work should always be evaluated for the total stress, which is now

$$\mathsf{S} = \mathsf{S}_{\text{con}} + \mathsf{S}_{\text{non}}, \tag{2.83}$$

with the first term from the chosen strain energy density. Dissipation can also be modelled as non-conservative contributions to boundary traction or body force, according to the discussion above.

2.6.4 Power and Work

While Eq. (2.63) is valid when no exterior forcing is present, a general view must consider that mechanical energy changes due to exterior work in and on the region. The mechanical energy balance can then be given in incremental work and power form as

$$\mathrm{d}\Pi_k = \mathrm{d}W_p + \mathrm{d}W_{\text{ext}} \quad \text{and} \quad \frac{\mathrm{d}}{\mathrm{d}t}\Pi_k = P_p + P_{\text{ext}}, \tag{2.84}$$

with expressions, for general and special cases, given above.

Incremental exterior work, together with changing strain energy, thereby lead to changes in kinetic energy Π_k. Equation (2.84) is valid for any velocity variation $\dot{\mathbf{U}}$ over the region, with its corresponding displacement $\mathrm{d}\mathbf{U} = \mathrm{d}t\,\dot{\mathbf{U}}$. All quantities $\mathbf{U}$, $\dot{\mathbf{U}}$, $\overline{\mathbf{T}}$ and $\mathbf{B}$ are functions of $\mathbf{X}$ and t, and the expressions are instantaneous.

Equation (2.84) is fundamental for the coming treatment of equilibrium and motion. It should be noted that the energy, work and power expressions above are global quantities, in the sense that they integrate effects over the whole considered system. No specific assumptions are made on the nature of acting traction and body force in Eq. (2.84), but $\mathrm{d}W_{\text{ext}}$ and P_{ext} may be simplified if a potential for the forcing is available and more attractive.

2.6.5 Conservative Systems

For a conservative system, when strain energy and exterior potential are available, the energy equations in Eq. (2.84) are simplified to

$$\mathrm{d}\Pi_{\text{tot}} = 0 \quad \text{and} \quad \frac{\mathrm{d}}{\mathrm{d}t}\Pi_{\text{tot}} = 0, \tag{2.85}$$

where a total mechanical energy is defined as

$$\Pi_{\text{tot}} = \Pi_k + \Pi_p + \Pi_{\text{con}} \tag{2.86}$$

The energy and potential terms in Eq. (2.86) are dependent on the displacement and velocity fields within the considered region at time t. Equation (2.85) states that the total mechanical energy is constant in a mechanically conservative system, when the potential of exterior forcing is considered.

Although the potential expression is valid and can be considered as a general fundament, it is not, as noted by Holzapfel (2000), a mechanical principle in itself; it just follows as a consequence of the balance of linear momentum.

In the absence of dynamical contributions, i.e., in equilibrium, the total potential for the conservative system is the sum

$$\Pi = \Pi_p + \Pi_{\text{con}}, \tag{2.87}$$

where the notation without indices is chosen due to the fact that conservative forcing together with strain energy is an important case of equilibrium in engineering analyses. The total potential in Eq. (2.87) is also a key quantity in judging stability of equilibrium, cf. Sect. 2.9.1.

2.7 Physical and Virtual Displacement Increments

The previous sections develop several aspects of work increment and power related to a small incremental displacement $\mathrm{d}\mathbf{U}$ corresponding to a velocity field $\mathrm{d}\mathbf{U} = \mathrm{d}t\,\dot{\mathbf{U}}$ and a small time increment $\mathrm{d}t$. Equation (2.84) is valid for any mechanical state for the considered region, be it stationary or transient. The displacement increments considered are thereby physical, and part of a process. For the solution to the problem, the increments must fulfill all the boundary conditions, and can thereby be non-zero on all boundaries, if $\overline{\mathbf{U}}$ changes with time, cf. Sect. 2.5.

When formulating the fundamental equations for mechanical response in the following section, also virtual displacements are needed. These are arbitrary (small) displacement fields around a current state $\mathbf{U}$, but need to vanish on the boundary part Γ_U, where displacement is prescribed, even when this condition is dependent on time. The virtual displacement field, denoted $\mathfrak{D}\mathbf{U}$ over the whole region including boundary is thereby restricted compared to the full displacement field $\mathbf{U}$.

As the virtual displacement field $\mathfrak{D}\mathbf{U}$ is included in the more general field $\mathrm{d}\mathbf{U}$, all the expressions derived above are valid also for the virtual displacement. In particular, virtual work terms $\mathfrak{D}W$ can be derived from above, with a correspondence to the terms in Eq. $(2.84)_1$, as

$$\mathfrak{D}\Pi_k = \int_\Omega \rho_X \ddot{\mathbf{U}} \bullet \mathfrak{D}\mathbf{U}\,\mathrm{d}V, \tag{2.88}$$

$$\mathfrak{D}W_p = -\int_\Omega \mathsf{S}{:}\mathfrak{D}\mathsf{E}\,\mathrm{d}V, \tag{2.89}$$

and

$$\mathfrak{D}W_{\text{ext}} = \int_{\Gamma_T} \overline{\mathbf{T}} \bullet \mathfrak{D}\mathbf{U}\,\mathrm{d}A + \int_\Omega \mathbf{B} \bullet \mathfrak{D}\mathbf{U}\,\mathrm{d}V \tag{2.90}$$

which are immediately found from Eqs. (2.63), (2.65) and (2.70)–(2.72). Equation (2.89) gives the possibility for non-conservative stress contributions representing dissipation, cf. Eq. (2.83), but the expression $\mathfrak{D}W_p = -\mathfrak{D}\Pi_p$ is valid only in a conservative setting. Equation (2.90) can, in order to allow both conservative and non-conservative forcing, be expanded as

$$\mathfrak{D}W_{\text{ext}} = -\mathfrak{D}\Pi_{\text{con}} + \int_{\Gamma_T} \overline{\mathbf{T}}_{\text{non}} \bullet \mathfrak{D}\mathbf{U}\, \mathrm{d}A + \int_{\Omega} \mathbf{B}_{\text{non}} \bullet \mathfrak{D}\mathbf{U}\, \mathrm{d}A. \tag{2.91}$$

The energy balance for an arbitrary virtual displacement $\mathfrak{D}\mathbf{U}$ can thus be formulated from current $\mathbf{U}$, $\dot{\mathbf{U}}$, S, $\overline{\mathbf{T}}$ and $\mathbf{B}$, when region and boundary are known. The strain increment $\mathfrak{D}\mathsf{E}$ must correspond to $\mathfrak{D}\mathbf{U}$, and the stress S evaluated for the strain E at displacement $\mathbf{U}$.

2.8 Fundamental Relations

Very general basic formulations for the analysis of mechanically affected structures, Figs. 2.6 and 2.10, define the setting within a region Ω with boundary Γ. For the interior, Eq. (2.44) defines the residual force on a differential interior element. The boundary is divided into two parts, where boundary conditions are defined in the forms of either defined traction[42] or displacement.[43] It is emphasized in Sect. 2.5.4 that a complete description of the mechanical response can be built on the displacement field $\mathbf{U}$, if the local material response is defined. Here, this is done through a strain energy density function, rather than a stress–strain constitutive relation. The prescribed boundary traction gives indirect constraints on the displacement at the boundaries, while the displacement boundary conditions are more direct. With this setting, the displacement field within the whole region, including boundaries, is the only variable to solve for.

In full agreement with this basic view, mechanical energy, potential and work expressions are given above; power and incremental work are consistently closely related. These formulate the energy balance as integrals over the considered region, and include the displacement and velocity fields. The energy expressions, and, in particular, the virtual work forms in Sect. 2.7, are used as basis for solution methods, and for quantitative descriptions of the state of the structure.

It must in this context again be emphasized that, even if the setting above is described as complete, the treatment is based on models of the real structures. The relevance, completeness and accuracy of these models are determinants for the reliability of the results obtained, and the conclusions from those.

2.8.1 General Equation

The previous section discusses the mechanical problem in an energy context, where power and incremental work represent interior and exterior actions on the region.

[42] in engineering interpreted as driving force

[43] in engineering interpreted as supports, with needed reactive force

Using Eq. (2.84) together with the expressions for virtual work in Sect. 2.7, the virtual energy balance equation gives the very general mechanics equation

$$\int_{\Omega} \rho_X \left(\ddot{\mathbf{U}} \bullet \mathfrak{D}\mathbf{U}\right) \mathrm{d}V + \mathfrak{D}\Pi_p + \mathfrak{D}\Pi_{\mathrm{con}} = \int_{\Gamma_T} \overline{\mathbf{T}}_{\mathrm{non}} \bullet \mathfrak{D}\mathbf{U} \, \mathrm{d}A + \int_{\Omega} \mathbf{B}_{\mathrm{non}} \bullet \mathfrak{D}\mathbf{U} \, \mathrm{d}V \tag{2.92}$$

expressing how the total mechanical energy during the virtual displacement is changed by the virtual work done by non-conservative exterior forcing. The equation is related to a virtual displacement increment $\mathfrak{D}\mathbf{U}$ from the displacement field $\mathbf{U}$.

One interpretation of Eq. (2.92) is that the acceleration field $\ddot{\mathbf{U}}$ is decided by the displacement field $\mathbf{U}$ at each particular time instance t. The equation is obtained from an energy balance formulated by introduction of an arbitrary virtual displacement $\mathfrak{D}\mathbf{U}$. In the continuum case, this must be valid for any legal virtual displacement increment.[44] The same equation is used for subsets of possible increments in the discretized settings of Chap. 3. This usage of the fundamental relations is the main argument for the chosen format of Eq. (2.92).

One main limitation of the stated equation is that an elastic situation is considered, where interior stress is derived from a strain energy density. A consideration of also interior dissipation, according to Sect. 2.6.3, needs[45] modifications to also the right hand side with respect to non-elastic stress $\mathsf{S}_{\mathrm{non}}$.

2.8.2 *The Time Dimension*

In addition to the modelling assumptions regarding the geometry, material and boundary conditions, a fundamental assumption is related to time. Although forcing and response aspects are in reality always time-dependent, it is many times relevant to disregard the dynamics of the processes, and consider the problem in a stationary, time-independent, configuration, where no velocities, and thereby no accelerations, are present. This implies that geometry, material models and boundary conditions, with all their defining parameters, are fixed; this is a common assumption in many engineering analyses.[46]

The distinction between different settings of the mechanical problem is briefly mentioned in the introduction to this Chapter, cf. Sect. 2.1.

A motion problem, where the qualification 'dynamic' is redundant,[47] considers all terms in the mechanics equation, and is necessary when the time dependence of the

[44] where 'legal' here implies that $\mathfrak{D}\mathbf{U} = \mathbf{0}$ on the boundary part Γ_U, as the prescribed value is introduced in $\mathbf{U}$, and no further variation is allowed.

[45] formally rather obvious, but implementation-wise possibly more complex

[46] In the numerical setting of coming Chapters, fixed aspects are denoted 'hard-coded' in the problem definition.

[47] The common term 'dynamic equilibrium' is avoided in this treatise, as it can be considered a contradiction in terms

setting can not be neglected. The response is traced in physical time, possibly under time-varying boundary conditions. An equilibrium case, where also the term 'static' is redundant is time-independent and can be solved as one stationary configuration,[48] with all its response quantities. A parametric equilibrium problem seeks a set of equilibrium solutions for a fictitious, non-physical, time-scale

2.8.3 Time-Dependent Motion

When the setting of the problem is time-dependent in some aspect, a motion problem is solved, and the complete Eq. (2.92) is needed. The interior force residual function in Eq. (2.44) then leads to acceleration within the region. As the residual is referring to a volume element $\mathrm{d}V$ of the initial reference configuration, where the density is ρ_X, the residual force in Eq. (2.44) gives the strong form of the equation of motion, which is written as a balance

$$\rho_X \ddot{\mathbf{U}} = \mathbf{B} + \mathrm{div}_X\,(\mathsf{FS})\,, \tag{2.93}$$

with the body force $\mathbf{B}$ defined at each point $\mathbf{X}$, and the deformation gradient F as well as the 2nd Piola-Kirchhoff stress S consequences of the current displacement field $\mathbf{U}$, with the constitutive parameters $\underline{\Xi}$, cf. Sect. 2.5.4. On the left hand side, $\ddot{\mathbf{U}}$ is the acceleration field, evaluated at point $\mathbf{X}$ and time t, as are the quantities $\mathbf{B}$, F and S, which are truly dependent on physical time[49]; the acceleration field is thereby also a time-dependent quantity. As also the boundary conditions in Sect. 2.5.3 are possibly dependent on t, these conditions use

$$\overline{\mathbf{T}} \equiv \overline{\mathbf{T}}(\mathbf{X}, t) \quad \text{and} \quad \overline{\mathbf{U}} \equiv \overline{\mathbf{U}}(\mathbf{X}, t), \tag{2.94}$$

for their respective boundary surface parts.

The problem is thereby an initial boundary value problem, where initial conditions for the displacement and velocity fields are needed for all $\mathbf{X}$, as

$$\mathbf{U}(t=0) \equiv \overline{\mathbf{U}}_0 \quad \text{and} \quad \dot{\mathbf{U}}(t=0) \equiv \overline{\dot{\mathbf{U}}}_0. \tag{2.95}$$

From the initial conditions, and Eq. (2.93), the time-dependent displacement field is integrated. It is implicitly assumed that the initial conditions fulfill also the boundary conditions, $\overline{\mathbf{U}}_0 = \overline{\mathbf{U}}(\mathbf{X})$ and $\overline{\dot{\mathbf{U}}}_0 = \frac{\mathrm{d}}{\mathrm{d}t}\overline{\mathbf{U}}(\mathbf{X})$ for all points $\mathbf{X}$ in Γ_U.

---

[48] even if several configurations can be possible for the same problem setting

[49] This is a necessary consequence of the assumed velocity for F and S, but is less common for $\mathbf{B}$, as this often represents the gravity of the material; inclusion of centrifugal-type force is one exception.

2.8.4 Time-Independent Equilibrium

Time-independent solutions under constant boundary conditions is a common setting in analyses of the mechanics of engineering structures. This is the case of equilibrium: a stationary situation, in which a configuration remains constant over time if introduced in a time-dependent treatment as an initial condition, together with zero velocity.

Equilibrium can also be an asymptotic state, when all time-dependent effects have been damped out, after a transient introduction or modification to exterior forcing. This solution can be obtained with a motion setting, if exterior and interior parameters are subsequently held constant over time, and some amount of damping is introduced in the system. This corresponds to the dynamic relaxation approach mentioned in Sect. 4.3.1 as one method to solve an equilibrium state. It is noted that not all equilibria can be reached with this approach; a basic requirement is that the equilibrium is stable.

While equilibrium demands that one configuration can be maintained by the structure under constant boundary conditions, stability of the equilibrium state demands even more. Focus is set on neighboring configurations, and motions introduced from these. Stability demands that the deviations from the equilibrium state are limited over time, if a disturbance—in displacement or velocity—to the state is introduced as an initial condition for a motion; all parameters for the problem are frozen. It must also be possible to limit the deviations to any low magnitude by limiting the magnitude of disturbance. Referring to the damping mentioned, the deviation will be decreasing in magnitude, and thereby converge to the equilibrium.

The assumption of stationary conditions allows a simplified solution method, where the stationarity is utilized, and velocity and acceleration are recognized as zero. When the solution to an equilibrium problem is sought, all inertia effects are ignored, and the solution is described by the general Eq. (2.92), with the first term removed. In the balance of linear momentum, Eq. (2.93), this corresponds to the right-hand side vanishing at every point, as any non-zero residual creates acceleration. The defining equation for interior force is then the strong form of the equation of equilibrium

$$\mathbf{B} + \mathrm{div}_X\,(\mathsf{FS}) = \mathbf{0}, \tag{2.96}$$

with body force $\mathbf{B}$ defined for every $\mathbf{X}$ within Ω. The deformation gradient F and the 2nd Piola-Kirchhoff stress S are dependent on the displacement field $\mathbf{U}$ and the constitutive parameters in $\underline{\Xi}$. Boundary conditions are defined, according to Sect. 2.5.3, as

$$\mathbf{T}(\mathbf{X}) = \overline{\mathbf{T}}(\mathbf{X}) \quad \text{and} \quad \mathbf{U}(\mathbf{X}) = \overline{\mathbf{U}}(\mathbf{X}), \tag{2.97}$$

on Γ_T and Γ_U, respectively.

Equations (2.96) and (2.97), together with a constitutive relation, e.g., the used strain energy density expression, define equilibrium as the solution to a strong form

boundary value problem for the displacement field $\mathbf{U}$. All quantities are referred to the initial reference configuration.

A weak form of the stationary boundary value problem demands that a weighted and integrated residual over the region, rather than the point-wise Eq. (2.96), must vanish. Introducing a vector-valued weight function field $\boldsymbol{\omega}$ over the region, this approach evaluates a scalar functional, evaluated from integrals over the initial region and boundary. Starting from

$$\int_{\Omega} (\mathbf{B} + \mathrm{div}_X (\mathsf{FS})) \bullet \boldsymbol{\omega} \, \mathrm{d}V = 0, \tag{2.98}$$

the functional, after some algebra, can be re-written as

$$F(\boldsymbol{\omega}) = \int_{\Omega} \left((\mathsf{FS}) : \mathrm{grad}_X \boldsymbol{\omega} - \mathbf{B} \bullet \boldsymbol{\omega} \right) \mathrm{d}V - \int_{\Gamma_T} \overline{\mathbf{T}} \bullet \boldsymbol{\omega} \, \mathrm{d}A = 0, \tag{2.99}$$

where both F and S are dependent on the displacement field $\mathbf{U}$. The equation must be fulfilled for any field $\boldsymbol{\omega}$ which respects the essential boundary conditions by vanishing on Γ_U.

With the weight functions chosen as $\boldsymbol{\omega} = \mathfrak{D}\mathbf{U}(\mathbf{X})$, i.e., the virtual displacement field in Sect. 2.7, the equations can be interpreted as the principle of virtual work, with Eq. (2.99) identified as the work balance

$$F(\mathfrak{D}\mathbf{U}) = \mathfrak{D}W_p(\mathfrak{D}\mathbf{U}) + \mathfrak{D}W_{\mathrm{ext}}(\mathfrak{D}\mathbf{U}) = 0, \tag{2.100}$$

which is the expression in Eq. (2.92). The virtual displacement field $\mathfrak{D}\mathbf{U}$ is here related to the equilibrium configuration $\mathbf{U}$.

Equation (2.100) describes the balance between the work done by acting interior stress S, body force $\mathbf{B}$ and prescribed boundary traction $\overline{\mathbf{T}}$ during a virtual displacement $\mathfrak{D}\mathbf{U}$. The virtual strain $\mathfrak{D}\mathsf{E}$ is the increment in strain when adding the increment $\mathfrak{D}\mathbf{U}$ to the current displacement field $\mathbf{U}$.

For a conservative exterior forcing, the two terms of Eq. (2.100) are obtained from virtual analogues to Eqs. (2.65) and (2.79), respectively. Also, the right hand side of Eq. (2.92) vanishes, and equilibrium can be interpreted as a demand for a stationary total potential Π, cf. Eq. (2.87). Any (legal) small disturbance $\mathfrak{D}\mathbf{U}$ to the equilibrium displacement field $\mathbf{U}$ must conserve Π. Fulfilling this for any $\mathfrak{D}\mathbf{U}$ demands that

$$\mathrm{grad}_U \Pi = 0. \tag{2.101}$$

The expressions are further simplified if the forcing is displacement-independent.

2.8.5 *Parametric Equilibrium*

The discussion above considers an equilibrium problem, where the setting and parameters are hard-coded, and one solution in most cases can be obtained. In connection with non-linear structural problems and stability analyses, there is always an implicit need to evaluate the parametric dependence of solutions. A sequence of equilibrium configurations is then solved, with the assumption that the sequence sufficiently well describes the parametric dependence. The primary usage of this parametric equilibrium setting is to step-wise solve equilibrium for an increasing forcing, but the same basis can be utilized in other parametric or optimization contexts, cf. Sect. 4.4.

Step-wise solutions in the form of displacement fields $\mathbf{U} = \mathbf{U}_i$ are obtained as equilibria related to a fictitious time, here denoted by τ.[50] Reflecting the usage, the parameter τ is in Chap. 4 used as a fictitious increment measure, often focussing on the graphical presentation of results. Each step i in the sequence is individually solved as above so that $\mathbf{U}_i \equiv \mathbf{U}(\tau_i)$, the difference being that either the body force, the boundary conditions, or, possibly, the material parameters are dependent on τ:

$$\mathbf{B} = \mathbf{B}(\tau), \quad \overline{\mathbf{T}} = \mathbf{T}(\tau), \quad \overline{\mathbf{U}} = \overline{\mathbf{U}}(\tau), \quad \text{or} \quad \underline{\Xi} = \underline{\Xi}(\tau). \tag{2.102}$$

No differentials with respect to τ are relevant in a mechanics interpretation.

Solving the parametric sequence gives a set of equilibrium states, which can be evaluated and interpreted individually, as no time or history is considered. The engineering force-displacement graphs are a typical example, when forcing is successively introduced, but methods for the introduction of general parameters, in a discretized setting, are extensively discussed in Chap. 4.

2.9 Stability

The previous section discusses the fundamental equations for equilibrium and motion. The developed expressions are set within a context of energy, potential, power and work; they emphasize the differences in form due to the assumed form of the acting exterior forcing.

Stability is a key concept for the solutions. The term can be interpreted—and the corresponding quantitative measures evaluated—in different ways dependent on context, but in loose terms implies an insensitivity to small deviations. The fundamental stability criterion used here is the one by Liapunov (1966), which states that stability demands that a small disturbance to a configuration of a mechanical system keeps limited with time; it must not grow. Referring to the cases in Chap. 1, where deflected equilibria are analyzed, these show that neighboring equilibria exist, and thereby that an additional displacement in this direction will not disappear.

[50] to distinguish it clearly from physical time t

In essence, and avoiding some technical details, the Liapunov criterion for stability can be described through a bound for possible disturbances to a state or process, which do not significantly modify the response. The criterion for stability states that for any bound ε on the resulting deviation, however small, there exists a bound γ for the magnitude of an initial disturbance from which the resulting deviation will always be limited by ε. The magnitudes ε and γ are some norms of the deviations. This, in general, causes problems in the continuous case, but these are limited in an energy context.

This section discusses some basic aspects of stability in a continuum context, while the more detailed analyses are discussed in the discretized setting of Chap. 3. The discussion here primarily handles stability of equilibrium, which is the primary focus, and also gives some comments on stability in connection with motion.

2.9.1 Stability of Equilibrium

Equilibrium can, in the general case, be defined through the boundary value problem in Eq. (2.92) with the first term of the left-hand side vanishing. This equation states that, for any virtual displacement increment $\mathfrak{D}\mathbf{U}$, the exterior work $\mathfrak{D}W_{\text{ext}}$ from acting traction and body force creates an increase in strain energy. The exterior work is simplified by Eq. (2.79) for conservative forcing, and even more to Eq. (2.82) when it is displacement-independent. Within the general setting of Eq. (2.92), equilibrium for a conservative problem is defined by Eq. (2.101).

Investigations of the stability of equilibrium traditionally have focussed on cases with conservative forcing, demanding for equilibrium a stationarity of the total potential Π, defined by Eq. (2.87). With all forcing and parameters fixed, this demands that Π must be constant for virtual changes $\mathfrak{D}\mathbf{U}$ to the displacement field $\mathbf{U}$ in the region.

The common static stability criterion for equilibrium demands that the total potential Π is at a local minimum for the current state, i.e., is positive definite. A minimum total potential at the equilibrium state is identified from the second variation of Π. The picturesque interpretation, often shown in literature, is that a ball does not significantly leave the bottom of a bowl when slightly disturbed from its equilibrium, while it rolls off from a hilltop, even if it can be in equilibrium at the precise top. The more mechanical interpretation is that additional positive work from exterior forcing is required for the system to leave the stable equilibrium.

The analogy to a ball in a bowl shows some important properties of the stability of equilibrium. Imagining that the ball is placed, without velocity, at any point within the bowl,[51] the ball will start rolling towards the lowest point, possibly oscillate within the bowl, but can not leave it unless the rim of the bowl is somewhere lower than the position from which the ball was released; with any degree of mechanical damping, the ball will come to rest at the bottom. Depending on the local shape of

[51] which must be higher than the minimum

the bowl, the possible initial disturbed position of the bowl is restricted, but at least a small region must exist around the minimum. Larger disturbances may, however, lead to a departure from the local minimum, and possibly an arrival in another bowl with even lower minimum level. This shows that static stability is a local minimum of the potential. The interpretation of stability is further discussed, for a discretized setting, in Sect. 3.7.

As most treatises on stability of equilibrium discuss cases with displacement-independent exterior forcing, the minimum of the total potential is dependent on the strain energy only, due to the linearity of the exterior potential on $\mathbf{U}$. The same approach is, however, also valid for any conservative problem, when the incremental work $\mathrm{d}W_{\text{ext}}$ is obtained from an exterior potential, according to Eq. (2.79). This quantity is a function of $\mathbf{B}$, $\mathbf{T}$ and $\mathbf{U}$, but in general not linear in $\mathbf{U}$. This implies that terms related to exterior forcing also enter the expressions deciding stability.

With stability demanding a minimum, an unstable equilibrium corresponds to a local maximum of the total potential along, at least, some direction of virtual displacement $\mathfrak{D}\mathbf{U}$; the total potential function resembles a saddle around the equilibrium. The borderline critical equilibrium case, with a neutral energy variation is often the situation sought in investigations. This, primarily, demands an evaluation of the second differential of the energy along any additional displacement from the equilibrium state, but can, in more exotic cases (for which this is zero) demand studies of also higher differentials.

The minimum of the total potential at an equilibrium state can also be interpreted in a dynamic context, where stability demands that the configuration of the structure must stay in a close vicinity to the static equilibrium state if a small disturbance to it is introduced as an initial condition for a motion setting, cf. Sect. 2.8.4. This demand can be studied by considering the total mechanical energy Π_{tot} in Eq. (2.86), which is evaluated for any displacement and velocity fields as $\Pi_{\text{tot}} = \Pi + \Pi_k$, with Π the total potential in Eq. (2.87), and Π_k the kinetic energy, coming from current velocity. After an introduction of a disturbance to displacement and velocity, the configuration contains a total energy Π^*_{tot}. As the kinetic energy Π_k can never be negative, this means that the subsequent motion is bounded by the region in $(\mathbf{U}, \dot{\mathbf{U}})$ space where $\Pi \leq \Pi^*_{\text{tot}}$. Since this region is containing the equilibrium studied, the motion necessarily occurs in the vicinity of the equilibrium. If, further, the region can be made smaller, still containing the equilibrium, by reducing the magnitude of the disturbance, the equilibrium is stable, and is a state of (local) minimum total potential. Any disturbance will then, due to damping, return to the equilibrium. A large enough disturbance may still allow the configuration to escape from the vicinity, and possibly, to arrive at another equilibrium state.

The dynamic viewpoint can also be used in another setting, based on the conservation of Π_{tot} in Eq. (2.86). With a non-zero velocity, and a constant total energy, the movement must lead to a constant exchange of the forms of energy. For stability, the disturbance to initial conditions must therefore lead to a movement around the equilibrium, being an overlay of the harmonic oscillations of the structure. The basis for these oscillations are the eigenmodes of the model, evaluated at the equilibrium.

As further discussed in the context of discretized models, cf. Sect. 3.7, the minimum of total potential or the existence of vibrational eigenmodes are two criteria for the stability of a conservative equilibrium. These are similar, but different in their consideration of structural mass. The conclusions regarding stability are, however, in general the same.

As mentioned above, stability is a property of an equilibrium state, for fixed model and parameters of geometry, material and forcing. This implies that the stability conclusion can vary with any of these parameters, not only the level of forcing. Typically, a certain parameter range corresponds to stable equilibria, while other ranges are unstable. In the general situation, where several parameters are considered, more or less exotic instability situations can exist for specific parameter combinations. Such situations are discussed within catastrophe theory, cf. Gilmore (1981) or Thompson and Hunt (1984), but do not occur for practical problems.[52] The nearness in parametric space and interaction between different instability phenomena can, however, significantly affect the response of a structural model around the instability states.

Quantitatively, judging stability for a continuous formulation has some inherent technical problems regarding norms, as discussed by Como and Grimaldi (1995). With the clear aim set at discretized models, the further discussion on static stability is postponed until Chap. 3.

Non-conservative systems

For structural models where the exterior forcing is non-conservative, and therefore no total potential exists, the investigation of stability of equilibrium is considerably more complex, and no general statements are easily available. The evaluation for a particular situation must therefore always go back to the fundamental definition of Liapunov stability, and investigate the outcome from an arbitrary disturbance to the configuration.

2.9.2 Stability of Motion

Also for a motion, stability is an important aspect. The concept is, however, not unique and can refer to several situations. One instability situation, which is similar to the static stability consideration above, is when a periodic motion is left by a disturbance, and the motion either enters another periodic motion,[53] or diverges into an exponential motion. This instability can occur for disturbances to any of the problem parameters.

[52] unless, e.g., a structural optimization demanding a high lowest value of particular response quantities has given a coincidence between two phenomena (which is a common outcome of such procedures)

[53] typically, with another frequency

The stability criterion from Liapunov (1966) is still, in essence, applicable, but needs some minor modification, where the definition of disturbance must be reconsidered, and related to the orbit of the movement, rather than to the position at each specific time. With such a problem-dependent adaptation, the basic criterion is still valid and useful. In the rather simple example of the rotational movement of a rigid body in Sect. 1.9, with a symmetric body spinning around an axis, stability exists if the axis of the body stays (close to) vertical, regardless of the rotational position of the body.

The problem of stability of motion is not further considered in the present treatise, but the problem is considered in literature.

2.10 Modelling of Reality

The sections of this Chapter develop a general view on structural mechanics problems based on energy and work concepts, leading up to the general mechanics equation in Eq. (2.92). This equation describes the momentum balance in a solution.

The equation is written in order to show the mechanical aspects of different assumptions as clearly as possible. The two main aspects underlying the formulation are the consideration of the dynamics of the region and the properties of the exterior forcing affecting it. The forcing is thereby divided into boundary traction and body force intensity. Both classes of forcing can also be divided into conservative and non-conservative actions. An important class of forcing for the engineering applications consists of displacement-independent cases.

These aspects reflect the assumptions made in engineering analyses, when a physical object or structure is represented by a mathematical or numerical model. This modelling necessarily needs simplifications of the real situation in order to facilitate the needed treatment. A first step is the determination of the physical model of the object, which decides the aspects to consider, as a preparation for the choice of mathematical (and, probably, numerical) models needed for evaluation. The physical model thereby has to be comprehensive enough to cover all relevant responses, but still simplified as far as possible, in order to avoid irrelevant details and excessive calculations. A balance between the details and accuracies of the assumptions made is a key aspect in good structural modelling.

The description above focusses on the modelling of reality in a few aspects. One important aspect is the identification of the relevant region, and—often in engineering—subregions, to describe in a model. The breaking up of complex reality into smaller problems possible to handle has always been a key competence among engineers.

The decision on whether consideration of dynamics, i.e., inertia effects, can be neglected is an important choice, where the inclusion of dynamics normally leads to considerably more demanding analyses. The above general mechanics equation allows the consideration of dynamics, by including the kinetic energy term, but does not include damping and other dissipative terms. Such effects can, with some efforts,

be included as energy losses if a relevant model of the dissipation is available, and possible to express in terms of the displacement and velocity fields.

The representation of acting exterior forcing is also a key aspect in the physical modelling. As clearly seen in the general equation, the treatment of conservative exterior forcing, for which potentials can be formulated, is essentially straight-forward in a physical modelling, while non-conservative contributions are always adding to complexity. As most engineering objects are designed to suffer only limited deformation, the distinction is often of limited importance, and forcing can in the majority of cases be represented as conservative, and even displacement-independent. Exceptions are, e.g., pressure-affected deformable structures, and rotating structures where centrifugal effects need be considered.

A final key aspect in the physical modelling of an object is related to the description of the material used. Although different materials can give very different responses to forcing, the treatment above is limited to elastic materials, for which a strain energy can be formulated. This implies a path-independence of the material response. Within the elastic material descriptions, the developed formulation is, however, very general and allows many common engineering material models, each with several constitutive parameters.

Conclusions from this Chapter

The main conclusion from this Chapter is that full stability evaluations for structural models have to be based on complete and general description of the region kinematics, and the derivations above are thereby completely displacement-based. The formulations must also include non-linear terms in displacement and strain. Although other forms of continuum mechanics formulations are possible and sometimes used, the Chapter proposes a consistent set of strain, stress and energy as the basis for investigations; all are based on the displacement field of the considered region and on the initial, unstrained, reference configuration. The discussed approaches are explicitly aimed at the discretized forms of analysis, being the topics of coming Chapters.

With a strain energy density as the definition of material properties, hyper-elastic material models fit very well into this approach, and some common models are briefly discussed. The strain energy density replaces the more common constitutive relations where stress is defined as a function of strain[54]; stress comes out as a derived quantity here.

The total mechanical energy of a structural model consists of the kinetic and strain energies within the considered region, and it is shown how this energy can be modified by mechanical work from exterior forcing: the energy balance is formulated for increments in displacement, and a distinction is made between physical and virtual increments.

[54] often as a linear constitutive operator

In the setting of energy, potential and work, exterior forcing can be described in different ways. Conservative components, which can be described in the energy form allow somewhat simplified formulations, and more systematic solution approaches. Displacement-independent exterior forcing, which is a common assumption in engineering analyses, allows further simplification of the formulation.

The virtual work balance leads to a general equation for mechanics, which is stated in weak, integrated form. From the general equation, conditions for equilibrium and motion are obtained. Stability is discussed, in general terms, in relation to these expressions. All concepts are further discussed for a discretized setting in the following Chapter.

Tasks for this Chapter

1. A unit cube is defined as $0 \leq (X_1, X_2, X_3) \leq 1$. It is deformed according to: $x_1 = 0.8X_1 + 0.2X_2$, $x_2 = -0.1X_1 + 1.1X_2 + 0.1X_3$, $x_3 = 0.1X_1 - 0.1X_2 + 1.1X_3$. What are the maximum and minimum values of all 2nd Piola-Kirchhoff stress components, if the cube is assumed to follow a Mooney-Rivlin material model with $c_1 = 1\,\text{MPa}$, $c_2 = 0.2\,\text{MPa}$. Verify first that the deformation is incompressible.
2. For the example case in Fig. 2.8 (based on Fig. 2.3), evaluate for three cases the traction vectors T for the displaced area, corresponding to all sides of the initial square, with their respective normal vectors $\mathbf{N}$. From these, evaluate also the traction vectors t on all edges, and related to the deformed area. The three cases are $S_{11} = 1$, $S_{12} = S_{21} = 1$ and $S_{22} = 1$, respectively, with all other stress components zero.
3. Develop, in energy terms, an analytical model for the pressurized spherical membrane in Sect. 1.8, for a linearly elastic material with (E_m, ν_m) as parameters, assuming a local plane stress situation. Describe the displacement field by just the current radius r, with $r = R$ the unstrained configuration. Document necessary and reasonable assumptions in the derivation of equilibrium and stability conditions.
   Hint: the exterior potential from an interior over-pressure is given on page 66.
4. A typical engineering model for a plane beam problem is visualized by a figure below. Give one reasonable and complete set of boundary conditions for the same problem, but modelled as an $L \times h \times w$ continuum problem, identifying the meanings of Γ_T and Γ_U as parts of the total boundary Γ. Use the more general notation for coordinates and components.

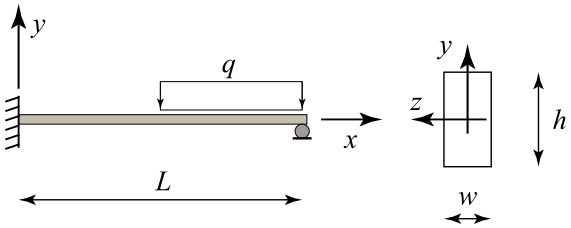

5. Evaluate for the region in the figure below, which is of constant thickness w, the total potential of the problem, if the displacement field and the prescribed boundary traction on the indicated edge are (with a and t the parameters)

$$\mathbf{U} = \begin{pmatrix} -2aX_1X_2 \\ aX_1^2 \\ 0 \end{pmatrix}, \quad \overline{\mathbf{T}} = \begin{pmatrix} -tX_2 \\ 0 \\ 0 \end{pmatrix}.$$

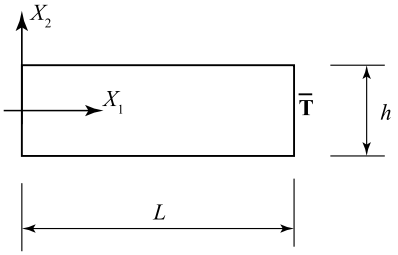

The material of the region is linearly elastic with constants (E_m, ν_m). Use the potential to find the relation between a and t, within these assumptions. **Note** that this is not a solution to a stated problem, but there is still some reason for the assumptions. Which, and to what extent does it make sense?

References

Como M, Grimaldi A (1995) Theory of stability of continuous elastic structures. CRC Press, Boca Raton, FL

Crespo J, Latorre M, Montáns FJ (2017) WYPIWYG hyperelasticity for isotropic, compressible materials. Comput Mech 59(1):73–92

Eriksson A, Nordmark A (2014) Non-unique response of Mooney-Rivlin model in bi-axial membrane stress. Comput Struct 144:12–22

Fung YC (1993) Biomechanics: mechanical properties of living tissues, 2nd edn. Springer, New York

Gilmore R (1981) Catastrophe theory for scientists and engineers. Wiley, New York

Gurtin ME (1982) An introduction to continuum mechanics. Academic Press, Boston

Holzapfel GA (2000) Nonlinear solid mechanics. A continuum approach for engineering. Wiley, Chichester

Holzapfel GA, Gasser TC, Ogden RW (2000) A new constitutive framework for arterial wall mechanics and a comparative study of material models. J Elast 61(1–3):1–48

Liapunov AM (1966) Stability of motion. (Mathematics in science and engineering, Volume 30). Academic Press, New York/London (translated from Russian Doctoral dissertation, Univ. Kharkov 1892)
Malvern LE (1969) Introduction to the mechanics of a continuous medium. Prentice-Hall, Englewood Cliffs
Nguyen QS (2000) Stability and nonlinear solid mechanics. Wiley, Chichester
Thompson JMT, Hunt GW (1984) Elastic instability phenomena. Wiley, Chichester

Chapter 3
Discretization of Structural Models

This Chapter discusses the discretized settings of non-linear and instability-affected structures. The discretization uses a finite set of numerical values to describe the state of the physical model. A key aspect is the introduction of sufficiently wide kinematics in the continuum setting from the previous Chapter.

The discretization is developed as an approximation, with best-fit criteria coming from the governing equation. Several approximation techniques are adopted for the solution of the general mechanics equation. The localized uniform interpolation used in most finite element formulations is developed as an important special case; finite elements are today the main tools for discretization of complex structures. Isogeometric approximation is a recent development with strong potential, and the derivations are equally applicable for this setting. Thin structures, which are particularly sensitive to loss of stability are preferably treated by dimensionally reduced models.

Necessary numerical settings are developed. A special aspect in this is the handling of boundary conditions for the structural problem, as are discretization aspects of symmetry in a problem. The introduction of mechanical constraints for the model is treated. The Chapter also develops the basic forms for evaluation of static stability in discretized models.

Brief Objective of this Chapter

The Chapter discusses, in a general form, efficient and reliable discretization methods for structural mechanics, their basic formulations, constraints and properties, and their capacity to describe stability properties.

A. Eriksson and A. Nordmark, *Structural Stability and Its Computational Modelling*, Computational Methods in Engineering & the Sciences,
https://doi.org/10.1007/978-3-031-36072-5_3

3.1 General Discretization

The previous Chapter develops a consistent set of theoretical concepts and expressions for the treatment of stability-affected structures, or—to be precise—physical models of such structures. The fundamental formulations are stated in an analytical continuum form, based on the consideration of energy and potential terms, and the relations of these to power and work during real and virtual displacement. The main result is a rather general energy-based equation for mechanics, Eq. (2.92), from which solutions are obtained.

The key ingredient in the equation is the displacement field, given as $\mathbf{U} \equiv \mathbf{U}(\mathbf{X}, t)$, i.e., a function of the material point reference position $\mathbf{X}$ and the current time t. All relevant quantities are based on this displacement, with $\mathbf{U}$, as well as $\mathbf{X}$, measured in a fixed $3D$ Cartesian coordinate space. The formulation is thus completely displacement-based; all relevant quantities are derived from $\mathbf{U}$ and a set $\underline{\Xi}$ of material, or constitutive, parameters, and related to a known initial unstretched reference configuration.

In the formulation developed, a differential or incremental virtual displacement $\mathfrak{D}\mathbf{U} \equiv \mathfrak{D}\mathbf{U}(\mathbf{X})$ is introduced. This is of similar form as the displacement $\mathbf{U}$, but is demanded to vanish at the part Γ_U of the region boundary, where $\mathbf{U}$ is prescribed.

As both the displacement and its virtual counterpart are described as functions of material coordinates $\mathbf{X}$, the solution space for the defining equations is of infinite dimension. Analytical solutions to the equations are thereby only available in special cases of clear-cut problems with regular geometries and forcing conditions.

The formulations are based on the geometrical definitions of a region, and, thereby, its boundary. Although the development in Chap. 2 is performed for the full $3D$ continuum, Sect. 2.5 described how engineering objects can often be described as dimensionally reduced to $2D$ or $1D$ regions, with consequent modifications to boundaries, forces and results; this is further discussed below. Even with this simplification, engineering objects are, more often than not, geometrically complex.

The infinite-dimensional displacement description, together with the complex geometries, make analytical solutions impossible, or at least extremely demanding, and some approximation technique is necessary.

Approximations to the analytical solutions can be obtained in several ways, but in order to make maximum use of computers, discretization techniques are the preferred approach. In particular, methods with high degree of generality, in the sense of a maximally wide range of tractable problems, are sought. A few different basic methods are discussed below, with displacement-based finite element ('FE') methods presently considered most relevant for systematic stability investigations.

The fundamental step in the discretization is to replace an analytical function of some arguments[1] with a set of numerical values, the discrete variables, which are used to evaluate the function at needed argument values through some inherent expressions. The discrete variables are collected as a set of N_d values in a numerical

[1] which, in this treatise, are almost exclusively the Cartesian coordinates for the material points in the region

vector $\underline{d}$, which is not a physical vector (as in Chap. 2), but a column matrix of dimension N_d-by-1[2]. The notation for such vectors is the underlined variable name, $\underline{x}$, with a double underlining to denote the corresponding matrices, $\underline{\underline{A}}$. Related to the set of discrete variables, a functional representation is chosen for the representation of the solution field. Through necessary conditions on the representation, the approximation is often a necessary—or, at least strongly suggested—consequence from the choice of discretization variables. Even if other choices are available, the description here starts with considering interpolation descriptions, where function values at a specific set of points are used as discrete variables; this is the situation for (most) finite element methods, but not for isogeometric analysis approximations, for which control point values are the discrete variables.

3.1.1 Interpolation and Curve-Fitting

Discretization can be partly explained as an interpolation or a curve-fitting procedure. Figure 3.1a shows a sine half-wave function $f(t) = \sin \pi t$, approximated by a set of $N_d = 10$ function values at equidistant points in the interval $0 \leq t \leq 1$. With an assumed linear interpolation between these values, denoted as $f_d(t)$ with a subindex 'd' used to denote the approximate function, the function is reasonably approximated[3]. Figure 3.1b shows a square wave function $f(t) = 1$ over a limited interval $0.3 \leq t \leq 0.9$, and its approximation $f_d(t)$ by a sum of $N_d = 64$ sine functions, where amplitudes are the discrete variables, which are chosen for best fit through a least-square criterion. The two examples show the difference between local and global representattion of functions, to be further discussed below. The example also shows the difference in discretization variables: in (a), the variables are the function values at specific arguments, while they are amplitudes without immediate interpretation in (b).

One comment for the further development concerns the interpolation approach. As the discrete points used are all placed on the correct function values, this implies that the approximate function is always on the same side of the correct one for a case with constant sign of curvature. The average error could therefore have been reduced by choosing slightly different discrete values; these could have been obtained through another criterion for best approximation, e.g., a least-squares demand.

The examples also show a few other aspects of discretization. First. it should be obvious that, for both cases, a systematically increased number N_d of discrete variables—within some basic form of approximation—will always give more accurate results; this must be considered as a demand on any useful discretization strategy. Second, the subfigures (c) and (d), which show the first derivatives of the two

[2] N_d is often very large in structural problems

[3] Rather few points are used, to show the difference, which would in this case visibly disappear with higher N_d.

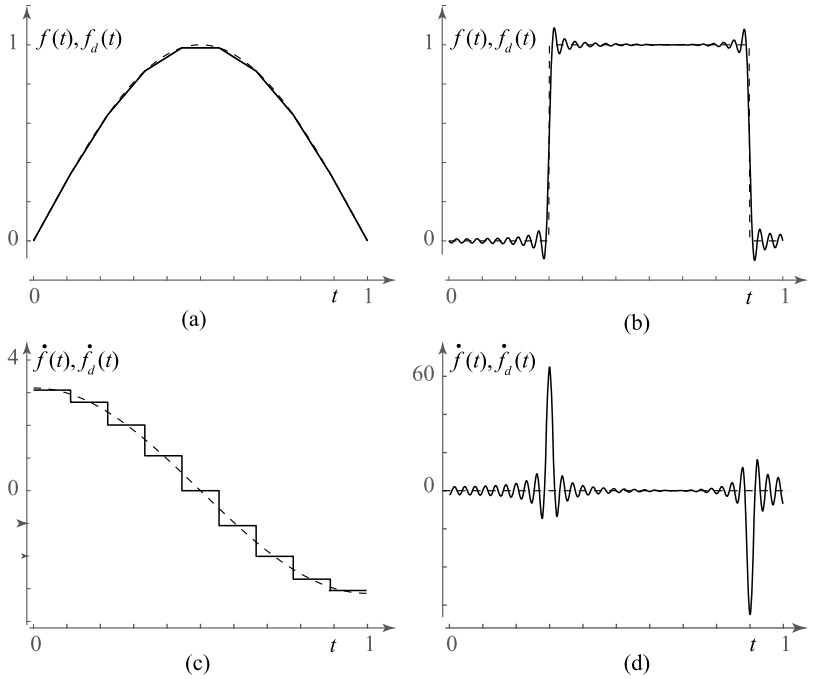

Fig. 3.1 Discretization of known functions. **a** Local approximation by discrete values. **b** Global approximation by function amplitudes. **c**, **d** First derivatives of **a** and **b**, respectively. Dashed lines for function $f(t)$, solid for discretized $f_d(t)$. Superposed dot is time differential

approximate functions, illustrate how the accuracy in relation to the correct functions deteriorates significantly when the approximate function is operated upon.

Two important comments must be made regarding the examples. First, when solving a mechanics problem, the solution is not known as in the figures, but defined by an equation. The fitting or interpolation thereby relates to this equation rather than to the solution. Regarding Fig. 3.1a, the problem could be which discrete function values at the $N_d = 10$ points give the best approximation to the unknown solution of a defining equation. To solve this, a choice must be made of functions using the discrete variables. Second, a criterion is also needed for how the 'best' approximation is defined and evaluated. The obtained result is sometimes strongly affected by these choices.

The basic method of discretized solution, based on local interpolation, can be demonstrated by a simple $1D$ problem example, seeking a function $f_d(t)$ over an interval $0 \leq t \leq 1$, as in Fig. 3.2. Equidistant argument positions t_i, $(1 \leq i \leq N_d)$ are chosen, and the unknown discrete variables are the function values $d_i = f_d(t_i)$, which fully define the sought approximate solution.

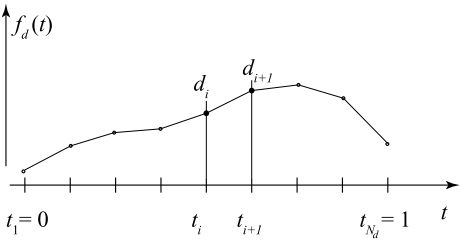

Fig. 3.2 Schematic example of discretized, linearly interpolated, function in $1D$. Function values d_i are used as discrete variables to represent approximations to $f_i = f_d(t_i)$

If the strongly suggested linear interpolation is chosen together with the discrete variables, the solution can be described as a sum of a set of functions over one subinterval each, according to

$$f_d(t) = d_i + \frac{t - t_i}{t_{i+1} - t_i}(d_{i+1} - d_i) = d_i \underbrace{\frac{t_{i+1} - t}{t_{i+1} - t_i}}_{N_i(t)} + d_{i+1} \underbrace{\frac{t - t_i}{t_{i+1} - t_i}}_{N_{i+1}(t)}, \tag{3.1}$$

for $(t_i \leq t \leq t_{i+1})$.

The final member in the equation emphasizes that each discrete variable gives a distinct contribution to the resulting solution, when it acts on a local function within the interval; these are the shape functions in FE terminology; here the term is restricted to cases where all considered variables[4] are uniformly interpolated from their nodal values. The derivative of the local approximation is thereby obtained as

$$\frac{\mathrm{d}f_d}{\mathrm{d}t} = \frac{d_{i+1} - d_i}{t_{i+1} - t_i}. \tag{3.2}$$

for $(t_i < t < t_{i+1})$. This is a constant square wave function within the subinterval, but it is discontinuous at the interval ends; this also applies to the full f_d.

Equation (3.1) is defined only on the interval $t_i \leq t \leq t_{i+1}$. Similar expressions can be formulated for $1 \leq i \leq N_d - 1$, with a function continuity at the discretization points[5]. These function values are the only unknown quantities in the result, as the chosen interpolation is well-defined; at once the discrete variable values are decided, the approximate function, and all its properties are fully known.

[4] which is here just one

[5] With a continuous function, but discontinuous derivatives, the approximate function is said to be C^0 continuous.

3.1.2 Differential Equation

The approximation above is general for the $1D$ case—in the sense that no problem is yet formulated—when a linear interpolation between each pair of two points is defined. To solve for the discrete variables, the expressions is used together with a specific equation, e.g., the ordinary first order differential equation

$$\frac{\mathrm{d}f_d}{\mathrm{d}t} = \pi \cos(\pi t), \tag{3.3}$$

which obviously has a relation to Fig. 3.1a. As the right-hand side of Eq. (3.3) is continuously varying, while Eq. (3.2) is piece-wise constant, perfect matching of the approximation to the equation is impossible. It is, however, possible to demand equality in the midpoint of each subinterval, i.e.,

$$\frac{d_{i+1} - d_i}{t_{i+1} - t_i} = \pi \cos\left(\pi \frac{t_i + t_{i+1}}{2}\right) \quad \text{for} \quad (1 \le i \le N_d - 1); \tag{3.4}$$

this is a collocation approach[6]. As each equation connects two of the unknowns, and Eq. (3.4) states $N_d - 1$ equations in the N_d unknowns, the set of equations is solvable when one solution value, e.g., $d_1 = f_d(0) = 0$ is defined as a boundary condition[7]. The solution to the example problem is shown in Fig. 3.3, where the dotted lines show the contributions from each point to the approximate solution. The discrete variables are here not exactly on the correct solution, as when the function was itself approximated in Fig. 3.1a, but are visibly very close to it, and represent it well, on average.

In the figure is emphasized how each discrete variable contributes by a triangular function with local support on the two subintervals neighboring its argument point. The sum of the triangles gives the final function.

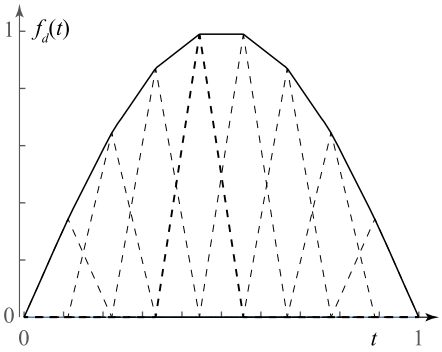

Fig. 3.3 Solution by midpoint collocation to the example $\frac{\mathrm{d}f}{\mathrm{d}t} = \pi \cos(\pi t)$, $f(0) = 0$, obtained by 10 equidistant discrete variables and linear interpolation. Dashed triangles show contribution from each discrete variable, and solid line the final approximate function

[6] which is easily understood, but may be not optimal with respect to accuracy

[7] Of course, this matches the order of the differential equation

It is noted that the choice of criterion for solving the discrete variables in Eq. (3.4) is just one of many reasonable ones. A more natural alternative choice is the least-squares solution, which minimizes the integral, over the whole interval, of the squared residual between the derivative of the discretized function and the defining equation. This gives other values for the discrete variables. even if the solutions are very close in this particular example. Also, the argument points are equidistantly spread over the interval here. This is not necessary, as Eq. (3.1) is equally valid for other sets of t_i. In more realistic problems, such choices of arguments could have been more favorable, for instance, with denser nodes in high curvature intervals. Different methods for evaluating (or estimating) the error in the solution can be used to develop systematic adaptation strategies.

The method suggested by the example shows a rather general approach, but is only applicable when the ordinary differential equation is of order one. In cases with higher order equations, the interpolation described by Fig. 3.2 is not sufficient, as all higher order derivatives of the approximate function are then identically zero. A discretization allowing sufficiently high derivatives is therefore needed. As just one example, sequences of three consecutive argument point could be the basis for quadratic function interpolation, thereby giving meaningful second derivatives in the approximate function. The interpolation and shape functions in general FE methods are extensively discussed in literature, and will be somewhat further discussed below in connection with the mechanical problems.

The basic technique used to solve discretized problems in the examples above will in coming sections be directed towards the mechanical problems of Chap. 2, where the displacement field in a continuum is the basic variable.

3.2 Discretized Balance

When solving mechanics problem, a very general fundamental equation is given in Eq. (2.92); this equation is repeated here as

$$\int_\Omega \rho_X \left(\ddot{\mathbf{U}} \bullet \mathfrak{D}\mathbf{U}\right) \mathrm{d}V + \mathfrak{D}\Pi_p + \mathfrak{D}\Pi_{\mathrm{con}} = \underbrace{\int_{\Gamma_T} \overline{\mathbf{T}}_{\mathrm{non}} \bullet \mathfrak{D}\mathbf{U} \,\mathrm{d}A + \int_\Omega \mathbf{B}_{\mathrm{non}} \bullet \mathfrak{D}\mathbf{U} \,\mathrm{d}V}_{\mathfrak{D}W_{\mathrm{non}}} .$$

Here, the left-hand side expresses the increment in the total mechanical energy, cf. Sect. 2.6.5, coming from virtual work done by the non-conservative exterior forcing on the right-hand side; if this is zero, the energy in the problem is constant during the virtual displacement. All terms in the equation are related to (small) increments $\mathfrak{D}\mathbf{U} \equiv \mathfrak{D}\mathbf{U}(\mathbf{X})$, and to the current displacement field $\mathbf{U} \equiv \mathbf{U}(\mathbf{X}, t)$, with its derivatives, over the whole region $\mathbf{X} \in \Omega$ and for any time t. The arguments to displacement and other fields are omitted below, unless they are of particular interest in an expression.

The first term uses the acceleration, being the second time derivative of $\mathbf{U}$, while the differentials of the strain energy and exterior force potential terms can be replaced by the negatives of the corresponding incremental work forms. The increment $\mathfrak{D}\Pi_p$ to the strain energy in Eq. (2.19)—which is formulated from a chosen strain measure, directly from the displacement—is formulated in differential work form in Eq. (2.89). Increments in potential from conservative exterior force are also given in incremental work as parts of Eq. (2.91). The right-hand side of the equation uses the explicitly formulated non-conservative exterior force together with the virtual displacement field, cf. Eq. (2.91).

A discretized solution method for the mechanics problem must thereby be based on an approximate description of the displacement field $\mathbf{U}_d$ through a set of discrete variables $\underline{d}$, The discrete variables can be dependent on time, as further discussed below. The displacement approximation can thus be time-differentiated for the acceleration field approximation.

3.2.1 Continuum Displacement

Compared to the $1D$ example in Fig. 3.2, the displacement approximation introduces two complexities. According to Fig. 3.4a, the displacement field $\mathbf{U}$ is expressed by three components in the Cartesian coordinate directions, but it is also variable with the three point coordinates[8]. A discretized displacement field in a region, with linear variation of displacement components is thereby

$$\mathbf{U}_d = \begin{pmatrix} U_1 \\ U_2 \\ U_3 \end{pmatrix} = \begin{pmatrix} \alpha_1 + \alpha_2 X_1 + \alpha_3 X_2 + \alpha_4 X_3 \\ \alpha_5 + \alpha_6 X_1 + \alpha_7 X_2 + \alpha_8 X_3 \\ \alpha_9 + \alpha_{10} X_1 + \alpha_{11} X_2 + \alpha_{12} X_3 \end{pmatrix}, \tag{3.5}$$

where the three displacement components in $\mathbf{U}_d$ are independent, and the twelve variables α_i in a discrete vector $\underline{d}$ are polynomial coefficients; note their different dimensions.

When the expression in Eq. (3.5) is adopted for a general tetrahedron with four vertices in space, cf. Fig. 3.4b, the displacement is formulated as an interpolation between nodal displacement components. Following the idea from Eq. (3.1), this is written

$$\mathbf{U}_d = \sum_{j=1}^{4} N_j(\mathbf{X})\, \mathbf{U}_j, \tag{3.6}$$

[8] All expressions in this Chapter use a Lagrangian form, with all quantities expressed in the initial reference coordinates for the points in the region. All quantities are also related to the same Cartesian coordinate system, cf. Sect. 2.1

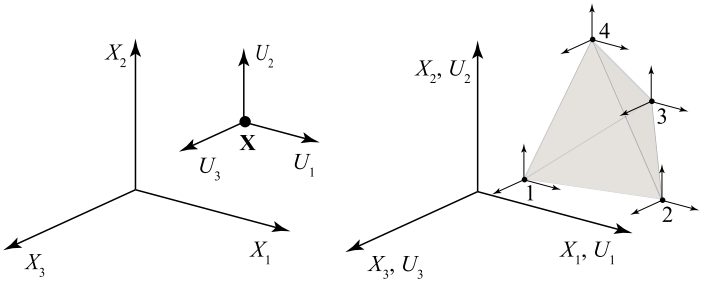

Fig. 3.4 Discretized displacement in $3D$ space. **a** Principle. **b** Interpolation in tetrahedron

where $\mathbf{U}_j$ is a 3-by-1 discrete vector of displacement components

$$\mathbf{U}_j = \begin{pmatrix} U_1(\mathbf{X}_j) \\ U_2(\mathbf{X}_j) \\ U_3(\mathbf{X}_j) \end{pmatrix}. \tag{3.7}$$

with the notation $U_k(\mathbf{X}_j)$ used for the displacement component in direction $\mathbf{e}_k$ at node j with initial reference coordinates $\mathbf{X}_j$. With a uniform interpolation of the displacement components from their nodal values, the four interpolating scalar shape functions $N_j(\mathbf{X})$ are implicitly related to one node each, in the sense that $N_j(\mathbf{X}_\ell) = \delta_{j\ell}$, the Kronecker delta function. The form emphasizes the connection between nodal displacement components and the shape functions, and is common in many discretization efforts, such as the finite elements for continuum problems.

When not necessarily demanding that discrete variables are displacement components at specific points in the region, a more general form of the displacement approximation is

$$\mathbf{U}_d = \underline{\mathbf{N}}\,\underline{d}, \tag{3.8}$$

where $\underline{\mathbf{N}}$ is a displacement operator taking a set of discrete variables into the displacement field; the operator varies with point $\mathbf{X}$. The symbol for this operator emphasizes that the result is (the approximation to) a physical vector, but coming from discrete variables, hence the bold font combined with underlining. The operator should be interpreted as a 1-by-N_d row matrix of basis vector fields $\mathbf{N}_i$ for the displacement representation[9]. These are multiplied by the corresponding discrete variables and added. Although not necessary until later, the expression is given in component form as

$$U_{d\,\alpha} = N_{\alpha i}\, d_i \tag{3.9}$$

[9] each with value dependent on $\mathbf{X}$

where Greek letters are used for components related to material coordinates, and lower-case Arabic letters to components in the discrete variables, with a summation over repeated indices implied. The component form resolves any ambiguity in the use of matrices and vectors.

Specifically for the uniformly interpolated tetrahedron example, this formalism uses twelve basis vectors for the displacement field

$$\underline{\mathbf{N}} = (N_1(\mathbf{X})\mathbf{e}_1, N_1(\mathbf{X})\mathbf{e}_2, N_1(\mathbf{X})\mathbf{e}_3, N_2(\mathbf{X})\mathbf{e}_1, \ldots, N_4(\mathbf{X})\mathbf{e}_3), \tag{3.10}$$

and twelve discrete variables in

$$\underline{d} = \begin{pmatrix} U_1(\mathbf{X}_1) \\ U_2(\mathbf{X}_1) \\ U_3(\mathbf{X}_1) \\ U_1(\mathbf{X}_2) \\ \vdots \\ U_3(\mathbf{X}_4) \end{pmatrix}. \tag{3.11}$$

The dots in the expressions emphasize the identical repetitions for the considered nodes. It must also be noted that the indices on N do not agree between Eqs. (3.9) and (3.10). The components in Eq. (3.9) can here be identified from the shape functions in Eq. (3.6) as

$$\begin{aligned} N_{11} = N_{22} = N_{33} = N_1(\mathbf{X}) \quad ; \quad N_{14} = N_{25} = N_{36} = N_2(\mathbf{X}); \\ N_{17} = N_{28} = N_{39} = N_3(\mathbf{X}) \quad ; \quad N_{1\,10} = N_{2\,11} = N_{3\,12} = N_4(\mathbf{X}), \end{aligned} \tag{3.12}$$

with all other components zero. This is a consequence from the uniform interpolation of the three displacement components in the example. For other representations, e.g., the cases in Sect. 3.4.2 below, nodal quantities have different meanings and are not identically approximated. These cases are still described by Eq. (3.8), but not necessarily similar to the simple structure of shape functions multiplied by axis unit vectors as in Eq. (3.10).

The example form above is obviously not good enough for the full representation of a solution to any interesting problem consisting of just a tetrahedron-shaped structure. Forms of higher complexity can be formulated from the same logic as above by introducing more nodes, and interpolating from these, i.e., in the form in Eq. (3.6), cf. Sect. 3.3.1.

Leaving the example, the general displacement interpolation defined in Eq. (3.8)—which is the basis for further development below—allows much more freedom in the choice of discrete variables and corresponding approximations; the connection to displacement components at nodes is not necessary. The key requirement in the expression is the linearity in the discrete variables.

In contrast to the example above, a non-uniform treatment of the three displacement components in Eq. (3.5) is also sometimes preferable. This can imply different orders of interpolation in the three directions, or other types of variables for the displacement description, e.g., rotations. Other strategies for approximation, like in isogeometric analysis methods introduce specific meanings of discrete variables and, thereby, corresponding basis vector fields in the approximation. All these cases fit formally well into Eq. (3.8), but special properties of a chosen approximation may strongly affect the algorithmic handling of resulting expressions.

3.2.2 Derivatives and Differentials

The previous section discusses a discretized representation of the displacement field in a $3D$ continuum, expressed in the general form of Eq. (3.8), with a set of basis vector fields, which are combined through the set of discrete variables. For the solution to specific problems, the setting can be further clarified by emphasizing the dependencies of the parts as

$$\mathbf{U}_d \equiv \mathbf{U}_d(\mathbf{X}, t) = \underline{\mathbf{N}}(\mathbf{X})\, \underline{d}(t), \tag{3.13}$$

where the scalar functions used for creation of the basis fields $\underline{\mathbf{N}}$ are representing the interior geometry of the initial reference configuration, while the whole description of a current configuration lies in the discrete variables $\underline{d}$. This form is relevant whether or not a real time-dependence is implied by t.

For any discretized continuum, the operator $\underline{\mathbf{N}}$ is of dimension 3-by-N_d, when the vector $\underline{d}$ contains N_d variables. In the interpolated tetrahedron example (with $N_n = 4$ nodes), the number $N_d = 3N_n = 12.$, but N_d need not be connected to a number of nodes in other approximation approaches.

As the approximation, regardless of which approach is used, is required to be linear in the discrete variables, this implies that

$$\mathbf{U}_d + \mathrm{d}\mathbf{U}_d = \underline{\mathbf{N}}\left(\underline{d} + \mathrm{d}\underline{d}\right) = \underline{\mathbf{N}}\,\underline{d} + \underline{\mathbf{N}}\,\mathrm{d}\underline{d}, \tag{3.14}$$

when any incremental displacement is described by the same basis fields, and a set of corresponding discrete components. This must be considered a fundamental—and very natural—requirement on the choice of approximation, and gives the virtual displacement field as

$$\mathfrak{D}\mathbf{U}_d = \underline{\mathbf{N}}\,\mathfrak{D}\underline{d} \tag{3.15}$$

with $\mathfrak{D}\underline{d}$ a numerical vector representing an arbitrary discretized virtual displacement field.

That the current and virtual displacement fields are given identical descriptions does not utilize that the virtual displacement field is more restricted and does not allow any virtual displacement in the boundary part Γ_U. This restriction is introduced

as constraints at a later stage of the treatment. It is also noted that the virtual term included in Eq. (3.15) is completely arbitrary within the displacement approximation, but is still only a subset of the displacement fields possible in the continuum view.

The linearity and the separation in Eq. (3.13) also imply that the time differentials of the approximate displacement field are easily obtained as the velocity field

$$\dot{\mathbf{U}}_d = \underline{\mathbf{N}}\,\dot{\underline{d}}, \tag{3.16}$$

and the acceleration field

$$\ddot{\mathbf{U}}_d = \underline{\mathbf{N}}\,\ddot{\underline{d}}, \tag{3.17}$$

with $\dot{\underline{d}}$ and $\ddot{\underline{d}}$ the successive time differentials of the discrete variables.

In the mechanics equation, first derivatives of the displacement field $\mathbf{U}$ with respect to the reference coordinates $\mathbf{X}$ frequently occur. Related to the approximate deformation gradient F_d, a displacement gradient is expressed as a tensor

$$\mathsf{D}_d = \mathrm{grad}_X \mathbf{U}_d = \mathsf{F}_d - \mathsf{1} = \underline{\mathsf{N}}_F\,\underline{d}, \tag{3.18}$$

where $\underline{\mathsf{N}}_F$ is a displacement gradient operator, being formally a 1-by-N_d row matrix of basis tensor fields, and gives the requested displacement gradient when combined through the discrete variables in $\underline{d}$. In component form, Eq. (3.18) is expressed as

$$D_{d\,\alpha\beta} = N_{F\,\alpha\beta i}\,d_i, \tag{3.19}$$

using the summation convention.

The operator $\underline{\mathsf{N}}_F$ is a structure with three dimensions, where two are residing in the physical space, and one in the discrete variable vector, hence the notation with sans serif font and one underline. It is described by the components

$$N_{F\,\alpha\beta i} = \frac{\partial}{\partial X_\beta} N_{\alpha i}, \tag{3.20}$$

which are the derivatives of the expressions in Eq. (3.8) with respect to the material coordinates. It is obvious that large parts of the operator are identically zero, as only a limited number of discrete variables affect each of the displacement components. The displacement gradient operator can be evaluated at any point $\mathbf{X}$.

Returning to the tetrahedron example, the uniform interpolation of the displacement field components simplifies the formulation of the operator $\underline{\mathbf{N}}_F$.

The expressions in Eqs. (3.13)–(3.17) are systematically introduced in Eq. (2.92), after some algebra on the terms included. The displacement gradient in Eq. (3.18) is used in the development of differentials to the residual equation, needed in the treatment of the problems. The results from these expressions are discussed in the next section.

3.2.3 *Virtual Work Terms*

A general form of displacement approximation is introduced by Eq. (3.8), and the consequent approximations to other displacement-related quantities are derived in the previous section. These are here introduced in the general mechanics Eq. (2.92), in order to allow discretized solutions. The result is a general discretized mechanics equation, which is consistently based on Eq. (3.8).

Kinetic energy

The first term in Eq. (2.92) is related to the acceleration and inertia, and comes from the increment in kinetic energy, according to Eqs. (2.63) and (2.88). Using Eqs. (3.15) and (3.17) for the discretized form, the term can be written

$$\begin{aligned} \mathfrak{D}\Pi_k &= \int_\Omega \rho_X \left((\underline{\mathbf{N}}\, \mathfrak{D}\underline{d}) \bullet (\underline{\mathbf{N}}\, \ddot{\underline{d}}) \right) \mathrm{d}V = \mathfrak{D}d_i \left(\int_\Omega \rho_X \, N_{\alpha i} N_{\alpha j} \, \mathrm{d}V \right) \ddot{d}_j \\ &= \mathfrak{D}\underline{d}^{\mathrm{T}} \underline{\underline{M}}\, \ddot{\underline{d}}. \end{aligned} \tag{3.21}$$

where the component form in the third member—which is a triple sum—is used to more clearly demonstrate the contents. In the final member, $\underline{\underline{M}}$ is the mass matrix for the discretized structural model region.

The component form shows that the mass matrix is related to the discrete variables from both sides, and thereby is of dimension N_d-by-N_d. From the formulation, it is also ascertained to be symmetric and positive-definite[10], i.e., non-singular, and defined completely by the geometry and material.

With $\underline{\mathbf{N}}$ interpreted as a 3-by-N_d matrix, the mass matrix is expressed as

$$\underline{\underline{M}} = \int_\Omega \rho_X \, \underline{\mathbf{N}}^{\mathrm{T}} \underline{\mathbf{N}} \, \mathrm{d}V. \tag{3.22}$$

where the $\underline{\mathbf{N}}$ operator is dependent on $\mathbf{X}$; it is straight-forwardly evaluated when the displacement approximation is developed from Eq. (3.8)

Strain energy

The virtual term $\mathfrak{D}\Pi_p$ in Eq. (2.92) is a bit more complex. The contraction of the two tensors S and $\mathfrak{D}\mathsf{E}$ in Eq. (2.89) is not easily and clearly set in linear algebra form, without re-formulation of its contents.

[10] given that density is positive everywhere

A common treatment is based on the so-called Voigt form, where the symmetric stress tensor S is handled through a 6-by-1 vector. With a slight abuse of notation, S is symbolically expressed as a column vector

$$\mathbf{S} = (S_{11}, S_{22}, S_{33}, S_{23} = S_{32}, S_{31} = S_{13}, S_{12} = S_{21})^{\mathrm{T}}\,, \tag{3.23}$$

with components related to the physical vector space. Correspondingly, the Green-Lagrange strain tensor is expressed as a vector

$$\mathbf{E} = (E_{11}, E_{22}, E_{33}, E_{23} + E_{32}, E_{31} + E_{13}, E_{12} + E_{21})^{\mathrm{T}}\,, \tag{3.24}$$

with a virtual counterpart $\mathfrak{D}\mathbf{E}$. In the Voigt form, the virtual strain energy in the continuum case can be expressed as a scalar product of these vectors

$$\mathfrak{D}\Pi_p = \int_{\Omega} \mathfrak{D}\mathbf{E} \bullet \mathbf{S}\,\mathrm{d}V \tag{3.25}$$

again with a simplified notation, and noting that stress and virtual strain are point-wise values, i.e., dependent on $\mathbf{X}$, but also related to time t.

In the virtual strain energy term, S and $\mathbf{S}$ contain the current stress at the solution, independent of how it is calculated. The virtual strain must consider the non-linearity in the strain-displacement relation; this is further discussed below.

While Eq. (3.25) can be used after a modification of the stress and strain tensors, a formulation more consistent with the form of Eq. (3.8) is developed and used here.

Based on the component form of the Green-Lagrange strain tensor E as, cf. Eq. (2.17),

$$E_{\alpha\beta} = \frac{1}{2}\left(\frac{\partial U_\alpha}{\partial X_\beta} + \frac{\partial U_\beta}{\partial X_\alpha} + \frac{\partial U_\gamma}{\partial X_\alpha}\frac{\partial U_\gamma}{\partial X_\beta}\right), \tag{3.26}$$

the components of the discretized strain can be written

$$E_{d\,\alpha\beta} = \frac{1}{2}\left(N_{F\,\alpha\beta i}\,d_i + N_{F\,\beta\alpha i}\,d_i + d_j\,N_{F\,\gamma\alpha j}N_{F\,\gamma\beta i}\,d_i\right), \tag{3.27}$$

and the approximate strain tensor is evaluated from a discretized strain operator

$$\mathsf{E}_d = \left(\underline{\mathsf{B}}_0 + \underline{d}^{\mathrm{T}}\underline{\underline{\mathsf{B}}}_1\right)\underline{d}, \tag{3.28}$$

giving the strain tensor—at a point $\mathbf{X}$—from current discrete variables $\underline{d}$. The notation with a strain operator named 'B' is very common, and kept here. This should not cause any confusion with the body force, denoted as the vector $\mathbf{B}$.

The operators in Eq. (3.28) are, respectively, a row vector and a matrix of tensors, i.e., structures of dimensions three and four. The notation is chosen to reflect that the operators $\underline{\mathsf{B}}_0$ and $\underline{\underline{\mathsf{B}}}_1$ take one and two discrete vectors to create a tensor. This

emphasizes the property of this particular strain tensor to consist of one part linear and one quadratic in the displacement. As with the operators defined above, these need be re-formulated for the algorithmic implementation, where typically only linear algebra tools are immediately available.

The two operators needed to define the discretized strain tensor are component-wise defined as

$$B_{0\alpha\beta i} = \frac{1}{2}\left(N_{F\,\alpha\beta i} + N_{F\,\beta\alpha i}\right), \tag{3.29}$$

and

$$B_{1\,\alpha\beta ij} = \frac{1}{2} N_{F\,\gamma\alpha j} N_{F\,\gamma\beta i}, \tag{3.30}$$

which are completely defined by the chosen approximation. With a current displacement, described by $\underline{d}$, the current strain can be evaluated by Eqs. (3.28)–(3.30) for any point $\mathbf{X}$.

A discretized virtual strain operator—giving $\mathfrak{D}\mathsf{E}_d$ from a virtual displacement increment $\mathfrak{D}\underline{d}$ at a displacement defined by $\underline{d}$—is formally derived based on Eq. (3.28). Noting the quadratic term, this becomes

$$\mathfrak{D}\mathsf{E}_d = \left(\underline{\mathsf{B}}_0 + \underline{d}^{\mathrm{T}}\underline{\underline{\mathsf{B}}}_2\right)\mathfrak{D}\underline{d} = \underline{\mathsf{B}}(\underline{d})\,\mathfrak{D}\underline{d}, \tag{3.31}$$

where the components of $\underline{\underline{\mathsf{B}}}_2$ are

$$B_{2\,\alpha\beta ij} = \frac{1}{2}\left(N_{F\,\gamma\alpha j} N_{F\,\gamma\beta i} + N_{F\,\gamma\alpha i} N_{F\,\gamma\beta j}\right) \equiv B_{1\,\alpha\beta ij} + B_{1\alpha\beta ji}, \tag{3.32}$$

which indicates a degree of symmetry in expressions. The operator $\underline{\mathsf{B}}$ is a non-linear basis tensor field for virtual strains.

The strain components in Eq. (2.17) agree with Eq. (3.26) for $(\alpha, \beta) = (1, 1)$, and $(1, 2)$, respectively. Equation (3.28) gives for the discretized strain components

$$\begin{aligned} E_{d\,11} &= \frac{\partial U_{d\,1}}{\partial X_1} + \frac{1}{2}\frac{\partial U_{d\,\gamma}}{\partial X_1}\frac{\partial U_{d\,\gamma}}{\partial X_1}, \\ E_{d\,12} &= \frac{1}{2}\left(\frac{\partial U_{d\,1}}{\partial X_2} + \frac{\partial U_{d\,2}}{\partial X_1} + \frac{\partial U_{d\,\gamma}}{\partial X_1}\frac{\partial U_{d\,\gamma}}{\partial X_2}\right), \end{aligned} \tag{3.33}$$

The corresponding virtual strain increments are, according to Eq. (3.31),

$$\begin{aligned} \mathfrak{D}E_{d\,11} &= \frac{\partial \mathfrak{D}U_{d\,1}}{\partial X_1} + \frac{\partial U_{d\,\gamma}}{\partial X_1}\frac{\partial \mathfrak{D}U_{d\,\gamma}}{\partial X_1}, \\ \mathfrak{D}E_{d\,12} &= \frac{1}{2}\left(\frac{\partial \mathfrak{D}U_{d\,1}}{\partial X_2} + \frac{\partial \mathfrak{D}U_{d\,2}}{\partial X_1} + \frac{\partial U_{d\,\gamma}}{\partial X_1}\frac{\partial \mathfrak{D}U_{d\,\gamma}}{\partial X_2} + \frac{\partial U_{d\,\gamma}}{\partial X_2}\frac{\partial \mathfrak{D}U_{d\,\gamma}}{\partial X_1}\right). \end{aligned} \tag{3.34}$$

As formulated here, it is obvious that the common linear virtual strain terms are obtained for small—or zero— displacement, when all $\frac{\partial U_{d\alpha}}{\partial X_\beta} \approx 0$. The linear strain operator $\underline{\mathsf{B}}_0$ at any point $\mathbf{X}$ is thereby independent of the current displacement. The operator $\underline{\underline{\mathsf{B}}}_2$ is also in itself independent, but is multiplied by a specific $\underline{d}$ in the virtual strain operator $\underline{\mathsf{B}}$.

The current discretized stress tensor S_d at any point $\mathbf{X}$ is evaluated from the strain coming from Eq. (3.28) at a specific $\underline{d}$, and is thereby also non-linearly dependent on current displacement. This follows from the assumption of an elastic[11] material model.

The virtual strain work term in Eq. (2.92), following the above expressions, is evaluated from Eqs. (2.64), (2.65) and (2.89) as

$$\begin{aligned} \mathfrak{D}\Pi_p = \int_\Omega \mathsf{S}_d : \mathfrak{D}\mathsf{E}_d \, \mathrm{d}V \equiv \int_\Omega \mathfrak{D}\mathsf{E}_d : \mathsf{S}_d \, \mathrm{d}V = \\ = \mathfrak{D}\underline{d}^{\mathrm{T}} \left(\int_\Omega \underline{\mathsf{B}} : \mathsf{S}_d \, \mathrm{d}V \right)^{\mathrm{T}}, \end{aligned} \tag{3.35}$$

with a contraction of the virtual strain operator and the current stress tensor. The seemingly unnecessary transposition of the factors is performed in order to obtain all terms in the final equations as column vectors. After this, a discrete internal force[12] vector of dimension N_d-by-1 is defined as

$$\underline{p} = \left(\int_\Omega \underline{\mathsf{B}} : \mathsf{S}_d \, \mathrm{d}V \right)^{\mathrm{T}}, \tag{3.36}$$

Derived here from a virtual energy term, the expression is more general, and allows also non-conservative stress formulations, according to Eq. (2.83). This is not a main consideration in the sequel.

As a special case, the strain operator is $\underline{\mathsf{B}} \equiv \underline{\mathsf{B}}_0$ for linear strain assumptions, or for small initial displacement. If also the constitutive relation is linear, then Eq. (2.24) gives $\mathsf{S}_d = \mathcal{K}\,\mathsf{E}_d$ for any strain, with a constitutive tensor $\mathcal{K}$. The virtual work expression is then further simplified into

$$\mathfrak{D}\Pi_p = \mathfrak{D}\underline{d}^{\mathrm{T}} \underline{\underline{K}}\, \underline{d} \qquad \text{or} \qquad \underline{p} = \underline{\underline{K}}\, \underline{d}, \tag{3.37}$$

[11] but not necessarily linearly elastic

[12] where internal is used for the representation of the interior forces in the form of stresses, in a vector form conjugated to the discrete variables used,

with a constant, linear stiffness matrix, of which the components are

$$K_{ij} = \int_{\Omega} \left(B_{0\alpha\beta i} \mathcal{K}_{\alpha\beta\gamma\delta} B_{0\gamma\delta j} \right) \mathrm{d}V, \tag{3.38}$$

which is symmetric in i and j, following from geometry and material. The expression is recognized from common linear finite element forms.

Without the linearity assumptions, no stiffness matrix can be formulated to give the virtual strain work immediately from the discretized displacement, and the discrete internal force must be evaluated through Eq. (3.36).

Exterior forcing

The exterior forcing of a structural model gives rise to one term on the left-hand side of Eq. (2.92), and two terms on the right-hand side. Conservative forcing is described through a variation of the potential Π_{con}, while non-conservative ones are introduced more directly through their incremental work during a virtual displacement.

In a general case, all forcing is introduced—in a form conjugated to the discrete displacement variables—as a discrete external force vector[13]

$$\underline{f} = \underline{f}_{\text{con}} + \underline{f}_{\text{non}}. \tag{3.39}$$

The conservative exterior force is obtained from the virtual work expression

$$\mathfrak{D} W_{\text{con}} = -\mathfrak{D} \Pi_{\text{con}} = \mathfrak{D} \underline{d}^{\mathrm{T}} \, \underline{f}_{\text{con}}, \tag{3.40}$$

where the force vectors are obtained as[14]

$$\underline{f}_{\text{con}} = \left(\int_{\Gamma_T} \underline{\mathbf{N}} \bullet \operatorname{grad}_U \pi_t \, \mathrm{d}A + \int_{\Omega} \underline{\mathbf{N}} \bullet \operatorname{grad}_U \pi_b \, \mathrm{d}V \right)^{\mathrm{T}}. \tag{3.41}$$

The non-conservative terms can similarly be collected and re-written as

$$\underline{f}_{\text{non}} = \left(\int_{\Gamma_T} \underline{\mathbf{N}} \bullet \overline{\mathbf{T}}_{\text{non}} \, \mathrm{d}A + \int_{\Omega} \underline{\mathbf{N}} \bullet \mathbf{B}_{\text{non}} \, \mathrm{d}V \right)^{\mathrm{T}}. \tag{3.42}$$

---

[13] where a notational distinction is made between the exterior forcing in the form of boundary tractions and body force, and the external force vector being conjugated to the discrete variables in $\underline{d}$.

[14] using Eq. (2.79) and its virtual counterpart together with Eq. (3.15)

The expressions above transform the exterior traction and the body force to a discrete external equivalent force vector of dimension N_d-by-1. In most cases, the exterior force expressions $\overline{\mathbf{T}}_{\text{non}}$ and $\mathbf{B}_{\text{non}}$ are dependent on the current displacement $\mathbf{U}_d$, i.e., on the discrete components in $\underline{d}$.

For a conservative setting, only $\underline{f}_{\text{con}}$ is left as the representation of exterior forcing. It is noted that also conservative forcing can be evaluated through the more general Eq. (3.42) if this is considered a more attractive form than Eq. (3.41).

It is obvious from the notation, which brings discrete variables into vector space displacement, that the discrete representation of the exterior forcing is inherently related to the chosen discrete variables and the corresponding approximation functions for the structural model. The 'equivalent' reflects this relation to the specific displacement representation.

When the force is displacement-independent, Eq. (3.41) is further simplified, by the linearity of the exterior force potential in the displacement, according to Sect. 2.6.3, and

$$\underline{f}_{\text{con}} = -\left(\int_{\Gamma_T} \underline{\mathbf{N}} \bullet \overline{\mathbf{T}} \, \mathrm{d}A + \int_{\Omega} \underline{\mathbf{N}} \bullet \mathbf{B} \, \mathrm{d}V \right)^{\mathrm{T}}, \tag{3.43}$$

where the forcing quantities $\overline{\mathbf{T}}$ and $\mathbf{B}$ are constant fields[15]. This is a very common situation in engineering analysis, when the expressions for the forcing can be of arbitrary complexity, as long as they are independent of the displacement. This is the case when exterior forcing is defined through directions and positions in relation to the material configuration. A computational advantage is that the discrete external force vector need be evaluated just once.

3.2.4 Discretized Mechanics Equation

The previous section develops the virtual work terms in the general Eq. (2.92) with respect to the discretized displacement representation in Eq. (3.8), with its consequent expressions in Eqs. (3.15) and (3.17). Collecting all the resulting terms gives the discretized mechanics equation

$$\mathfrak{D}\underline{d}^{\mathrm{T}} \left(\underline{\underline{M}}\ddot{\underline{d}} + \underline{p} - \underline{f}_{\text{con}} \right) = \mathfrak{D}\underline{d}^{\mathrm{T}} \left(\underline{f}_{\text{non}} \right), \tag{3.44}$$

which must be valid for any legal virtual discretized displacement increment $\mathfrak{D}\underline{d}$.[16] With a problem definition through a constitutive expression, and expressions for the

[15] This is the key difference in relation to the more general Eq. 3.42, which formally looks very similar, but allows arbitrary descriptions of exterior forcing.

[16] fulfilling the essential boundary conditions, as discussed in Sect. 3.5, but this is neglected at this stage

exterior forcing, the equation is only dependent on the operator $\underline{\mathbf{N}}$, which reflects the geometry and the chosen discrete variables. The equation is straight-forwardly adapted to any specific setting.

The expression in Eq. (3.44) is a very general formulation for a mechanical problem, including dynamics, but without damping; consideration of this aspect would include terms related to velocity. In the most general form, it includes conservative and non-conservative contributions to the external force vector. Non-conservative stress, as in Eq. (2.83), is included in the internal force in Eq. (3.36), but is not further considered here.

3.2.5 *Discretized Equilibrium*

The first term in Eq. (3.44) vanishes when studying equilibrium, and the remainder can be written, noting the arbitrariness of $\mathfrak{D}\underline{d}$, as the discretized equilibrium equation

$$\underline{p} = \underline{f} \quad \text{or} \quad \underline{r} \equiv \underline{p} - \underline{f} = \underline{0}, \tag{3.45}$$

with $\underline{r}$ a discrete residual force vector expressed in relation to the discrete variables, and representing a balance between internal force $\underline{p}$ and external force $\underline{f}$. The latter may contain conservative as well as non-conservative contributions.

Regarding the discrete internal force $\underline{p}$ in Eq. (3.45), this is derived from the incremental strain energy or work $\mathfrak{D}\Pi_p \equiv -\mathfrak{D}W_p$ in Eq. (3.35). The simplification of this term in Eq. (3.37)—as a stiffness matrix $\underline{\underline{K}}$ multiplied with the total discrete vector $\underline{d}$—is, however, normally not relevant in any stability problem; some non-linearity must be present in the problem. This non-linearity is very seldom present only in $\underline{f}$, and such cases are not further considered.

When equilibrium is defined by either of the forms in Eq. (3.45), this defines a set of non-linear equations in the discrete variables. It must be noted that the equation is expressed as the full set of equilibrium equations, where no consideration is given to the displacement boundary conditions on the boundary part Γ_U. The equations should thereby be read in such a way that either these boundary conditions are introduced at a later stage, or that the two force vectors are already condensed such that only forces conjugate to 'free' or unrestricted displacement variables remain, cf. the discussion in Sect. 4.1.

Problem classes

The discretized equilibrium equation in Eq. (3.45) is quite general, and can be adapted to many problem classes. A few special settings are common in engineering, and are considered here, as a background to the solution methods in Chap. 4. The cases are distinguished through the arguments to the force vectors.

The least complex form of non-linear equilibrium function is

$$\underline{r}(\underline{d}) = \underline{p}(\underline{d}) - \underline{f}, \tag{3.46}$$

with a fixed, displacement-independent, external force[17]. The discrete vector $\underline{d}$ is solved for equilibrium using, e.g., the methods in Sect. 4.1.5.

Commonly, non-linear problems consider a parametric exterior forcing, giving[18]

$$\underline{r}(\underline{d}, \lambda) = \underline{p}(\underline{d}) - \lambda \underline{f}', \tag{3.47}$$

where the prime denotes a constant 'force pattern' $\underline{f}' \equiv \underline{f}_{,\lambda}$, and the forcing level is defined through λ. The force is displacement-independent, thus conservative. A set of equilibrium states for variable λ is solved in this case, e.g., according to Sect. 4.1.6.

For more complex situations, the forcing is dependent also on displacement, and the equilibrium equation is

$$\underline{r}(\underline{d}, \lambda) = \underline{p}(\underline{d}) - \underline{f}(\underline{d}, \lambda), \tag{3.48}$$

where the forcing level is described by λ and the displacement-dependence coming from, e.g., pressure on a structure undergoing finite displacement. When also internal force is affected by some parameter, the defining form is

$$\underline{r}(\underline{d}, \lambda) = \underline{p}(\underline{d}, \lambda) - \underline{f}(\underline{d}, \lambda). \tag{3.49}$$

The two latter forms are best treated by methods in Sect. 4.4. They also allow non-conservative forcing situations.

Depending on the problem at hand, the non-linearity is more or less pronounced, and demands versions of iterative solution methods, as discussed in Chap. 4.

3.2.6 *Differential of Equilibrium*

Equation (3.45) expresses equilibrium for a discretized model, by demanding work balance for an arbitrary virtual displacement from the state. For full investigation of the equilibrium, it is also necessary to express how increments to exterior forcing relate to increments in displacement.

The most general expression considered for the residual force in Eq. (3.49) gives that the full differential of the residual force is

$$\mathrm{d}\underline{r} = \underline{r}_{,\underline{d}}\, \mathrm{d}\underline{d} + \underline{r}_{,\lambda}\, \mathrm{d}\lambda, \tag{3.50}$$

[17] evaluated from the exterior forcing, through the reference geometry

[18] It is conceivable, but uncommon, to introduce the force description through a general function $\underline{f} \equiv \underline{f}(\lambda)$

where the comma index notation denotes a differentiation with respect to the index variable. Repeated differentiation of the equation gives expressions for higher order relations between differential increments in discrete displacement variables $\underline{d}$ and forcing parameter λ.

Starting from an equilibrium with $\underline{r} = \underline{0}$, and setting $\mathrm{d}\underline{r} = \underline{0}$ in Eq. (3.50) gives requirements on first-order increments in λ and $\underline{d}$ to keep the zero residual. The first term expresses how residual force changes with discrete variables $\underline{d}$,

$$\underline{r}_{,\underline{d}} = \underline{p}_{,\underline{d}} - \underline{f}_{,\underline{d}}, \tag{3.51}$$

where the expression defines an N_d-by-N_d matrix. Referring to Eqs. (3.45) and (3.39), the matrix is written as

$$\underline{r}_{,\underline{d}} = \underline{p}_{,\underline{d}} - \underline{f}_{\mathrm{con},\underline{d}} - \underline{f}_{\mathrm{non},\underline{d}} = \underline{\underline{K}}^t + \underline{\underline{K}}^e + \underline{\underline{K}}^{\mathrm{non}} \tag{3.52}$$

Here, $\underline{\underline{K}}^t$ is the tangential stiffness matrix, which comes from strain energy increments,

$$\underline{\underline{K}}^t = \Pi_{p,\underline{d},\underline{d}} \tag{3.53}$$

and an expression for the variation of strain energy with respect to the displacement variables

$$\mathrm{d}^2\Pi_p = \sum_i \sum_j \frac{\partial^2 \Pi_p}{\partial d_i \, \partial d_j} \, \mathrm{d}d_i \, \mathrm{d}d_j = \underline{d}^{\mathrm{T}} \underline{\underline{K}}^t \underline{d}. \tag{3.54}$$

Similarly, the internal force comes from the first variation,

$$\underline{p} = \left(\Pi_{p,\underline{d}}\right)^{\mathrm{T}}, \tag{3.55}$$

which is an alternative form for Eq. (3.36), when only conservative stress is considered.

After some algebra, the tangential stiffness matrix components are expressed as

$$K^t_{ij} = \int_\Omega \left(B_{\alpha\beta i} \mathcal{K}_{\alpha\beta\gamma\delta} B_{\gamma\delta j} + N_{F\,\gamma\alpha i} S_{d\,\alpha\beta} N_{F\,\gamma\beta j} \right) \mathrm{d}V, \tag{3.56}$$

where $\mathcal{K}_{\alpha\beta\gamma\delta}$ are the components of the fourth order tensor in Eq. (2.24), and S_d the current stress tensor; the result is obtained by using the symmetry of S_d. The terms reflect the change in stress and strain, respectively, in a displacement increment from the current state. The operators $\underline{\mathsf{B}}$ and $\underline{\mathsf{N}}_F$ come from Eqs. (3.31) and (3.19), respectively. In the expression, the incremental strain operator $\underline{\mathsf{B}}$ and the stress S are dependent on the current displacement, while $\underline{\mathsf{N}}_F$ is not so, and the constitutive $\mathcal{K}$ might be.

Similarly, the conservative force stiffness matrix $\underline{\underline{K}}^e$ is related to the second variation of the exterior potential, and is expressed as

$$\underline{\underline{K}}^e = \Pi_{\text{con},\underline{d},\underline{d}}, \tag{3.57}$$

which gives an expression for the variation of the external potential as

$$\mathrm{d}^2\Pi_{\text{con}} = \sum_i \sum_j \frac{\partial^2 \Pi_{\text{con}}}{\partial d_i \partial d_j} \mathrm{d}d_i \, \mathrm{d}d_j = \underline{d}^{\mathrm{T}} \underline{\underline{K}}^e \underline{d} \tag{3.58}$$

while the conservative external force is, cf. Eq. (3.41),

$$\underline{f}_{\text{con}} = -\left(\Pi_{\text{con},\,\underline{d}}\right)^{\mathrm{T}}. \tag{3.59}$$

For displacement-independent exterior forcing, which gives a potential linear in displacement, the force stiffness disappears.

From the definition of the total potential Π in Eq. (2.87), the above expressions show that the differential is

$$\mathrm{d}^2\Pi = \underline{d}^{\mathrm{T}} \left(\underline{\underline{K}}^t + \underline{\underline{K}}^e\right) \underline{d} = \underline{d}^{\mathrm{T}} \underline{\underline{K}}^i \underline{d}, \tag{3.60}$$

which defines an incremental stiffness; this matrix relates—for a conservative system—increments in discrete residual force to increments in discrete variables according to

$$\mathrm{d}\underline{r} = \underline{\underline{K}}^i \, \mathrm{d}\underline{d} \quad \text{or} \quad \underline{r}_{,\underline{d}} = \underline{\underline{K}}^i. \tag{3.61}$$

This matrix is of major importance in the solution of non-linear equilibrium equations, and in describing properties of an equilibrium state, cf. Chap. 4.

The third part of Eq. (3.52) refers to non-conservative forcing, and is not possible to express in any other form. In general, this differential matrix is unsymmetric. Addition of this term to the differential expression may be an important part in the solution of non-conservative equilibrium problems. but the expression is not obviously useful for property evaluation, and is not denoted a stiffness matrix here. A similar modification to the differential matrix is needed if interior dissipation is considered, as in Eq. (2.83). The solution methods in Chap. 4 are almost exclusively discussing conservative settings.

The second term in Eq. (3.50) describes the effects on the residual from a differential increment to the parameter λ. In equilibrium formulations like Eqs. (3.47) or (3.48), the result is of a type resembling a discrete force vector, while the similarity can be more distant for the case in Eq. (3.49), if other types of parameters are introduced. This term is non-existing in the form of Eq. (3.46).

3.2.7 Discretized Motion

The previous section considers equilibrium, where inertia effects are neglected. The first term in Eq. (3.44) is therefore omitted, which leads to the discretized equilibrium equation in Eq (3.45). When this assumption is not relevant, another form of Eq. (3.44) must be used to solve the discretized motion problem.

Re-organizing Eq. (3.44) with respect to the discretized acceleration, again considering that virtual displacement is arbitrary, gives

$$\underline{\underline{M}}\,\underline{\ddot{d}} = \underline{f}_{\text{con}} + \underline{f}_{\text{non}} - \underline{p} \tag{3.62}$$

or, comparing this to the expressions in Eq. (3.45)

$$\underline{\ddot{d}} = \underline{\underline{M}}^{-1}\left(\underline{f} - \underline{p}\right) = -\underline{\underline{M}}^{-1}\underline{r}, \tag{3.63}$$

where the mass matrix in Eq. (3.21) is non-singular and the residual $\underline{r} \equiv \underline{r}(t)$, measured in relation to the discrete variables, is introduced. The equation states that an unbalance between current external and internal force gives an acceleration, cf. Sect. 2.8.3.

Identification of the terms shows that the right-hand side is dependent on the current displacement $\underline{d} \equiv \underline{d}(t)$, and the exterior forcing, which is possibly time-dependent[19] $\overline{\mathbf{T}} = \overline{\mathbf{T}}(t)$ and $\mathbf{B} \equiv \mathbf{B}(t)$. At a time instance t, with a displacement measured by $\underline{d}$, the equation thus gives an acceleration. The second-order differential equation

$$\underline{\ddot{d}} = -\underline{\underline{M}}^{-1}\,\underline{r}(\underline{d}, t) \tag{3.64}$$

gives a time-dependent solution $\underline{d}(t)$, if initial discrete displacement and velocity vectors $\underline{d}(t=0)$ and $\underline{\dot{d}}(t=0)$, are provided. The solution need be traced in time t by some time evolution procedure.

Reliable and efficient general methods for this time evolution of the solution over a prescribed interval is a technically demanding issue, and several basic methods—with many variations—are available in literature and software implementations. A basic description of some available classes of methods is given in Sect. 4.2, but the topic is not pursued to any greater depth in this treatise.

With respect to the more limited aspect of stability of equilibrium, the dynamic setting of major interest is related to free vibrations around the equilibrium state, i.e., the vibrations possible at frozen parameters for model and exterior forcing. Utilizing a known equilibrium state, where $\underline{r} = \underline{0}$ and $\underline{\ddot{d}} = \underline{0}$, a linearization of the residual in a conservative system gives a dynamic equation

$$\underline{\underline{M}}\,\mathrm{d}\underline{\ddot{d}} = -\mathrm{d}\underline{r} = -\underline{\underline{K}}^{i}\,\mathrm{d}\underline{d}, \tag{3.65}$$

[19] suppressing the dependence on $\mathbf{X}$, which is considered through the spatial integration

with frozen exterior forcing. This gives a discretized harmonic differential equation

$$\underline{\underline{M}}\, \mathrm{d}\underline{\ddot{d}} + \underline{\underline{K}}^{i}\, \mathrm{d}\underline{d} = \underline{0}, \tag{3.66}$$

for which eigenmodes $\underline{d}_0$ and eigenvalues Σ can be solved, through the exponential ansatz

$$\mathrm{d}\underline{d} = \mathrm{d}\underline{d}_0 \exp(\Sigma t). \tag{3.67}$$

This free vibration setting as a tool for stability investigations is further discussed in Sects. 3.7, 4.2.1 and 4.5.2.

3.2.8 *Conclusions from Sect. 3.2*

The aspects covered in this section show how a discretized mechanics problem is systematically modelled, based on a choice of discrete variables and an approximation to the displacement field, according to Eq. (3.8). The expressions can be used in different contexts, with global or local approximation bases, not least in finite element forms. The coming section discusses the possibilities, requirements and limitations for a variety of approaches.

The implementation of the developed expressions in an algorithm needs a method for the handling—and in particular the integration—of terms coming from a set of operators, which are not trivially handled in most computing environments; the complications come from three-and four-index operators, but also from the abundant number of zeroes in them.

With the explicit expressions for many quantities involved in the equations, an attractive method for treatment is in many cases an analytical development in a computer algebra software for large parts of the equations, allowing parametric description of a problem or a problem class. For instance, many element expressions in finite element methods can be given in closed parametric forms, replacing the common numerical integration approach.

3.3 Approaches to Discretization

The derivation of the discretized mechanics equation in Sect. 3.2 starts from an example situation of a general tetrahedron solid region in Fig. 3.4. It uses an approximation of the displacement field as a uniform interpolation between vertex nodal values, based on nodal shape functions. The dependence on this specific setting is, however, very limited. The number of nodes, $N_n = 4$, and the number of discrete variables[20], $N_d = 12$ are essentially only affecting the sizes of the variables in

[20] or, the number of degrees of freedom

Eqs. (3.10) and (3.11), which is emphasized by the . . . notation for repetitive nodes. The key aspect of this approximation is the uniform interpolations of the Cartesian displacement components in $\mathbf{U}_d$ from the displacement variables in $\underline{d}$. This allows approximations through shape functions $N_j(\mathbf{X})$, which are only dependent on the Cartesian coordinates of the nodes defining the region.

The example is thereby only a background for the very general Eq. (3.8) when this is used for other models of a solid continuum region. Such approximations may use an arbitrary number of discrete variables, and any approximation using these. This section discusses other approximation possibilities for solid regions, starting from some general requirements.

When, as in the example, the approximation is in the form of an interpolation such as Eq. (3.6), some requirements are obvious. The first requirement on an interpolation is that it must give the correct displacement components at the nodes, for any displacement state. Each displacement component must therefore be completely determined by the discrete variable corresponding to this component at the node. This is a demand on the components of the displacement operator $\underline{\mathbf{N}}(\mathbf{X})$ at the nodes, according to

$$N_{\alpha j}(\mathbf{X}_\ell) = \delta_{j\ell} \qquad (\alpha = 1, 2, 3) \tag{3.68}$$

for all related (j, ℓ). This demand is directly related to the approximation being an interpolation, and simplifies the form of $\underline{\mathbf{N}}$ in Eq. (3.8).

Another demand is that a rigid translation must be correctly reproduced. With equal displacement of all nodes, any point within the region must have the same displacement, which requires that

$$\sum_{j=1}^{N_d} N_{\alpha j} \equiv 1 \tag{3.69}$$

for $(\alpha = 1, \ldots, 3)$ and at any $\mathbf{X}$.[21] This demand is related to any description where the discrete variables are the displacement components at a set of points, and is valid also for non-uniform approximations. With other choices of variables[22], this demand is not valid.

3.3.1 Global Approximation

Other approximations, and thereby other discrete variables, are fully possible, and most of the derivations in Sect. 3.2 can still be used. An obvious choice is to introduce more nodes in the region, e.g., on its edges, but still describe an interpolation between

[21] the basis vectors must together give a 'partition of unity' for all three components.

[22] such as polynomial coefficients

nodal values. The corresponding global approximation through shape functions then becomes of increasingly high order.

As an example, introduction of one additional node at the midpoint of each edge in the tetrahedron in Fig. 3.4b gives a total of ten nodes, which matches the number of coefficients of a complete quadratic polynomial for each component. The shape functions, related to each node, can be formulated by matching ansatz polynomials successively to the coordinates of the used nodes, such that Eq. (3.68) is fulfilled. This can be done algorithmically, when nodal coordinates are known, either explicitly for all nodes, or by defining just the vertices and automatically place also midpoints. If the number of nodes introduced does not match the number of coefficients in a complete polynomial of a certain order, a choice of terms will be necessary.

With increased number of nodes, any general interpolation technique is still possible, but the shape functions will get more expansive. The addition of nodes, and the increased polynomial degree, will improve the approximation, but also make the formulation less numerically well-conditioned. This refinement strategy is thereby normally not useful for high accuracy. Similar aspects are discussed in relation to finite element settings in Sect. 3.3.3.

Approximations not based on nodal interpolation are fully possible, and a global approximation based on trigonometric series functions is assumed in many stability problems. The amplitudes of the series terms are then used as the discrete variables. This is not an interpolation, and Eq. (3.68) is not relevant. As the discrete variables are not displacement components, Eq. (3.69) is also not relevant. As the approximation still can be written as in Eq. (3.8), most of the expressions in Sect. 3.2 are, however, still valid. The expressions also need obvious modifications when the displacement components are differently approximated. This approach is very common for semi-analytical treatment of beam, plate and shell stability, cf. Chap. 1, but is not suited for general approximation in a $3D$ region. The approach is much more relevant for the cases of dimensionally reduced models in Sect. 3.4, with a more individualized treatment of the displacement components.

Trigonometric functions are also an important ingredient in finite strip models, which are sometimes used for long prismatic structural components. The approximation is global-local with a product of global trigonometric functions for longitudinal behavior and local simple polynomial functions in the transversal.

Boundary element methods and field-consistent approaches fall into the category of global shape functions, but are of limited applicability in general cases.

3.3.2 Local Approximation

While global shape functions have significant drawbacks for general $3D$ regions, the discretized mechanics equation in Eq. (3.62)—which is based on expressions developed in Sect. 3.2—points to other possibilities. With the terms of the equation formulated as integrals of discretized field variables over the region and its boundary, a possibility is to use a sum of local approximations, where each is non-zero only over

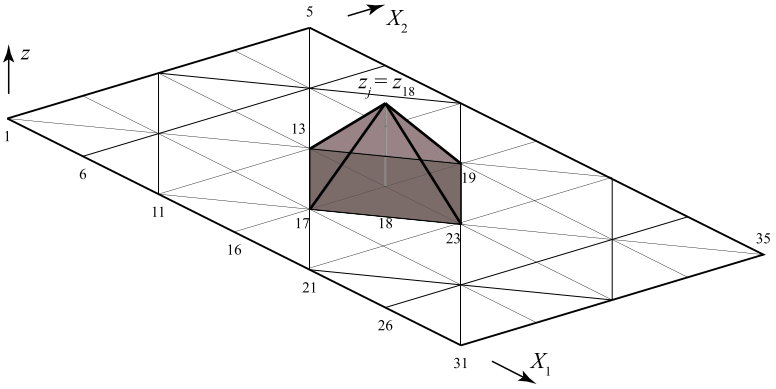

Fig. 3.5 $2D$ region with one shape function. Template subregion around one node. The contribution from a value at point 18 linearly decreases to zero at points 13, 17, 19 and 23 and on the edges connecting these

a limited subregion. With functions identically zero—and, thereby, also vanishing derivatives—outside the respective subregions, the integrals for each basis field need only be evaluated for a limited part of the whole, the support region for each function[23]. For a $1D$ region, Fig. 3.3 illustrates this approach, while Fig. 3.5 shows the same for a $2D$ region, where the area is divided into regular triangles. For simplicity, a single scalar variable z is indicated in the figure, with nodal values $z_j = z(\mathbf{X}_j)$. Figure 3.5 shows how a discrete variable z_j at node j only gives a contribution to the approximate function $z_d = z_d(X_1, X_2)$ in a set of four triangular subregions attached to the argument point[24]. Conversely, the function z_d at any interior point in a subregion is the sum of contributions from just the nodes defining it. A point on an edge between triangles, necessarily gives the same value from all connected subregions.

With a linear interpolation of the quantity z in the neighboring triangles, the first derivatives of it are well-defined, and constant in each triangle, but discontinuous at all triangle edges. Higher derivatives vanish identically at all points within a subregion, but are giving infinite spike values at edges. The form would not be useful in connection with physical equations demanding these derivatives. A general demand on an approximation in a discretized setting is that derivatives are available to a sufficient order for the integrals, with the order decided by the physics equation modelled.

For the $3D$ continuum setting discussed above, an illustration is troublesome, but a general region can always be divided into tetrahedron-shaped subregions[25]. The

[23] or, even the common support regions for two shape functions appearing in product integrals

[24] but also that other discrete variables would affect subregions of up to eight triangles in this figure; in general, the number can be higher.

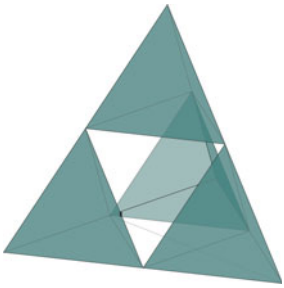

Fig. 3.6 Tetrahedron region with four marked subregions, from each initial vertex, which leaves an interior octahedron hole, which is not possible to fill regularly. More nodes might be needed for complete definition of subregions

variables are typically three displacement components at each nodal point $\mathbf{X}_j$, and a uniform interpolation through nodal shape functions is assumed. Each variable appears in a number[26] of tetrahedron subregions, and there gives a contribution to the final approximate displacement.

For the present problem class, first order derivatives of displacement are needed. This demands an approximate function with (at least) complete linear variation. The demand that first order derivatives of the approximate function must be finite implies a demand for continuity of the function itself. This has strong implications on the functions used for the approximation.

A conceptual challenge is illustrated by Fig. 3.6, which should be compared to Fig. 3.4b. Figure 3.6 attempts to visualize what happens if the solid tetrahedron is divided into a set of smaller tetrahedra. This subdivision is more complex than might be initially assumed, and no simple symmetric pattern exists; this may affect results, cf. Sect. 3.5.1. In general, however, tetrahedra of variable shapes can geometrically fill any region, even if symmetry is lost. After the division into subregions, the local shape functions are chosen such that the weighted sum of these define a linear interpolation between nodal values of the components for the subset of nodes. Compared to the approach with several nodes, and higher order polynomials mentioned above, the local interpolation is now piece-wise linear.

It is important to note that the complete linear polynomial over the $3D$ solid subregion implies that the variation of it is also linear (in two local variables) on each face of the tetrahedron, and linear (in one local variable) along any of its edges. As the values of variables at the three nodes on any face, and at the two on each edge, define these interpolations uniquely, subregions meeting at a face or an edge will share interpolation and give a continuity of the approximated variable. This is a fundamental requirement on any local approximation.

Figures 3.5 and 3.6 indicate that many subregions—but also the surroundings of many nodes—are identical in shape and size. In the interior of the rectangular region in Fig. 3.5, only two different node types, and four different triangles appear. In a linear setting, this can be utilized for increased efficiency in the needed integrations,

[25] with some level of approximation to curved region edges

[26] often rather few, but in principle unbounded when a sphere is modelled by tetrahedra using the center point as one vertex, and three point on the sphere surface as the others

but this is not trivial in a general context, where expressions are supported on, and use individual surroundings and sets of discrete variables. A general approach must therefore treat each subregion individually, and this is the basis for finite element approximations.

3.3.3 Finite Elements for 3D Continuum

Among local interpolation methods for structural analysis, the finite element (FE) techniques have been the clearly dominant choices in engineering for at least 50 years, and are expected to remain so for a foreseeable future due to the enormous investments in knowledge and implementations. A vast literature exists on these methods, with key references to Zienkiewicz and Taylor (2000) and Bathe (2014). Only a few aspects are discussed here, with a focus on the modeling of stability problems, and based on the energy viewpoints promoted in this treatise. This section focusses on FE-based formulation for $3D$ continuum situations[27], while more application-oriented dimensionally reduced situations are discussed in Sect. 3.4.

The description of discretized models above is, in its assumptions and concepts, fully valid for the displacement-based finite elements in common use. In particular, the usage of the displacement components at a set of nodes as the discrete variables is introduced, with a corresponding uniform polynomial interpolation through nodal shape functions. With some care in the choice of interpolation, the displacement field is C^0 continuous between elements, which is a requirement for the integration of constituent quantities. This choice has a minor advantage in its direct interpretation of some important result variables[28]. The philosophy of the techniques is, however, somewhat different here than in most engineering literature.

Element-wise integration

The description above is focussed on the influence on the solution from one node (and its related discrete variables) through integrals over the subregions surrounding the node, cf. Fig. 3.5. The traditional engineering view sees each subregion, i.e., element as an—almost physical—building block. The integration of the contributions to the relevant discrete vectors and matrices is therefore performed one element at the time, considering all integrands with support within the element, i.e., those using the variables at nodes connected to the element. Figure 3.7a attempts to illustrate this for a plane case with one approximated variable, as a contrast to subfigure (b), which is essentially reproducing a part of Fig. 3.5, where matrices and vectors are built column- and component-wise, respectively, based on the contribution from one discrete variable at the time.

[27] even if this not the most common situations where stability is an issue

[28] like the point-wise deflection under an acting force

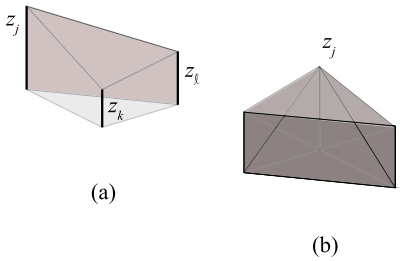

Fig. 3.7 Visualization of the difference between integration of contributions: **a** Element-based. **b** Node-based

The engineering approach also commonly uses the basic mechanical quantities, e.g., strain and stress, to evaluate the element interior equilibrium. The element quantities are block-wise added to the complete structural matrices and vectors. This approach is here replaced by the expressions from Sect. 3.2. The final quantities, and therefore the results, are identical for the same choices of discrete variables, shape functions and mechanical formulation.

The integration is now performed as if the element subregions were instead considered as individual regions. This can be done by an 'extract-and-assemble' strategy, where the complete region is broken down into elements. The information for these is calculated and processed, whereafter the results are assembled as contributions to the whole. This approach thereby successively focusses on one of the triangles in Fig. 3.5 or one of the tetrahedra in Fig. 3.6, and performs the integrations over these.

The extraction part formally uses a displacement extraction operator for the element to withdraw all its displacement variables from the full set, according to

$$\underline{d}_e = \underline{\underline{L}}_e \, \underline{d}, \tag{3.70}$$

where $\underline{d}_e$ are displacement components for the relevant element e, and $\underline{\underline{L}}_e$ an extraction matrix, typically consisting of just N_ℓ unit values in an N_ℓ-by-N_d matrix, when N_ℓ is the number of displacement components affecting the subregion[29].

With this approach, each element can be considered through the expressions in the tetrahedron example above, giving contributions to internal and external force, but also to the mass and stiffness matrices. Primarily, a mass matrix $\underline{\underline{M}}_e$, internal force p_e and an incremental stiffness matrix $\underline{\underline{K}}^i_e$ are evaluated from the displacement $\underline{d}_e$, combined with material and geometry data for the element. Commonly, also element external force $\underline{f}_e$ is evaluated.

Noting that all the expressions for structural mechanics come from integrals over the whole region, but are evaluated for a subregion element, it is obvious that the element expressions are contributions to the whole. The full expressions are the assembled sums from the elements, considering their subregion definitions. The summation of force contributions is thereby

[29] which is $N_\ell = 3$ for the interpolation of z in one triangle of Fig. 3.5, and $N_\ell = 12$ for one solid tetrahedron element in Fig. 3.6

$$\underline{p} = \sum_{e=1}^{N_e} \underline{\underline{L}}_e^{\mathrm{T}} \underline{p}_e \qquad \text{and} \qquad \underline{f} = \sum_{e=1}^{N_e} \underline{\underline{L}}_e^{\mathrm{T}} \underline{f}_e, \tag{3.71}$$

with N_e the number of elements in the structural model. Similarly, the contribution to matrix quantities are assembled as

$$\underline{\underline{K}}^i = \sum_{e=1}^{N_e} \underline{\underline{L}}_e^{\mathrm{T}} \underline{\underline{K}}_e^i \underline{\underline{L}}_e \qquad \text{and} \qquad \underline{\underline{M}} = \sum_{e=1}^{N_e} \underline{\underline{L}}_e^{\mathrm{T}} \underline{\underline{M}}_e \underline{\underline{L}}_e. \tag{3.72}$$

Being a fundamental part of finite element techniques, these summations are often symbolically described by an assembly operator, e.g., as

$$\underline{p} = \mathbb{A}\underline{p}_e; \qquad \underline{f} = \mathbb{A}\underline{f}_e; \qquad \underline{\underline{K}}^i = \mathbb{A}\underline{\underline{K}}_e^i; \qquad \underline{\underline{M}} = \mathbb{A}\underline{\underline{M}}_e, \tag{3.73}$$

being a short-hand notation for the full expressions above, and implicitly using the element extraction operators for the N_e elements in the model.

The needed information for the integral contributions is conveniently given as topology information, in the format of a translation of the discrete variable numbers in a template form of the element integrals to the numbers of the complete region model. With the same number of components for each node, this can be defined as node numbers. In Fig. 3.5a, element areas are defined by the numbers: (13, 17, 18), (17, 23, 18), (23, 19, 18) and (19, 13, 18) in the hatched subregion[30]. The integration region is easily handled algorithmically when the positions of all nodes are known.

Numerical or Gauss integration, which is optimally accurate for polynomial integrands[31], are extensively described in all text books on finite element techniques. The method evaluates the integrand quantity at a set of points within the element, and refers a part of the element volume to this. The weighted sum is an approximation to the integral. In several contexts, pre-integrations of terms can also be utilized, when developing a formulation for a specific setting.

Element types

Many elements for structural continuum analyses are available through literature or in commercial software. On the surface, these differ in their geometries and node placements, but they may also differ in their interior approximations. They may also differ in their possibilities to model different materials. As results from FE-based stability investigations can be rather strongly affected by the elements used, it is important to understand their underlying assumptions. For the present discussion, the geomet-

[30] Imagining three discrete variables per node for the plane problem, the first triangle relates to variables 37, 38, 39, 49, 50, 51, 52, 53, 54

[31] but uses coordinates and weights with rather irregular numerical values—which can not be too much rounded

ric and interpolation properties are of particular interest. A basic understanding of element assumptions and capabilities is therefore needed, even—or, in particular—when general software is used for the analyses. For non-linear and stability analyses based on energy concepts, some convergence-enhancing and locking-reducing modifications to the fundamental element descriptions—which are sometimes introduced in software implementations—can make conclusion less clear.

The basic geometrical shapes for $3D$ structural FE analysis are the tetrahedron, which is discussed above, and a regular hexahedron brick; these have four and eight vertex nodes, respectively, Fig. 3.8a–b. The tetrahedron element allows arbitrary shapes through the definition of the coordinates of the vertices, and can give good results even for rather irregular shapes. The brick element, on the other hand, is basically defined by its lengths in the coordinate directions. Through an iso-parametric mapping of the coordinates, the brick can be transformed into an arbitrary solid region with eight defining vertex nodes as in Fig. 3.8c, giving twelve straight edges and six surfaces; these are not necessarily plane, but fully compatible between adjacent elements. While this mapping can reliably handle changes of the element orientation in $3D$ space, the distortion of the basic brick shape must be kept within certain limits to be legal, and within even stricter limits to give a well-behaving element[32]. The limits are typically given as maximum aspect ratios for side lengths and limits for the distortion of right corner angles.

The term iso-parametric here refers to the identical representations of the reference point and the displacement. In the terminology of Chap. 2, this means that $\mathbf{X}$ and $\mathbf{U}$—and, consequentially also $\mathbf{x}$—are completely consistent, in the sense that they all are described from a set of normalized local coordinates, and thereby allow constant strain conditions within the element. This implies that, e.g., a straight element edge in the material configuration will keep straight when deformed, if based on a linear interpolation. Higher order displacement variations are needed for curved edges, but demand a higher number of nodes.

Both the basic types of element also demand that vertex nodes are given in an order prescribed by the implementation[33]; this information must be obtained from the software documentation. The elements should be objective with respect to the coordinate directions, but incorrect node number ordering in the element definition may lead to incorrect results. The geometrical aspects of element definition are normally handled and safe-guarded by a commercial software.

With respect to the possibilities to handle complex region geometries, sets of tetrahedron elements can be combined to reliably represent any shape, with the only restriction that curved edges and faces are represented by sets of straight lines and flat surfaces[34]. The element sizes are also easily gradually changed within the region. The brick elements are, even with the iso-parametric approach, less flexible in this respect; as an example, the modelling of a solid sphere through a set of reasonably

[32] as finite element methds are fundamentally aproximate, and therefore can be of different qualities

[33] or the volume will be calculated as negative, with disastrous results

[34] and, consequently, also gives too small areas and volumes, if defining vertices are placed on the exact geometry of a convex region

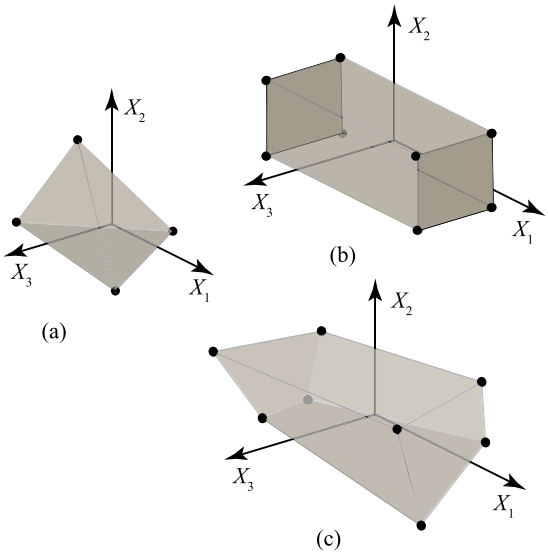

Fig. 3.8 Typical low order finite element types for $3D$ continuum structural simulations. **a** Tetrahedron element. **b** Regular hexahedral brick element. **c** Iso-parametrically transformed brick element

shaped hexahedra is impossible. For any element type, it is always advantageous to use elements of similar measures in the coordinate directions.

While the geometric definition of elements in a region can be more or less automatically handled by a software, a choice is often needed for the interpolation, and implementations may offer several possibilities, through named element types with different assumptions, or by switches given as input.

Improved interpolation

In the tetrahedron representation above, the four vertex nodes allow an interpolation based on a complete linear polynomial, cf. Eq. (3.5). The eight vertex nodes of the basic brick element can be used in different interpolations, all fulfilling the demands in Eqs. (3.68) and (3.69), but the eight nodes are not sufficient for a complete quadratic polynomial. As isotropy of an element formulation with respect to axis directions is a highly desired quality, the uniform interpolation is often chosen as the product form

$$N_{\alpha j}(\mathbf{X}) = (a_1 + a_2 X_1)\,(a_3 + a_4 X_2)\,(a_5 + a_6 X_3) \tag{3.74}$$

for $(\alpha = 1, \ldots, 3)$ in the regular brick, with a consequent modification for the iso-parametric transformation[35]. This gives a complete linear polynomial for each component, with addition of three quadratic terms and one cubic, i.e., a slight improvement of the tetrahedron interpolation.

[35] where the interpolation of both geometry and displacement is written based on three local coordinates, instead

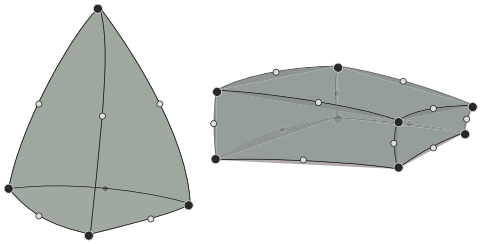

Fig. 3.9 Higher order finite element types, as improvements, through addition of mid-edge nodes, to the elements in Fig. 3.8. **a** Tetrahedron element. **b** Iso-parametrically transformed brick element. Only the visible nodes are marked

The interpolation in Eq. (3.74) can be assured to fulfil the needed C^0 continuity over element boundaries. Considering one face of the regular brick (e.g., $X_1 = \text{const.}$), the interpolation gives an incomplete quadratic function, which is fully defined by the four corner nodes of the face. On any edge, the interpolation is linear, and defined by the two end nodes. This uniqueness ensures the continuity of displacement between adjoining elements; no gaps or overlaps between elements will appear. The same reasoning shows that first derivatives are not continuous.

Higher order interpolation in finite element models, and thereby smoother results[36], demands elements with higher numbers of nodes than in the basic elements in Fig. 3.8[37]. Systematic procedures for this add nodes on all element edges, on all surfaces or as a regular grid within the element. The choice of polynomial terms which match the nodes available is not always unique, and may be difficult, due to the continuity demands on faces and edges.

The first step of improvement of the basic tetrahedron element is in this context straight-forward, when six new nodes at the midpoints of each edge are added to the four vertex nodes, Fig. 3.9a. The midpoint nodes allow curved edges and faces of the refined tetrahedron. Having ten nodes, the element perfectly fits a choice of a complete quadratic polynomial. It is noted that 'midpoints' here is not necessarily the geometric midpoint of the edge; any placement rather near this is fully useful. This choice satisfies the continuity requirements.

A further improvement with only edge nodes is not obvious, as two nodes on each edge gives a total of 16 nodes, while a complete cubic polynomial has 20 terms. Placement of nodes also at the midpoints of the four element faces is a possible solution to this, and this form observes the continuity demands. For even higher order elements based on the tetrahedron, a similarity to the Pascal triangle shows that complete polynomials can always be obtained, but that these will demand interior nodes within the element volume.

For the basic brick element, adding one node at all edge midpoints as in Fig. 3.9b gives a total of 20 nodes. Seemingly, this would allow a cubic polynomial in three coordinates. Such a choice would, however, not uniquely define the approximation on a face, as only eight nodes are available, and ten terms exist in the polynomial for

[36] for the same number of elements, at least

[37] Other possibilities exist, such as non-node variables, but these are outside the present scope

a constant value of one coordinate. The same conclusion is valid for the edges of the brick, where three available nodes can not uniquely define a cubic function.

A useful element based on the nodes in Fig. 3.9b is the so called 20-node 'serendipity element'. This interpolates geometry and displacement by an incomplete fourth-order polynomial. The next element in this group has 32 nodes, all on element edges. Another group of elements is the Lagrange elements which are based on products of functions in the coordinates, and has a regular grid of—also interior—nodes.

Not least due to the extensive geometry handling, only the simplest versions of the elements are possible choices for self-made implementations. In commercial FE software, a set of tested element types are available[38]. The documentation of these should describe the underlying interpolations, the restrictions on usage, and the input needed for the division of a region into set of elements. For high-order elements, this meshing needs assistance from an automatic procedure; ideally, the user should just define the region and the requested order of interpolation by the elements.

Regarding the choice of element most suited for a specific analysis, this has been a constant discussion in literature for several decades, but still without firm conclusion. Without any ambition to settle the issue, it is just noted that the non-linear formulations needed here tend to move the main computational burden from the solution of sets of equations towards the repetitive evaluation of element quantities. This would thereby be an argument for lower order element types, with less complex element expressions, at the cost of higher numbers of discrete variables for equal accuracy in results. This conclusion is then primarily valid for practical engineering simulations, while high-order interpolations are invaluable for high-accuracy results, if computational demands are not major issues.

3.3.4 Isogeometric Analysis

Isogeometric analysis ('IGA') is a more recently developed technique for numerical modelling and analysis of structures. The approach has major potential, but is yet not as developed as the FE techniques; this implies that general commercial software is sofar more rare. The main references for the method are works by Hughes et al. (2005) and Cottrell et al. (2009).

The isogeometric analysis models share some properties with FE models, but also include some important differences, which demand a good understanding of the methods and results. Based on FE knowledge, IGA was developed with an objective to bridge the conceptual and implementation-related gaps between design and analysis software. This ambition, but also a demand for analysis formulation with higher smoothness than the basically C^0 continuous finite elements, have been stated as main motivations for the IGA development.

[38] even if the element testing is perhaps not always directed towards the element performance in stability analyses

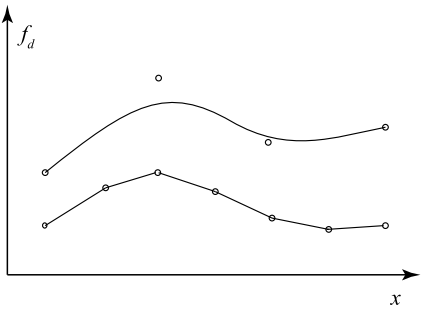

Fig. 3.10 Schematic comparison of main differences between approximate functions $f_d(x)$ as obtained from FEM interpolation (bottom) and IGA approximation (top). The figure shows two fictitious and unrelated cases

In relation to the descriptions above, the IGA modeling of a $3D$ continuum uses the form of Eq. (3.8), with basis fields and discrete variables, and uses uniform approximation for the displacement components. The approximate displacement is in IGA described through non-uniform rational B-spline (NURBS) functions—the same for each component—which are a further development of the B-spline functions commonly used as the basis in constructive solid geometry (CSG)[39]. These are not interpolating, as the discrete variables relate to the displacement at a set of control points not attached to the physical region. As shown by the simplified $1D$ comparison in Fig. 3.10, the control points in IGA are rather 'attractors' to the displacement variations in the region than the nodal values used in FEM.

The main advantage of the IGA modeling for structural analyses is the higher degree of continuity inherent in the form, and obtained with fewer discrete values, even if this does not necessarily imply a lower computational cost. The continuity improves the smoothness of both the geometric model and the calculated results, as IGA is fundamentally iso-parametric. The continuity is described through knot vectors[40], which give very good possibilities to model complex geometries from few data. The knot vectors describe patches of the complete model, which in the FE context could be described as super-elements, which are divided into elements for numerical treatment.

The higher degree of continuity obtained by the NURBS functions is a desirable quality in stability analyses, and comes from the wider support regions for the functions. The increased smoothness adds some complexity to, e.g., the algorithmic integration of the constituent terms in the needed equations. The less localized approximation on the other hand makes the introduction of several classes of boundary conditions less straight-forward. As the approximation is not interpolatory, all results from IGA also need some degree of post-processing prior to interpretation.

Although considered as having a very interesting potential in stability investigations of structures, the IGA methods are not further discussed here. Their basic

[39] B-splines are, in turn, developments of the spline functions, being the mathematical expressions for the engineering spline tool, a flexible ruler used to connect a set of points in a drawing by a smooth graph

[40] which are really tensor-like products of knot vectors for each spatial dimension of the model

features, however, fit well with the description in earlier parts of this Chapter and in the solution methods of Chap. 4.

3.3.5 Mesh-Free Methods

Another potentially interesting possibility for the discretized approximation of the displacement in a structural model lies in the mesh-free methods. The basic idea in these methods is to avoid the creation of artifact geometry and topology information for the algorithmic definition of the model, like nodes, elements and patches. The method therefore only operates by a set of nodal points more or less uniformly spread over the region. The possibilities to adaptively change this node set is an interesting feature of the method.

The approximation within the modeled region is interpolatory, in the sense that point source functions are attached to each node, however, not in general fulfilling the partition of unity quality in Eq. (3.69). Commonly, radial functions around the nodes are used. With the limited geometric information about the model utilized, the definition of model edges and the corresponding boundary conditions become considerably more complicated than for FEM or IGA formulations.

As very few commercial implementations of the mesh-less methods are available, and a self-made implementation demands the solutions to several complicated numerical problems, related to, e.g., numerical well-posedness, the mesh-less methods are not further discussed here. With strategies for the placement of nodes, and choices of source functions, a successful implementation can be based on most of the expressions in this and the following Chapter.

3.4 Dimensionally Reduced Models

The previous sections of this Chapter discuss discretization methods for $3D$ continuum regions, representing general solids and structures. The discretization, based on finite elements or through other approaches, is then isotropic in the sense that all directions are treated identically. The developed elements for the analyses are also assumed to be similar in all directions.

Stability problems are on the other hand primarily relevant for other classes of slender structures, which are thin in one or two dimensions. Methods for treatment of such problems are needed. Even if the methods from above can be used, they become impossibly unattractive, due to the very large numbers of—roughly cube-shaped—elements needed; a beam of length 4 m, with a rectangular section of $0.1 \times 0.2\,\mathrm{m}^2$ needs $80 \times 2 \times 4$ elements of side lengths 5 cm for a reasonable representation[41].

[41] in order to have at least two elements in each direction; non-rectangular sections are even worse

This section gives a brief overview of methods for the modeling of slender structures, i.e., structural components where at least one material dimension is considerably smaller. In addition to the slenderness of the components, this also introduces the concept of component orientation, when the components, although $1D$ or $2D$ in their individual response, are normally combined into a $3D$ structure.

The description below is related to finite element discretizations, but similar approaches can be developed in other contexts. The description is brief, just pointing to some aspects of these elements, which are relevant to stability investigations. For a more complete description, the reader is referred to more comprehensive finite element texts.

3.4.1 Membranes and Trusses

Flat membrane elements and straight truss elements are assumed to be very thin in one and two dimensions, respectively. They are thereby represented as a geometrical surface or line. Figure 3.11 shows the simplest possible, linearly interpolated, elements of the two classes. More complex elements—curved or with higher numbers of nodes—are possible, but need extensive algebra, based on more complex assumptions. In the figure, the elements are shown in a local coordinate system adapted for their basic geometries, with the membrane arbitrarily situated in an $(X_{1'}, X_{2'})$ plane, and the truss on the $X_{1'}$ axis. The prime superindex here denotes a local coordinate, adapted to the element initial position.

The elements possess thickness and sectional area, respectively, even if they are thin in their geometry definition. These quantities are therefore defined as just properties of the elements, without geometric implications. The key assumption underlying the description is that interior quantities are constant over the neglected dimensions.

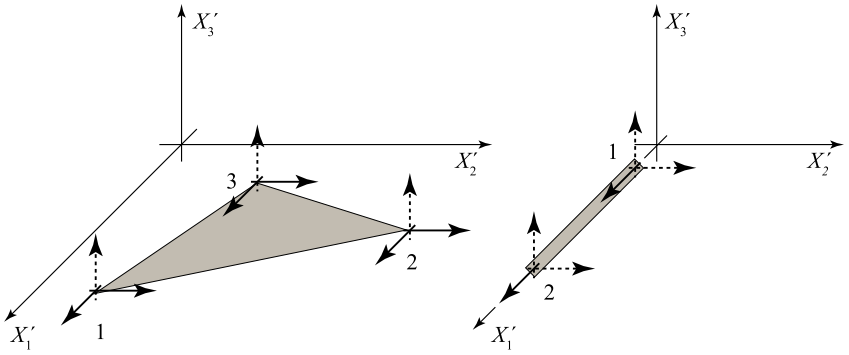

Fig. 3.11 Linear finite elements, represented in local coordinate systems. **a** Membrane element. **b** Truss element

The integral of this quantity thereby corresponds to just a multiplication by the thickness or sectional area. Consequently, the same applies to the boundary conditions: prescribed displacement and traction are valid for (points on) the mid-surface and mid-line, respectively, with traction components often integrated to resultants.

Neglecting the behaviour in the transversal directions makes it impossible to consider deformation normal to the defined geometry, i.e., bending effects. Transversal traction is therefore effectively considered as resultants at the nodes. This is indicated by the dashed arrows in Fig. 3.11. The presentation is chosen in order to be compatible with element descriptions using the full three displacement components. The element displacement is then measured in the local system as $\mathbf{U}_j = (U_{j1'}, U_{j2'}, U_{j3'})^{\mathrm{T}}$ for each node j. A uniform interpolation through nodal shape functions is implied; the element remains flat or straight.

In order to utilize the general expressions for these classes of elements, expressions for the neglected transversal deformation components are developed. They are thereby evaluated from the in-plane displacement components, and from interior relations, e.g., stress relations.

For the membrane element with local plane-stress assumptions, the full strain state is introduced through an unknown normal strain component[42] $E_{3'3'}$ in the local $X_{3'}$-direction. This is solved—within the used constitutive relation—such that the corresponding stress component $S_{3'3'} = 0$. For an incompressible constitutive material, e.g., the Mooney-Rivlin material model in Sect. 2.4.2, the incompressibility constraint must also be fulfilled, with an unknown p calculated from the strain components, such that the invariant $I_3(\mathsf{E}) = 1$.

Together with the in-plane strain from the interpolated displacement, these fictitious variables allow the evaluation of all relevant quantities. Necessary integrations thereby must be performed also over the real thickness, based on the assumption of constant values through the neglected dimensions.

For the truss element in Fig. 3.11, the two normal strains in the (arbitrarily chosen) directions orthogonal to the axial direction $X_{1'}$ are handled in the same way by an introduction of fictitious normal strain components; these are chosen to give zero transversal stresses, and, possibly, incompressibility.

The internal force for either of the elements can be evaluated with the procedures described above, seeing the element as a complete structure, with its interior interpolation. The result is a local element internal force vector[43]

$$\underline{p}'_e = \underline{p}'_e(\underline{d}'_e) \tag{3.75}$$

completely calculable from the local element displacement variables. The simple geometrical forms of the element types allow extensive pre-calculation of the expres-

[42] 'unknown' since it is not evaluated from a deformation gradient; shear strain components are here irrelevant

[43] Subindex e denotes the isolated element, the prime that force is described in the local coordinate directions

sions for this force. This makes it straight-forward to introduce parametric definitions of geometry and material.

When transversal traction is introduced for the triangular membrane element, the total transversal force is distributed as external force components in the $3'$ direction for the nodes, in an element external force vector $\underline{f}'_e$, which also considers body-force contributions. For the truss element, exterior traction and body force similarly contributes to nodal external force components in the $X_{2'}$ and $X_{3'}$ directions. For uniform intensities, these are equally distributed to the nodes.

Accounting for element orientation

Equation (3.75) gives a symbolic expression for the internal force in a membrane or truss element as a function of its current displacement, all measured in local coordinates. The expression is used for each element, when it is part of a complete $3D$ structure subjected to stability investigation[44]. For this, it is important to note that the overall mechanics equations are based on integrals of certain quantities over the full region, and that the individual element is considered as a subregion for these integrations; the total is the sum of the parts.

Integrating the expressions as above thereby leads to contributions to the needed (global) discrete vectors and matrices. After consideration of the above restrictions on transversal components, internal and external force contributions as well as incremental stiffness and mass matrices are obtained in the local element coordinate system. Similarly as in Eq. (3.75), also $\underline{f}'_e$, $\underline{\underline{K}}'_e$, and $\underline{\underline{M}}'_e$ may be dependent on $\underline{d}'_e$ and local geometry.

Even if the expressions give correct values to the fundamental scalar quantities, the addition of the element quantities demands that all contributions refer to the same global displacement components, when differentials of energy are needed. A geometric transformation is thus needed for the element displacement components in $\underline{d}'_e$, which are individual for the element described by the $(\mathbf{e}_{1'}, \mathbf{e}_{2'}, \mathbf{e}_{3'})$ orthonormal coordinate axes. Referring to Fig. 3.12, an orientation operator is introduced to define the orientation of local axes. This operator, in physical vector form, has the components

$$\Theta_{e\,ij} = \mathbf{e}_{j'} \bullet \mathbf{e}_i, \tag{3.76}$$

where $\mathbf{e}_i$ are the unit vectors of the global coordinate system. This operator has an obvious interpretation as an element orientation matrix $\underline{\underline{\Theta}}_e$.

Equation (3.76) allows a projection of the global displacement components $\underline{d}_e$ on the local ones $\underline{d}'_e$ according to

$$\underline{d}'_e = \left\lceil \underline{\underline{\Theta}}_e^{\mathrm{T}} \right\rfloor \underline{d}_e. \tag{3.77}$$

[44] For the truss element, also a plane, $2D$ structure can be relevant with respect to stability

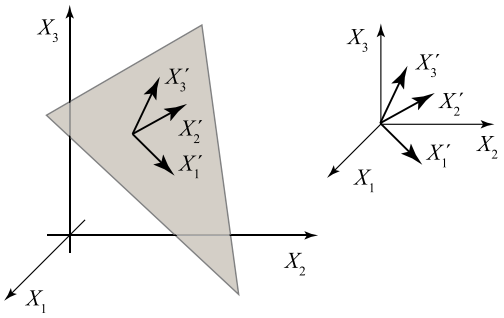

Fig. 3.12 Membrane element in its own local coordinate system, and basis for transformation of local to global quantities

where the schematic notation implies that the orientation matrix is repeated on the diagonal for each node in the element, i.e., three times for the membrane element, two for the truss element.

After this transformation of the extracted nodal displacement, the $3'$ nodal displacement components for the membrane element and the $2'$ and $3'$ components for the truss element are describing displacements transversal to the initial plane and line, respectively[45]. It is noted that all local nodal displacement components are normally non-zero, when the element is part of a $3D$ structure.

The calculated element quantities must also be transformed into the global component directions before addition; this is obvious going back to the basic equations, where the virtual displacement components (in the global directions) were on the left-hand side of all terms. A transformation of these to the local system is needed. This implies that element quantities must be pre-multiplied by the inverse orientation transformation, according to

$$\begin{aligned} \underline{p}_e &= \left\lceil \underline{\underline{\Theta}}_e \right\rfloor \underline{p}'_e \qquad & \underline{f}_e &= \left\lceil \underline{\underline{\Theta}}_e \right\rfloor \underline{f}'_e \\ \underline{\underline{K}}^i_e &= \left\lceil \underline{\underline{\Theta}}_e \right\rfloor \underline{\underline{K}}^{i\,\prime}_e \left\lceil \underline{\underline{\Theta}}^{\mathrm{T}}_e \right\rfloor \qquad & \underline{\underline{M}}_e &= \left\lceil \underline{\underline{\Theta}}_e \right\rfloor \underline{\underline{M}}'_e \left\lceil \underline{\underline{\Theta}}^{\mathrm{T}}_e \right\rfloor \end{aligned} \tag{3.78}$$

before assembling their contributions to the whole[46]. The right-hand transformation for the stiffness and mass matrices is needed as they operate on local displacement components from both sides.

After the orientation transformation, the element contribution to the whole is described through the extraction operator in Eq. (3.70), which decribes the topology of the element in relation to the structural model.

[45] which does not, in the non-linear context, imply that they are not affecting the interior response

[46] even if the transformation of the mass matrix is often not necessary, as the element gives the same node contributions in all directions

3.4.2 Shells and Frames

Shell and frame elements share some aspects with membranes and trusses, but are considerably more complex from several viewpoints. In fact, accurate, reliable and efficient shell elements are still a research challenge, even if the TRIC elements as described by Argyris et al. (1997), and the MITC group of elements discussed by. e.g., Ko et al. (2017) are highly reliable for most purposes.

Regarding terminology, a shell element is here considered as a combination of a membrane and a plate element, while a frame element is similarly a combination of a truss and a beam element. The formulation problems primarily relate to the plate and beam parts, where bending must be considered. As many treatises exist on these situations, the description here is brief, even if stability problems often relate to these response aspects and to models based on such elements.

Essentially, the formulation and usage of plate and beam elements adds two complexities to the descriptions above, and these can be well described already for the simplest situation, namely a straight plane beam element. This setting is used for demonstration, and is similar to Fig. 3.11b: a line element, which is directed along a local $X_{1'}$ axis, and represents the beam element midline. It has a small beam section height measured in the $X_{2'}$ direction, while the width in the $X_{3'}$ direction is arbitrary, without variation of the strain and stress[47].

In analogy to the membrane and truss elements above, plates and beams also have one and two dimensions, respectively, that are small. They are, however, not as small as above, implying that quantities like interior stress can not be considered constant over the smaller dimensions. For a beam element in the $(X_{1'}, X_{2'})$ plane, according to Fig. 3.13a, this implies that both displacement components $U_{1'}$ and $U_{2'}$ need be described. Obviously, this can be done, with similar approximations as in the membrane case in Fig. 3.11a, using the corner node displacement components indicated in the figure, but the result would be of low accuracy due to the very anisotropic aspect ratio of the region.

In order to describe the beam element by just its $1\,D$ midline, the common approach introduces a rotation variable, here around the $X_{3'}$ axis. The variations of $\vartheta_{3'} = \vartheta_{3'}(X_{1'})$ and the transversal displacement $U_{2'} = U_{2'}(X_{1'})$ along the beam axis are used to describe the beam element kinematics, with the description related to the straight initial element midline, i.e., the $X_{1'}$ axis.

If also the axial truss action is included, in order to create a plane frame element, the axial displacement approximation $U_{1'} = U_{1'}(X_{1'})$ is also considered.

When introducing also rotations as variables, these allow different kinematic interpretations, and consequent assumptions for the interior response of the beam subregion. In either case, rotations are assumed to be small, as the treatment of large rotations is not linear. Figure 3.13b interprets the rotation as the change of orientation of the initial $X_{2'}$ axis. Together with the axial and transversal displacement components $U_{1'}$ and $U_{2'}$, this gives a kinematic approximation, according to

[47] It just enters in the integration as the area and area moment of inertia in the integrals, and the treatment of non-rectangular sections is thereby almost trivial.

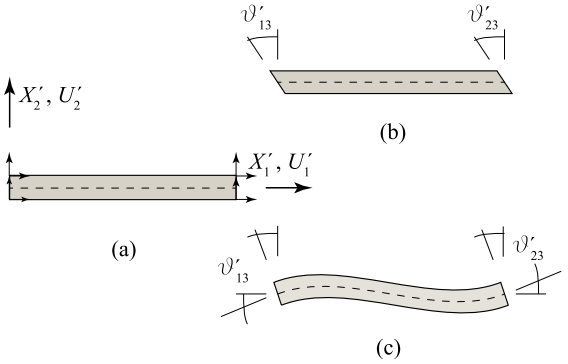

Fig. 3.13 Element assumptions for plane beam element. **a** General view, with small but not infinitely small transversal measure. **b** Timoshenko beam theory assumption with rotation as section orientation. **c** Euler-Bernoulli beam theory assumption with rotation as both section and midline orientation

$$\mathbf{U}'_d = \begin{pmatrix} U_{1'}(X_{1'}) - X_{2'}\,\vartheta_{3'}(X_{1'}) \\ U_{2'}(X_{1'}) \\ 0 \end{pmatrix}. \tag{3.79}$$

where the point coordinate along the $X_{2'}$ axis appears together with the displacement components.[48]

Introducing three variables at each element end node, and using a linear variation for each variable, the $\underline{\mathbf{N}}$ operator in Eq. (3.8) is obtained as

$$\underline{\mathbf{N}} = \begin{pmatrix} N_1 & 0 & -X_{2'}N_1 & N_2 & 0 & -X_{2'}N_2 \\ 0 & N_1 & 0 & 0 & N_2 & 0 \\ 0 & 0 & 0 & 0 & 0 & 0 \end{pmatrix}. \tag{3.80}$$

The functions N_1 and N_2—both functions of the local axial coordinate $X_{1'}$—are the shape functions interpolating linearly between two nodes, cf. Eq. (3.1). This interpolation relates to the element discrete displacement variables as

$$\underline{d}_e = (U_{11'},\ U_{12'},\ \vartheta_{13'},\quad U_{21'},\ U_{22'},\ \vartheta_{23'})^{\mathrm{T}} \tag{3.81}$$

The kinematic description of Eq. (3.79) is commonly, and naturally, used together with the so-called Timoshenko beam theory, which considers the shear strain originating in the difference between the section orientation (as described by the rotation variable $\vartheta_{3'}$) and the slope of the beam midline described by the derivative of the transversal deflection $U_{2',X_{1'}}$, where the comma subindex denotes a derivative of the approximation functions with respect to the local axial coordinate $X_{1'}$.

The element integrals are evaluated after an introduction of the same conditions on strains in the neglected directions as in the previous section. Compared to the $3D$ solid case above, the appearance of a coordinate multiplied with the shape functions

[48] The $U_{3'}$ component is obviously not really meaningful, but included for consistence with Eq. (3.8)

is noted[49]; this represents a simplification of the kinematics in the $X_{2'}$ axis direction not described in detail[50], ensuring that the beam section remains plane, although not necessarily normal to the midline.

The linear and independent interpolation of the three nodal variables makes the usage of this approach straight-forward.

Another approach, commonly connected to the Euler-Bernoulli beam theory, uses the same nodal displacement variables, but interprets them in another way, cf. Fig. 3.13c. While the rotation, as above, is used to describe the changing direction of the midline normal, it now also describes the slope of the beam midline itself. This implies that the beam section is always plane and normal to the midline, and shear strain is thereby defined to vanish. A non-uniform approximation is used as

$$\begin{aligned} U_{1'} &= N_1 U_{11'} + N_2 U_{21'} \\ U_{2'} &= N_3 U_{12'} + N_4 \vartheta_{13'} + N_5 U_{22'} + N_6 \vartheta_{23'} \\ U_{3'} &= 0 \end{aligned} \tag{3.82}$$

adding four third-degree polynomial functions[51] in the local axial coordinate $X_{1'}$ for $U_{2'}$; the functions are available in any treatise of finite elements. The key aspect of the form, compared to the situations above, is that two nodal variables[52] are merged together in one approximation.

The approximation leads to an expression for the element midline slope, which is now the rotation $\vartheta_{3'}$ as

$$\vartheta_{3'} = U_{2',\,X_{1'}} = N_{3,X_1'} U_{12'} + N_{4,X_1'} \vartheta_{13'} + N_{5,X_1'} U_{22'} + N_{6,X_1'} \vartheta_{23'}, \tag{3.83}$$

The total approximation in the form of Eq. (3.8) then uses

$$\underline{\mathbf{N}} = \begin{pmatrix} N_1 & -X_{2'} N_{3,X_1'} & -X_{2'} N_{4,X_1'} & N_2 & -X_{2'} N_{5,X_1'} & -X_{2'} N_{6,X_1'} \\ 0 & N_3 & N_4 & 0 & N_5 & N_6 \\ 0 & 0 & 0 & 0 & 0 & 0 \end{pmatrix} \tag{3.84}$$

to represent Eq. (3.82) with the same element discrete variables as in Eq. (3.81).

The two forms of kinematic assumptions for the 2-node plane frame element in Eqs. (3.80) and (3.84), based on nodal displacement components in Eq. (3.81), can be used to develop finite elements following the general procedures above. The discussion below will show that the obtained elements are not necessarily optimal. Before considering possible improvements, three comments are given on the formulations above.

---

[49] With a symmetric beam section, this will only appear in squared form, leading to the bending stiffness of the beam section, in the final expressions.

[50] The $X_{3'}$ direction is neglected through the 'plane' assumption

[51] not denoted shape functions here, due to the non-uniform approximation

[52] which are also of different kinds

The first comment relates to the introduction of rotation variables, in the plane beam case the rotation $\vartheta_{3'}$, which is of another type than the translation components used in the $3D$ solid models. Obviously, this rotation is of another unit (e.g., [rad.] instead of [m]), but this difference in unit also implies that the conjugated quantity appearing in the element internal force $\underline{p}'_e$ is not a force, but a moment quantity. That this will come automatically is seen from the $X_{2'}$ coordinate in the kinematic descriptions, which will propagate to strain and stress expressions. The different types of quantities appearing in $\underline{p}'_e$—and thereby also in $\underline{f}'_e$—is one of the reasons for the notational distinction between, e.g., exterior forcing and external force vector.

The second comment concerns only the Euler-Bernoulli model, where the rotation variable is used for an improved description of the transversal displacement. The higher order of approximation will give, but its treatment also demands, a higher degree of continuity in the displacement description. This has some implications on the possibilities to connect elements, but will normally not give any major problems.

Third, the introduction of exterior forcing will demand some extra care for the frame element, and does not lead to just equal nodal external force components at both ends. A consistent equivalent external force representing boundary traction and body-force must consider the corresponding displacement, as defined by the adopted kinematic assumptions. This comment is particularly valid for the Euler-Bernoulli beam element, with its high order approximation and mixed types of variables.

A straight space frame element, intended for $3D$ situations can be developed along the same lines, when displacement in the $X_{3'}$ direction is described by the $U_{3'}$ translation and the rotation $\vartheta_{2'}$. Torsion is linearly interpolated from the nodal values for the rotation $\vartheta_{1'}$.

Thin and thick situations

The two kinematic models for a plane frame element above are both suited for implementations. They will, however, give elements with different capacities and properties. Practical recommendations typically suggest element of Timoshenko type for ‘thick’ beams and those of Euler-Bernoulli type for ‘thin’ ones, reflecting the dominant shear and bending deformations typically occurring.

While the Euler-Bernoulli element will give a somewhat over-stiff response for thick beams, due to the neglected shear deformation, the Timoshenko element—which has some desirable advantages in implementations—can give extremely over-stiff results for thin beams, due to locking phenomena. Such effects occur in elements due to inconsistencies in kinematic approximations, and are here related to the shear angle. In a problem where bending should dominate response, accompanying shear stress will become excessively high in the approximation, and thereby consume almost all work introduced by exterior forcing; the resulting deflection can be orders of magnitude too low[53].

[53] An example cantilever of height $1/1000$ of length, gives a deflection under uniform transversal load on the order of 10^{-5} times the correct, when using the form of Eq. (3.79).

The problem can be remedied, and a frame element useful for all thicknesses developed, by a modification to the strain expression, still keeping the energy-based formulation favoured here. Within the MITC ('mixed integration of tensor components') approach, promoted by Bucalem and Bathe (1993), Ko et al. (2017), and many authors, the in-plane shear strain, which comes from the linearly varying rotation $\vartheta_{3'}$ and the constant midline slope angle, can instead use the average value for rotation $\frac{1}{2}(\vartheta_{13'} + \vartheta_{23'})$ for the whole length; this is a modification to the kinematic description used for the strain expressions. This removes the excessive shear variation over the element length, and thereby the locking, and gives much improved results for thin beams, without any noticeable effect on thick ones. Even if the form is slightly inconsistent in relation to the continuum formulations, the results are predictable and more well-behaving than for other methods of locking removal.

Also other forms of locking, due to inconsistencies in kinematics, may occur in beam elements, but these are in most cases less severe.

Plates and shells

For plate and shell elements and structures, essentially the same aspects appear. Rotation variables are used to represent the kinematic situation over the small but not infinitesimal thickness. For a flat plate element, these are the rotations around the in-plane local axes, which are connected to the transversal displacement, the direction of the normal to the surface, or both these. Corresponding to the Timoshenko beam theory, the Mindlin plate (or thick-plate) theory uses rotations as orientations of the normal, while the Euler-Bernoulli beam theory corresponds to the Kirchhoff plate (or thin-plate) theory. Related to the discussion above, the two theories are more or less suited for problems of different thicknesses: the Mindlin theory considers the shear stiffness coming from a relatively thick situation, while the Kirchhoff theory only considers bending deformations. As with the beam models, the former thereby considers shear effects on the transversal displacement, at the cost of a less precise representation of the plate bending.

As with the frame elements discussed above, the kinematic assumptions for the two models can lead to locking effects when an element type is used outside its intended scope. Different methods are used to remedy these problems in general software, where 'tuning' efforts modify the clear-cut derivations in order to give optimal properties for a chosen set of test problems. Again, the MITC approach is preferred, as it is well-defined in relation to the energy-based approaches promoted in this treatise. As the class of shell problems ia always potentially troublesome, critical testing of an element type is recommended for increased credibility in results. Published results are valuable guides, but need be evaluated as conclusions are highly problem related.

Assemblies of elements

Like the membrane and truss elements, the shell and frame elements need a geometric transformation from the local geometry used in their derivation to the global geometry used for the complete structural model. This first demands that the element is trivially re-written to relate to a complete set of nodal components

$$\underline{U}_j = \left(U_{j1'}, U_{j2'}, U_{j3'}, \quad \vartheta_{j1'}, \vartheta_{j2'}, \vartheta_{j3'}\right)^{\mathrm{T}}, \tag{3.85}$$

for node j, and relating to the three local axes.

The transformation of the three translation components is identical to the previous description, but the rotation components need care, at least if a $3D$ model is employed. Only when rotations are small, the three components can be considered a vector, and handled in the same way as translations. For large rotations in space, this is not possible, and other measures and methods must be introduced. These are transformed to their local counterparts for the element evaluations.

For the representation of large space rotations, several approaches are available, e.g., Euler angles and the rotation vector. All methods have some advantages in handling or generality, but also some limitations. Related to the representation of the rotations, the differential rotation expressions needed in the element transformations can be derived. The full treatment of this is outside the present scope.

The discussion of total and differential rotations is not least valid in the context of co-rotational element types. Such element formulations are rather frequently discussed in literature today, but are based on older concepts of 'adapted' and 'ghost' reference configurations. The method can be described as a removal of (large) rigid displacement, and in particular the rotation, from the deformation. When the resulting deformation is considered as small and treated as linear, but only then, the approach leads to simplifications in the element expressions. As the formulations are still based on a Lagrangian formulation with an unstretched initial reference state, cf. Sect. 2.1, the co-rotational formulations fit well into the setting described above.

3.5 Displacement Boundary Conditions

The boundary conditions in the form of tractions on the boundary part Γ_T are extensively discussed above within the treatment of exterior forcing. Also displacement boundary conditions on the boundary part Γ_U must be considered, when using a discretized modelling of a structure. Essentially, these only appear in relation to the virtual displacement field used in the derivation of the mechanics equations. These must fulfil the essential boundary conditions that $\mathfrak{D}\mathbf{U} = \mathbf{0}$ on boundary part Γ_U, when prescribed displacement conditions are introduced as part of the frozen parameter setting.

Although it is very common in engineering problems that the displacement boundary conditions demand that the displacement components $U_i(\mathbf{X}, t) = \text{const.}$, or even $= 0$ on (part of) the part Γ_U, it is fully possible to specify the components as any function of $\mathbf{X}$ and t. In an interpolating approximation, like a finite element model, this must be represented by the discrete displacement variables, and the shape functions used, which sets some limits to what can be represented. After an introduction of fixed values to a set of discrete variables in the solution, the interpolation defines the displacement variation between the nodal points; the variation will therefore be linear with a linear element interpolation, which is the natural situation in most engineering problems. Higher order elements have more edge nodes, and prescribed values for the displacement gives corresponding interpolation along the boundary; if boundary conditions are more rapidly varying than the shape functions can reproduce, they will be approximately satisfied.

Even if the identification and introduction of prescribed displacement components is in most cases very natural—when some boundary nodal points are given prescribed displacement components—a few situations exist where the identification can be misleading. The most prominent one is related to prescribed transversal deflections for plate (and shell) models, when rotation nodal variables are included in the approximation. Whether to include a prescribed rotation around the plate edge normal is debatable, and related to the used element type[54]. With hard boundary conditions, this rotation is typically set to zero when the edge should undergo a constant (often zero) transversal deflection. This many times leads to a kind of locking response, with significantly over-stiff results as a consequence. Soft boundary conditions, which allow unphysical rotations around an edge normal, are often more appropriate for a good approximation, given that a not too low number of elements are used in modelling; the results, however, may appear somewhat strange.

When some displacement variables are prescribed for the analysis of the structural model, reactive force components appear in the conjugate internal force components; these are the forces needed to enforce the displacement condition. The solution method is described for linear cases in Sect. 4.1.1, and is in essence the same also for non-linear situations. A more elaborate treatment of boundary conditions as mechanical constraints is given in Sect. 3.6 below.

3.5.1 Symmetry Modelling

Nature shows many aspects of symmetry, and engineering often uses geometrical symmetry and repetition of structural components for aesthetical as well as mechanical reasons. From the computational viewpoint, the identification of symmetries was also a necessity in early days of numerical analyses, due to limited resources. Creating or identifying such aspects is also well in line with the engineering ideals

[54] Note also the discussion on the notation for moment components in Sect. 1.6.

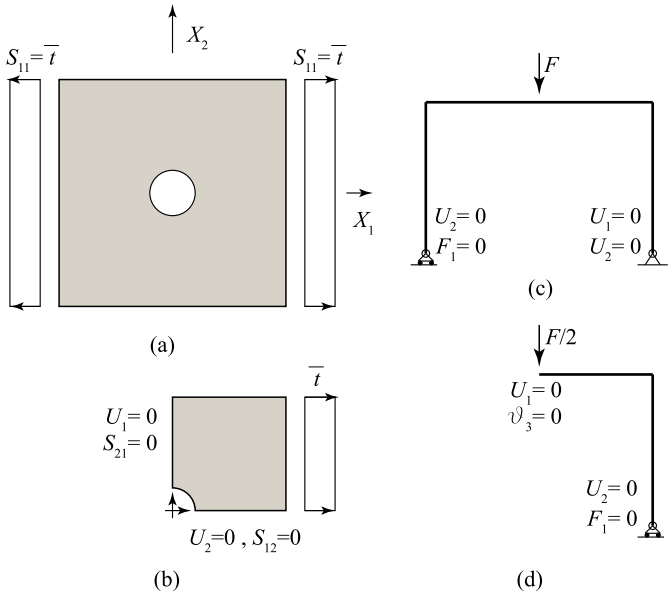

Fig. 3.14 Macro-symmetry in two simple plane examples

of reducing a problem to relevant and tractable pieces, but this section shows that this intuition is mis-leading in some cases.

From the modelling viewpoint, symmetry can be considered from two viewpoints. The previous paragraph primarily relates to a macro-symmetry, where the symmetry is related to the structural problem at hand. A symmetry in geometry and boundary conditions is then assumed to lead to a symmetry in response. Two simple but illustrative plane examples are given in Fig. 3.14. For these, symmetry is often introduced in the modelling. Micro-symmetry, which relates to the interior approximation—e.g., through finite elements—is discussed below. Both aspects of symmetry are further discussed in Sect. 5.3.

Considering macro-symmetry, the square region in subfigure (a) has only boundary traction conditions, even if some of the traction intensities are defined to zero. i.e., all boundaries belong to Γ_T, cf. Fig. 2.6[55]. Any arbitrary rigid translation or rotation is thereby fully possible. In a computational model for equilibrium, which demands some displacement constraints, this situation is not trivially described, but the treatment in Sect. 3.6.3 gives a reliable method.

A common engineering approach for modelling this case is shown in Fig. 3.14b. This identifies two reflection planes and a 180° rotation as the symmetries of the problem. For equilibrium analyses, the two mirror planes are replaced by displacement boundary conditions, in the component normal to the reflection plane, i.e., a

[55] except that the reduction to a plane problem implies that the midplane of the model is assumed to stay in the (X_1, X_2) plane, which is a displacement boundary condition for the U_3 component

new boundary part in Γ_U. The other component on these edges belongs to Γ_T, with necessarily zero traction components parallel to the symmetry edges. The isolation of the quarter part thereby removes the rigid displacement possibilities, by fixing the center point and the edge orientations.

The conclusion on symmetry for the problem is related to both the structure and the forcing. For an alternative case, with a forcing consisting of identical traction also on the horizontal boundaries $X_2 = \text{const.}$, the symmetry of the structure is even higher, with four obvious reflection planes[56], and 90° rotations as symmetry operations. In fact, the symmetry is even higher, due to the up-down symmetry in relation to the plane of the structure. The representative subregion is then a one-eighth part of the square region, as further discussed in Sect. 5.3.

Figure 3.14c shows a simple plane frame with symmetric shape and forcing. The support conditions are unsymmetric, but express that the lower column ends are moment-free, and not connected by any horizontal coupling[57]. The left support thus moves left-wards under this forcing. With respect to interior force, the response is, however, symmetric, and Fig. 3.14d shows a possible analysis model, with new—and one removed—displacement boundary conditions. With U_i and F_i denoting the displacement and integrated force components in the axis directions, boundary conditions must reflect that the frame bottom can change its length under forcing; the displacement conditions for the right-hand support must allow this, and change the condition for component U_1[58].

It has been emphasized for both examples that symmetry considerations are common—and useful—for equilibrium analyses, i.e., static settings. In neither of the two cases, symmetry should, however, be introduced in a dynamic analysis, as the introduction of displacement boundary conditions removes or distorts some vibration modes[59]. A full structural model without any fictitious conditions is always recommended, when (the correct number of) rigid body modes showing zero eigenfrequencies can be easily disregarded when interpreting simulation results.

The present topic of stability is closely related to dynamic response, and the same recommendation is given. This is further motivated by the discussion in Sect. 3.7, which shows that buckling, or bifurcation, is fundamentally symmetry-breaking. This implies that the problem symmetry must be fully respected in the initial model. The same recommendation is obtained from the plate buckling analysis in Sect. 1.6, where it is shown that the buckling response modes are different, dependent on the geometric relations of the region considered.

---

[56] i.e., also through the diagonals

[57] which is in most cases a necessary, albeit not necessarily a fully correct, assumption in order to isolate the model from its surroundings

[58] Note that already the plane frame assumption introduces a restriction to the full $3D$ response, prescribing $U_3 = 0$

[59] Note, for instance, the much smaller mass active in a horizontal mode vibration in cases (d)

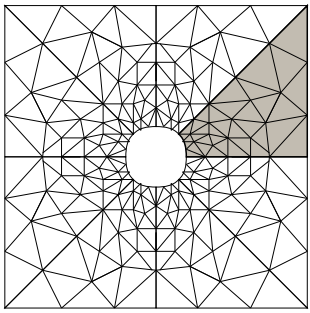

Fig. 3.15 (Coarse) meshing of the representative subregion of a problem with higher symmetry than the case in Fig. 3.14a. The one-eighth mesh must be repeated in two versions for a quarter model and eight versions for a complete model

Discretization symmetry

When considering the discretization of a structural model, micro-symmetry demands that the approximation does not destroy the symmetry existing in the original problem. For the example in Fig. 3.14a this means that a finite element mesh must be identical—with the obvious reflections—for all quarters of the complete structure, or results will be more or less incorrect. As the subregion in Fig. 3.14b already has introduced all symmetries present in the problem, this subregion model can be described by any element mesh without negative effects (in this respect).

For the alternative case discussed above, where equal tractions act on all four edges of the model in Fig. 3.14a, the higher degree of symmetry demands further consideration. Figure 3.15 show how the repetitive subregion of one-eighth of the structure can be arbitrarily approximated by elements, but that this must be identically repeated over the full considered region, twice for a quarter model and eight times for the complete region. The key aspect of this, which is further demonstrated in Sect. 5.3, is that a discretized model must keep, and must not destroy, any symmetry existing in the original problem, if reliable results are requested for dynamic or stability problems. The demands are thereby higher than for a linear equilibrium analysis, where symmetric forcing on a symmetric structure will always lead to symmetry in results.

One further aspect in the treatment of symmetry is that adopted finite elements must be objective in the sense that their formulation is not dependent on any particular coordinate axis directions. Without this, even a visibly symmetric element mesh can give unsymmetric results.

3.5.2 Coupling of Subregions

The approximation of the displacement on a boundary surface of a model is also of fundamental importance, when a structure is divided into components, like the schematic discussion in Sect. 2.5.5. The regions are then either included in the same

simulation model, with definitions of their respective geometries and properties together with the coupling information, or they are separately and successively analyzed with a transfer of boundary data between the simulations.

In either case, the continuity of the approximate representation of displacement across the boundary between the subregions need be carefully considered. The problem lies in the appearance of gaps between the interpolated subregion surfaces (or edges), which are a major source of inaccuracy, due to the work done by interface stresses over the gap. This is often a major challenge, when different element types are used for the regions[60], or when the meeting regions are independently meshed with non-regular element shapes and sizes.

3.6 Mechanical Constraints

In almost every relevant engineering problem, the structural equilibrium solutions must fulfil additional mechanical constraints. These are one way to define the supports for the structure, but constraints can also be used to restrain rigid body movements with an objective method, e.g., for a thin sphere when conventional point supports are not suited. The same idea is also used to prescribe more general displacement relations, such as symmetry conditions.

Several kinds of constraints, e.g., support conditions in the form of prescribed displacement variables, can be trivially introduced by straight-forward modifications to the established equilibrium equations. A more systematic approach can handle also other forms of constraints. This section will discuss constraint equations of rather general form in relation to the discretized form of Eq. (3.45), i.e., as residual functions of the problem variables. The constraints are considered as passive, i.e., enforced by the structure itself, as opposed to active ones, when externally supplied energy modifies the response following some strategy.

The introduction of a set of N_c constraints on the equilibrium solution demands a corresponding set of N_c constraint-enforcing variables $\underline{C}$. Being fundamental mechanical quantities, these are included in the solution variables, together with discrete displacement variables $\underline{d}$.

3.6.1 Energy Form

Following the energy-based formulation from Eq. (2.87), which is valid for conservative problems, the total potential Π is augmented by the two terms

$$\Pi_{\text{constr}} = \underline{C}_\ell^{\mathrm{T}} \underline{R}_\ell(\underline{d}) + \Pi'_{\text{constr}}(\underline{d}, \underline{C}_c), \tag{3.86}$$

[60] which can be, e.g., beam-plate connections, or elements of the same class but with different orders of approximation

reflecting common engineering settings of constraints; each set can consist of several terms. The terms are implicitly dependent on problem parameters. The second set of terms is the more general form, and is based on constraint variables $\underline{C}_c$, in addition to the displacements; these may appear non-linearly in Eq. (3.86).

The first type of terms in Eq. (3.86) is a special case of the second, and is introduced as it is commonly useful in engineering problems. This type uses Lagrange multipliers $\underline{C}_\ell$ to enforce residual equations $\underline{R}_\ell = \underline{0}$, and is simpler to handle as long as the functions in R_ℓ are linear in the components of $\underline{d}$. The corresponding Lagrange multipliers are often physically meaningful results, e.g., discrete support forces. As a special case, hard contact conditions can be handled based on this approach, cf. Sect. 3.6.4.

The two vectors of constraint variables are collectively denoted as $\underline{C} = (\underline{C}_\ell^{\mathrm{T}}, \underline{C}_c^{\mathrm{T}})^{\mathrm{T}}$. These variables are typically independent, in the sense that each individual term of Π_{constr} only contains one of them.

With the terminology used, a total constrained potential is defined for the constrained conservative problem setting, as

$$\Pi_c = \Pi_p + \Pi_{\text{con}} + \Pi_{\text{constr}} \tag{3.87}$$

The constraints affect the discrete residual of equilibrium, giving an N_d-by-1 constrained residual force

$$\underline{r}_c = \Pi_{c,\underline{d}} \equiv \underline{r}_0(\underline{d}) + (\underline{R}_{\ell,\underline{d}})^{\mathrm{T}} \underline{C}_\ell + \Pi'_{\text{constr},\underline{d}}. \tag{3.88}$$

where $\underline{r}_0$ is the equilibrium residual discussed in Sect. 3.2.5, without the constraints, and the final term contains $\underline{C}_c$. The assumption about linearity of $\underline{R}_\ell$ simplifies the handling of the second term, and $\underline{R}_{\ell,\underline{d}}$ is often only a set of constants.

Differentiating the potential expression in Eq. (3.87) with respect to the components in $\underline{C}$, gives a set of constraint functions

$$\underline{R}_c = \Pi_{c,\underline{C}}, \tag{3.89}$$

which must vanish at a constrained equilibrium. The functions in $\underline{R}_c$ depend on the discrete variables $\underline{d}$, the constraint-enforcing variables $\underline{C}$, and problem parameters. Due to the assumed independence, each variable in $\underline{C}$ gives one constraint function. For Lagrange multipliers according to the first part of Eq. (3.86), $\underline{R}_c \equiv \underline{R}_\ell$, but the term Π'_{constr} demands a formal differentiation. The final $\underline{R}_c$ in Eq. (3.89) may contain functions of both types.

As the residual equation together with the physical constraints define the problem at hand, the setting demands solutions to a constrained equilibrium equation

$$\underline{R} \equiv \begin{pmatrix} \underline{r}_c \\ \underline{R}_c \end{pmatrix} \equiv \begin{pmatrix} \Pi_{c,\underline{d}} \\ \Pi_{c,\underline{C}} \end{pmatrix} = \underline{0}, \tag{3.90}$$

being $N_d + N_c$ equations in the $N_d + N_c$ state space variables, collectively denoted as

$$\underline{D} \equiv \begin{pmatrix} \underline{d} \\ \underline{C} \end{pmatrix}; \tag{3.91}$$

these are the fundamental variables of the constrained problem.

A constrained stiffness matrix

$$\underline{\underline{K}}^c = \begin{pmatrix} \underline{\underline{K}}^i & \underline{r}_{c,\underline{C}} \\ \underline{R}_{c,\underline{d}} & R_{c,\underline{C}} \end{pmatrix}, \tag{3.92}$$

relates differential increments in the constrained residual to increments in the variables. This matrix is fundamental to the constrained mechanical problem, and needed for the stability conclusions, cf. Sect. 3.7.

It is important for implementations of the described setting to note that Eq. (3.90) establishes a set of $N_d + N_c$ equations, which represents a problem with only $N_d - N_c$ free variables. Elimination approaches, where some variables in $\underline{d}$ are condensed out from the set of equations by using $\underline{R}_c = 0$ lead to a smaller set, but normally demand more specific problem knowledge and information, in particular if constraints are non-linear. The existence of the $2N_c$ additional variables and equations is of importance, e.g., in the evaluation of eigensolutions for the constrained system, cf. Sects. 3.7 and 4.5.2.

As one non-trivial example, the treatment of a closed membrane pressurized by internal over-pressure can—under some assumptions—enforce a specific gas amount, according to a constraint potential term

$$\Pi_{\text{constr}} = A \ln \frac{C_1 + p_0}{p_0} - C_1 V, \tag{3.93}$$

where A is a parameter representing gas amount, and p_0 the hard-coded ambient pressure, while C_1 is the single constraint-enforcing variable, the over-pressure. The volume V is calculated from current displacement $\underline{d}$. The seemingly complicated form is demanded in order to obtain the relation in a form resembling energy. The residual function from this energy term is $R_c = A/(C_1 + p_0) - V(\underline{d})$, when differentiated with respect to C_1[61]. When differentiated with respect to the displacement variables in $\underline{d}$, the potential term gives

$$\Pi_{\text{constr},\underline{d}} = -C_1 V_{,\underline{d}}, \tag{3.94}$$

which is the external force term representing the internal over-pressure on the structure, and part of the residual function $\underline{r}_c$ in Eq. (3.90).

[61] Demanding R_c to vanish implies that $A = pV$, with p the total pressure and V the volume, and represents the general gas law under isotheral conditions.

The over-pressure is just a forcing parameter when no constraints are considered, but changes role with the introduction of the constraint. It here reflects a fundamental mechanical requirement, which must be considered in a stability evaluation. When this gas amount is not constrained, but only a convenient alternative expression for the forcing, a similar expression is used as a parametric selector function in Sect. 4.4.

3.6.2 Supports

Structural supports are displacement boundary conditions belonging to the boundary part Γ_U in Sect. 2.5, as discussed in Sect. 3.5. In the discretized setting, these lead to a set of prescribed discrete variables in the solution. This implies that the representation of the boundary tractions as equivalent reactive forces is unknown, and part of the equilibrium solution. The engineering interpretation is that of support point reactions.

In common finite element equilibrium simulations, the introduction of displacement constraints is considered as a necessity in order to remove rigid body motions from the solution. The basic method to remove this singularity is to remove rows and columns corresponding to prescribed displacement components in the residual and stiffness matrix, cf. Sect. 4.1.1.

As an alternative to this approach, the prescribed solution components are introduced through constraint functions augmenting the residual expression. Being of very simple form, these are formulated as functions $\underline{R}_\ell(\underline{d})$ in Eq. (3.86), in which case the reactive force components appear in the solution as the corresponding Lagrange multipliers $\underline{C}_\ell$. They are parts of the external force on the structure, but can also, after convergence to equilibrium, be found as parts of the resisting internal force $\underline{p}$, when applied force $\underline{f}$ is subtracted from it.

As noted above, the addition of support conditions expands the equilibrium equations by a set of constraint equations, rather than condensing it. This approach leads to a system with an increased number of unknowns, but it also has several advantages. One example is when non-localized support conditions can avoid the localized effects created by point-wise supports, another the generality in problem modelling.

3.6.3 Symmetry Conditions

Although not recommended in Sect. 3.5.1 for problems of dynamics and stability, many structural problems are analyzed with an assumed macro-symmetry. Such an approach uses a model of a part of the whole structure. Symmetry planes are thereby typically replaced by displacement conditions related to the plane; these are well described by displacement constraints, as in Sect. 3.6.2. In this case, the constraint equations are normally of very simple form, e.g., specifying one displacement variable to zero, or the sum of (or difference between) two axis components vanishing;

this is the situation on the diagonal of the one-eighth subregion in Fig. 3.15, and fits well as functions $\underline{R}_\ell(\underline{d})$ in Eq. (3.86).

Similar approaches can also be used for other relations between displacement components, with an obvious one being the modeling of anti-symmetries. Such anti-symmetries are noted to be valid only in linear and linearized settings. A discussion on how symmetries and anti-symmetries can be used for a complete investigation of structural stability, based on a minimal representative subregion is given by Eriksson and Nordmark (2016).

3.6.4 Hard Contacts

As a special case of constrained equilibrium setting, this method is used to include mechanical contact conditions, assumed as hard, frictionless and exact. The description is focussed on contacts in chosen discretized nodes of a finite element model, but can be modified to other displacement-based models. It is similar to the introduction of supports and prescribed displacements. If N_z nodes are known to be in contact, the form is through a potential contribution from each contact node, summed as

$$\Pi_{\text{constr}} = \sum_{j=1}^{N_z} C_j (z_j - \overline{z}_j) \tag{3.95}$$

where a nodal position coordinate denoted z_j is constrained to be a prescribed value $\overline{z}_j$ in the solution[62], and C_j is a corresponding contact force component in the direction of z, ensuring the exact fulfilment of the contact condition. In the sense of Eq. (3.86), the contact situation can be described as a contribution

$$\Pi_{\text{constr}} = \underline{C}_\ell^{\mathrm{T}} \left(\underline{\underline{T}}_z (\underline{X}_d + \underline{d}) - \underline{\overline{z}} \right), \tag{3.96}$$

independent from any non-contact prescribed function values. In the equation, the vector $(\underline{X}_d + \underline{d})$ represents the current nodal position, when $\underline{X}_d$ gives the reference nodal coordinates in a form compatible to $\underline{d}$, and $\underline{\overline{z}}$ a corresponding description of the contact surface coordinates. The transformation operator $\underline{\underline{T}}_z$ is a constant N_z-by-N_d matrix independent of $\underline{d}$ and $\underline{C}$, but in general dependent on problem parameters. Each row in $\underline{\underline{T}}_z$ expresses one displacement constraint, and transforms the current point coordinate to the surface normal direction.

The N_z constraint functions are parts of the complete $\underline{R}_c$ in Eq. (3.89), and are related to contributions $(\underline{\underline{T}}_z^{\mathrm{T}} \underline{C}_\ell)$ to the residual force $\underline{r}_c$ in Eq. (3.88).

[62] with z a general coordinate normal to the contact surface, which does not need to be in the same direction for all nodes

The formulation assumes that the active constraints are known, when solving for an equilibrium state. The constraints are introduced in the same way as the supports[63]. With this setting, it is straight-forward to obtain an equilibrium solution in which displacement conditions are exactly fulfilled at all supports, but also at the defined set of contacts.

When a sequence of equilibrium states is obtained for a pre-defined active set of constraints, a solution is illegal when it contains contact forces of the incorrect sign, or if any node outside the active set has crossed the contact surface. The algorithm must signal such incorrect solutions, and modify the set of contacting nodes when they appear. When tracing an equilibrium sequence, this is a case of transition equilibrium state, as discussed in Sect. 4.5.6, and shown by an example in Sect. 5.4.

3.7 Discretized Stability

Stability has been discussed for a continuum setting in Chap. 2. While the reasoning is strictly not valid in continuous cases, as described by Como and Grimaldi (1995), theories for discrete systems can be defined, and are discussed here.

The treatment is primarily related to the consideration of static stability, i.e., stability of an equilibrium configuration. The structural models can be mechanically constrained, i.e., completely described by Eq. (3.90), but affected by conservative forcing only.

The basic view on stability, based on the work by Liapunov (1966), is formulated in Chap. 2. This defines static stability as the capacity of the structure, or rather the model used for it, to stay close to the equilibrium state after a small perturbation. An asymptotic stability, where the effects from a perturbation are gradually decreasing to zero, is then ensured for any structure possessing some damping. Within the present setting, stability thereby refers to one equilibrium state for a structure, and discusses this stability property from two different starting points.

For models without constraints, common views demand for static stability a minimum total potential energy at the equilibrium state, as discussed by Koiter (1970), and Thompson and Hunt (1973), among others. For a discretized problem without constraints, this is a sufficient condition, and corresponds to positive definiteness of the incremental stiffness matrix, which describes the second variation of the total potential around the equilibrium, as defined by Eqs. (3.53) and (3.60). This is also the differential of the residual force in Eq. (3.61), for the expression evaluated at a particular equilibrium state, with all parameters fixed. Using the incremental stiffness matrix allows all classes of conservative forcing.

[63] A support can be treated in the same way, as an always existing row of $\underline{\underline{T}}_z$.

The positive definiteness of $\underline{\underline{K}}^i$ is defined from all eigenvalues Σ_ℓ^K being positive in the one-matrix eigenvalue problem (no summation)

$$\underline{\underline{K}}^i \, \underline{\varphi}_\ell^K = \Sigma_\ell^K \, \underline{\varphi}_\ell^K . \tag{3.97}$$

with eigenvalues Σ_ℓ^K and corresponding eigenvectors $\underline{\varphi}_\ell^K$ for $(\ell = 1, \ldots, N_d)$. The symmetry of the matrix ensures the existence of a complete set of orthonormal eigenvectors, spanning the N_d-dimensional discrete displacement space.

As an alternative view on static stability, closer to the basic Liapunov definition, a perturbation must not lead to divergence, but to a movement composed of the harmonic vibration modes around the equilibrium. These are evaluated from an equation for undamped free vibration, as in Eqs. (3.65)–(3.67), in the form of a two-matrix eigenvalue problem (no summation)

$$\underline{\underline{K}}^i \, \underline{\varphi}_\ell = \Sigma_\ell \underline{\underline{M}} \, \underline{\varphi}_\ell . \tag{3.98}$$

with $\underline{\underline{M}}$ the mass matrix, cf. Sect. 3.2.3, and again for $(\ell = 1, \ldots, N_d)$. The problem gives a full set of eigenvectors, as both matrices are symmetric.

Given that all Σ_ℓ are positive, the solutions are free vibration modes $\underline{\varphi}_\ell$ and frequencies $\sqrt{\Sigma_\ell}$ in small linearized vibrations around the equilibrium state. With any $\Sigma_\ell \leq 0$, non-vibration responses exist, which can lead to divergence, if triggered by the perturbation. Stability is thereby judged by the sign spectrum of the eigenvalues Σ_ℓ, demanding all $\Sigma_\ell > 0$ for stability.

It is noted that the results from Eqs. (3.97) and (3.98) give different eigenvalues and eigenvectors, with only the sign spectra of eigenvalues the same. The simpler notation for quantities in Eq. (3.98)—without a super-index—reflects that the eigenvalues from Eq. (3.98) are the preferred ones.

3.7.1 Constrained Stability

As discussed above, stability of an unconstrained equilibrium state demands a local minimum of the total potential at the calculated solution. With constraints included as energy-like terms, stationarity is sought for equilibrium, and the second variation of the constrained total potential in Eq. (3.87) is studied for stability conclusions. This can be written as a second variation of constrained potential

$$\mathrm{d}^2 \Pi_c = \mathrm{d}\underline{D}^{\mathrm{T}} \, \underline{\underline{K}}^c \, \mathrm{d}\underline{D}, \tag{3.99}$$

with $\underline{\underline{K}}^c$ the constrained stiffness matrix, cf. Eq. (3.92). It is noted that the displacement and constraint-enforcing variables must be allowed to vary together.

While two methods for evaluation of stability are discussed above, and considered as equivalent, the difference between the approaches is more significant in connection

with constrained equilibrium settings. It is here only appropriate to judge stability from the existence of vibration frequencies, i.e., the eigenvalues Σ_ℓ corresponding to eigenvectors $\underline{\varphi}_\ell$, solved from the two-matrix problem (no summation)

$$\underline{\underline{K}}^c \, \underline{\varphi}_\ell = \Sigma_\ell \, \underline{\underline{M}}^c \, \underline{\varphi}_\ell \tag{3.100}$$

with stability demanding all eigenvalues Σ_ℓ to be positive, cf. Eq. (3.98). The constrained stiffness $\underline{\underline{K}}^c$ is defined in Eq. (3.92). As the constraints are mass-less, the constrained mass matrix to use in Eq. (3.100) is of the form

$$\underline{\underline{M}}^c = \begin{pmatrix} \underline{\underline{M}} & \underline{\underline{0}} \\ \underline{\underline{0}} & \underline{\underline{0}} \end{pmatrix} \tag{3.101}$$

with $\underline{\underline{M}}$ the structural mass matrix—or any relevant simplification of it. With this setting, vibration modes around the studied equilibrium and their corresponding frequencies are estimated.

When only the eigenvalue sign spectrum is needed for the stability conclusions, any relevant structural mass representation can be used, as long as it is positive definite. A simple version is to use a diagonal matrix of equal nodal masses $\underline{\underline{M}} = \underline{\underline{1}}_{N_d}$. With this choice, neither the stability coefficients Σ_ℓ nor the corresponding eigenvectors have any physical meaning. In a sequence of evaluated equilibria, the variations of the calculated eigenvalues along the sequence, however, can have some predictive capacity for approaching critical situations, where any $\Sigma_\ell = 0$, somewhat similar to—but more powerful than—the LPB ideas of Sect. 4.1.3.

Numerical treatment of the eigenproblem in Eq. (3.100) is discussed in Sect. 4.5.2.

3.7.2 *Comparison of Criteria*

The stiffness and mass expressions in the eigenvalue settings above are evaluated at a particular configuration, and express differential relations, linearized around this configuration. They are thereby only valid for infinitesimal variations to the state, and this must be considered when interpreting results. This is illustrated already in Sect. 1.2, e.g., by Fig. 1.2, which shows a secondary equilibrium branch graph at the critical state. The graphs are initially horizontal, but deviate from this at finite deflections, at least for the more refined models.

The two seemingly very different views on the stability of an equilibrium state above reflect the basic criteria. The positive definiteness of the incremental stiffness matrix, corresponding to the eigenvalue problem in Eq. (3.97), shows that the total potential has to be increased, and additional energy supplied for the structure to leave the equilibrium. Stability demands that small changes to acting forces lead to only small changes to the equilibrium configuration. The eigenmodes obtained from the equation are further discussed below.

The vibration viewpoint, as expressed by the eigenvalue problems in Eq. (3.98) and (3.100), focusses on whether the structure will be able to sustain small linearized vibrations around the current equilibrium state, if an initial disturbance is introduced as an initial condition to a motion. Positive values for Σ_ℓ give real values for $\sqrt{\Sigma_\ell}$, and these correspond to frequencies in a vibration-type response, which continues without any additional exterior action[64]. With a zero eigenvalue, introduction of a small disturbance in the corresponding eigenvector direction will not lead to vibration. The existence of a negative eigenvalue indicates a possibility for an exponentially growing magnitude of the disturbance.

Either of the two views clearly shows that only the sign spectrum of the eigenvalues is of importance for the stability conclusion, not the precise values. The eigenvalues are evaluated for one particular equilibrium state, where displacements in $\underline{d}$—and constraint-enforcing variables in $\underline{C}$, if included—are in equilibrium at frozen parameters. This implies that interior stress and exterior forcing for this particular state are affecting the incremental (or constrained) stiffness matrix through the non-linear formulation.

For the common engineering setting, where a fixed structural model is considered when affected by some exterior forcing described by a single parameter λ, cf. Sect. 4.1.6, the non-linear response evaluation commonly interprets equilibrium variables as functions of this single parameter. The stability conclusions for the evaluated equilibria are thereby also related to the parameter λ. As most simulations of this type start from an unforced stable initial state, successively increases forcing, and focusses on finding the first critical equilibrium state for the model[65], the view is typically that the used force parameter is the one causing the loss of stability. Although fundamentally debatable, this is a reasonable view for this particular setting.

In the more general setting of Chap. 4, with several parameters for the model and forcing, and possibly parameters of very different kinds, the view on a forcing creating unstable response is no longer relevant, and other causal relations must be considered. The basic definition of stability for one particular equilibrium state—with all parameters frozen—must be used, disregarding any parameterization which has been used in finding this state. The notion of a particular parameter causing the loss of stability is thereby in general incorrect, cf. the discussion already around Eqs. (1.10)–(1.11). Along a parametric sequence of equilibrium states, stability conclusions thereby relate to certain parametric regions, which are delimited by critical states, where the stability properties change.

It is again emphasized that the constraint-enforcing variables in $\underline{C}$ are not parameters in this discussion, but are fundamental physical quantities included in the equilibrium solutions and in the eigenvectors evaluated. The effects of the expanded system in Sect. 3.6 must therefore be considered in the evaluation and interpretation of eigensolutions, cf. Sect. 4.5.2.

---

[64] but is eventually reduced by the ever-existing damping

[65] even if it is conceivable that a structure becomes stable with increasing force

Role of mass matrix

The two common eigenvalue settings for unconstrained problems in Eqs. (3.97) and (3.98) come from different criteria, and may demand different methods for their evaluation. With a stiffness matrix $\underline{\underline{K}}^i$, and a mass matrix $\underline{\underline{M}}$ coming from the used discretization of the structural model, the matrices are easily evaluated, but eigenvalue extraction is a computationally demanding task, always[66] based on iterative techniques, cf. the works by Wilkinson (1988) and Bathe (2014). Knowledge about the characteristics of the matrices involved can improve efficiency and reliability of the algorithms.

When comparing the formulations for eigenvalues, it is noted that the one-matrix problem in Eq. (3.97) can be written as (no summation)

$$\underline{\underline{K}}^i \underline{\varphi}_\ell^K = \Sigma_\ell^K \underline{\underline{1}}_{N_d} \underline{\varphi}_\ell^K . \tag{3.102}$$

where an identity matrix is introduced on the right-hand side. It is obvious that this equation is a variation of Eq. (3.98) with a much simplified uniform mass matrix. This refers equal masses to all discrete displacement components, and avoids all mass-coupling components existing in the mass matrix built consistently from the discretization through Eq. (3.21). The identity is thereby even more simplified than so-called lumped mass matrices. The form in Eq. (3.102) shows that the eigenvectors obtained are unphysical, as a re-scaling of the variables in the discretized setting will change the results. The eigenvectors obtained from Eq. (3.102), and thereby from Eq. (3.97), can not be used for any conclusions on the vibration modes of the model.

It is, however, shown by Strang (1988) that the sign spectra for the eigenvalues from the two forms must be identical, as both $\underline{\underline{M}}$ and $\underline{\underline{1}}_{N_d}$ are positive definite matrices. As only the signs of the eigenvalues are interesting, the two formulations are equivalent, in this particular respect. This reasoning also shows that both eigenvalue formulations identically show critical equilibria, with zero eigenvalues, which is of major interest in stability investigations.

The issue of a relevant mass matrix representation is an important aspect in the treatment of constrained problem settings, and will be further discussed in Sect. 4.5.2. A two-matrix eigenvalue problem is used for the formulation, but this can be re-written for efficiency in the treatment.

Interpretation of modes

For problem settings without constraints, the eigenvalues obtained from Eq. (3.97) are unphysical—as shown by the form in Eq. (3.102)—in contrast to the vibration properties obtained from Eq. (3.98). The magnitudes of the eigenvalues give no information on the stability properties of an equilibrium. The signs of the eigenvalues from both settings, however, provide this information.

[66] for models of interesting size

The same comments refer to the eigenvectors. With a consistent mass matrix, the eigenvectors from Eq. (3.98) define modes, which allow free vibrations at a specific frequency when the corresponding eigenvalue is positive. While these do not give any immediate information on the stability of equilibrium, they are, however, of major importance in connection with critical situations, as discussed in Sect. 4.6.

The set of eigenvectors in this case has the property that they diagonalize both stiffness and mass matrices, creating scalar equations, symbolically written as (no summation)

$$k_\ell \, \underline{\varphi}_\ell = \Sigma_\ell \, m_\ell \, \underline{\varphi}_\ell, \tag{3.103}$$

where k_ℓ and m_ℓ are the diagonalized stiffness and mass components[67]. These are interesting from the vibration viewpoint, as the set of eigenvalues is obtained by $\Sigma_\ell = k_\ell / m_\ell$. The diagonalization de-couples the discretized system into a set of single degree of freedom systems, on which the incremental force can be projected, and the response evaluated. This can be of major interest, when dealing with critical equilibrium states, in which case the eigenvectors are preferably mass-normalized so that $\underline{\varphi}_\ell^{\mathrm{T}} \, \underline{\underline{M}} \, \underline{\varphi}_\ell = 1$.

Further, as both matrices are symmetric[68], the eigenvectors are spanning the whole N_d-dimensional discrete displacement space. This implies that any increment to the state variables[69] can be written as a sum of contributions parallel to the eigenvectors, according to

$$\mathrm{d}\underline{d} = \sum_{\ell}^{N_d} \alpha_\ell \underline{\varphi}_\ell, \tag{3.104}$$

where the amplitude α_ℓ measures the contribution from eigenvector $\underline{\varphi}_\ell$.

Although the evaluated eigenvectors constitute a basis for any displacement vector of the problem at a particular equilibrium state, the diagonalization is only meaningful at this particular state. It is also noted that the eigenvectors in general are global, affecting large parts of a structural model, and not localized to a particular structural component, as is commonly—and necessarily—done in manual stability investigations.

Modes for constrained problem

The previous discussion was concerned with problem settings without constraints, where the displacement variables $\underline{d}$ are the only unknowns, and define the configuration in state space. When constraints are included in the problem formulation, several aspects change. When $(N_d + N_c)$ state variables are introduced to define the configuration, as in the collected vector $\underline{D}$ in Eq. (3.91), and the corresponding residual

[67] emphasizing that Σ does not denote a sum, but an eigenvalue

[68] but the incremental stiffness matrix not necessarily positive definite for the non-linear situation

[69] which are now just $\underline{d}$

equations in Eq. (3.90), the differential is given in Eq. (3.92), and the corresponding mass matrix by Eq. (3.101). Compared to the unconstrained case, a main difference lies in the just semi-definite mass matrix, with zero rows and columns.

Although the eigenvalues problem for this setting, given by Eq. (3.100) is of dimension $(N_d + N_c)$, the problem has only $(N_d - N_c)$ free variables, and only this number of eigenvectors exist. This demands specific algorithms for their solution.

The $(N_d - N_c)$ eigenvectors obtained are linearly independent, and thereby give a basis for the solutions in the constrained state space. Implicit in these solutions are the relations between increments in displacements $\underline{d}$ and constraint-enforcing variables $\underline{C}$. As in the unconstrained case, the obtained eigenvectors diagonalize the constrained stiffness and mass matrices.

Algorithms for eigenvalue extraction handle the semi-definite mass matrix in different ways[70]. If they allow such problem forms, they may add fictitious eigenvectors, which correspond to the zero mass part. As an example, the software Matlab[71], being more or less industry standard for numerical linear algebra procedures, adds $2\,N_c$ eigenvectors, with non-zero components only in the $\underline{C}$ part of $\underline{D}$, and gives eigenvalues marked as infinite for these vectors.

The numerical treatment in Sect. 4.5.2 replaces the zero masses for constrains by very small positive values, transforming the infinite eigenvalues to very high ones, which are easily discarded in the algorithm, when their very small norms of the $\underline{d}$ part of $\underline{\varphi}_\ell$ are noted.

3.7.3 Unstable Equilibrium

In the treatment above, stability of a structural model—at a particular parametric instance—is characterized by a complete set of positive eigenvalues for either the operative stiffness matrix itself[72]—representing the second differential of a total potential—or the combination of it and a mass matrix for the model—representing the vibration properties. The treatment thereby presupposes a consistent representation for both matrices, coming from the general displacement-based approximation in Eq. (3.8). With other basic formulations, the criteria may need a re-formulation.

Instability, interpreted as a lack of stability is thereby the opposite, and implies that a certain perturbation from the equilibrium releases energy or results in a divergent motion. It is important to note that unstable response is normally described by one, or a very low number of negative eigenvalues[73]; the remaining ones are positive. This means that unstable response is always related to a particular direction, or a space

[70] even when the problem is within their capacity

[71] Release R2017b, MathWorks, Inc., Natick, MA.

[72] where 'operative' is 'tangential', 'incremental' or 'constrained', depending on context

[73] The matrix formulation is thereby not negative definite, as written in many research papers, as this would imply that all eigenvalues are negative

spanned by a low number of base vectors. The situation is thereby best visualized as a saddle surface in the energy space, and not through a mountain-top maximum.

It is noted that—at least in theory—equilibrium states can be maintained for perfect structures with perfect forcing even if the equilibrium is unstable. One example is the Euler buckling case in Sect. 1.4, which can carry compressive forces well above the critical forcing, as long as no imperfections appear. Due to their nature, unstable equilibrium states are, however, often of limited interest to engineering objects, but note the initial discussion in Sect. 1.1. They, however, can provide some qualitative information on phenomena in structural response, when they appear as solutions in an analysis. It is thereby sometimes of interest to evaluate also unstable equilibria, and to trace them in a parametric space; this is further discussed in connection with multi-parametric solution methods in Sect. 4.4.

3.7.4 Critical Equilibrium

While stability and unstable equilibrium (with respect to certain perturbation directions) are conclusions related to a calculated equilibrium state, a main focus in structural investigations is set on critical equilibrium states, being the intermediate case[74].

Critical equilibrium states are thereby the states where one or a few eigenvalues of the formulations in Eqs. (3.97), (3.98) or (3.100) vanish. In the interpretation of the total potential, this implies a structural situation, where the configuration can be perturbed, at least a small distance, at constant energy, or without any force creating or resisting it. The simple examples described by Eqs. (1.3) and (1.25) illustrate how a deflected shape of any magnitude can exist for some forcing; a neutral equilibrium appears. In many complex models, similar situations occur, but then for particular eigenvectors, representing critical—or, buckling—modes. Typically, most eigenvalues are still positive, while one or a few vanish[75].

The critical situation implies that a mechanism is formed, i.e., a state where no stiffness exists and the linearized relation implies that additional displacement can be created by an infinitely small force, in a particular mode direction. This mechanism is infinitesimal, in the sense that only small movements can appear without force. The critical equilibrium reflects a ‘forced mechanism’ as it is existing only at a particular exterior forcing, cf. Fig. 3.16. This is the situation reproduced by the deflected equilibrium used in several analyses in Chap. 1. It is noted that this reasoning is mainly an attempt to visualize the effects of critical equilibrium, and that the reasoning is based purely on a linearized stiffness viewpoint; introducing gravity or mass properties can change the view.

---

[74] very often termed the instability forcing magnitude, when adopting the view of this as the loss of stability in an increasing forcing scenario

[75] even if a critical equilibrium also exists, e.g., between parametric regions of five- and six-fold unstable response

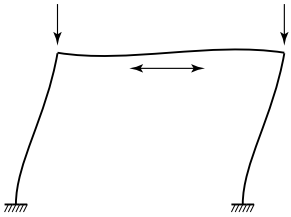

Fig. 3.16 Forced mechanism as an illustration of critical equilibrium, with zero horizontal stiffness indicated for the linearized setting

While most engineering approaches seek the critical states as a particular forcing level, a wider view, further discussed in Chap. 4, identifies the critical states as borderline cases between regions giving equilibria of different stability properties.

With more than one vanishing eigenvalue, the set of orthogonal critical eigenvectors define a subspace of critical response. This situation will occur for structural models possessing symmetry, and occasionally for structures where parameters have been optimized, cf. the work by Ashwear et al. (2016).

In the most common engineering setting, critical equilibria can be of two different kinds[76]. The discussion takes its starting point in Eq. (3.50), which—for an unconstrained problem—formulates the differential of the residual equation from differentials in discrete variables and in the single parameter λ. Evaluated at an equilibrium state, this differential describes neighboring equilibria, on an equilibrium branch imagined for the parametric variation. When the incremental stiffness matrix has no vanishing eigenvalues, the equation is invertible, and a vanishing differential of the residual

$$\mathrm{d}\underline{r} = \underline{\underline{K}}^i \, \mathrm{d}\underline{d} + \mathrm{d}\lambda \, \underline{r}_{,\lambda} = \underline{0}, \tag{3.105}$$

leads to

$$\mathrm{d}\underline{d} = -\mathrm{d}\lambda \left(\underline{\underline{K}}^i \right)^{-1} \underline{r}_{,\lambda}. \tag{3.106}$$

This is an expression for the only tangent vector, on which neighboring equilibria can exist. This expression is valid as written for the cases in Eqs. (3.48) and (3.49). For the case in Eq. (3.47) the tangent expression is somewhat simplified from $\underline{r}_{,\lambda} \equiv -\underline{f}_{,\lambda}$ and $\underline{\underline{K}}^i \equiv \underline{\underline{K}}^t$; the criteria below are often stated in these more restricted terms. The tangent vector is discussed in a more general context in Sect. 4.5.4.

When mechanical constraints are included in the formulation together with one parametric external force, Eq. (3.92) expresses the same relation between the residual components and the variables considered, giving the tangent vector as

$$\mathrm{d}\underline{R} = \underline{\underline{K}}^c \mathrm{d}\underline{D} + \mathrm{d}\lambda \, \underline{R}_{,\lambda}, \tag{3.107}$$

with the collective terms from Eqs. (3.90) and (3.91).

[76] even if more complex situations can appear for very specific parametric combinations, as discussed by catastrophe theory

A non-critical increment along the equilibrium branch demands that the matrix $\underline{\underline{K}}^c$ is invertible, and the connected variations of all fundamental variables can be written

$$\mathrm{d}\underline{D} = -\mathrm{d}\lambda \left(\underline{\underline{K}}^c\right)^{-1} \underline{R}_{,\lambda} \tag{3.108}$$

with $\underline{R}_{,\lambda}$ the differential of the exterior forcing representation.

It is obvious that the case without constraints in Eq. (3.106) is a special case of the more general Eq. (3.108). The following is therefore considering the more general case, and introduces the operative stiffness matrix $\underline{\underline{K}}$, which—depending on context—is $\underline{\underline{K}}^c$, $\underline{\underline{K}}^i$ or even $\underline{\underline{K}}^t$.

At a critical equilibrium, the matrix $\underline{\underline{K}}$ is singular, i.e., has at least one zero eigenvalue. One or more critical eigenvectors then exist, for which

$$\underline{\underline{K}}\,\underline{\varphi}_{\mathrm{cr}} = 0\,\underline{\varphi}_{\mathrm{cr}}, \tag{3.109}$$

where $\underline{\varphi}_{\mathrm{cr}}$ is evaluated from Eq. (3.100) in the general case. If more than one eigenvalue vanishes at a critical equilibrium state, the corresponding eigenvectors are collected as an orthonormalized set $\underline{\underline{\Phi}}_{\mathrm{cr}}$.

The implication of Eq. (3.109) is that any non-zero right-hand side, which is not orthogonal to $\underline{\varphi}_{\mathrm{cr}}$, creates infinite displacement increments. It is noted that an eigenvector $\underline{\varphi}_{\mathrm{cr}}$ contains displacement variables, and—if included—constraint-enforcing variables.

Referring to Eq. (3.109), this implies that only $\mathrm{d}\lambda = 0$ is possible for a case when $\underline{R}_{,\lambda}$, i.e., the λ derivative of the residual vector, has any component in the direction of (any of the) $\underline{\varphi}_{\mathrm{cr}}$. This can be evaluated through a demand on the projection of this derivative on the critical eigenvector(s). With one critical eigenvector, the criterion is evaluated from

$$\underline{\varphi}_{\mathrm{cr}}^{\mathrm{T}}\,\underline{R}_{,\lambda} \neq 0. \tag{3.110}$$

If this is true, a limit state exists, where the only incremental equilibrium solution is an additional displacement in the direction of the $\underline{\varphi}_{\mathrm{cr}}$ together with a zero increment to the parameter.

With several critical eigenvectors[77] the same criterion can be used for all the critical vectors, and evaluates whether the current parameter differential of the residual vector is out of the range of the current incremental stiffness. Limit states are rather easily handled in computations, even if they normally need a displacement stepping approach, cf. Sect. 4.3.2.

The opposite case is when the parameter differential of the residual $\underline{R}_{,\lambda}$ is completely within the range of the operative stiffness, i.e., has no component in the direction of any of the critical eigenvectors. A bifurcation state exists when, at a particular equilibrium,

$$\underline{\varphi}_{\mathrm{cr}}^{\mathrm{T}}\,\underline{R}_{,\lambda} = 0, \tag{3.111}$$

[77] assumed as orthonormalized with respect to the mass matrix

for all the critical eigenvectors in $\underline{\underline{\Phi}}_{\mathrm{cr}}$ at the critical state. Thus, non-zero stiffness exists for this increment, and an increment $\mathrm{d}\underline{D}_{\perp}$ is formally solved from the two simultaneous equations[78]

$$\begin{aligned} \underline{\underline{K}}\,\mathrm{d}\underline{D}_{\perp} &= -1 \cdot \underline{R}_{,\lambda}, \\ (\underline{\varphi}_{\mathrm{cr}})^{\mathrm{T}}\,\underline{\underline{M}}\,\mathrm{d}\underline{D}_{\perp} &= 0 \end{aligned} \tag{3.112}$$

where the notation is intended to emphasize that this displacement increment is orthogonal to the critical eigenvector(s).

In addition to this orthogonal increment, the critical eigenvectors are also solutions, as any of them $\mathrm{d}\underline{D} = \alpha\underline{\varphi}_{\mathrm{cr}}$, together with $\mathrm{d}\lambda = 0$ also fulfills the differential residual Eq. (3.107). This equation can thereby be fulfilled by any increment of the form

$$\mathrm{d}\underline{D} = \mathrm{d}\lambda\,\mathrm{d}\underline{D}_{\perp} + \underline{\underline{\Phi}}_{\mathrm{cr}}\,\underline{\alpha}, \tag{3.113}$$

for arbitrary vectors $\underline{\alpha}$ of dimension matching that of the critical eigenvectors space.

Higher order differentials, however, show that only a specific number of branches—defined by combinations $(\mathrm{d}\lambda, \underline{\alpha})$—are possible; these are solved from an algebraic bifurcation equation. At a bifurcation state, with just one vanishing stability coefficient, two crossing branches exist, and a common situation is that possible branches are defined by $\underline{\alpha} = \underline{0}$ and $\mathrm{d}\lambda = 0$, respectively[79]. Other situations, where other combinations are solved, give unsymmetric bifurcations. Solution of the equation gives important information on the properties of the secondary equilibrium branch, including the stability of solutions on it and the imperfection sensitivity around the critical state. The numerical treatment is discussed in Sect. 4.5.3.

While limit states with respect to the parameter normally appear as critical equilibria with one vanishing eigenvalue and one equilibrium branch, bifurcation states demand handling of—at least—two possibilities and are more algorithmically demanding. This is further discussed in Chap. 4.

A general conclusion is also that the critical eigenvector at a limit state has the same symmetry as the equilibrium solution, while a bifurcation state give modes of lower symmetry. The existence of critical eigenvectors with another symmetry than the equilibrium solution is thereby an alternative criterion for a bifurcation state; this is rather easily noted for a particular problem.

As bifurcations are always symmetry-breaking in the response, they demand models where a chosen discretization is considered in the light of symmetry aspects, cf. Sect. 3.5.1, the work by Eriksson and Nordmark (2016) and the example in Sect. 5.3. Macro-symmetries in models also often give (at least) two eigenvalues vanishing at the same state. The solution of secondary equilibrium branches is somewhat complicated, and needs tools not commonly available in general analysis software.

[78] even if this demands some specialized algorithmic implementation

[79] This is the situation at what is commonly called a symmetric bifurcation state in structural stability

An example

A fictitious but relevant simple example of total potential for a structure modelled with two discrete displacement components, $\underline{d} = (d_1, d_2)^{\mathrm{T}}$ is

$$\Pi = \frac{1}{2}d_1^2 + \frac{1}{2}d_2^2 + \frac{1}{3}d_2^3 + \frac{1}{2}d_1^2 d_2 - \lambda(\frac{1}{2}d_1^2 + d_2), \tag{3.114}$$

where the terms containing λ may be seen as representing the driving force, and the others the resisting force. An identity matrix is assumed for the mass matrix $\underline{\underline{M}}$. The problem is also treated from several viewpoints in Sect. 4.6.

The system is symmetric under the transformation $d_1 \to -d_1, d_2 \to d_2$.

From the total potential, residual force and incremental stiffness are

$$\underline{r} = \Pi_{,\underline{d}} = \begin{pmatrix} d_1 + d_1 d_2 - \lambda d_1 \\ \frac{1}{2}d_1^2 + d_2 + d_2^2 - \lambda \end{pmatrix}, \quad \underline{\underline{K}}^i = \Pi_{,\underline{d},\underline{d}} = \begin{pmatrix} 1 + d_2 - \lambda & d_1 \\ d_1 & 1 + 2d_2 \end{pmatrix}, \tag{3.115}$$

and the parameter derivative of driving force

$$-\underline{r}_{,\lambda} = \begin{pmatrix} d_1 \\ 1 \end{pmatrix}. \tag{3.116}$$

The residual equation allows two classes of equilibrium solutions, where the primary one is symmetric of the form

$$\underline{d} = (0, \tau)^{\mathrm{T}} \quad \text{for} \quad \lambda = \tau(1 + \tau), \tag{3.117}$$

and one is unsymmetric of the form

$$\underline{d} = (\sqrt{2}\cos\tau, \sin\tau)^{\mathrm{T}} \quad \text{for} \quad \lambda = (1 + \sin\tau) \tag{3.118}$$

Regarding the solutions, it is obvious that symmetric solutions exist for $\lambda \geq -\frac{1}{4}$, while the unsymmetric solutions exist for $0 \leq \lambda \leq 2$, and that $\underline{d} = (0, 0)^{\mathrm{T}}$ is a symmetric solution for $\lambda = 0$.

On the symmetric solution where $d_1 = 0$, the incremental stiffness is

$$\underline{\underline{K}}^i = \begin{pmatrix} 1 - \tau^2 & 0 \\ 0 & 1 + 2\tau \end{pmatrix}. \tag{3.119}$$

Critical situations with a singular $\underline{\underline{K}}^i$ exist at three states, for $d_2 = -1, -\frac{1}{2}, 1$, and $\lambda = 0, -\frac{1}{4}, 2$, respectively. For $\tau = -\frac{1}{2}$, the critical eigenvector is $\underline{\varphi}_{\mathrm{cr}} = (0, 1)^{\mathrm{T}}$, which keeps the symmetry from the primary solution, and also gives $\underline{\varphi}_{\mathrm{cr}}^{\mathrm{T}} \underline{r}_{,\lambda} \neq 0$; both criteria indicate a limit state at this solution.

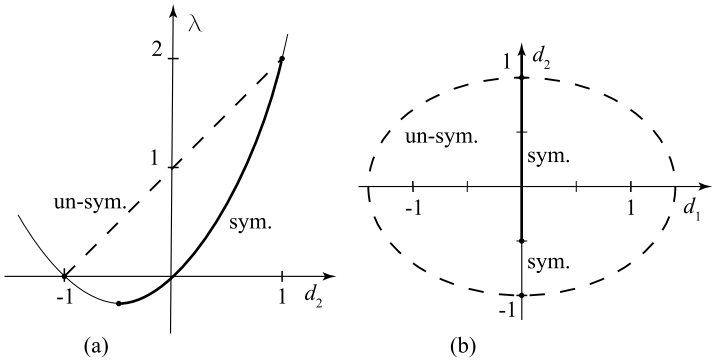

Fig. 3.17 Solution to example in two projections

The critical solutions at $\tau = \pm 1$ give a critical eigenvector $\underline{\varphi}_{\text{cr}} = (1, 0)^{\text{T}}$, which does not keep the symmetry from the primary solution, and also gives $\underline{\varphi}_{\text{cr}}^{\text{T}} \underline{r}_{,\lambda} = 0$; these are symmetry-breaking bifurcation states.

On the primary solution branch, where the incremental stiffness is diagonal, the eigenvectors are always of the two forms above, and the diagonal reveals the eigenvalues. It is obvious that the eigenvalue corresponding to the symmetric mode $\underline{\varphi} = (0, 1)^{\text{T}}$ is positive when $\tau > -\frac{1}{2}$, and the one corresponding to the unsymmetric mode $\underline{\varphi} = (1, 0)^{\text{T}}$ when $|\tau| < 1$. The stable region of the primary branch, with two positive eigenvalues, is thereby $-\frac{1}{2} < \tau < 1$.

Similar investigations of the incremental stiffness on the unsymmetric solution branch show one positive and one negative eigenvalue for all solutions where $d_1 \neq 0$.

The solution to the example problem is summarized in Fig. 3.17

3.7.5 Classification of Critical States

The simple example above shows the two most common critical situations occurring for elastic structural equilibrium evaluations. Both situations are characterized by a change of stability for the equilibria on the branch. The situations are, however, still fundamentally different.

The simplest, and most common, type of critical state on an equilibrium branch is the limit state, commonly appearing as an extremum for the forcing parameter, λ in the example. The limit state is found for $d_2 = -\frac{1}{2}$, $\lambda = -\frac{1}{4}$, cf. Fig. 3.17a. The limit state exists on the symmetric primary branch with $d_1 = 0$. The neighboring equilibria are unstable for lower d_2 and stable for higher[80]. The limit state can be

[80] This corresponds to the common structural situation that stability corresponds to increasing forcing parameter for increasing displacement, but this is not necessarily true in a more general case.

interpreted as two branches of different properties meeting at the critical state, even if only one continuous branch exists through the state.

The other common class of critical state is the bifurcation state, and two such states exist at $d_2 = \pm 1$ in Fig. 3.17a. Subfigure (b) shows that symmetry-breaking secondary equilibrium branches emanate at these states[81]; the continuation is thereby not unique through the state. The bifurcation states lead to changes of the stability of the states on the connected branch segments. In the example case, the primary branch changes from giving stable equilibrium for just below $d_2 = 1$ to unstable above this state. Equilibria are also one-fold unstable for d_2 just above -1, and changing to two-fold unstable for lower d_2. The secondary branch loop consists of one-fold unstable equilibria. In general, bifurcations always lead to changes of stability.

Obviously, both types of critical equilibrium states are characterized by vanishing eigenvalues of the operative stiffness matrix valid for the model. The corresponding eigenvectors give contributions to the possible equilibrium branches passing through the critical state, as discussed above. Even if the two classes are fundamentally different from several aspects, they both consist of connections between solution branches with different properties. They are special cases of the general cases discussed within catastrophe theory, singularity theory or the mathematical branch of bifurcation analysis, where the bifurcation concept has a wider meaning than in the structural buckling cases discussed in the present treatise.

Bifurcation analysis in general can loosely be described as investigating whether variations to the parameters of a dynamical system can lead to qualitative changes in the dynamics of the systems. Qualitative changes include, but are not limited to, changes in the number of equilibrium points and/or changes to their stability. For systems where small parameter variations can change the qualitative dynamics, the goal of bifurcation analysis is also to predict the changes. This setting of bifurcation theory is described by, e.g., Strogatz (2019).

Mostly as a curiosity in the present context, 'structural stability' in the mathematical context refers to systems which are not sensitive to small parameter variations, and a system that is not 'structural stable' is at a 'bifurcation point', and the latter includes systems with limit points.

3.8 Model Creation

The present Chapter gives a general basic formulation for discretized non-linear structural mechanics, based on a consistent displacement-based form. Although not complete in its details, the objective is to create an understanding of the underlying

[81] In this example problem, the secondary branch is a loop between the bifurcation states, but this is not generally true, cf., e.g., the results in Sect. 5.3

formulations in general analysis software. When using such tools for analyses of equilibrium and stability investigations, the following aspects need be considered[82]:

- the physical model i.e., the choice of continuum, frame or shell representation;
- the geometry, often through a set of defining measures or point coordinates;
- the topology, defining connections in the model;
- the material as material models and corresponding parameters;
- the support conditions, and other displacement constraints or connections;
- the forcing considered;
- the results requested;
- the sensitivity of the result, e.g., response to perturbations or variations;
- the stability properties of solutions.

Depending on the software used, the aspects may—or, may not—be available to some extent. The software documentation must be consulted for this, and also on how the different features are introduced; in professional software, there are often many different possibilities available for the definition of a model.

In relation to the completely consistent treatment above, formulations in available software often introduce modifications in order to avoid, e.g., locking problems or to enhance convergence in the solutions. These modifications are also described in the documentation, and must be judged in relation to the problem at hand: even if they are normally improving the discretized model, they sometimes affect, e.g., the stability conclusions. Different modifications to the pure displacement-based formulations are extensively discussed in literature.

Commercial finite element software also offer different possibilities for creating a mesh for a structural region. While the creation of the mesh, with nodes and element topologies, is today often more or less automatic from minimal geometric information, two aspects are commonly needed as input. The first relates to the order of the element, and thereby the number of nodes in the element definition. This affects the capabilities of the elements to accurately represent the boundary geometry of the model. The choice of suitable element type is strongly context dependent, but rather simple elements[83] can be slightly recommended in many engineering applications, due to a more robust behavior, while higher order elements may be more interesting for detailed academic investigations.

The other meshing choice refers to the fineness of the mesh, and thereby the number of elements. This choice is also supported by user information regarding the software, in some more or less obvious way. With an element type chosen, the number of elements gives the accuracy obtainable in results. This choice is even more context dependent with respect to application type and need for accurate results, and no general indications can be given, especially since convergence results obtained for linear analysis are no longer necessarily relevant when non-linear and stability analyses are concerned. The best recommendation is to perform the analysis with a

[82] and should in some way be defined for an analysis model, even if the software input can be defined in other categories

[83] and thereby a higher number of them

rather coarse model, then refine it uniformly and compare results between the two analyses; the differences in important results can give hints on how much meshing should be refined for a desired accuracy.

Some aspects which need particular care and consideration, not least regarding symmetry of a problem, are mentioned in Sect. 5.5.

Conclusions from this Chapter

The starting point and the motivation for the Chapter is that numerical analyses in most cases are necessary for the full stability investigation of complex structures. The numerical treatment demands a discrete form, where continuous functional representations are replaced by a set of discrete variables, and accompanying approximative functions. The Chapter proposes the use of finite element techniques for the simulations, even if other locally based discretizations are also possible. The finite element approach is supported by a wide range of available commercial software.

Any approximation of the displacement field in a stability-affected structure need be based on functions with sufficient kinematic complexity to capture the potential loss of stability. The numerical representation must also be based on sufficiently detailed assumptions regarding strain and energy, in order to allow the necessary consideration of non-linear effects

Even if finite element techniques are the primary target for the development, a consistent treatment is given on non-linear discretized mechanical formulations, based on approximations to the displacement field over the region, or a subregion. Within this general form, any discretization can be developed, the only requirement being that the chosen discrete variables are appearing linearly in the approximation. Based on this form, all virtual work terms can be systematically derived. An implementation needs to find efficient representations of developed operators. For several classes of assumptions on the exterior forcing of the structure, important concepts—like internal and external force representations, mass and different types of stiffness matrices—are derived and related to a problem setting.

The Chapter discusses constraints on the equilibrium solutions, which are presented as a systematic method capable of handling support conditions, avoiding rigid body modes, enforcing symmetry and modelling hard, frictionless contact conditions. The treatment shows how such constraints are a fundamental part of the mechanical problem, with effects on the quantitative evaluation of stability.

In addition to the formulations for equilibrium and motion, the main quantities developed are key indicators for the evaluation of stability for an equilibrium, where the treatment only considers conservative systems. Stability of the discretized structural model is shown to be decided by the signs, even if not the magnitudes, of the eigenvalues to either of two settings. The corresponding eigenvectors allow an approximate evaluation of unstable modes or vibration components. From the basic expressions developed here, solution methods for the stated problem are the topic of the next Chapter.

Tasks for this Chapter

1. Solve the same problem as in Eq. (3.3) using the same discrete values as in Fig. 3.3, but with cubic, third-order, functions $f_d(t)$ for $t_i \leq t \leq t_{i+3}$, $(i = 1, 4, 7)$. Use the same collocation criterion as in the text, demanding perfect match at the points $\frac{t_i+t_{i+1}}{2}$ for all i. Assume that the argument points t_i are uniformly distributed over the interval, when writing the three local functions.

2. For a tetrahedron with nodes in $\mathbf{X}_1 = (1, 2, 2)^{\mathrm{T}}$, $\mathbf{X}_2 = (3, 0, -1)^{\mathrm{T}}$, $\mathbf{X}_3 = (-1, 1, -1)^{\mathrm{T}}$ and $\mathbf{X}_4 = (1, 5, 0)^{\mathrm{T}}$ (all measures in consistent units), evaluate the shape functions $N_i(\mathbf{X})$, $(i = 1, \ldots, 4)$. Then evaluate their sum $\sum_{i=1}^{4} N_i(\mathbf{X})$, and consider the result. Also, evaluate the shape functions for the barycenter of the tetrahedron[84]. If these results do not come out as something slightly remarkable, the solution is not correct.

3. Investigate the properties of Gauss integration through a test problem. For simplicity, a $2D$ region $1 \leq X_1 \leq 3, -1 \leq X_2 \leq 2$ is considered. First, evaluate and list the coordinates and weights for 2×2 and 3×3 integration in this region (and, possibly, also 4×4). Then, use this information to integrate functions of the form $f(X_1, X_2) = (1 + (X_1)^m)\,(1 + (X_2)^n)$ for $m, n = 1, \ldots$. Compare the results to analytical values, and find the limits for m and n at which the numerical integration is still (very close to) correct. As an extra study, investigate the effects of rounding of the (rather boring) numbers in the quadrature formulae.

4. In an available general FE-based software, investigate which element types and variations of these are provided for non-linear $3D$ continuum analyses. List their properties with respect to generality in geometry (with restrictions and/or recommendations) and interpolation. Note any 'special numerical tricks' which are used. Write down how useful they would be for modelling of massive (or hollow) cube and sphere regions, possibly by automatic routines in the software. If possible, create and visualize examples of these models.

5. For a rectangular region in $2D$: $0 \leq X_1 \leq a, 0 \leq X_2 \leq b$, it could be tempting to use an interpolation for, e.g., the displacement component U_1 as

$$U_1 = U_{11} \cos\left(\frac{\pi X_1}{2a}\right) \cos\left(\frac{\pi X_2}{2b}\right) + U_{21} \sin\left(\frac{\pi X_1}{2a}\right) \cos\left(\frac{\pi X_2}{2b}\right) + \\ + U_{31} \sin\left(\frac{\pi X_1}{2a}\right) \sin\left(\frac{\pi X_2}{2b}\right) + U_{41} \cos\left(\frac{\pi X_1}{2a}\right) \sin\left(\frac{\pi X_2}{2b}\right),$$

[84] which is the center of gravity, if a constant density is assumed

based on the four corner points, and with U_{j1} the displacement component at node j. Discuss the advantages and disadvantages with this approach: is it useful? Draw a figure to explain the geometry.

6. Consider a structure according to the figure, which is a $3D$ generalization of the example in Sect. 1.3. The basic structure is symmetric in the (X_1, X_2)-plane, but has two different length measures; the sectional properties EA are equal for all bars. It is affected by a downwards vertical force. Formulate the total potential based on three displacement components of the top vertex. Differentiate once for equilibrium, and twice for stability. Find critical vertical force magnitudes. Investigate the case when $L = w$.

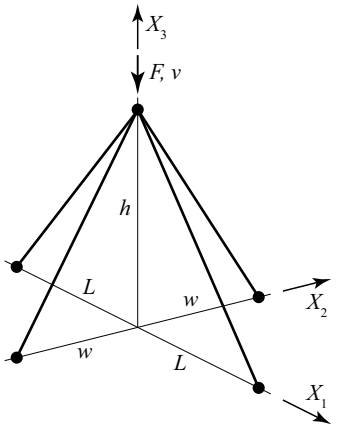

7. In an available general FE-based software, model a 4 m simply supported prismatic beam of section $20 \times 10\,\text{cm}^2$, when affected by a central point force by continuum elements (of chosen type). Solve the problem, and compare the results to a solution based on elementary beam theory. In particular, note all modelling choices needed for the continuum model. Additionally, test with different meshes, and different force magnitudes (if a non-linear setting is available).

8. Assuming a system described by two variables (X_1, X_2), and a total potential $\Pi = aX_1^2 + bX_2^2 - c(X_1 - X_2)^2$, decide the limits for stability around $(0, 0)$, and the lowest mode of critical response in terms of the parameters a, b, c. Use some software to create and plot the potential surface for some interesting parameter values, including a critical combination.

References

Argyris J, Tenek L, Olofsson L (1997) TRIC: a simple but sophisticated triangular element based on 6 rigid-body and 12 straining modes for fast computational simulations of arbitrary isotropic and laminated composite shells. Comput Meth Appl Mech Eng 145:11–85

Ashwear N, Tamadapu G, Eriksson A (2016) Optimization of modular tensegrity structures for high stiffness and frequency separation requirements. Int J Solids Struct 80:297–309

Bathe KJ (2014) Finite Element Procedures, 2nd edn. KJ Bathe, Waterton, MA, also published by Higher Education Press, China, 2016. First edn published by Prentice-Hall, 1996

Bucalem M, Bathe KJ (1993) Higher-order MITC general shell elements. Int J Num Meth Eng 36(21):3729–3754

Como M, Grimaldi A (1995) Theory of stability of continuous elastic structures. CRC Press, Boca Raton, FL

Cottrell JA, Hughes TJR, Bazilevs Y (2009) Isogeometric analysis: toward integration of CAD and FEA. Wiley, Singapore

Eriksson A, Nordmark A (2016) Symmetry aspects in stability investigations for thin membranes. Comput Mech 58:747–767

Hughes TJR, Cottrell JA, Bazilevs Y (2005) Isogeometric analysis: CAD, finite elements, NURBS, exact geometry and mesh refinement. Comput Meth Appl Mech Eng 194(39–41):4135–4195

Ko Y, Lee P, Bathe KJ (2017) A new MITC4+ shell element. Comput Struct 182:404–418

Koiter W (1970) The stability of elastic equilibrium. Technical report Report AFFDL-TR-70-25, Air Force Flight Dynamics Laboratory, Wright-Patterson Air Force Base, Ohio, a translation of the Dutch original from 1945

Liapunov AM (1966) Stability of motion. (Mathematics in science and engineering, Volume 30). Academic Press, New York/London (translated from Russian Doctoral dissertation, Univ. Kharkov 1892)

Strang G (1988) Linear algebra and its applications, 3rd edn. Brooks/Cole, Thomson Learning

Strogatz SH (2019) Nonlinear dynamics and chaos. With applications to physics, biology, chemistry, and engineering. CRC Press

Thompson JMT, Hunt GW (1973) A general theory of elastic stability. Wiley, Chichester

Wilkinson JH (1988) The algebraic eigenvalue problem. Oxford Science Publications, Oxford, New York

Zienkiewicz OC, Taylor RL (2000) The finite element method. Volume 1: the basis, 5th edn. Butterworth-Heinemann, Oxford

Chapter 4
Solution Algorithms

This Chapter discusses non-linear settings of discretized equilibrium and motion problems, with a focus on the former. Basic solution methods for these are presented. With a parametric setting of the problem, for instance of the forcing, it is necessary to solve for a sequence of equilibria, describing the response of the structure in more detail. Choosing a sequence of states is a challenge in itself, when maximum information is desired with limited computations. The Chapter proposes a setting of the parametric non-linear equilibrium problem, which is suited for an incremental and iterative solution algorithm. A generalized sequence-tracing algorithm is presented, which can handle any parameters for the problem modelled. The algorithm uses Newton iteration to find each solution point, but Dynamic relaxation approaches are mentioned as an alternative. Methods for evaluation of the stability properties of equilibria are discussed. For complete stability investigations in a parametric structural model, the generalized algorithm gives wide possibilities to trace the parametric space with different selections of solutions. The dependence of critical states on structural parameters, and the sensitivity to imperfections are main objectives. Such investigations are of major interest in the design phase, but also relevant in structural optimization.

Brief Objective of this Chapter

The development in this Chapter facilitates solution of the response of a parametric structural model with full quantitative information on its stability properties under diverse forcing situations.

A. Eriksson and A. Nordmark, *Structural Stability and Its Computational Modelling*, Computational Methods in Engineering & the Sciences,
https://doi.org/10.1007/978-3-031-36072-5_4

4.1 Discretized Equilibrium Analyses

This Chapter discusses how stability problems for structures can be solved in a computational discretized setting. The key ingredient in such an approach is that the structural model created is sufficiently comprehensive to admit the treatment of unstable equilibria. Commonly, this implies a need for a more complex description of the displacement: a bar becomes a beam, a plate becomes a shell, et cetera. This is a reason why displacement-based forms are preferred for the analyses. The computational modelling also needs some aspect of non-linearity in the formulation, as the response to forcing level is no longer proportional. As demonstrated in previous Chapters, the discretization of a structural model can take several forms, from the series solutions in traditional semi-analytical methods, via finite difference ('FD') approximations to systematic finite element methods ('FEM'), and isogeometric analysis ('IGA').

All the mentioned approaches are potentially useful for structural stability analyses, and share many common aspects. The main focus here is on FEM formulations, as these are easily available in commercial software, and also systematic enough for self-developed algorithms in special application settings. Most aspects covered in the FEM terminology below can also be used for the other settings.

The Chapter has a main focus on the treatment of structural time-independent equilibrium for conservative systems, but some aspects will be given concerning non-conservative equilibrium and time-dependent situations.

As many aspects of modular FEM procedures can be used also in the context of stability investigations, the description starts from the linear FEM setting, and then progressively develops this into the non-linear form needed for parameter-dependent forcing, which is the basis for stability investigations. Due to the non-linearity of the formulations, some iterative method must be used to reach solutions.

Introducing parameters in the problem, it is also necessary to solve for several such equilibria; this is a parametric approach, with a fictitious time scale, cf. Sect. 2.8.5. A non-linear formulation is used in an incremental and iterative solution algorithm, where a sequence of equilibria is solved. For complete stability investigations in a parametric structural model, the generalized algorithm gives wide possibilities to consider the solution space from many different viewpoints. It is thereby fully possible to seek out, for instance, critical parameter and force combinations. In the design phase of a structure, such investigations can be of major interest. They are also highly relevant in mathematical structural optimization. The properties of these equilibria with respect to stability can be evaluated, and stable parametric regions isolated.

For the solution of each equilibrium, it is proposed to use Newton iteration, but Dynamic relaxation approaches are discussed as an alternative with some advantages for certain classes of problem settings. The choice of states to solve for is a challenge in itself, when maximum information is desired with minimum computational effort. This shows that the non-linear form is considerably more demanding than a corresponding linear problem.

The discussion in the Chapter also allows the inclusion of physical constraints for the possible solutions. As discussed in Sect. 3.6, these constraints can be of several types, where simple ones describe the supports or the macro-symmetries of the model, while more complex ones refer to potential contact situations. The constraints affect the obtained solutions themselves, not least regarding stability conclusions. Their usage also has significant impact on the possibilities and setting of the solution algorithm used.

The notation in this Chapter is heavily relying on concepts from numerical linear algebra. As in Chap. 3, vectors, denoted as $\underline{x}$, are column matrices of dimension n-by-1, while matrices, denoted as $\underline{\underline{A}}$ are of dimension m-by-n.

4.1.1 Linear Stiffness

The linear form of FEM equilibrium analysis has at its core the solution of a linear set of equations in the discrete variables[1], $\underline{\underline{K}}^{\ell}\,\underline{d} = \underline{f}$. This is here, aiming at the development in the sequel, stated in the equivalent residual form

$$\underline{r}(\underline{d}) = \underline{\underline{K}}^{\ell}\,\underline{d} - \underline{f} = \underline{0} \tag{4.1}$$

which is a special case of Eq. (3.46), with a linear internal force $\underline{p} = \underline{\underline{K}}^{\ell}\,\underline{d}$ in the structure, and the equivalent conservative external force $\underline{f}$, both expressed as conjugate variables to the chosen discrete variables. An alternative viewpoint defines the solution to the equilibrium as the minimization of the norm of this residual.

The form chosen is based on equilibrium being a stationary state of the total potential[2] Π, with respect to a set of discrete variables in $\underline{d}$. The inclusion of these as arguments to $\underline{r}$ emphasizes that these are the unknowns.

The system matrix $\underline{\underline{K}}^{\ell}$ in Eq. (4.1) is systematically built on the constituent N_e elements in the model, according to

$$\underline{\underline{K}}^{\ell} = \mathbb{A}\underline{\underline{K}}_e^{\ell} \tag{4.2}$$

with $\mathbb{A}$ used for the assembly operator, cf. Sect. 3.3.3: an index-based summation of element contributions[3]. Dependent on precise algorithmic implementation, the assembly procedure contains an identification of model topology, and, possibly, the space orientations of elements, cf. Chap. 3.

An important observation is that Eq. (4.1) cannot, in general, be used in the natural view that the external force $\underline{f}$ immediately gives the resulting $\underline{d}$. This comes from a

[1] As this treatise has more ambitious objectives, the linear stiffness is considered a special case, and gets a qualifying index.

[2] which contains the strain energy in the structural region, and the potential for acting conservative forcing, cf. Sect. 2.6.3.

[3] implicitly using a set of element extraction operators $\underline{\underline{L}}_e$ and a number of elements N_e.

singularity of $\underline{\underline{K}}^{\ell}$, reflecting rigid motion modes of the model. Boundary conditions for prescribed displacement components, e.g., supports are introduced through a modified system

$$\underline{\underline{K}}^{\ell}_{\text{free}}\,\underline{d}_{\text{free}} = \underline{f}_{\text{free}} \tag{4.3}$$

where the subindex 'free' refers to the discrete variables with known forcing[4] on the boundary part Γ_T of the model[5]. Formally, the procedure implied is a part-inversion of Eq. (4.1), utilizing the boundary condition for each discrete variable. A more generalized view on constraints on solutions is introduced in Sect. 3.6, and is used in the general formulations below.

When also the prescribed discrete variables are introduced through $\underline{d}_{\text{presc}}$, which reflects the conditions on boundary part Γ_U, the full displacement field approximation is known, and the complete acting force, including reactions, is evaluated from the internal force $\underline{p} = \underline{\underline{K}}^{\ell}\,\underline{d}$. All relevant response aspects and results are then easily obtained from the full set of discrete variables.

After providing information on geometry, topology, material, supports and forcing for a specific model, the algorithm for solving a FEM problem within a class of structures is highly modular. Procedures for the needed substeps are given in all text books on basic FEM techniques, and can be easily programmed. In addition to this straight-forward method, advanced software normally provide several refined methods for result presentation.

Linear equations

For linear FE-based problems, the dominating task is to solve the set of linear equations in Eq. (4.3), and this can put severe demands on computer capacity for large-scale problems with millions of discrete variables. These demands can sometimes be mediated by algorithms making full use of the properties of the established stiffness matrix $\underline{\underline{K}}^{\ell}$, primarily that it is symmetric and positive definite, due to the energy and displacement-based form. The matrix is also, in particular for large problems, sparse. Earlier FEM implementations often used elaborate strategies to reduce a bandwidth or skyline measure for $\underline{\underline{K}}^{\ell}$, but this is no longer of major interest.

Direct solution methods do not lend themselves favorably to parallelization, but some efforts have been directed to iterative methods within this approach. For in-house specialized software development, only direct methods are reasonable choices.

In engineering practice, many cases of forcing are commonly considered on a structural model. If possible, efficiency can be improved by defining all cases at once, and then treating them in parallel. It is also noted that superposition of cases is always possible for linear cases, a fact which also ensures proportionality. None of the comments in this section is of major importance for users of general software. The comments are also less relevant to non-linear formulations, which are the main interests in stability investigations.

---

[4] and, thereby, unknown displacement.

[5] Refer to the discussion in Sect. 2.5 on the relation between boundary parts with prescribed traction or prescribed displacement.

4.1.2 Secant Stiffness

For mildly non-linear structural equilibrium problems, secant stiffness methods are sometimes used. Examples of application are for some total deformation material descriptions, or when joints change their stiffness during deformation. The approach, which should seldom be a first-hand choice, is formulated for fixed external equivalent force $\underline{f}$, as

$$\underline{r}(\underline{d}) = \underline{\underline{K}}^s(\underline{d})\,\underline{d} - \underline{f} = 0, \tag{4.4}$$

where the structural secant stiffness matrix $\underline{\underline{K}}^s$ is again assembled from element contributions, all possibly affected by the non-linearity. The equation, which is of the form in Eq. (3.46), differs from Eq. (4.1) in the dependence of the stiffness matrix on the discrete variables. As these are also the solution to the problem, iteration procedures must be used, hoping that the solution converges to equilibrium with a low residual norm.

Iterative solution

The equilibrium equation in Eq. (4.4) is solved by an iteration technique, with successive solutions to problems of the same type as Eq. (4.3). With supports considered, the solution is thereby obtained through a process

$$\underline{d}_{\text{free}}^{j+1} = \left(\underline{\underline{K}}^s_{\text{free}}(\underline{d}^j)\right)^{-1} \underline{f}_{\text{free}}, \tag{4.5}$$

where the superindex is the iteration counter, and $\underline{d}^0, \underline{d}^1, \ldots$ are successive approximations to the equilibrium state. Without any prior knowledge about the solution, $\underline{d}^0_{\text{free}} = \underline{0}$ is normally a reasonable assumption. The iterations must be safe-guarded against divergence, and are continued until some norm of the residual $\underline{r}(\underline{d}^{j+1})$ is acceptably low[6], and $\underline{d} = \underline{d}^{j+1}$ is accepted as the solution.

The calculations of reactive and interior force are similar to the linear case above, based on the secant stiffness expressions $\underline{p} = \underline{\underline{K}}^s\,\underline{d}$. The exception is that superposition of cases is no longer possible; all interesting cases must be successively iterated to convergence[7].

Problems of this type can preferably be treated as fully non-linear problems instead, cf. Sect. 4.1.4.

[6] where acceptable should normally demand a norm considerably lower than what is initially planned, perhaps of the order 10^{-10} of the norm of the internal force $\underline{p}$.

[7] even if good initial approximations can often be found from neighboring cases.

4.1.3 Geometric Stiffness

Another common form for simplified treatment of non-linear structural equilibrium is through the inclusion of a geometric stiffness term. The residual equation, through a secant stiffness expression, is thereby given as

$$\underline{r}(\underline{d}) = \left(\underline{\underline{K}}^{\ell} + \underline{\underline{K}}^{g}(\underline{d})\right)\underline{d} - \underline{f} = 0, \tag{4.6}$$

where $\underline{\underline{K}}^{\ell}$ is the linear stiffness matrix, and $\underline{\underline{K}}^{g}$ is a geometric stiffness matrix, which is based on the interior forces, i.e., stress existing at discrete variables $\underline{d}$. Typical examples are the effects from axial stress on the bending stiffness for beams, cf. the examples in Sects. 1.4 and 1.5. It should be noted that this splitting of the secant stiffness matrix is not the same as the splitting of the incremental stiffness in Eq. (3.60): the geometric stiffness is not identical to the force stiffness.

In most cases, compressive interior force will—in loose terms—lead to negative, de-stabilizing contributions from $\underline{\underline{K}}^{g}$, while tensile forces tend to stabilize the model. The geometric stiffness is linear in the interior forces.

In the second order treatment in Sect. 1.4, the inclusion of $\underline{\underline{K}}^{g}$ in some respects improves the description of non-linear response, but this approach still lacks some non-linear terms[8]. The one-way coupling potentially leads to strange results, and the approach is only useful for classes of problems, where response is linear and geometric distortion under forcing is limited.

In order to solve Eq. (4.6), the expression is a special case of Eq. (4.4), and the same iterative approach used. Due to the necessary restriction of the method to problems with small deformations, only one iteration is often applied[9], which can give mis-leading results for statically indeterminate systems.

Linear pre-buckling prediction

Variants of the formulation in Eq. (4.6) are often used for estimation of instabilities through linear pre-buckling ('LPB') analyses. This approach is available in most commercial software, as it is efficient in implementation, and results are easily interpreted, cf. the example in Sect. 5.2. Although not identical, the approach is closely related to second order methods, and several deflected equilibrium methods.

[8] In the example Sect. 1.4, the omission is related to the shortening of the beam due to bowing.

[9] in some software without even questioning the convergence.

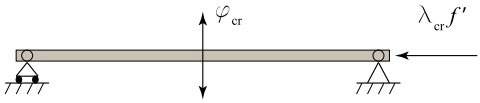

Fig. 4.1 Plane beam model, where a compressive axial force gives a vanishing transversal stiffness

The software implementations may differ, but the method always uses for representation of exterior forcing a unit vector $\underline{f}'$. This is multiplied by a small multiplier[10] λ, i.e., $\underline{f} = \lambda \underline{f}'$ in the form of Eq. (3.47) with $\underline{f}'$ here a constant force vector. The equivalent force evaluated from traction and body force at the undeformed state, suitably scaled, is a common choice for $\underline{f}'$. Solving $\underline{d}_1$ linearly from $\underline{f}'$ gives the geometric stiffness $\underline{\underline{K}}^g(\underline{d}_1)$ corresponding to $\underline{f}'$.

The assumption of linearity in all response aspects implies that the secant stiffness matrix at force $\lambda \underline{f}'$ is

$$\underline{\underline{K}}^0 + \underline{\underline{K}}^g(\lambda \underline{d}_1) = \underline{\underline{K}}^0 + \lambda \underline{\underline{K}}^g(\underline{d}_1). \tag{4.7}$$

Using this stiffness in Eq. (4.6) gives the solution for external force $\underline{f} = \lambda \underline{f}'$.

The linear pre-buckling approach uses Eq. (4.7) to evaluate an LPB estimator for the critical force multiplier λ_{cr} from

$$\left(\underline{\underline{K}}^0 + \lambda_{cr} \underline{\underline{K}}^g(\underline{d}_1)\right) \underline{\varphi}_{cr} = \underline{0}, \tag{4.8}$$

which makes the secant stiffness matrix singular. The eigenvector $\underline{\varphi}_{cr}$ describes the critical mode, for which a displacement increment $\mathrm{d}\underline{d} = \alpha \underline{\varphi}_{cr}$ is possible without additional forcing; a forced mechanism is formed, cf. Sect. 3.7.4. This critical direction is normally not in the direction of the forcing. The critical external force is $\underline{f}_{cr} = \lambda_{cr} \underline{f}'$.

The situation is very schematically described for a compressed plane beam model in Fig. 4.1. Given that the problem is well formulated, the interesting eigenvalue is the lowest positive one, while higher ones are in general practically unreachable[11], and negative ones normally point to irrelevant inverted solutions. The same approach can be used also for much more complex structures, when effects from compressed components may affect the structural response.

The method is well correlated with engineering procedures, in the sense that the eigenvalue gives a safety factor against critical (buckling) response of the structural model for the specific case of forcing defined by $\underline{f}'$. In general, the mode is a combined displacement for the whole structural model, and does not allow the characterization of a particular type of instability, as is done with semi-analytical and design code instabilities.

[10] where both 'unit' and 'small' must be read as flexible terms.

[11] unless they are very close to the lowest one, which can create numerical as well as mechanical problems.

The LPB formulation described here does not formally agree with the general discussion on discretized stability in Sect. 3.7, as the latter derives the stability conclusion from the tangential, rather than the secant, stiffness matrix. From a practical viewpoint, the conclusions are in many—but, definitely, not all—contexts compatible. The usage of LPB approaches demands good problem knowledge, as they are highly unreliable in general cases.

It should also be noted that the eigenvalue λ in the above equations is not related to the stability coefficients Σ used elsewhere in this treatise, even if those are also eigenvalues, cf. Sect. 3.7. The eigenvalues λ here are positive multipliers, which predict the forcing level at which a stability coefficient $\Sigma_\ell = 0$.

4.1.4 Non-linear Equilibrium

The previous sections describe the solution of equilibrium problems, where the models are linear or close to linear. For more general non-linear equilibrium problems, the equations above are no longer relevant, and the formulation must take its basis in Sect. 3.2.5, where the equilibrium is defined by the residual form in Eq. (3.45), with some different common setings defined by Eqs. (3.46)–(3.49). All cases express a requirement for balance between internal force $\underline{p}$ and external force $\underline{f}$, both being equivalent force vectors coming from the virtual interior and exterior work, according to Eq. (3.44). The equilibrium residual force vector, in an FE context, is evaluated according to

$$\underline{r} \equiv \underline{p} - \underline{f} = \mathbb{A}\underline{p}_e - \mathbb{A}\underline{f}_e, \tag{4.9}$$

with $\underline{p}_e$ and $\underline{f}_e$ evaluated for current element discrete variables $\underline{d}_e$, and assembled according to Sect. 3.3.3[12].

In a general case, the differential of the residual related to differentials in the discrete variables is given by Eq. (3.52), which considers non-conservative forcing. Also this matrix is evaluated from element contributions, similar to Eq. (3.72).

Restricting the discussion to conservative cases without constraints, the residual is obtained from

$$\underline{r} = \Pi_{,\underline{d}}, \tag{4.10}$$

ordered as a column vector. The differential of the equilibrium residual is described by an incremental stiffness matrix $\underline{\underline{K}}^i$ defined by Eq. (3.60), (3.53) and (3.57), and coming from

$$\underline{\underline{K}}^i = \Pi_{,\underline{d},\underline{d}} \tag{4.11}$$

with the convention that the index variables create one row and one column index in the matrix[13]. As discussed in Sect. 3.2.6, the incremental stiffness is the sum of

[12] even if external force is often created more easily through a direct definition of components.

[13] and the matrix is obviously symmetric.

the tangential stiffness and the force stiffness matrices—corresponding to the strain energy Π_p and the external potential Π_{con}, respectively[14].

A few important special cases of conservative systems were expressed in Sect. 3.2.5. In Eq. (3.46), for a displacement-independent forcing, $\underline{f}$ is just a constant vector, evaluated at the reference configuration. When such a forcing is magnified by a forcing parameter λ, this case is described by Eq. (3.47). For conservative, but not displacement-independent, forcing, $\underline{f}$ is also dependent on $\underline{d}$ as in Eq. (3.48), and follows from definitions of traction $\overline{\mathbf{T}}$ and body force $\mathbf{B}$. When parameters affect also the internal force vector $\underline{p}$, Eq. (3.49) defines the setting.

The incremental stiffness matrix need be evaluated for the different cases, noting their dependencies on displacement variables $\underline{d}$. The matrix is needed for the solution of the non-linear equilibrium based on the residual in Eq. (4.9). It is also an important property indicator for the obtained equilibria, not least related to stability aspects. This is further discussed in Sect. 4.5.

4.1.5 Basic Solution Method for Non-linear Equilibrium

For non-linear formulations, neither Eq. (4.1) nor Eq. (4.4) is useful, since no total stiffness matrix is available, and iterative methods based on the residual Eq. (3.45) and its differential in Eq. (3.52)—or Eq. (3.61), for conservative cases—must be used.

As an introduction, this section develops a solution method for the simplest case, where a displacement-independent, thereby conservative, problem setting without mechanical constraints is formulated. From this setting, a general numerical formulation is established, the solution of which is discussed in coming sections. This general setting will allow the introduction of multi-parametric formulations and classes of mechanical constraints, discussed in Sect. 3.6, within the same basic format.

Fixed exterior forcing

The solution method is first discussed for the case in Eq. (3.46) where a non-linear structural model is affected by a specified external force $\underline{f}$. For such cases, the incremental stiffness matrix $\underline{\underline{K}}^i \equiv \underline{\underline{K}}^t$. The treatment also assumes that displacement boundary conditions, in the form of prescribed values for a set of displacement variables, are the only mechanical constraints on the equilibrium; this implies that a treatment as above, with 'free' and 'prescribed' displacement variables is relevant.

For this setting, Newton iteration[15] is considered the first-hand choice. For fixed force $\underline{f}$, and a predictor to the discrete solution $\underline{d}^0$, the residual can be assumed to be reduced by a repetitive update to the discrete variables through correctors

[14] noting that the latter vanishes for displacement-independent exterior forcing.

[15] often denoted a Newton-Raphson method.

$$\underline{d}^{j+1} = \underline{d}^{j} + \delta \underline{d}^{j}, \tag{4.12}$$

with δ a forward difference operator, and the superindex denoting the iteration cycle. The iterative correctors are evaluated from the solution to a linear set of equations

$$\delta \underline{d}^{j}_{\text{free}} = -\left(\underline{\underline{K}}^{i}_{\text{free}}(\underline{d}^{j}) \right)^{-1} \underline{r}_{\text{free}} \qquad \text{with} \qquad \underline{r} \equiv \underline{r}(\underline{d}^{j}) = \underline{p}(\underline{d}^{j}) - \underline{f}. \tag{4.13}$$

A common choice for the predictor is $\underline{d}^{0} = \underline{0}$, and the iteration continues until the norms of both the corrector $\delta \underline{d}^{j}$ and the residual $\underline{r}_{\text{free}}(\underline{d}^{j+1})$ are small enough; this is noted for some $j = \hat{j}$, which gives the solution as $\underline{d} = \underline{d}^{\hat{j}+1}$.

The same treatment of free and prescribed displacement components as above is used. If the prescribed displacement variables are introduced in the predictor $\underline{d}^{0}$, the further iterations give zero corrections to these. The equilibrium residual should be assumed to be reduced with each iteration, and should normally give a quadratic convergence to very low norm with increasing j.

Difficulties in the procedure can be related to very large deformations, to nearness to critical states (where $\underline{\underline{K}}^{i}_{\text{free}}$ is close to singular), or to the existence of several nearby equilibrium states. The iterations should be aiming at very low residual norms, perhaps on the order of 10^{-10} times the norm of current internal force $\underline{p}$[16]. It should also be noted that convergence, in some cases of more significant non-linearities, can occur to equilibria not on the primary branch, demanding a careful interpretation of the obtained result.

A solution algorithm based on this clear-cut Newton iteration scheme is very easily created, when algorithmic formulations are available for the evaluation of residual and consistent incremental stiffness from current discrete variables.

Stability evaluation

When convergence is reached through Eqs. (4.12)–(4.13) to an equilibrium state $\underline{d} = \underline{d}^{\hat{j}+1}$, evaluation of the residual shows vanishing values for the free components, while the prescribed components describe the reaction forces needed to enforce the displacement boundary conditions.

The obtained equilibrium state can be evaluated with respect to its properties and stability. Referring to Sect. 3.7, the stability coefficients Σ_ℓ of the equilibrium are obtained from either a one-matrix eigenvalue problem with the incremental stiffness matrix $\underline{\underline{K}}^{i}$ or a two-matrix problem with also a mass matrix; these settings will give the same sign spectra of eigenvalues, cf. Sect. 3.7. Stability demands that all coefficients Σ_ℓ, $(\ell = 1, \ldots, N_d)$ are strictly positive, while any negative stability coefficient indicates that equilibrium is unstable, and zero ones identify a critical state.

[16] For the further developed settings below, this can be of major importance, in order to avoid a build-up of deviations from the correct solutions.

To be precise, the eigenvalue extraction is based on the free components of the matrix, which may need the same condensation of the full matrix as in the iterations. For the full incremental stiffness matrix, a precise and predictable number of zero eigenvalues related to rigid body modes appear in the extraction.

Methods for obtaining a relevant subset of the N_d eigenvalues for the problem are discussed in Sect. 4.5.2. In particular, simple methods to evaluate the number of negative eigenvalues exist. When the eigenvalue analysis indicates a stability coefficient close to zero, the equilibrium is a critical state. Such states are more algorithmically demanding, but are also more interesting, as further discussed below.

A final comment in this section is that the iteration procedure described above normally converges equally well to both stable and unstable equilibria, so no conclusion on stability can be drawn from the iteration progress. Nearness to a critical state can, however, create convergence problems, due to the singular tangential stiffness.

4.1.6 One-Parametric Forcing

The treatment above used the setting of the non-linear problem from Eq. (3.46), where a fixed external force $\underline{f}$ is defined, and the corresponding displacement state solved. Even with this state evaluated, together with corresponding reaction force components and (signs of) stability coefficients, the information on the non-linear response is limited. In order to obtain further information, the solution is normally defined through some problem parameter, most commonly a scalar forcing parameter λ as in Eq. (3.47). The parameter λ is here a special case of the fictitious time parameter τ in Sect. 2.8.5, but it must be noted that no dynamical aspects are considered.

The objective of the parametric form is to solve the equilibrium branch, on which the solution is situated; this provides important information on, e.g., the sensitivity of the solution. Noting in Fig. 4.2, that one obtained equilibrium can be situated on branches of many shapes; it is seen that just one state gives limited information. In the figure, d^* is a relevant discrete displacement component in the solution, e.g., the deflection under a concentrated exterior point force.

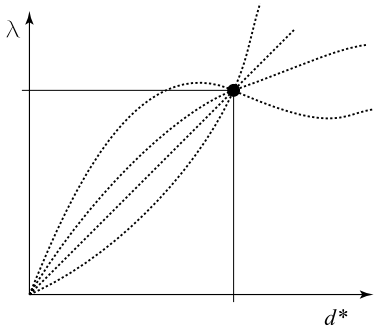

Fig. 4.2 One converged non-linear equilibrium state gives limited information about the branch on which it is situated

A sequence of equilibria is then requested, aimed to reflect the dependence of the response—primarily the displacement vector $\underline{d}$—on λ. In an engineering interpretation, the analysis is aiming at a force-displacement graph with the parameter λ as abscissa, cf. Fig. 4.2. The sequence of equilibrium states aims to represent an equilibrium branch.

Equilibria are sought for a set of parameters λ_i $(i = 1, \ldots)$, chosen to represent the full response to desired accuracy[17], and solutions $\underline{d}_i \equiv \underline{d}(\lambda_i)$ are obtained from

$$\underline{r}(\underline{d}_i) = \underline{p}(\underline{d}_i) - \lambda_i \underline{f}' = \underline{0}, \tag{4.14}$$

where $\underline{f}'$ is a unit external force vector, representing the pattern of exterior forcing as in Sect. 4.1.3. Each solution is obtained iteratively—for fixed λ_i—by Eqs. (4.12)–(4.13), which now become

$$\underline{d}_i^{j+1} = \underline{d}_i^j + \delta\underline{d}_i^j \quad \text{with} \quad \delta\underline{d}_i^j = -\left(\underline{\underline{K}}^i(\underline{d}_i^j)\right)^{-1} \underline{r}(\underline{d}_i^j) \tag{4.15}$$

neglecting the notation for the free displacement variables, and with prescribed displacements introduced in the predictor $\underline{d}_i^0$ for each parameter increment.

As the stepping parameter λ has no fundamental meaning to the equilibrium, each converged equilibrium solution $\underline{d}_i$ can be evaluated as in the previous section, including reactions and (signs of) stability coefficients. After reaching converged equilibria for all intended forcing levels λ_i, the results can be visualized by some suitable presentation.

One important aspect for an interpretation is the non-linearity in displacement response, which can have important functional implications for the structure. From the stability viewpoint, the evolution of the stability coefficients as functions of λ are of major importance, as a vanishing Σ_ℓ indicates a critical situation, where stability is lost. If all stability coefficients are positive for all the equilibria found, an extrapolation of the lowest Σ_ℓ to zero may give an estimate for the critical forcing level λ_{cr}, where stability can be lost; this is an improvement compared to the LPB approach in Sect. 4.1.3. An important conclusion is, however, that the parameter λ does not affect the stability evaluation in any direct way; it is just a selector function for the cases to investigate, and also a measure for the forcing.

The setting and method is rather general for the treatment of cases without a too pronounced non-linearity. A major limitation lies in the assumption that equilibria can be successively solved for increasing λ, i.e., for increased forcing, which demands that no limit state in the force is present. Methods to trace also such equilibrium states, and to continue on the unstable branch of decreasing forcing are discussed from Sect. 4.3 onwards.

[17] With $\underline{f}'$ representing the practical design forcing, the parameters might be, e.g., $\Lambda_i = 0.1, 0.2, \ldots, 2$ in order to describe the response, but also the sensitivity of the solution.

Other forms of one-parametric forcing

When the force in the structural model is conservative, but not displacement-independent, some modifications will appear in the expressions above. These are, primarily, that $\underline{f}$ is dependent on the current discrete vector $\underline{d}_i^j$, through the definitions of $\overline{\mathbf{T}}$ and $\mathbf{B}$. The differential of the potential in Eq. (3.59) gives the equilibrium expression in Eq. (3.48) and employs the full incremental stiffness matrix $\underline{\underline{K}}^i$. Introducing the dependence of $\underline{f}$ on $\underline{d}_i^j$, the procedure defined by Eq. (4.15) is still valid.

For general forcing, with non-conservative terms, the basic Eqs. (4.14)–(4.15) are still valid, if the internal[18] and external force vectors are correctly evaluated. The incremental stiffness matrix must also be replaced by the differential matrix in Eq. (3.52) for the forcing and a similar modification related to internal dissipation. In a non-conservative setting, this matrix is normally unsymmetric, which has some effects on the numerical implementation. This would also demand the treatment of complex eigensolutions; this problem is not further considered here.

Problem formulations including mechanical constraints could be modified to fit into the form used above, but are better treated within the more general setting below.

4.2 Discretized Motion Analyses

As the main focus of this treatise is set on equilibrium states, only a brief account will be given of motion problems. Extensive specialized literature on the topic is available, e.g., the books by Géradin and Rixen (1997) and Bathe (2014).

Several solution methods for dynamic problems are developed for different settings and objectives, and some of these are relevant in connection with stability investigations for equilibria. So is the extraction of eigensolutions a fundamental tool in stability analyses, and this is discussed in Sect. 4.5.2. While spectral response formulations are out of the present topic, mode superposition is related to branch-switching, cf. Sect. 4.6. A very brief account of the basis for direct time evolution of dynamic processes is given in this section.

4.2.1 Dynamic Solution Methods

Without mechanical constraints, the basic equation for treatment of discretized structural dynamics is Eq. (3.63). Inclusion of mechanical constraints in more general forms needs a careful consideration of the method, as briefly noted below.

Equation (3.63) gives an expression for the discrete acceleration at time t through the mass matrix and the current residual. The mass matrix is evaluated from the

[18] only modified if internal dissipation is included.

chosen approximation, cf. Eq. (3.21), only using information from the reference configuration. The residual force expresses the unbalance between current external and internal force. When the internal force is dependent on displacement, and the external force is time dependent, Eq. (3.63) expresses the acceleration from the current state in an assumed time evolution.

The present treatise does not to any depth consider damping in the structural model, even if dissipation is mentioned in Sect. 2.6.3 and Sect. 3.2.6. With a consideration of viscous damping, additional terms are added to Eq. (3.63), typically involving the discrete velocity $\dot{\underline{d}}$.

The most basic dynamics problem, which seeks eigenfrequencies and their corresponding mode vectors for a conservative model is discussed in Sect. 3.2.7, with the defining Eq. (3.66), when the small harmonic vibration $\mathrm{d}\underline{d}$ around an equilibrium state is governed by the mass matrix, which is constant, and the incremental stiffness matrix, which is dependent on the current state, typically evaluated as in Sect. 3.2.6. Compared to the most common setting of harmonic analysis, the form considers both the non-linear response, and a distribution of internal and external force. This is the reason why the smallness of vibration is emphasized, as large non-linear vibrations demand more specialized methods. The treatment of harmonic vibrations around an equilibrium, and the relation of this to stability, is given in Sect. 4.5.2.

In the treatment of structural response to general dynamic forcing, the properties of the forcing affect the choice of method. With a more extensive discussion in the referenced literature, a loose distinction can be made between quick, i.e., explosive forcing primarily as localized force impulses, and slower, perhaps also repetitive, events with more extensive effects on the structure. The time scale is thereby related to the eigenspectrum, or dynamic signature, of the model. As a general rule of thumb, literature commonly states that explicit methods are preferred for the quicker processes, while implicit methods are recommended for the slower.

For the detailed analyses needed in connection with stability affected structural models, the implicit methods are often the most appropriate, even if catastrophic rapid events can be the results of instability. The implicit methods also have a stronger connection to the solution method for parametric equilibrium discussed in Sect. 4.1.6, and several time evolution methods for this task are discussed by Eriksson (1991).

4.2.2 Stability and Accuracy

As extensively discussed in reference and research literature, the time evolution methods have significantly different properties, and need a careful choice for a particular problem. The first choice is whether an explicit or an implicit method should be used, the next one selects the specific method within the class, and its governing parameters. This and the following sections gives a brief review of arguments for these choices.

Both basic settings involve a time sequence of steps valid at time $t_0, t_1, \ldots$, often with uniform intervals[19]. For this, the space and time variations of $\overline{\mathbf{T}}$ and $\mathbf{B}$ are known, together with an initial state, described by discrete displacement $\underline{d}(t = 0)$ and velocity $\dot{\underline{d}}(t = 0)$. The result consists of the discrete solutions at the time steps, $\underline{d}_i \equiv \underline{d}(t_i)$ and $\dot{\underline{d}}_i \equiv \dot{\underline{d}}(t_i)$, which allow the evaluation of also the corresponding current discrete acceleration $\ddot{\underline{d}}_i \equiv \ddot{\underline{d}}(t_i)$ from the basic equation.

The difference between explicit and implicit time evolution methods[20] is whether a new solution $(\underline{d}_{i+1}, \dot{\underline{d}}_{i+1})$ is calculated from just information related to the time $t < t_{i+1}$, or if the solution at $t = t_{i+1}$ is used iteratively. As a general rule, the explicit methods are less algorithmically demanding, and this in particular when lumped mass descriptions are introduced. As the implicit methods are not affected by numerical stability issues in the same way as the explicit ones, they allow longer, and thereby fewer, time steps for a given time duration. The same aspect also implies that they do not have to reduce time step length when an element model is spatially refined.

Discussions of the numerical time evolution methods are commonly related to their stability and accuracy properties. This is related to the aspect that the time evolution methods introduce a discretization of time, in addition to the spatial discretization extensively discussed in Chap. 3. This includes some assumptions for the response between the discrete time stations t_i. This implies that solutions to a motion problem are to some degree always affected by the time history. The accuracy and stability of the time evolution is thereby discussed in relation to the spatially discretized models, disregarding the approximations existing in these in relation to the physical reality.

Numerical stability of a time evolution method is a necessary demand on its properties. Although completely different from the structural stability aspects being the main theme of this treatise, there are some similarities, in the sense that stability demands that small deviations must not grow with time: the effects from unavoidable numerical errors introduced in one time step must be limited in the coming steps.

The stability properties of the numerical time evolution method is investigated by expressing the solution at one time instance in the results from preceding steps. For a homogeneous problem and a linear structural model without damping, the new solution can be expressed as an operator equation. Stability demands that this operator must have eigenvalues of magnitude not greater than one, or some deviations may be amplified by the operator. The conclusion from the investigation is that a method is un-conditionally or conditionally stable[21], where the latter implies that the method is only stable for time steps shorter than a certain value. This time step limit is commonly dependent on the properties of the structural model, and often implies that time steps need be shorter for more finely spatially discretized models[22]. This aspect increases computational complexity quickly when using accurate models. Commercial software sometimes evaluate, or even enforce, the critical time step limits.

---

[19] and this is now physical time.

[20] There exist many proposed variations of each class.

[21] Unstable time evolution methods are not useful.

[22] e.g., related to the wave speed in the material.

While numerical stability is a necessary demand on a used time evolution method, it does not necessarily imply accuracy in obtained results. Even if the used method is un-conditionally stable, results may be inaccurate—or even irrelevant—if long time steps are used. The inaccuracies from the time evolution methods are essentially of two types, where amplitude errors correspond to an un-physical increase of energy in the system with time. Periodicity errors relate to an inaccurate representation of the harmonic free vibration frequencies of the structural model[23].

One further aspect of numerical time evolution methods is commonly discussed in comparison of methods. Numerical damping of higher vibration modes is often a desired property of a time evolution method, and such damping is often introduced by the numerical method. This damping is often advantageous, as it focusses the computed dynamical motion response on the major phenomena, removing small-scale high-frequent vibration effects; as these in most structural contexts contain rather small portions of the total kinetic energy, their removal is of little importance. Several time evolution methods can be provided with selectable parameters to control this numerical damping.

For non-linear problems, or problems with rapidly changing exterior forcing, the strict stability investigations can not be performed, and problem-specific tests must be performed to evaluate the reliability of results.

4.2.3 Explicit Algorithms

Given that $\underline{d}(t_i)$ and $\dot{\underline{d}}(t_i)$ are known, and $\ddot{\underline{d}}(t_i)$ thereby calculable, it is a tempting approach to introduce a series expansion around t_i for a time increment $\Delta t_i = t_{i+1} - t_i$ in order to find $\underline{d}(t_{i+1})$ and $\dot{\underline{d}}(t_{i+1})$. This straight-forward setting of an explicit method is, however, seldom used, and many explicit time evolution methods use a re-formulation of the second order initial value problem into a first order form

$$\frac{\mathrm{d}}{\mathrm{d}t}\begin{pmatrix}\underline{d}\\ \dot{\underline{d}}\end{pmatrix} = \begin{pmatrix}\dot{\underline{d}}\\ \ddot{\underline{d}}\end{pmatrix} = \begin{pmatrix}\dot{\underline{d}}\\ -\underline{\underline{M}}^{-1}\underline{r}\end{pmatrix}, \tag{4.16}$$

with a doubled number of discrete variables. As the right-hand side exists and can be evaluated for a solution at time instance t_i, any general method for time evolution of a first order problem can be used as described by Dahlquist and Björk (1974). One option is the forward Euler method, which is expressed according to

$$\begin{pmatrix}\underline{d}\\ \dot{\underline{d}}\end{pmatrix}_{i+1} = \begin{pmatrix}\underline{d}\\ \dot{\underline{d}}\end{pmatrix}_{i} + \Delta t_i \begin{pmatrix}\dot{\underline{d}}\\ -\underline{\underline{M}}^{-1}\underline{r}\end{pmatrix}_{i}. \tag{4.17}$$

For rapidly changing structural forcing and response, the time steps are often required to be very short for relevant solutions.

[23] as evaluated for the discretized, not the physical model.

More elaborate, but still explicit, methods can be devised using intermediate configurations for some $t_i < t < t_{i+1}$. A simple, but not optimal, method takes half the forward Euler step in Eq. (4.17), evaluates the derivative at the configuration valid at $t = t_i + \Delta t_i/2$, and uses this for the whole step Δt_i. In the same basic approach, e.g., systematic Runge-Kutta methods can be used for the setting in Eq. (4.16), with improved accuracy, but with a higher computational cost per time step; the hope is that this can facilitate the use of fewer, longer time steps. For the present setting, without severe discontinuities in the response, the more elaborate methods are often preferable.

Explicit methods are not easily adapted to problem settings including mechanical constraints, unless these are of a form such that they can be immediately condensed out from the setting.

4.2.4 Implicit Algorithms

One main drawback of the explicit time evolution methods is that they do not consider the acceleration $\underline{\ddot{d}}_{i+1}$ at the new time instance t_{i+1} in the calculation: this can be loosely interpreted as an unbalanced residual at the end of the taken time step, if the integrated $\underline{d}_{i+1}$ and $\underline{\dot{d}}_{i+1}$ do not match the derivative of the process leading up to this state. The implicit methods for time evolution aim to reduce this shortcoming by an iterative method, where $\underline{\ddot{d}}_{i+1}$—calculated from provisional $\underline{d}_{i+1}$ and $\underline{\dot{d}}_{i+1}$—is used in the time evolution of $\underline{d}$ and $\underline{\dot{d}}$ over the time interval $t_i \leq t \leq t_{i+1}$. Several different algorithms are proposed in literature, differing in basic ideas and algorithmic parameters, cf. the type of discussion by Noh and Bathe (2019). The new solution is iteratively improved to give force balance at the new time instance, but also to maximally utilize the information at both ends of the time interval. Noting that some approximations are introduced for the variations of the discrete variables during the time step, all methods will tend to accumulate inaccuracies during the time sequence; the order of the inaccuracy is predictable from the method definition.

Implicit time evolution methods allow the introduction of general mechanical constraints in the structural model, and can be adapted to handle particular forms of these. The issue is discussed by, e.g., Noh and Bathe (2023).

Efficient implicit methods of high accuracy have been presented in recent research literature, and are introduced in some advanced simulation codes. General commercial software, however, commonly use, e.g., the Newmark and Hilber-Hughes-Taylor ('HHT') implicit time evolution procedures, each with a few algorithmic parameter choices. These methods, with default parameters, are generally reasonably reliable for many, not too complicated, problems in structural motion analyses.

4.3 Parametric Equilibrium Analyses

The treatment of a non-linear equilibrium problem in Sect. 4.1.6 considers a one-parametric forcing on a structure, where a force pattern is hard-coded in the model, but its magnitude variable. The solution method evaluates a sequence of equilibria, each valid for a specific value of the forcing parameter λ. The solution method assumes a monotonously increasing forcing. As presented, it can only handle trivial constraints on the equilibrium, in the form of specified values for displacement variables. In order to remove the limitations mentioned, this section develops a more general setting, from which the case above is a special case. The following sections describe a number of algorithmic aspects of such a general setting. A schematic description of an implementation is given in Sect. 4.7 and Fig. 4.11; an example of usage for stability investigations of a simple model is given in Sect. 4.6.

The generalized form of the equilibrium problem is here stated as a non-linear set of N equations

$$\underline{R}_y(\underline{y}) = \underline{0} \tag{4.18}$$

in N variables $\underline{y}$.

The N functions in the extended residual $\underline{R}_y$ are all set in a residual form, so that a vanishing value is required in a solution. The discrete vector $\underline{y}$ contains all variables for the problem. These are always the N_d discrete displacement variables $\underline{d}$ and a set of N_p parameters $\underline{P}$[24]. If mechanical constraints are introduced, N_c constraint-enforcing variables $\underline{C}$ are also included, cf. Sect. 3.6.

In the general case, the relevant vectors of variables and functions are thereby

$$\underline{y} = \begin{pmatrix} \underline{D} \\ \underline{P} \end{pmatrix} \equiv \begin{pmatrix} \underline{d} \\ \underline{C} \\ \underline{P} \end{pmatrix} \quad \text{and} \quad \underline{R}_y = \begin{pmatrix} \underline{R} \\ \underline{R}_x \end{pmatrix} \equiv \begin{pmatrix} \underline{r}_c \\ \underline{R}_c \\ \underline{R}_x \end{pmatrix}. \tag{4.19}$$

where the subsets of fundamental state space variables $\underline{D}$ and corresponding residual functions $\underline{R}$ from Eqs. (3.90) and (3.91) are augmented by a set of parameters $\underline{P}$ and a set of selector functions $\underline{R}_x$. The further elaboration will be based on the fact that displacements and contact-enforcing variables are fundamental to the mechanical problem, and are strongly connected to equilibrium and constraint equations, while parameters and selectors are much more loosely—if at all—connected. The latter fact is the reason why the index on $\underline{R}_x$ is not 'p'.

With the exception of cases where constraints represent hard contact conditions, cf. Sect. 3.6.4, the solution to the constrained equilibrium problem is well-defined and allows solution methods discussed below. With hard contacts introduced, the solution of equilibrium has to be based on an assumption concerning the contact status at the equilibrium, and methods included in the algorithm for handling of changing status, cf. Sect. 4.5.5.

[24] with $N_p = 1$ and $\underline{P} = \lambda$ in the mentioned example.

The parametric setting focusses on diverse forms of parameters in $\underline{P}$, while the basic structural model and the constraints are considered as specified; this includes all hard-coded parameters. The form emphasizes the parametric dependence in the equilibrium states. A special focus is often set on investigations of parametric regions where equilibria give the same stability conclusions[25], and the boundaries for these, which are the critical states. The main tool is a general algorithm for parametric traces[26] in the solution space.

As one example, the problem in Eq. (4.14)—without constraints, and with just one parameter—is in the generalized form defined as

$$\underline{R}_y(\underline{y}) \equiv \begin{pmatrix} \underline{r}(\underline{d}, \lambda) \\ \lambda - \overline{\tau} \end{pmatrix} \quad \text{with} \quad \underline{y} \equiv \begin{pmatrix} \underline{d} \\ \lambda \end{pmatrix} \tag{4.20}$$

adding to the demand for a vanishing force residual a request for a specific forcing parameter value through a prescribed fictitious time $\overline{\tau}$. This is a selector equation of the form $R_x = 0$ related to the parameter λ, which is part of the solution vector $\underline{y}$, but does not affect the stability conclusions.

With the general setting of the extended residual in Eq. (4.18), the solution is again obtained through Newton iteration, where an incremental-iterative algorithm uses a two-level loop. For every increment i in a sequence, a cycle of iterations j is evaluated according to

$$\begin{aligned} \underline{y}_{i+1}^{0} &= \underline{y}_i + \Delta \underline{y}_i^0 \\ \underline{y}_{i+1}^{j+1} &= \underline{y}_{i+1}^{j} + \delta \underline{y}_{i+1}^{j} \quad \text{for} j = 0, \ldots, \hat{\jmath} \\ \underline{y}_{i+1} &= \underline{y}_{i+1}^{\hat{\jmath}+1}. \end{aligned} \tag{4.21}$$

In the iteration scheme, $\Delta \underline{y}_i^0$ is a chosen predictor to the increment, and the iterative correctors are repeated until iterate $\hat{\jmath}$, decided by small enough $\delta \underline{y}_{i+1}^{\hat{\jmath}}$ and $\underline{R}_y(\underline{y}_{i+1}^{\hat{\jmath}+1})$. Here, 'small' is below a low tolerance, as discussed above. The iterative correctors in the increment are calculated from

$$\delta \underline{y}_{i+1}^{j} = -\underline{\underline{J}}^{-1} \underline{R}_y(\underline{y}_{i+1}^{j}), \tag{4.22}$$

where the Jacobian of the system

$$\underline{\underline{J}} = \underline{R}_{y,\underline{y}} \tag{4.23}$$

is the derivative of all the functions $\underline{R}_y$ with respect to all variables $\underline{y}$, and evaluated at a particular $\underline{y}$. In the most general case, the Jacobian is of the form

[25] interpreted as the same sign spectra of stability coefficients, i.e., eigenvalues.

[26] or 'sequences' or 'curves', which are often, but not always, representing 'branches'.

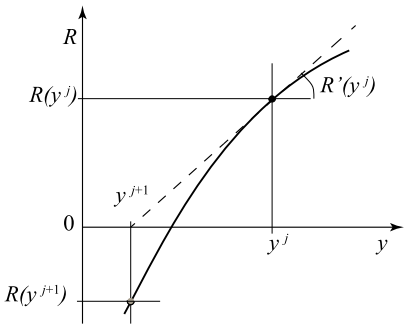

Fig. 4.3 Schematic illustration of one step of Newton iteration for a scalar problem $R(y) = 0$. The slope at the current iterate y^j is used to find an improved iterate y^{j+1}. The prime is here the differential with respect to y

$$\underline{\underline{J}} = \begin{pmatrix} \underline{\underline{K}} & \begin{pmatrix} \underline{r}_{c,P} \\ \underline{R}_{c,P} \end{pmatrix} \\ \begin{pmatrix} \underline{R}_{x,d} & \underline{R}_{x,C} \end{pmatrix} & \underline{R}_{x,P} \end{pmatrix}, \tag{4.24}$$

with simplifications for specific cases. In particular, the operative stiffness matrix $\underline{\underline{K}}$ is equal to $\underline{\underline{K}}^i$—or even $\underline{\underline{K}}^t$—if no mechanical constraints are considered, and equal to $\underline{\underline{K}}^c$ if they are. Without constraints, $\underline{R}_{c,P}$ and $\underline{R}_{x,C}$ are not present.

In the example case above, the Jacobian is

$$\underline{\underline{J}} \equiv \begin{pmatrix} \underline{\underline{K}}^t & -\underline{f}' \\ \underline{0}^{\mathrm{T}} & 1 \end{pmatrix} \tag{4.25}$$

when the external force is $\underline{f} = \lambda \underline{f}'$, cf. Eq. (3.47), and $\underline{\underline{K}} \equiv \underline{\underline{K}}^t$, the tangential stiffness.

One step of the Newton iteration can be schematically described for a scalar problem $R(y) = 0$ by Fig. 4.3; the working for a set of equations is analogous. The current derivative of the function is used to improve the approximate solution. In the case of the figure, one more iterate will come very close to the correct solution.

Referring again to the example problem in Eq. (4.20), the final equation plays a special role. Without any mechanical meaning, it is an algorithmic increment selector function controlling the evolution of the solution sequence. In this case, it is specifying the forcing parameter values for which solutions are sought. The selector equation is kept in its form, but modified by a new value $\overline{\tau}_i$ for each new increment.

This force stepping procedure is the most basic form for a non-linear equilibrium trace in the context of conservative one-parametric forcing, and is in general highly reliable for many classes of problems as long as no limit states appear on the solution branch. It must be noted that λ is just a parameter, and not a state variable in the stability investigation.

As the choice of the form of increment selector function, and the updating of it, are both of major importance for the success of the numerical simulations, more

reliable and general methods are discussed below in Sect. 4.3.2. These aspects affect the number and classes of variables in $\underline{P}$ and equations in $\underline{R}_x(\underline{y})$, and thereby also the contents of $\underline{\underline{J}}$, albeit not the operative stiffness $\underline{\underline{K}}$, which decides stability for the equilibria solved.

The forms of residual and Jacobian given by Eqs. (4.19) and (4.24), and the solution method defined by Eqs. (4.21)–(4.22) are consistently used in coming sections, when the settings introduce new aspects of the equilibrium problem.

4.3.1 Variations to the Newton Iteration

Several variations of the Newton iteration procedure described by Eqs. (4.21)–(4.22) are employed for diverse cases in literature, in particular for cases with one-parametric forcing. These may be motivated for particular problem settings, but are often made necessary from incorrect or incomplete forms of the Jacobian matrix, when this is inconsistent with the residual or increment selector expressions.

One modification, particularly used in early implementations with more limited computational resources, is the modified Newton iteration method, which evaluates the iterative corrections in Eq. (4.22) as

$$\delta \underline{y}_{i+1}^{j} = -\left(\underline{\underline{J}}(\underline{y}_{i+1}^{0})\right)^{-1} \underline{R}_y(\underline{y}_{i+1}^{j}) \tag{4.26}$$

with only one evaluation of $\underline{\underline{J}}$ at the predictor $\underline{y}_{i+1}^{0}$ for each new increment. Other implementations evaluate $\underline{\underline{J}}$ at, e.g., every third iteration[27]. The gain from fewer evaluations of $\underline{\underline{J}}$ is counteracted by the often significantly higher number of iterations needed, in particular when the tolerance is set low.

Other common modifications emanate from descent methods in optimization, and interpret the correction calculated by Eq. (4.22) as a search direction. A line search is then added to Eq. $(4.21)_2$, giving

$$\underline{y}_{i+1}^{j+1} = \underline{y}_{i+1}^{j} + \alpha_{i+1}^{j}\, \delta \underline{y}_{i+1}^{j} \tag{4.27}$$

with $\delta \underline{d}^{j}$ evaluated from Eq. (4.22), and α_{i+1}^{j} a scalar chosen from some criterion. As the Newton iteration step gives both direction and magnitude for the correction, not even 'slack' line searches are normally improving overall efficiency of the process, if accurate differential expressions are used. Factors $\alpha_{i+1}^{j} < 1$ may, however, be useful as safe-guards in the first few correctors in an increment if the predictor is rough.

[27] or when convergence is deemed to be too slow, based on some criterion.

Dynamic relaxation

A fundamentally different approach to solving a conservative equilibrium state, and primarily used in form-finding methods is through Dynamic relaxation ('DR'). The problem is then solved in a pseudo-dynamic setting, with more or less fictitious mass and damping matrices. A time evolution of the thereby stated problem is assumed to eventually—through the introduced damping—lead to an equilibrium, when residual force, and acceleration, is brought to zero. The damping is a necessary requirement for this convergence, and efficient formulations are discussed in literature; as the damping is completely fictitious, the choice is non-trivial.

Even if more elaborate and efficient methods for handling motion problems are briefly discussed in Sect. 4.2. the fictitious time evolution in the DR context can be performed with simpler methods.

Two main drawbacks of this method are related to the significant difficulties in choosing sufficiently good mass and damping descriptions without deep prior problem knowledge, and the low accuracy achievable without very long time sequences simulated. Experiences from tests within the present problem class show prohibitively high numbers of iterations needed for acceptably low residual norms. One of the few problem classes where this method has proven useful is described by Nakashino et al. (2020), dealing with a problem where different localized wrinkling patterns of a structure allow many similar and nearby solutions. For such cases, the Newton iteration approach tends to give convergence problems, due to near-singularity, while the dynamic relaxation can converge to one—essentially arbitrary—of the neighboring equilibria. When the engineering view is interested only in the occurrence of wrinkles, but not the exact location of them, this result is fully relevant. A hybrid approach starting the iteration with a number of DR steps—to localize an approximate equilibrium—and ending with Newton iteration—for high accuracy—can be an interesting choice for special problem settings.

4.3.2 Stepping Procedures

The most common parameter in a non-linear equilibrium problem is related to the representation of exterior forcing, and takes the form of Eq. (3.47), where a parameter λ magnifies a fixed external force pattern vector $\underline{f}'$. The structural model is here completely fixed with hard-coded geometry, sectional properties and material. In Sect. 4.1.6, the problem is solved through a force stepping strategy, where equilibrium is sought and evaluated for successively introduced prescribed values for λ. The same approach is useful for solving a case according to Eq. (3.48), if the displacement dependence in external force is introduced.

An implicit assumption in the method is that closely placed equilibria are analyzed, so that they can be assumed to represent a continuous equilibrium branch, or important response aspects can be missed. This aspect is closely related to the complexity of the equilibrium branch.

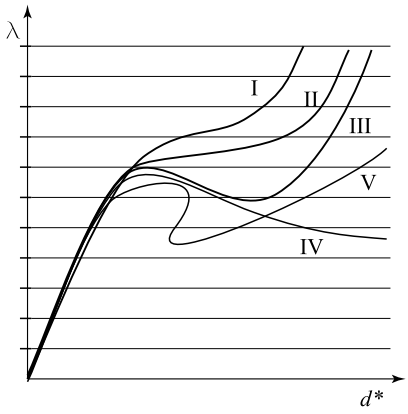

Fig. 4.4 Schematic equilibrium branches for structures under one-parametric forcing. Horizontal lines indicate levels for force stepping, defining the equilibrium states solved as the crossings of paths and levels

Figure 4.4, which is an elaboration of Fig. 4.2, shows a few possible classes of results, where force stepping is not well-suited, and other approaches must be introduced. The figure shows equilibrium branches, where a characteristic displacement value d^* is related to the forcing parameter λ, i.e., as a force-displacement graph[28]. The graphs in the figure are the true equilibrium branches for the model, while the horizontal lines indicate a set of fixed forcing parameters, for which the equilibria could be evaluated. The result from the simulation would thereby be just the points of the crossings, needing an interpolation between these for more complete results. Even with several equilibrium states evaluated, the question remains whether the solved equilibria represent all relevant aspects of the equilibrium branch, but it should be noted that each state is a correct equilibrium in itself; the question is whether the imagined connection lines between solved states are representative.

In the figure, branch I shows a mildly non-linear graph, describing a first softening, then stiffening response. This branch can be rather well represented by states with uniform increments in the forcing parameter, if these are not too large. Branch II, which is monotonous but more varying in stiffness, is more difficult to describe by uniform forcing increments, due to the almost horizontal projection over a significant (and interesting) interval. Branch III where a 'snap-through' response is showing two limit points, and branch IV showing one, are obviously not suited for force stepping increments. Branch V with a 'snap-back' response is even more challenging. At least the tracing of branches II–V needs other methods, in particular since the more dramatic response aspects are of major engineering interest.

Several strategies for increment stepping have been proposed, and are set in a common form by Eriksson (1989). The under-determined set of non-linear equations

[28] in the typical engineering projection, with the forcing parameter vertical and the displacement component horizontal.

reflected by Eq. (4.14), with N_d equations in $N_d + 1$ variables is then transformed into a solvable system, by adding an increment selector equation, as in Eq. (4.20).

The most obvious remedy to problems in the force stepping is to introduce displacement stepping for the choice of successive equilibrium states. All the branches I–IV can be well described by equilibria uniformly distributed along the horizontal axis d^* in the graph instead, with the fictitious time variable $\tau = d^*$. In the general form of Eq. (4.19), this means that the increment selector equation added to the equilibrium residual equation is

$$R_x \equiv d^* - \overline{\tau} = 0, \tag{4.28}$$

which gives a row matrix with just one unit component in $\underline{R}_{x,\underline{d}}$. Also, $\underline{R}_{x,\underline{P}} = 0$, as no parameter is involved in Eq. (4.28). The operative stiffness is the same as before, so the stability conclusions for an equilibrium state are the same, disregarding the stepping strategy.

Another common and popular choice, which potentially handles the tracing of equilibrium branch V, is commonly attributed to Riks (1979) and Crisfield (1981). The basic idea is to define a branch length, commonly denoted an arc length, as the fictitious evolution time τ, and to introduce increments in this quantity for evolution of the equilibria in the sequence. The method can be interpreted as a curve stepping strategy, as the measure focusses more on the presentation than on the physical response itself.

With variations in the specific implementation, one step along the branch is typically described by the secant length between equilibrium states, which for an incremental step, starting at state i, is

$$\Delta\tau_i = \sqrt{\left(\Delta\underline{d}_i\right)^{\mathrm{T}}\left(\Delta\underline{d}_i\right) + (\beta\,\Delta\lambda_i)^2}, \tag{4.29}$$

where $\Delta\underline{d}_i$ and $\Delta\lambda_i$ refer to the increments in the displacement and forcing parameter during step i, respectively. The arc length measures the radius of a hyper-sphere in $(N_d + 1)$-dimensional space centered at the state $\underline{y}_i = (\underline{d}_i^{\mathrm{T}}, \lambda_i^{\mathrm{T}})^{\mathrm{T}}$. This is best set in the form of Eq. (4.19) through a consistent, and easily differentiable, selector function

$$R_x(\underline{y}) \equiv \left(\underline{d} - \underline{d}_i\right)^{\mathrm{T}}\left(\underline{d} - \underline{d}_i\right) + \beta^2\,(\lambda - \lambda_i)^2 - \left(\overline{\Delta\tau}_i\right)^2, \tag{4.30}$$

with $\overline{\Delta\tau}_i$ a requested increment in the evolution parameter. A basic increment stepping strategy is to find equilibria with uniform increments in $\Delta\tau_i$ for $i = 0, 1, \ldots$, but the increment lengths can be variable in the sequence, as further discussed in Sect. 4.4.3.

The first two terms of this $R_x(\underline{y})$ expression can be evaluated as $\Delta\underline{y}_i^{\mathrm{T}}\,\underline{\underline{S}}\,\Delta\underline{y}_i$, with $\underline{\underline{S}}$ a diagonal scaling for the components of $\underline{y}$. This expression can be generalized for specific needs, and can be used also for more complex settings than one with just $\underline{d}$ and λ as variables, cf. below.

Although attractive from the graphical viewpoint, the curve stepping method needs care. One non-trivial, but manageable, aspect relates to the square root in Eq. (4.29)[29]—and an accompanying choice of sign—but the main problem lies in the different dimensions of the involved variables, when force, moment, translation and rotation variables might be involved; the β factor cannot remove this problem. If a 'spherical' arc length increment is requested, the constant β must be chosen such that the two first terms of $R_x(\underline{y})$ are—on average—reasonably similar in magnitude.

Several other strategies based on similar ideas have been published in order to distribute solution states for maximum information about equilibrium response with minimum computational effort. Experiences from many different problem areas indicate that the most efficient and reliable stepping strategy is highly problem dependent, and can not always be predicted before starting the analyses of a particular problem.

Some form of increment selection and control is available for parametric forcing in most professional software[30]. They are also rather easily introduced in self-made non-linear solution algorithms.

The increment selector function is needed to facilitate the solution of a new equilibrium in a sequence. In many cases, it also improves the condition number for the Jacobian matrix $\underline{\underline{J}}$ used in the iterations, but it has some potential computational drawbacks. These come from the structure of $\underline{\underline{J}}$, when the augmenting final row leads to a large fill-in during factorization. A direct solution of the complete set of equations is suggested, if sufficiently efficient algorithms are available for this task.

A new equilibrium state in the sequence can also be obtained from a two-term process, even if this is occasionally less numerically well-conditioned. For the form in Eq. (4.15)[31], the procedure is based on a re-writing of the equations, expressing the iterative correction to the displacement variables as

$$\delta \underline{d}_{i+1}^{j} = -\underbrace{(\underline{\underline{K}}^{i})^{-1}\underline{r}}_{\delta \underline{d}_r} + \delta\lambda_{i+1}^{j} \underbrace{(\underline{\underline{K}}^{i})^{-1}\underline{f}'}_{\delta \underline{d}_f}, \tag{4.31}$$

in the example setting. The 'free' subindex is again omitted, and $\underline{\underline{K}}^{i}$, $\underline{r}$ and $\underline{f}'$ all evaluated for the iterate $(\underline{d}_{i+1}^{j}, \lambda_{i+1}^{j})$. After solving the two systems of equations, with the same system matrix, an iterative correction to the force parameter $\delta\lambda_{i+1}^{j}$ is chosen such that the new iterate

$$\underline{d}_{i+1}^{j+1} = \underline{d}_{i+1}^{j} + \delta \underline{d}_{i+1}^{j} \quad , \qquad \lambda_{i+1}^{j+1} = \lambda_{i+1}^{j} + \delta\lambda_{i+1}^{j} \tag{4.32}$$

---

[29] but this is essentially removed by using Eq. (4.30).

[30] often under names such as 'arc length' or 'Riks' strategies with different implementations and specifications.

[31] Note that the increment index is changed to the one used here.

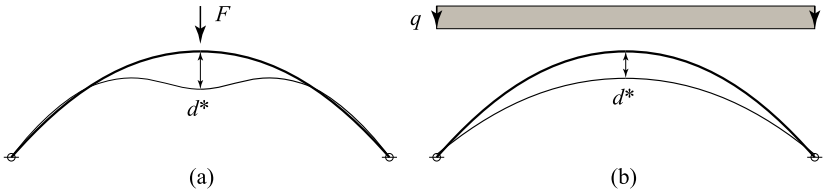

Fig. 4.5 Example of increment stepping methods in forced plane beam structure

satisfies the selector equation, which may use any of the increment stepping functions. It is noted that this approach uses the incremental stiffness matrix, which is close to singular around critical equilibria.

Comparison of increment selectors

Although the discussion above solves the same problem—but with different methods—the different approaches tend to change the view on results, as illustrated by Fig. 4.5. For the problem in subfigure (a), with a concentrated force F of fixed direction applied to a material point, the problem can be solved with a parametric forcing, i.e., force stepping, as long as no snap-through response occurs; the corresponding deflection d^* is a result. Alternatively, the same problem can be solved by a displacement stepping, using d^* as the fictitious time, and obtaining the acting force F as a reactive force result. For the distributed traction forcing in subfigure (b), the forcing can be described by a forcing parameter λ, and the solution force stepped in λ, or displacement stepped in d^*; the forcing parameter λ will be a result and give the traction corresponding to the d^* parameter. Both problems can be solved by curve stepping according to Eq. (4.30), if a forcing parameter λ is defined, and a suitable scaling parameter β selected.

Note, regarding the example, that the increment selector introduced is not a constraint on the equilibrium, but just acts to pick a set of solutions with a combination of displacements $\underline{d}$ and forcing parameter λ. The increment selector is thereby outside the operative stiffness $\underline{\underline{K}}$.

4.4 Multi-parametric Equilibrium

Common engineering analyses of non-linear equilibrium focus on the form in Sect. 4.1.6, where a hard-coded structural model is affected by a one-parametric forcing, i.e., a case with $N_p = 1$ in Eq. (4.19). The examples in Chap. 1 show that structural response, and not least stability, can be strongly dependent on other parameters, e.g., geometric, material or imperfection data. For improved understanding of mechanical response, it can thus be advantageous to investigate the dependence of

response on also other parameters. Parametric equilibrium solutions are therefore a main interest. This is the basis for the introduction of N_p parameters in the general form of the non-linear equilibrium problem in Eq. (4.19). This section discusses how equilibrium and stability can be studied in such a context. The parameters available in the part $\underline{P}$ of the discrete vector $\underline{y}$ allow variations to the model or the forcing, while the selector equations in $\underline{R}_x$ are used to define the cases for which equilibria are sought. The selection of cases gives wide possibilities to focus on specific investigations. As noted above, the fundamental variables $\underline{d}$ and $\underline{C}$ are very strongly connected to the functions $\underline{r}_c$ and $\underline{R}_c$, while parameters $\underline{P}$ and selectors $\underline{R}_x$ have no necessary connection.

The combination of parameters and selectors thereby reflect the analysis objective. The setting and method below has similar objectives as the work by Cox et al. (2018), while the numerical implementation essentially follows the works by Eriksson (1998) and Groh and Pirrera (2018). The basis for algorithms performing parametric analyses is well discussed by Rheinboldt (1986).

The coming sections discuss settings where N_d and N_c can be high numbers, while N_p is typically rather low. The primary interest here is focused on cases with $N_p \geq 2$. The more general setting also allows, as one special case, settings where $N_p = 1$, but with the parameter not related to the exterior forcing. In addition to the explicitly introduced parameters in $\underline{P}$, a large number of structural parameters are still implicitly considered as hard-coded in the simulation model.

Without mechanical constraints, the common one-parameter discretized setting in Sect. 4.1.6 is defined by N_d equilibrium residual equations in the $N_d + 1$ discrete variables, thus an under-determined system, with states on branch segments as the general solution. The solution for one particular equilibrium state demands the addition of an increment selector function, e.g., one of the stepping functions discussed in Sect. 4.3.2. For reasonable choices of function and increment length, convergence can be assumed to occur to a new state on the equilibrium branch. The equilibrium sequence is obtained when this selector function is updated between the increments in the solution process.

Constraints on the mechanical equilibrium enter through new variables in $\underline{C}$ and functions in $\underline{R}_c$ in Eq. (4.19). These are equal in number and strongly related; they form the constrained residual equations in Eq. (3.90) with its constrained stiffness in Eq. (3.92). The expressions show that parameters enter in the same way, whether or not constraints are introduced. This is even more clearly seen from Eq. (4.24), where the operative stiffness $\underline{\underline{K}}$ relates to all state variables together. A multi-parametric setting is thereby equally valid and relevant also for this case.

When the number of parameters is increased to N_p, the constrained equilibrium residual in Eq. (3.90), being also the two upper sets of $\underline{R}_y$ in Eq. (4.19), gives $N_d + N_c$ equations in the $N_d + N_c + N_p$ variables. The full equilibrium solution thereby consists of N_p-dimensional submanifolds, which may be difficult to visualize and interpret if $N_p > 1$. The linearized parametric response around an equilibrium state is described by the tangent space, as discussed in Sect. 4.5.3.

Lower dimensions of the solution space are reached by adding selector functions $\underline{R}_x$, where each reasonable function reduces the dimension by one. Introduction

of N_p selector functions thereby—under some assumptions—gives the solution as one state, and is necessary for the Newton iteration in one increment, as defined by Eqs. (4.21)–(4.22).

The selector functions can refer to any or all of the variables in $\underline{y}$, and have no necessary connections to the parameter introduced. The multi-parametric problem setting and parametric traces give wide possibilities to investigate structural response, and in particular stability properties. The coming subsections discuss some interesting classes of selectors and typical parameters briefly. It is noted that some of the selector functions discussed below are rather easily formulated as residual functions, but their derivatives with respect to problem variables may be more demanding, which strongly suggests a numerical differentiation. In any case, the formulations are highly specific for the problem setting.

Even if Sect. 4.4.4 briefly discusses two-dimensional solution surfaces, engineering typically views results as one-dimensional relations, i.e., graphs, which are easily presented and interpreted. This aspect is further discussed in Sect. 4.4.2

4.4.1 Selectors and Parameters

Selectors and parameters can be used in many different ways, dependent on simulation purpose. This section will discuss a few classes, where in most cases selectors and parameters are related.

Convenience parameters

An addition of further parameters in $\underline{P}$ and related functions in $\underline{R}_x$ can be used for transformations between variables. This is easily used for, e.g., summation of some displacement or reactive force components[32], intended for post-processing of results, or for convenience in interpretation. As one example, several papers by the authors use this method to connect gas pressure and included volume in a closed membrane to a gas amount quantity, allowing two different views on the forcing. The selector function is then of the type

$$R_x(\underline{d}, \underline{P}) \equiv (P_1 + p_0)\, V(\underline{d}) - P_2, \tag{4.33}$$

with P_1 the internal over-pressure, which is considered as the main forcing parameter (and related to ambient pressure p_0), P_2 a scaled measure for the gas amount[33], and the volume V calculated from displacement variables $\underline{d}$. Effectively, a passive parameter P_2 is included, demanding a minor extra computational effort, but simplifying

[32] A parameter is introduced for the summed quantity, and a selector function equates this to a sum of the discrete variables, or of some calculated quantities.

[33] through the ideal gas law, under iso-thermal conditions.

interpretation. With an added increment selector function successively updated, a sequence of equilibria is obtained, with pressure and amount immediately available in the solution vector; both are relevant in an inflation process.

The selector function in Eq. (4.33) reflects the same relation between variables as the constraint in Eq. (3.93), and leads to the same equilibria, but yields different stability conclusions. As the two variables P_1 and P_2 are both parameters here, they are frozen in a stability evaluation, and thereby have no effect on the resulting conclusions. The formulation of convenience transformation functions and their differentials is often straight-forward for a specific problem.

Response quantities

Geometric or material parameters for the considered structural model can be introduced by $\underline{P}$, thereby allowing variations. This is used, e.g., for evaluation of sensitivities, cf. Sect. 4.5.3. Examples are lengths or angles, thicknesses or section properties and constitutive parameters.

Such parameters are primarily used together with response quantities for the obtained equilibria. These can be one of the primary variables, e.g., a discrete displacement component, or a post-processed one, e.g., a stress component at a specified point[34]. As each state in the sequence is a complete equilibrium, any such property is easily evaluated.

As an example, if one geometric and one forcing parameter are introduced, a selector function can be used to fix a certain stress component in the model. The equilibrium sequence will then show for which forcing level this stress is reached under variation of the geometric parameter.

In an optimization context, this setting can be used to find parametric combinations for which a response quantity takes a specific value for specified forcing. Eriksson (1997) gives an example, sketchily shown in Fig. 4.6, where the plane frame is defined from the parameters angle β and sectional height h, together with all other data hard-coded. Equilibrium sequence No. 1 shows for which parametric combinations an interesting stress component takes a specified value for this forcing. Sequence No. 2 shows parameter combinations for which the equilibrium is critical for a chosen safety factor times the same forcing. The sequences together give the feasibility region for the structure under these optimization constraints[35]. The objective function is easily evaluated for all solutions in the sequences[36].

The response functions are often easily formulated for a specific problem, but their differentials may need a numerical differentiation.

[34] The maximum stress anywhere in the model can be used, but is more complicated, due to the discontinuity if the maximum point varies over the sequence.

[35] limiting stress under forcing and demanding a safety against loss of stability.

[36] assuming that the optimum solution will always have one optimization constraint activated.

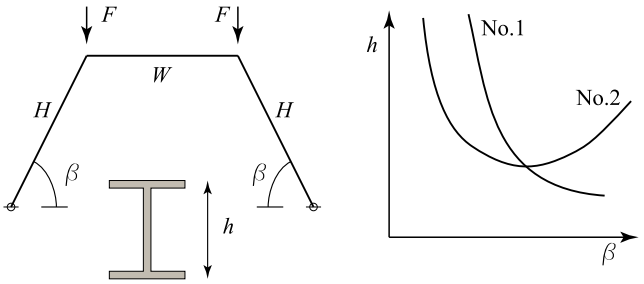

Fig. 4.6 Simplified result from an example of parametric response. Schematically re-drawn from Eriksson (1997). Curves show parametric combinations which give a particular response property

Forcing

The most common parameter for forcing is a force multiplier affecting $\underline{f}'$ or $\overline{\mathbf{T}}$ and $\mathbf{B}$, as in Sect. 4.1.6. Several contributions to forcing can be described by a set of parameters. For modelling imperfections, an inclined force component can be described by an added parameter, which is either an orthogonal force component or an orientation angle added to the main force parameter. The same basic idea is used when modelling the combined effect of a pre-forcing and a main forcing. This is typically combined with a response selector function for some important response quantity, e.g., deflection or stress.

Multi-parametric descriptions can also introduce a perturbation force component in a critical direction. A selector equation prescribing a specific secant distance from an isolated critical state defines a hyper-circle, revealing secondary equilibrium sequences through a vanishing perturbation force. This demands a reliable algorithmic treatment, which isolates states with a vanishing parameter, cf. Sect. 4.5.6.

Critical states

States of critical equilibrium, where the stability changes, are characterized by vanishing stability coefficients[37], cf. Sect. 3.7, and uses a function

$$R_x \equiv \Sigma_{\text{crit}} \left(\underline{\underline{K}} \right), \tag{4.34}$$

the lowest magnitude eigenvalue of the operative stiffness matrix[38]; this is normally rather easily found through, e.g., inverse power iterations, at least if the critical state shows only one vanishing stability coefficient.

[37] very commonly just one, but symmetry may lead to two or more.

[38] with or without constraints, with our without force stiffness.

In a one-parametric setting, this function replaces the increment stepping function, solving then one critical equilibrium state for a hard-coded structure and the parametric forcing. In an optimization context, the critical selector function seeks, e.g., a model parameter, for which the critical force has a hard-coded value. The result for these settings is one state, not a sequence.

In multi-parametric settings, this function is one of the selectors when seeking a sequence of critical equilibrium states. With one parameter for forcing and one for the model geometry (or material), the critical state with its forcing is solved as function of the other parameter. This is thereby a more systematic, but similar, method as the one used by Li and Healey (2016).

Parameter combinations can also be sought, where a specific forcing level gives a critical equilibrium. This is the situation for graph No. 2 in Fig. 4.6, for which three parameters—one related to forcing and two to geometry—are used. With one selector function specifying the forcing, one defining a critical state and one successively updated increment selector, this gives a sequence as result.

The search for critical states based on a criticality function such as Eq. (4.34) is limited to cases where a single vanishing eigenvalue of the operational stiffness vanishes. This is due to the implicit need for the eigenvector corresponding to the critical mode in the formation of the gradient of the eigenvalue with respect to state variables.

States of multiply critical equilibria with more than one vanishing eigenvalue are sometimes of interest. Under certain circumstances[39], the critical selector condition in Eq. (4.34) can be replaced by the function

$$R_x \equiv \sum_{c=1}^{N_0} (\Sigma_c - \Sigma_\varepsilon) \tag{4.35}$$

where the Σ_c are the N_0 lowest magnitude eigenvalues of the operative stiffness $\underline{\underline{K}}$, when a sequence of N_0-fold criticality is traced[40], and Σ_ε a positive numerical tolerance for a vanishing eigenvalue. A sequence traced with this selector follows a border line for the zone of critical equilibrium states, which is known to be on the more stable side of them. This approach is useful also with just one vanishing eigenvalue in a sequence of bifurcations with stable secondary branching. A (small) positive Σ_ε leads to stable equilibrium states, very close to becoming unstable, without a need to converge to the precise singular state.

Symmetry preservation

As further presented and discussed by Eriksson and Nordmark (2019), the tracing of critical equilibrium sequences is not always a robust procedure if based on Eq. (4.34).

[39] which exist for, e.g., the critical sequences of bifurcation states, for which the emanating secondary equilibrium paths are stable.

[40] where N_0 must be defined as a hard-coded input to the analysis.

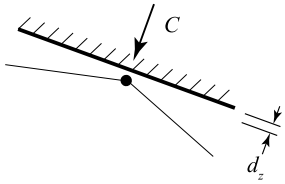

Fig. 4.7 Grazing contact, when a node is in perfect contact with constraint surface, but no contact force has yet been established

This is the case when the iterations tend to deviate to nearby adjoint secondary sequences, on which symmetry is broken; this deviation will typically grow with each step, regardless of very low residual tolerances. In order to keep the solutions on a specific sequence, selector functions are introduced. These express the desired symmetry, typically through a prescribed value for one displacement component. The addition of one selector equation demands also an additional parameter. In several cases analyzed, this has been a force related to the prescribed displacement, which will vanish at the solution, due to the nature of the problem setting. The inclusion of such equations decrease the condition number of the iteration matrix, but will not affect the equilibrium state. It is noted that this is not a constraint in the sense of Sect. 3.6, as the function does not appear in the fundamental residual expression $\underline{R}$. A demonstration example is given in Sect. 4.6.3.

Grazing contacts

Mechanical constraints introduced for the modelling of hard contact conditions are discussed in Sect. 3.6.4. The discrete contact condition at a model node is schematically described by Fig. 4.7, where a gap d_z between a structural node and a hard constraining surface is reduced to zero distance, and a constraint-enforcing contact force C appears. The transition between non-contact and contact conditions has some similarities to a critical equilibrium state, as it immediately changes aspects of structural response[41]. The grazing contact condition is relevant to investigate; an example is given in Sect. 5.4.

In the present setting, the grazing contact condition for a node allows two different formulations. These give two different situations and two independent stability conclusions. As one alternative, the node in question is considered as already constrained, giving a corresponding constraint function in $\underline{R}_c$. A selector function demands the constraint-enforcing variable in $\underline{C}$ to vanish as the grazing condition; the node is in contact, but with zero contact force. With respect to stability, this implies that the increased stiffness from the active contact will appear in the current operative stiffness $\underline{\underline{K}}$.

[41] Note that this is partly due to the discretized setting.

The second alternative is to consider the node as still free, but to introduce a selector equation prescribing the node to be on the contact surface, i.e., a selector based on one displacement variable; the node is not in contact, but the gap closed. In this approach, the grazing contact condition will not affect the operative stiffness.

Either of the two formulations can be used for the equilibrium. They are relevant for tracing a grazing contact sequence in parametric space. The solutions obtained are the same with respect to displacement and force, but stability coefficients are different. In general, the constrained case is evaluated as more stable. A particularly interesting situation is when, for a particular node in a grazing contact state, the two settings give different sign spectra for the eigenvalues.

The handling of contact conditions very clearly emphasizes the ever-present problem to define numerical equality and vanishing values in numerical simulations; relevant tolerances must always be introduced.

4.4.2 Sequence Definition

The previous section deals with some ideas for different classes of selector functions for a structural problem, and relevant parameters in relations to these selectors. The selector functions are all related to physical aspects of a structure. Obviously, many parameters in a structural design affect these response aspects. This makes them interesting to include in an investigation of the design. The present setting allows a number of such parameters to be included.

The investigation of the parametric solutions can focus on the sensitivity of a particular equilibrium state to small variations of the parameters around the present case. This linearized response is described by the tangent space, which is a local property of the particular state, and is further discussed below in Sect. 4.5.3. For more extensive investigations of the parametric response aspects, low-order subsets of the possible parametric equilibrium states need be studied. In this context, the first and foremost parameter is almost exclusively a parameter for the exterior forcing level.

With a set of N_p parameters included in $\underline{P}$, the constrained equilibrium equations in Eq. (3.90) lead to solution manifolds of dimension N_p, connected at critical states. When introducing N_s selector functions, the dimensions of the manifolds are reduced to $N_p - N_s$. For convenient handling and interpretation, the introduction of $N_s = N_p - 1$ selector functions leads to one-dimensional state sequences, and this is the main setting for the solution of structural equilibrium, even if two-dimensional equilibrium surfaces are briefly mentioned in Sect. 4.4.4. The sequences are represented in discretized form by parametric traces in the equilibrium space.

The N_s selector functions may be an arbitrary combination of the selectors discussed above. In order to allow introduction of many parameters in a common formulation, subsets of the parameters can be de-activated in a particular simulation run, by the introduction of selector functions prescribing them to particular values. This adds a few almost dummy equations to the system, at marginal computational cost.

With a focus on obtaining one-dimensional equilibrium sequences[42], one selector function in $\underline{R}_p$ is chosen as an increment selector function. In the present algorithm, this selector is always placed last in the set $\underline{R}_p$ of functions, and automatically updated by the algorithm from strategy rules, discussed below.

4.4.3 Increment Selection

In order to produce one-dimensional solution sequences, the set of N_p selector equations need be successively modified between increments. In the present algorithm, the increment selector function is kept in basic form but updated by a constant, which can be interpreted as a fictitious time variable. This is also the case in Eq. (4.20), where $\overline{\tau}$ is modified after convergence in one increment.

The increment selector function is similar to the stepping strategies for parametric forcing in Sect. 4.1.5, but can now relate to any of the problem variables, e.g., forcing, displacement or some geometric parameter. It gives one way to find a set of equilibrium states on what is really a continuous sequence, cf. the discussion around Fig. 4.4. In most settings of the multi-parametric equilibrium tracing, one—but, only one—of the selectors is such an increment stepping function, even if more complex combinations are fully possible for specific needs.

In the present version of the algorithm, an increment selector strategy based on step-wise increments along one of the problem variables is the main alternative. In each incremental step, either a displacement component or one of the parameters is held fixed during iterations[43]. The variable to use is decided based on the previous increment[44]. The basis for the choice is an evaluation of the most rapidly changing component, in the sense of the relative deviation from the predicted step increment. Only a set of the variables with largest increments is considered. An alternative, very commonly adopted in performed simulations, is to use the same specified variable for a whole sequence. The arc length curve stepping is not recommended, for the reasons above. With almost the same scaling problems, a hyperplane approach is, however, sometimes used, where all corrections $\delta \underline{y}_{i+1}^{j}$ in increment $i+1$ are orthogonal to the prediction $\Delta \underline{y}_i^0$.

A choice is thus needed for the class of increment selector function to use, but the algorithm also needs a strategy for the increment magnitudes in the overall evolution. In the general context, there is no reason why solutions should be placed uniformly along an equilibrium sequence, as measured by the incremental time parameter adopted. Several methods are published for choosing the parameter incre-

[42] which may—or may not—be equilibrium branches in the traditional sense of force-displacement relations.

[43] Stepping in any of the constraint-enforcing variable is fully possible, but considered rather unnatural in most cases.

[44] It is prescribed as input in the first increment.

ments automatically along the solution sequence. The problem is discussed, e.g., by Eriksson and Kouhia (1995).

An automatic regulation of increment step lengths in the present algorithm is based on the number of iterations needed in the previous step. The increment size is reduced when convergence is slow, and expanded when the tolerance is easily reached[45]. A fixed step length, rather than the algorithmic modification. is a commonly used option.

For the complex problems at hand, an important aspect is a re-start option, so that a full simulation can be performed in a sequence of limited trace intervals, allowing an inspection and re-direction of the simulation if this is deemed relevant; this is also useful for branch selection at bifurcation states.

As a very general comment on increment stepping strategies, the efficiency and reliability of any method implemented is highly problem-dependent, and no general answer on optimal strategies should be expected.

4.4.4 Equilibrium Surfaces

Even if engineering practice often prefers to see parameter dependence in a structure as graphs for the response, the multi-parametric problem setting also allows other means for obtaining and presenting the results. Eriksson and Pacoste (2001) develop methods for solving two-dimensional equilibrium surfaces in a multi-parametric space. The work is focussed on conservative stability problems, and the possibilities to visualize response aspects in terms of catastrophe theory.

One example of result in the reference shows a 3D surface, which illustrates the magnitude of a vertical point force at the apex of a clamped toggle frame as function of both the height of the frame and the vertical deflection under the force. A color scale is used to show the degree of instability for the model at the solutions. The drawing gives considerably more information on the phenomenological response than a set of parametric force-displacement graphs for fixed heights.

The solution method is a rather natural extension of the one-dimensional equilibrium sequence evaluation, but puts a focus on the measuring of the solution manifolds in the parametric space, i.e., the two-dimensional counterpart to the increment stepping in Sect. 4.4.3. The basis chosen for this is the two-dimensional tangent space at a solved equilibrium, which defines a local coordinate system. The tangent space of a multi-parametric equilibrium formulation is further discussed in Sect. 4.5.3. The solution manifold is successively expanded by a simplex mapping in the parametric space. Several technical aspects need be solved for a successful implementation of the idea, but results can show new information, not least from a phenomenological viewpoint.

[45] This happens when the number of iterations in the increment is $< N_w - 1$ or $> N_w + 1$, with N_w an algorithmic parameter for the desired number.

4.5 Equilibrium Properties

The solutions to the parametric constrained equilibrium problem in Eqs. (4.18)–(4.19), which are obtained from the incremental-iterative procedure in Eqs. (4.21)–(4.22), are complete equilibrium configurations. They can therefore be evaluated with respect to their equilibrium properties, exactly as the results from the more specialized setting in Sect. 4.1.5. All included parameters, and not only the forcing parameter, are now frozen, when stability of the equilibrium state is evaluated. In a parametric setting, the parameter variables in a solution are the results from the set of selector equations used, and thereby not necessarily equidistant.

The primary results are the discrete variables $\underline{d}$, which describe the displacement of the model, and constraint-enforcing variables $\underline{C}$. The parameters $\underline{P}$ are also immediately found from the solution vector $\underline{y}$, with very commonly at least one forcing parameter included. Convenience transformations related to $\underline{P}$ are discussed as a means for producing further interesting quantities for the state, cf. Sect. 4.4.1.

Other main results for the equilibrium state, like point-wise stress or section resultants, need a post-processing of the result within the discretization used. As indicated in Sect. 3.1.1, all such derived results should be considered to be of—at least somewhat—lower accuracy than the primary results.

4.5.1 Operative Stiffness

The above mentioned properties of an equilibrium state are all local in nature, but also several global quantities are important properties of the equilibrium. Not least, this is the case for the energy aspects deciding stability. From Eq. (3.90), a constrained equilibrium is defined by the stationarity of Π_c, with respect to displacement $\underline{d}$ and constraint-enforcing parameters $\underline{C}$. This implies that $\underline{d}$ and $\underline{C}$ are the fundamental state variables for the equilibrium state, with frozen parameters.

Dependent on the specific setting of the problem, the fundamental equilibrium equations are connected to the fundamental variables according to Eqs. (3.90) and (3.92), or, in compact form, Eq. (4.18). The operative stiffness matrix $\underline{\underline{K}}$ in the top-left part of the Jacobian matrix $\underline{\underline{J}} \equiv \underline{R}_{\underline{y},\underline{y}}$ in Eq. (4.24), can represent either of $\underline{\underline{K}}^t$, $\underline{\underline{K}}^i$, or $\underline{\underline{K}}^c$, depending on forcing class and the introduction of constraints.

The operative stiffness is symmetric if the constraints are expressed by Π_c in Eq. (3.87). This is the reason for the seemingly over-complicated form of the gas relation in Eq. (3.93)—in particular if this is compared to the more obvious convenience selector function for the same relation in Eq. (4.33)[46].

[46] noting the fundamental difference between a constraint and a selector.

4.5.2 *Stability Properties*

For the stability investigations, the treatment in Sect. 3.7 gives basic expressions, with two formulations for cases with or without constraints. The discussion below treats a general case, based on the operative stiffness $\underline{\underline{K}}$, which is formally simplified if no constraints are introduced.

Eigenvalue extraction

A problem setting without constraints allows two eigenvalue formulations according to Eqs. (3.97) or (3.98) giving identical stability conclusions. A constrained model must consider that the constraints are mass-less. In order to cover all cases, the two-matrix eigenvalue problem in Eqs. (3.100)–(3.101) is more relevant than the form in Eq. (3.97), and will be discussed here. The positive semi-definite constrained mass matrix in Eq. (3.101) makes the solution more complicated, and out of scope for many standard matrix algebra algorithms. The setting with such a mass matrix is extensively discussed by Eriksson and Nordmark (2019), where methods are given for its treatment. Without constraints, the choice of method offers other options, but this situation is covered by the treatment below, just introducing $N_c = 0$ and $\underline{\underline{M}}^c \equiv \underline{\underline{M}}$.

The setting is characterized by symmetric matrices, normally sparse, and a semi-definite mass matrix[47]. The problem class also often shows clusters of identical or very close eigenvalues, sometimes also situations where several eigenvalues coincide due to symmetries in the model. It is noted that, depending on the phase of the algorithm, several situations occur, demanding often only a limited number of eigenvalues, sometimes only their signs, sometimes their exact values and sometimes also the corresponding eigenvectors. A special case is when the criticality is part of the problem setting, in the form of a critical selector function, according to Eq. (4.34) or Eq. (4.35). In this case, also the differential of the critical eigenvalue with respect to fundamental variables is needed.

An analysis of the setting shows that suitable methods for the eigenvalue extraction in Eq. (3.100) are strongly dependent on the structure and components of the operative stiffness $\underline{\underline{K}}$ in Eq. (4.24), and in particular on whether the submatrix $\underline{R}_{c,\underline{C}}$ in its lower right part is zero, singular or has full rank, cf. Eq. (3.92).

When evaluating eigenvalues without too high demands on precision, a strategy based on a Sturm sequence, cf. the book by Strang (1988), can preferably be used. This employs an LDL-factorization of the operative stiffness matrix shifted by a multiplier of the relevant mass matrix. This method is in the present implementation used to decide the numbers of negative eigenvalues (below a certain tolerance $-\gamma$) and of zero ones (within $0 \pm \gamma$), but also to give a coarse estimate to the eigenvalue closest to zero in non-critical situations, as this can be used for predictions of approaching

[47] which is also diagonal if $\underline{\underline{M}}$ is a unit or lumped matrix.

critical states. A systematic usage of the same method in a bisection strategy can give also the eigenvalues, but is inefficient for an accurate determination.

A numerically feasible method for approximate, but potentially very accurate, solution to the eigenvalue problem described by Eq. (3.100) is based on an introduction of small fictitious masses for the constraints. Replacing the mass matrix $\underline{\underline{M}}^c$ in Eq. (3.101) by a matrix of the form

$$\underline{\underline{M}}^{\varepsilon} = \begin{pmatrix} \underline{\underline{1}}_{N_d} & \underline{\underline{0}} \\ \underline{\underline{0}} & \varepsilon^2 \underline{\underline{1}}_{N_c} \end{pmatrix}, \tag{4.36}$$

with ε a small value[48], the square root of the diagonal matrix $\tilde{\mathbf{M}}^{\varepsilon}$ can be used to transform the original problem to a one-matrix form for the matrix

$$\underline{\underline{K}}_{\varepsilon} = \begin{pmatrix} \underline{\underline{1}}_{N_d} & \underline{\underline{0}} \\ \underline{\underline{0}} & (1/\varepsilon)\underline{\underline{1}}_{N_c} \end{pmatrix} \underline{\underline{K}}^c \begin{pmatrix} \underline{\underline{1}}_{N_d} & \underline{\underline{0}} \\ \underline{\underline{0}} & (1/\varepsilon)\underline{\underline{1}}_{N_c} \end{pmatrix} \tag{4.37}$$

where the left- and right-hand operators are $(\sqrt{\underline{\underline{M}}^{\varepsilon}})^{-1}$, which operates on both $\underline{\underline{K}}$ and $\underline{\underline{M}}^{\varepsilon}$, yielding the latter as an identity matrix. The resulting matrix $\underline{\underline{K}}_{\varepsilon}$ is symmetric and, for wide ranges of ε, well-conditioned for the eigenvalue extraction. Standard matrix algebra algorithms give a chosen set—or range—of eigenvalues with selectable precision, and the corresponding eigenvectors. If needed, the obtained eigenvectors are multiplied by $(\sqrt{\underline{\underline{M}}^{\varepsilon}})^{-1}$ to give the eigenvectors for the original problem. In the present algorithm, eigenvectors are only extracted when eigenvalues are numerically zero, giving a set $\underline{\underline{\Phi}}_{\mathrm{cr}}$ of critical eigenvectors $\underline{\varphi}_{\mathrm{cr}}$, for which $\underline{\underline{K}}\,\underline{\varphi}_{\mathrm{cr}} \approx 0\underline{\underline{M}}^c\underline{\varphi}_{\mathrm{cr}}$, with the approximate equality representing the tolerance for a zero eigenvalue.

Due to the re-formulation of the problem discussed in Sect. 3.6.1, where constraints increase the number of residual equations rather than decrease it, the described procedures give $2\,N_c$ spurious eigenvalues of large magnitude. As these correspond to eigenvectors with low values in all displacement components, the irrelevant eigensolutions are easily discarded. This removal reduces the complete set of $(N_d + N_c)$ eigenvalues to the correct number, i.e., $(N_d - N_c)$.

The eigenvalues and their corresponding mode vectors are providing essential information on the properties of the equilibrium state investigated, and a stable equilibrium shows positive eigenvalues only. When the number of negative eigenvalues changes between the states in the sequence, this defines a transition equilibrium state, cf. Sect. 4.5.6.

Regarding the mass matrix in Eq. (4.36), it is noted from Sect. 3.7 that the usage of an identity structural mass matrix is unphysical, and does not allow any interpretation of neither eigenvectors nor eigenvalues, beyond the signs of the latter. This is particularly true if discrete displacement variables are of different types, e.g., both

[48] In applications of the method, $\varepsilon \approx 10^{-7}$ has often been used, when constraint equations are reasonably scaled in comparison to the equilibrium equations.

translations and rotations. For vanishing eigenvalues, i.e., at critical equilibria, the critical mode vectors are, however, independent of the mass assumptions, and results obtained with the mass matrix from Eq. (4.36) are thereby reliable and useful for the adopted discrete model.

4.5.3 Tangent Space

The multi-parametric setting of stability problems discussed here is primarily motivated by the possibilities to find the parameter dependence of phenomena. Examples are the parametric regions of stable responses, with parameters being related to, e.g., geometry or material. Similar arguments can also be used to motivate investigations of the sensitivity of equilibrium states, in the sense of effects from small variations to given parameters. This gives measures for the potential effects from imperfections, where a high sensitivity implies that small variations in parameters lead to large effects in response. While the parameter dependence in qualitative response reflects a global parameter variation, the sensitivity is a local property valid at a particular state. It is emphasized that the sensitivity is thereby only expressed in relation to the parameters introduced; the sensitivity to other variables can be much more pronounced. In such cases, additional hard-coded parameters may be transferred to be parts of $\underline{P}$, cf. the discussion in Sect. 4.4.2.

The discussion of sensitivity of equilibrium takes its starting point in a problem definition using $(N_d + N_c)$ fundamental displacement and constraint-enforcing variables, but also N_p parameters defining a particular instance[49]. As this gives $(N_d + N_c)$ constrained equilibrium equations, according to Eq. (4.19), the solutions to the non-linear equations consist of manifolds or hyper-surfaces of dimension N_p in the $(N_d + N_c + N_p)$-dimensional variable space. Such manifolds can be connected at different kinds of critical states, marking a non-smooth change of the solutions.

The sensitivity analysis investigates the linearized manifold around a solved equilibrium, which is defined by the local tangent space. The space is a property of the equilibrium state, in the sense that it describes important aspects of its surroundings. The differential of the constrained equilibrium equations from this state is written as

$$\mathrm{d}\underline{R} = \underline{\underline{K}}\,\mathrm{d}\underline{D} + \underline{\underline{J}}_p \mathrm{d}\underline{P} \tag{4.38}$$

using the combined state space variables and the corresponding residual function from Eq. (4.19). In the expression, the differential operator

$$\underline{\underline{J}}_p = \underline{R}_{,\underline{P}} \equiv \begin{pmatrix} \underline{r}_{c,\underline{P}} \\ \underline{R}_{c,\underline{P}} \end{pmatrix}. \tag{4.39}$$

[49] In the simplest case of Sect. 4.3, this is just one forcing parameter.

This matrix is part of the total Jacobian in Eq. (4.24), and is an $(N_d + N_c)$-by-N_p matrix.

The tangent space describes all possible increments to variables and parameters which let the linearized equilibrium differential in Eq. (4.38) vanish. The result is a matrix $\underline{\underline{T}}_y$, which satisfies the equation

$$\left(\underline{\underline{K}} \quad \underline{\underline{J}}_p\right) \underline{\underline{T}}_y = \underline{\underline{0}}. \tag{4.40}$$

The columns of the matrix $\underline{\underline{T}}_y$ thus belong to the null space of the matrix $(\underline{\underline{K}} \; \underline{\underline{J}}_p)$. The algorithm evaluates and makes use of a good basis for this null space.

In the one-parametric forcing situation of Sect. 4.1.6, the tangent space essentially describes the current differential displacement response to a unit increment of the forcing parameter, at least at a non-critical state. For a parametric displacement-independent forcing component, the corresponding column of $\underline{\underline{J}}_p$ is related to the (negative of the) external force. Other parameters lead to other forms, but always resembling a discrete force vector.

When several kinds of parameters are allowed, the columns of $\underline{\underline{J}}_p$ may be more or less similar, in the sense of a co-linearity in the $(N_d + N_c)$-dimensional space[50]. Almost parallel columns are normally uninteresting or reflecting trivial design relations, and can also cause numerical and algorithmic complications. It is here assumed that the columns are reasonably separated.

If the equilibrium is regular, as opposed to critical, with a non-singular operative stiffness, the positions of new equilibria, in the vicinity of the studied state, are indicated by the condition from Eq. (4.38). Demanding a zero increment $\mathrm{d}\underline{R}$, this is written

$$\mathrm{d}\underline{D} = -\underline{\underline{K}}^{-1} \underline{\underline{J}}_p \, \mathrm{d}\underline{P}, \tag{4.41}$$

where an increment in $\underline{D}$ is expressed as a consequence of variations in the parameters $\underline{P}$ through an $(N_d + N_c)$-by-N_p matrix. Expressed in relation to the solution vector $\underline{y}$, neighboring equilibrium states are reached through an arbitrary combination of the columns in the matrix

$$\underline{\underline{T}}_y = \begin{pmatrix} -\underline{\underline{K}}^{-1} \underline{\underline{J}}_p \\ \underline{\underline{1}}_{N_p} \end{pmatrix}, \tag{4.42}$$

spanning the possible variations. This matrix—to first order—shows the solution manifold around a non-critical equilibrium state. Even if particular choices of parameters can make the matrix less well-defined, this does not normally create severe numerical problems. If the process shows a dependence between the parameters, as mentioned above, some specialized handling is needed to effectively remove one of the parameter columns.

[50] This happens, for instance, when two geometric parameters introduced affect the equilibrium in rather similar ways.

Depending on purpose, the matrix for the tangent space basis can be modified in different ways, e.g., orthonormalized in connection with equilibrium surfaces, cf. Sect. 4.4.4. Such procedures also allow further investigations of parametric intra-dependence. A normalization can also be motivated by the scaling of the parameters.

At a critical equilibrium state, with a singular operative stiffness, the null space of the operative stiffness matrix contains vectors of the form

$$\underline{T}_\Phi = \begin{pmatrix} \underline{\underline{\Phi}}_{\mathrm{cr}} \\ \underline{\underline{0}} \end{pmatrix} \tag{4.43}$$

with columns consisting of orthonormal eigenvectors corresponding to vanishing eigenvalues of $\underline{\underline{K}}$, and showing possible differential increments to the fundamental variables at frozen parameters, i.e., no variation to $\underline{P}$. This is closely related to the discussion in Sect. 3.7, noting that the critical eigenvectors in general involve all state variables in $\underline{D}$, i.e., displacements and constraint-enforcing variables.

In the numerical treatment, the singularity of the operative stiffness is related to a tolerance for a zero eigenvalue. The implementation must define this tolerance, and formulate the used methods accordingly, cf. also Sect. 4.6.

With a numerically singular operative stiffness, it is not possible to use Eq. (4.42) as written. With an adapted numerical technique, it is, however, possible to solve the components of these basis vectors by making the columns of $\underline{\underline{J}}_p$ effectively orthogonal to all columns of the $(N_d + N_c)$-by-N_Φ-dimensional matrix of critical eigenvectors $\underline{\underline{\Phi}}_{\mathrm{cr}}$. This can be done in several ways, depending on the properties of the system. A very general approach is given here.

With N_Φ the number of orthonormal critical eigenvectors in $\underline{\underline{\Phi}}_{\mathrm{cr}}$, an orthogonal part is obtained from a stabilized system according to

$$\begin{pmatrix} \underline{\underline{K}} & \underline{\underline{M}}^c \underline{\underline{\Phi}}_{\mathrm{cr}} \\ \underline{\underline{\Phi}}_{\mathrm{cr}}^{\mathrm{T}} \underline{\underline{M}}^c & \underline{\underline{0}} \end{pmatrix} \begin{pmatrix} \underline{\underline{T}}_\perp \\ \underline{\underline{X}} \end{pmatrix} = \begin{pmatrix} -\underline{\underline{J}}_p \underline{\underline{N}}_p \\ \underline{\underline{0}} \end{pmatrix}, \tag{4.44}$$

where the matrix $\underline{\underline{N}}_p$ is a representation of the null space of the (small) matrix product $(\underline{\underline{\Phi}}_{\mathrm{cr}}^{\mathrm{T}} \underline{\underline{J}}_p)$. The multiplication by the null space matrix combines columns in $\underline{\underline{J}}_p$ in such a way that the resulting columns are all orthogonal to the critical eigenvectors. In the equation, $\underline{\underline{X}}$ is an auxiliary matrix, which comes out as numerically zero and is discarded. The useful result is thereby a matrix $\underline{\underline{T}}_\perp$, also with columns orthogonal to all critical eigenvectors.

With this formulation, it is obvious that different situations appear, depending on the relation between the number of parameters N_p and the number of critical eigenvectors N_Φ. The dimension of the null space decides the number of columns in the right-hand side of Eq. (4.44), and thereby also the number of columns in $\underline{\underline{T}}_\perp$. With $N_\Phi < N_p$, the number will be at least $N_p - N_\Phi$, but can be higher. With $N_\Phi > N_p$, on the other hand, the null space can be empty, and the right-hand side will disappear. This is also the case when $N_\Phi = N_p$, and the product $(\underline{\underline{\Phi}}_{\mathrm{cr}}^{\mathrm{T}} \underline{\underline{J}}_p)$ does not have a null space; this typically happens if the matrix consists of non-zero numbers. Special

situations appear when the matrix $(\underline{\underline{\Phi}}_{\text{cr}}^{\text{T}}\,\underline{\underline{J}}_p)$ contains a mixture of zeros and non-zero values. The number of columns in $\underline{\underline{T}}_\perp$ must always be $\leq N_p$, as the matrix $\underline{\underline{N}}_p$ can not expand the dimension of $\underline{\underline{J}}_p$. Note that it has been assumed that all N_p parameters are reasonably independent, so columns do not degenerate.

For the common case of one-parametric forcing, i.e., $N_p = 1$, critical states with $N_\Phi = 1$ or 2 commonly appear. If the scalar product(s) of critical eigenvector(s) and the single column of $\underline{\underline{J}}_p$ is non-zero, no null space exists, and $\underline{\underline{T}}_\perp$ is empty. If the scalar product(s) is zero, the null space is non-empty and $\underline{\underline{T}}_\perp$ can be evaluated as above.

Based on Eqs. (4.43) and (4.44), which give two different types of tangent space base vactors, a description of the total tangent space is obtained as

$$\underline{\underline{T}}_y = \begin{pmatrix} \underline{\underline{T}}_\perp & \underline{\underline{\Phi}}_{\text{cr}} \\ \underline{\underline{N}}_p & \underline{\underline{0}} \end{pmatrix}, \tag{4.45}$$

where the right part is always, present, but the left part may be empty. When this is the case, only the critical eigenvector(s) remain in the tangent space.

The conclusion from the discussion is that the dimension of the matrix $\underline{\underline{T}}_y$ is N-by-N_p^*, where $N = N_d + N_c + N_p$ and N_p^* the number of columns; the notation is chosen to emphasize that $N_p^* \geq N_p$, with $N_p^* > N_p$ only for particular states. The situation is easily evaluated from the matrix product $(\underline{\underline{\Phi}}_{\text{cr}}^{\text{T}}\underline{\underline{J}}_p)$, noting that this must be performed at the particular state considered.

The tangent space as discussed above only considers the constrained equilibrium equations according to Eq. (3.90), irrespective of the number of parameters introduced in the formulation; no selector equations are introduced, and the solution manifold spanned by the columns of the tangent space basis matrix $\underline{\underline{T}}_y$ considers all possible linearized variations to the parameters. As discussed above, the matrix can be orthogonalized and normalized for special purposes.

For the common limit state with one critical eigenvector for a one-parametric forcing, a limit state is characterized by Eq. (3.110), which implies that also the product $(\underline{\underline{\Phi}}_{\text{cr}}^{\text{T}}\,\underline{\underline{J}}_p)$ is non-zero, and thereby has no null space. This reduces the tangent space in Eq. (4.45) to just the right-hand part, i.e., the critical eigenvector for zero forcing parameter increment. If, on the other hand, $(\underline{\underline{\Phi}}_{\text{cr}}^{\text{T}}\,\underline{\underline{J}}_p) = 0$, also the orthogonal part remains, which creates a bifurcation state.

As noted in the introduction to this section, the tangent space has a clear relation to the sensitivity of results to parametric variations around an equilibrium state. With the procedure described, the columns show the sensitivity to the parameters in $\underline{P}$; the columns may be rotated, in order to emphasize the sensitivity to specific parameters For special purposes, this can be valuable information in the design process, and it can even be an aspect in an optimization setting.

4.5.4 Tangent Vector

The description above gives a basis for the tangent space, i.e., all linearized variations to state variables and parameters fulfilling differential equilibrium around a considered state with vanishing residual $\underline{R}$. The tangent space considers free and independent variations to all parameters in $\underline{P}$, and is a linear space tangential to the equilibrium manifold.

With the present focus on one-dimensional generalized equilibrium sequences, the selector equations define subsets of equilibria on the total manifold. The selector equations thereby reduce the tangent space. With an addition of N_s selector functions in $\underline{R}_x$ to the system in Eq. (3.90), which consists of the constrained equilibrium equations, the dimension of the tangent space basis matrix $\underline{\underline{T}}_y$ is normally reduced by N_s. The tangent space is contracted, by the demand for a non-trivial solution to the N_s equations in N_p^* unknowns stated as

$$\underline{R}_{x,\underline{y}}\, \underline{\underline{T}}_y\, \mathrm{d}\underline{\underline{P}}^* = \underline{0}, \tag{4.46}$$

with $\mathrm{d}\underline{\underline{P}}^*$ describing a basis for the null space to the combined matrix $(\underline{R}_{x,\underline{y}}\, \underline{\underline{T}}_y)$. This demands that a tangential direction must also fulfil the set of selector equations. The reduced tangent space is then obtained as

$$\underline{\underline{T}}_s = \underline{\underline{T}}_y\, \mathrm{d}\underline{\underline{P}}^*. \tag{4.47}$$

The form shows that, in general, the parameter-based columns of the tangent space matrix will be combined in order to solve also the selector equations.

When a one-dimensional equilibrium sequence is the objective of the simulation, the necessary number of relevant selector equations is $N_s = N_p - 1$, as discussed in Sect. 4.4.2. With this choice, Eq. (4.46) is under-determined, and will always give at least one vector $\mathrm{d}\underline{\underline{P}}^*$ as solution. Any column of $\underline{\underline{T}}_s$ includes all variables and parameters, and points to directions in $\underline{y}$ space in which linearized equilibrium is fulfilled. The tangent vectors define the possible evolution directions for equilibrium states on the sequence, which is defined by a set of selector functions. This agrees with the comments above that a number of physically relevant selectors is augmented by increment selector functions, which are just related to the numerical evaluation, giving a total of N_p selectors to fix one solution state.

At a non-critical equilibrium or a limit state, the evaluation of Eq. (4.47) gives a tangent vector in $\underline{y}$ space (if $N_p - N_s = 1$), for the problem at the current state. The vector shows the only linearized direction of neighboring equilibrium states[51]. This thereby gives a good predictor for a new increment in the sequence tracing, after a choice of increment length. With a reasonable increment along a tangent vector, convergence can be assumed to be rapid. This approach is used in the present algorithm.

[51] with the current selector functions, which puts demands on the selector around a limit state.

At a bifurcation state, where the expression in Eq. (4.46) is under-determined by at least two equations, a basis for the space of incremental solutions can also be obtained through the matrix $\mathrm{d}\underline{\underline{P}}^*$, with columns defining the basis. This basis, which now contains at least two columns can be transformed, dependent on the purpose and setting of the problem. For the most common case of one-dimensional sequence tracing in a problem setting with one main forcing parameter, the suitable form for tangent vectors at a bifurcation state with just one critical eigenvector, is an orthonormal matrix rotated such that the second vector has a vanishing component for the main forcing parameter. This gives the first column as the primary response direction. For more complex settings, other criteria for a suitable expression for the tangent vector matrix need be considered; a reasonable approach is to transform the basis vectors into a form where each of the parameters in $\underline{P}$—as far as possible—dominates one column, even if this may be difficult dependent on the selector equations used; a method can be based on a QR factorization of the $\underline{P}$ part of $\underline{\underline{T}}_s$.

The tangent vector matrix is therefore important for the choice of predictor in a new incremental step in the algorithm described by Eqs. (4.21)–(4.22). For the interpretation of analysis results, the magnitudes of the parameter components in the tangent vectors, and even more their signs, give important information on the qualitative aspects of equilibria. When the sign of any of the parameter components in the tangent vector changes, this is considered a transition equilibrium state, as further discussed in Sect. 4.5.6.

4.5.5 Contact Status

When hard contact conditions are considered in a problem formulation, according to Sect. 3.6.4, the contact status at each equilibrium is an important property of the state. In an FE context, this status shows which nodal points are in active contact.

As discussed in Sect. 3.6.4, the iteration within a certain step increment is in the present algorithm performed under an assumption of a specific set of active constraints. These are handled analogously as the boundary conditions representing structural supports, i.e., with prescribed displacement components, each defined through one constraint equation in the set $\underline{R}_c(\underline{y}) = 0$. In the converged solution, this condition is fulfilled through a corresponding Lagrange multiplier, being part of $\underline{C}$ in the solution $\underline{y}$.

A provisional new equilibrium state is found from the iterations in the increment, using the contacts valid from the previous accepted state. Before accepting this as a new solution in the sequence, a conclusion must be reached whether the provisional state fulfills the contact conditions.

The conclusion is based on the contact status list for the provisional equilibrium. This list contains all nodes being at the contact surface, and having a contact force of the correct sign[52], but also any node penetrating the contact surface. Nodes included

[52] physically outwards from the surface, but related to the definition of the constraint equation.

as contacts in the increment, but showing a contact force of incorrect sign at the provisional state are excluded from the contact status list.

If the contact status list for the provisional state agrees with the contact status used during the increment, the new state can be accepted as a solution, and all other interesting results evaluated. If not, a change of contact status has occurred and the provisional state is discarded. A transition equilibrium state is identified and sought within the increment, as further discussed in Sect. 4.5.6. Based on the results from this procedure, the incremental-iterative procedure is continued.

It is noted that the solution is based on a set of approximations, and obtained through an iterative procedure with a specified tolerance for convergence. The investigation of contact status must therefore also allow for some tolerances for defining the sign of the contact force, and for the penetration of the contact surface.

When contacts are modelled as soft, i.e., as one-sided contact penalty functions or springs, the treatment does not need any handling of a contact status list for the workings of the algorithm. If linear springs are used, this will, however, create problems in the interpretation of stability, due to their inherent discontinuity. Therefore, third order springs are preferred. For book-keeping reasons, it can still be interesting to investigate the contact status for each equilibrium state, in order to find the exact state where a particular contact is activated. Comparisons of contact modelling approaches are shown in Sect. 5.4.

4.5.6 Transition Equilibrium States

Stability investigations as presented in this treatise are to high degree focussed on the transitions between stable and unstable equilibrium states in some parametric description. This objective sets the focus on the critical situations of neutral equilibria. These are in engineering treatments often denoted as states of instability[53], giving in many cases an absolute maximum capacity of a structure to exterior forcing.

Being of fundamental importance to structural capacity, the evaluation of critical states demands high reliability. Accurate methods are thereby needed, not only in academic treatments of stability phenomena. The algorithmic treatment of transitions between parametric regions of different properties need to be reliable, and—as far as possible—efficient.

The treatment of transitions can be developed in several different ways dependent on scope and purpose of the analyses, but in the present context, where parametric incremental-iterative procedures are proposed as the main tool[54], it is natural to include the handling of transitions in the algorithm. This is based on a continuous monitoring of a set of important status quantities in the sequence. The main idea is to find, and isolate to desired accuracy, transition equilibrium states in the sequence. Dependent on the problem formulation, this can equally well be the forcing level at

[53] even if the term should rather be the creation of a forced mechanism, cf. Sect. 3.7.4.

[54] noting that not only forcing parameters are considered.

which equilibrium for a structure is no longer stable, the geometric parameter giving the highest buckling force, the thickness of a plate from which a specific traction can be carried in a stable configuration, or the length of a compressed plate, where the buckling mode of lowest critical forcing changes[55].

The equilibrium properties evaluated and collected at each converged equilibrium state, include—in addition to displacement variables—all parameters and reactive constraint-enforcing forces. Different signs of parameters at two successive states indicate a zero-crossing transition in the interval between them. Similarly, the tangent vector parameter components along the equilibrium sequence are of interest, with a zero-crossing indicating some kind of turning state situation.

The eigenvalues of the operative stiffness at an equilibrium state are, as is obvious from the treatment above, the main indicators of stability, and need be followed along the sequence. As the full and accurate evaluation of the eigenvalues is a computationally expensive operation, the Sturm sequence method mentioned in Sect. 4.5.2 is employed for each new state, giving the numbers of negative and zero eigenvalues as two integer values. A tolerance for 'almost zero' values must be defined in relation to the current problem setting, as further discussed in Sect. 4.5.2, leading to the numbers of negative, positive and zero eigenvalues. A change to the number of negative eigenvalues is a change of stability.

When hard contacts are considered with the method described in Sect. 4.5.5, the contact status for each equilibrium is recorded. If the contact status of the provisional state changes from the previous solution state, this is noted as a transition between the two states.

Dependent on the specific problem setting, some or all of these aspects are of interest. Also other equilibrium properties, where a transition is of importance to the qualitative interpretation of the results, can be considered and handled by similar approaches.

Isolation of transition states

The equilibrium properties discussed above are of different kinds, with continuous variable variations, integer value jumps or a changing list of numbers demonstrating a transition in the provisional increment. Although more efficient methods can be developed if only one kind is considered, a common method is used in the present algorithm. The key is thereby just that any—or several—of the equilibrium properties under observation changed between the previous equilibrium state $\underline{y}_i$ and the provisional new $\underline{y}_{i+1}$. The new state is not accepted until the transition state is handled.

The procedure used for isolation of such equilibrium states is schematically shown in Fig. 4.8 for the continuous case of a variable q changing sign, here from positive to negative in an increment described by a characteristic component y^*.

[55] which is a case when two critical situations coincide.

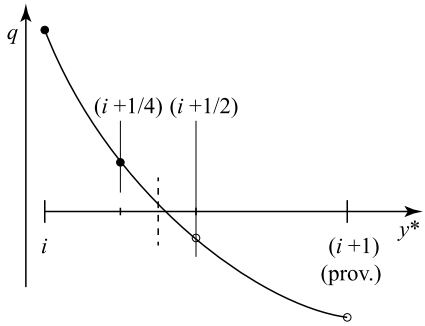

Fig. 4.8 Isolation of transition equilibrium state, with a transition between qualitatively different solution properties

Although secant or 'regula falsi' types of method could be used in this case, the general method uses a bracketing. The basic approach is essentially a bisection method where a bracket holds two solution states of different properties[56], and this bracket is successively reduced until a satisfactorily well isolated transition state is reached. Each new bisection point is iterated until equilibrium, using the same increment selector function[57] as in the provisional step. The very good predictions available normally make convergence fast.

The result from the procedure is thereby two new equilibrium states. One of these is ascertained to have the same properties as the previous accepted state, and can be included as a new state in the sequence, while the other has different properties, and may need some further treatment.

For a transition state involving signs of eigenvalues, the isolation gives two bordering states with different numbers of negative eigenvalues. Compared to Fig. 4.8, this implies that the bracketing solutions for a critical state will not meet, but indicate a range, delimited by states where the interesting eigenvalue is $+\varepsilon$ and $-\varepsilon$, respectively, with ε a numerical tolerance for an 'almost zero' eigenvalue. It is a valuable aspect of this treatment of critical states, that it handles multiple vanishing eigenvalues without extra measures.

In the cases of changing sign of a parameter or its tangent vector component, where properties can be assumed to vary continuously, both the second bracket state and the provisional state can be accepted, if these state share the same properties; otherwise a new isolation between these is started. The exact transition state can be well approximated by the midpoint of the bracket, if needed. This type of isolation is not always of interest, and can be turned off in the implementation.

For a transition state concerned with the contact conditions, the first bracket state has the same contact status as the previous state, while the second state is illegal. A new iteration must be started, with a new assumed active set of contacts. As an equilibrium state is known just before the changing contacts, the prediction of a new contact state is normally very good. The provisional solution state is normally useless

[56] with the diverse view on 'properties' from above.

[57] but, with a changed constant.

in this case, and is replaced by a new incremental step, based on the new contact status. Even then, the discarded provisional state may be a good predictor.

Occasionally, if long increments are attempted in the tracing of a sequence, it may happen that the provisional solution state is not situated on the same branch as the previous one. If these states differ in any of the observed quantities, an isolation will be initiated, but the bracketing will then break down when trying to find new midpoint solution states.

Another special situation, in cases where hard contact is considered, appears in the isolation of states beyond which no legal equilibria exist for the used increment selection, cf. Sect. 5.4. In such cases, a re-start with a more extensive identification of the grazing contact state is needed.

4.6 Critical States

As is obvious from the previous Chapters of this treatise, the handling of critical equilibrium states is a significant part of all stability investigations. This is obvious from the engineering viewpoint, where critical equilibrium is commonly interpreted as a loss of stability, or a structural instability[58]. It is also obvious from the treatment above that the critical equilibrium states lead to singular matrices and, thereby, potential numerical problems in a simulation. An important part of any stability investigation is therefore to find any critical equilibrium states for the problem setting at hand.

4.6.1 Identification

A critical equilibrium is here interpreted as any state on a parametrically traced equilibrium sequence, where the stability properties change. This may be states on an equilibrium branch of parametric forcing, which is the more traditional setting. It may also be a state on a sequence of a parametric geometry where the response to a particular forcing changes between stable and unstable equilibria. Cases are also included where a critical equilibrium sequence is traced, and the number of negative eigenvalues changes. This indicates the existence of a higher order critical state[59]. The more general view on critical states is thereby a state where the number of negative eigenvalues of the operative stiffness changes along a specified sequence.

On a trace of parametric forcing, a critical equilibrium state is first detected by a change of the number of negative eigenvalues in the provisional converged equilibrium, as compared to the previous accepted state. In the most basic case, this means a change from zero to one (or two, for problems of some symmetry), but more

[58] in common terminology, even if this term has been avoided here.

[59] which has probability zero to appear in a problem, unless it is specifically sought by the setting; normally, more than one problem parameter must be variable in order to find such states.

advanced settings of parametric tracing can show any increase or decrease of the number, as detected by a Sturm sequence method, according to Sect. 4.5.2.

When the existence of a critical equilibrium is detected in a new increment, two methods are realistic for finding the critical state more precisely. One method is to replace the increment selector function by the critical selector equations in Eq. (4.34) (or, for certain problems, the one in Eq. (4.35)). Continued iteration with this new selector included will with high probability lead to the critical state; the midpoint between the previous and the provisional state is normally a good predictor for this step. This demands an accurate evaluation of at least some eigenvalues around zero for each iterate, and expressions for their gradients with respect to the fundamental variables. The gradients normally need a numerical evaluation.

The other method—used in the present implementation, due to high generality in diverse problem settings—is based on the isolation of a transition equilibrium state, according to Sect. 4.5.6. The simple method for eigenvalue sign spectrum is still useful. After the solution of a sequence of new equilibria around the critical state, the bracketing is accurate, and the midpoint of the bracket interval can be assumed to be a good approximation to the critical state. The numerical tolerance for a zero eigenvalue, and the number of bisection steps used, need be decided for a particular problem. The tolerance is also involved in the evaluation of the tangent space and vector described in Sect. 4.5.3.

With the first strategy mentioned, the eigenvector[60] corresponding to low magnitude eigenvalues at the critical state is evaluated as part of the algorithm for isolation of the critical state. Using the bracketing strategy, the obtained estimate to the critical state need be further evaluated, in order to obtain the critical eigenvector(s). Either method relies on the continuity of all aspects of structural response, which excludes some problem settings.

The eigenvectors at critical states are important in the evaluation of the tangent space, as discussed in Sect. 4.5.3. They immediately give a basis for the discrimination between limit and bifurcation states, indicating the possible branch continuations from the critical state. The eigenvectors are also an important basis for further investigations of the properties of the critical state.

A special case appears when a critical equilibrium sequence is traced, as further discussed below. A critical eigensolution is then involved as a selector function in the problem setting. In addition to the critical zero eigenvalue, a certain number of eigenvalues are negative along the sequence. If this number changes in an increment, a state with higher criticality exists within the increment. This can be isolated by the method above, leading to a state with several critical eigenvalues, which may demand some special measures for the solution of equilibrium.

As discussed in Sect. 3.7, the eigenproblem at an equilibrium state gives the linearized response around the state. In particular, the eigenvector(s) corresponding to zero eigenvalue(s) span(s) a space of linearized equilibrium states around the equilibrium. This space can be investigated by the so called ‘asymptotic methods’, in which higher differential forms of the equilibrium equations are introduced. Catastrophe

[60] or eigenvectors, if a multiply critical state is sought.

theory discusses the interpretation of these results, which can be of particular interest in specific instances of multi-parametric formulations. Already for states with one critical eigenvalue, these methods can be used to distinguish between supercritical (stable) and subcritical (unstable) bifurcations. The higher order differentials also similarly give the basis for the algebraic bifurcation equation, which gives the possible branches at a bifurcation state.

An example

The small demonstration problem from Sect. 3.7 is used here for a description of the treatment of multi-parametric discrtized problems in the setting of the algorithm implementation described in Sect. 4.7. The formulation is somewhat generalized by the introduction of an extra parameter c, which is assumed to be variable, but with an initial reference value of $c = 0$; c is considered a finite parameter, not just a perturbation. The formulation is thereby based on the total potential

$$\Pi = \frac{1}{2}d_1^2 + \frac{1}{2}d_2^2 + \frac{1}{3}d_2^3 + \frac{1}{2}d_1^2 d_2 - \lambda(\frac{1}{2}d_1^2 + d_2 + cd_2^3), \tag{4.48}$$

with c affecting the part resembling exterior forcing. With the notation from the present Chapter, this means that

$$\underline{y} = \begin{pmatrix} \underline{D} \\ \underline{P} \end{pmatrix} \quad \text{with} \quad \underline{D} \equiv \underline{d} = \begin{pmatrix} d_1 \\ d_2 \end{pmatrix} \quad \text{and} \quad \underline{P} = \begin{pmatrix} \lambda \\ c \end{pmatrix} \tag{4.49}$$

as no constraints are considered. The residual force is thereby

$$\underline{R} = \begin{pmatrix} d_1(1 + d_2 - \lambda) \\ \frac{1}{2}d_1^2 + d_2 + d_2^2 - \lambda(1 + 3cd_2^2) \end{pmatrix}, \tag{4.50}$$

the operative stiffness is

$$\underline{\underline{K}} = \Pi_{,\underline{D},\underline{D}} = \begin{pmatrix} 1 + d_2 - \lambda & d_1 \\ d_1 & 1 + d_2(2 - 6c\lambda) \end{pmatrix}, \tag{4.51}$$

and the parameter derivative of the residual is

$$\underline{R}_{,\underline{P}} = \begin{pmatrix} -d_1 & 0 \\ -1 - 3cd_2^2 & -3\lambda d_2^2 \end{pmatrix}. \tag{4.52}$$

Hard-coding the parameter c to a specific value gives three problem variables, and just needs an increment selector function to specify the one-parametric problem according to Sect. 4.1.6. If several investigations are planned for the problem, it may be convenient to use the full $\underline{P}$, and use two selector equations, for instance,

$$\underline{R}_x(\underline{y}) = \begin{pmatrix} c - 0 \\ d_2 - \overline{\tau} \end{pmatrix}, \tag{4.53}$$

giving a four-component residual $\underline{R}_y$. In the algorithm, $\overline{\tau}$ is step-wise updated. The parameter derivatives $\underline{R}_{x,\underline{D}}$ and $\underline{R}_{x,\underline{P}}$ for Eq. (4.24) are easily found, giving the Jacobian $\underline{\underline{J}}$ for a particular increment[61].

A start from a tentative equilibrium state $\underline{y} = (0, 0, 0, 0)^{\mathrm{T}}$ allows step-wise Newton iterations for increasing d_2. All equilibria are evaluated as stable until $d_2 > 1$, when one eigenvalue of $\underline{\underline{K}}$ becomes negative. An isolation of the transition is performed, giving two closely situated equilibria with different eigenvalue sign spectra. For a performed simulation with fixed increments $\Delta d_2 = 0.15$, the seventh increment gave a state with one negative eigenvalue. From this provisional state, 5 isolation steps revealed that $0.9984 < d_{2\,\mathrm{cr}} < 1.0031$; the critical eigenvalues are 0.0031 and -0.0063, respectively, to be compared to the non-critical eigenvalue of around 3. The midpoint of the bracketing states gave the best approximation to the critical state $d_{2\,\mathrm{cr}} \approx 1.0008$, $\lambda_{\mathrm{cr}} \approx 2.0094$ with a critical eigenvalue of -0.0016. The isolation could have been continued for better approximation of the critical state.

From the same starting state, d_2 was also decreased in another simulation, and the two sequences combined into one. The decreasing part gave two critical states: one limit state with minimum λ, and the bifurcation state at $d_2 = -1$, cf. Figs. 3.17a and 4.9. These states were isolated and identified with the same method as above.

4.6.2 Secondary Branches

Although engineering interest is often primarily directed towards the evaluation of the first critical equilibrium state under increasing forcing, the existence of post-critical branches is of interest. The interest is related to the response after the passage of a limit point, or to the existence of buckled configurations on a secondary equilibrium branch emanating at a bifurcation state. Both situations play important roles in the investigation of the sensitivity to imperfections. Methods for treatment of such equilibrium branches are thereby needed.

The existence of post-critical branches is indicated by the tangent vector matrix evaluated at the critical state, according to Sect. 4.5.4. At a limit state in a one-parametric description of exterior forcing, the tangent vector indicates the single branch passing through it, and the continued tracing of the branch just may need a change of the increment selector, cf. Sect. 4.3.2.

At a bifurcation state for the same problem setting, the tangent space is (at least) two-dimensional, consisting of a primary, non-critical, tangent vector corresponding to a parameter increment[62], and the critical eigenvector(s), corresponding to zero parameter increments, cf. Eq. (4.45). Neither of these necessarily indicates even an

[61] Note that the Jacobian contains the increment selector equation.

[62] orthogonal to the critical eigenvector(s).

infinitesimal equilibrium sequence, but they often do so. In general, the algebraic bifurcation equation gives combinations for the columns of the matrix in Eq. (4.45), for which a sequence can be initiated.

Traces along secondary equilibrium branches from a bifurcation on a primary branch typically are initiated as a re-start from the critical state. The first continuation increment is solved, introducing a predictor and a selector function reflecting this. Using the critical eigenvector, scaled by a chosen constant, and a selector function fixing an increment to the displacement component of largest magnitude in it, is very often a good choice. After convergence for this first increment on the secondary branch, the general strategy for tangent vector evaluation is normally useful again. A new increment is thus performed with a tangent vector predictor, iterative correctors and property evaluation.

When a more complete stability investigation is performed, and several critical states detected on the primary branch, as in Sect. 5.3, a new re-start is needed at each isolated critical state.

Different forms of critical states may appear somewhere on the secondary branches, cf. the bifurcation tree in Fig. 5.7. The same procedures are followed also for these. Not least the treatment of critical states appearing on the secondary branches also may need careful considerations of the symmetry properties of solutions and modes.

In an application-oriented analysis of critical states for a parametrically forced model, the critical state effects may be more relevant than a very accurate isolation of their parametric position. For such situations, and in particular for bifurcation problems, the treatment can be simplified without significant loss of information, by the introduction of an imperfection to the studied model. The imperfection can be a (small) distortion of the model geometry, or a (small) disturbance force added to the parametric exterior forcing; the latter approach is often preferred, and is used in Sect. 5.2 for a case of buckling mode interaction.

If the distortion or disturbance is somewhat related to the critical mode at the first critical state, the distinct bifurcation branch crossings is replaced by a gradual transition from the primary to the secondary branch, triggered by the imperfection. The situation is schematically illustrated by a comparison of Figs. 1.2 and 1.3, where it is obvious that a larger imperfection reduces the more dramatic response effects close to the bifurcation.

After an introduction of the imperfection, the single equilibrium branch can be traced by standard methods, even if a smaller imperfection leads to sharper curvatures of the branch and a need for careful increment selector strategies. When using this approach, without any physical motivation for the magnitude of the imperfection, the smallest value of it, which still allows an uncomplicated numerical treatment, is chosen.

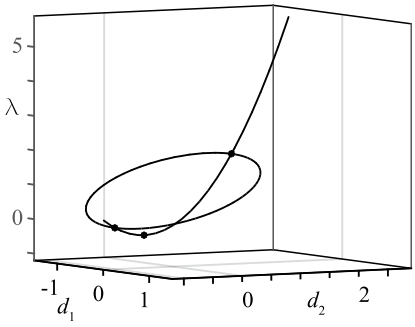

Fig. 4.9 Primary and secondary equilibrium sequences evaluated for example problem with $c = 0$. Critical states are marked

The example continued

The example in Sect. 4.6.1 is continued. The main results in the simulation were a provisional unstable equilibrium for $d_2 = 1.05$, and the approximate critical state at $d_2 = 1.0008$. As the provisional state is in equilibrium, it is accepted, and the primary path could be continued from it using the same method; the unstable states for larger d_2 do not lead to any problems for the Newton iterations.

The treatment of the critical state can be continued, preferably after a re-start from the interval midpoint. The tangent space is evaluated at the approximate critical state. If this is sufficiently well isolated, the critical eigenvalue is below the tolerance for what is considered as vanishing, and the tangent space is two-dimensional, containing the primary tangent and the critical eigenvector[63]. In the example problem, which is very well-defined, the normed basis vectors were evaluated as $(0, 0.316, 0.949, 0)^{\mathrm{T}}$ and $(1, 0, 0, 0)^{\mathrm{T}}$, respectively, for the setting used, with parameter $c = 0$ fixed.

The critical eigenvector was used to initiate the secondary equilibrium branch, by selecting the appropriate vector in the tangent space. A parameterization was chosen to reflect the secondary path direction, and a suitable increment length gave the predictor for a new step. From this, iterations were performed with exactly the same formulation as used for the evaluation of the primary sequence, with the exception that the second function in Eq. (4.53) was modified—not only by changing the constant $\overline{\tau}$, but also in form. In the example case, an increment $\Delta d_1 = 0.1$ from the approximate critical state was introduced as selector. With a variable parameterization along the sequence, the sequence followed the complete 'un-symmetric' branch of Fig. 3.17 in 61 increments[64]; all the states were identified as unstable with one negative eigenvalue[65]. Projections of the primary and secondary sequences evaluated for $c = 0$ are shown in Fig. 4.9.

[63] both evaluated to good accuracy, if tolerances are set appropriately for the problem.

[64] Fewer longer increments still converged, but gave a bad representation of the branch.

[65] even if this is very close to zero at the two connections to the primary sequence.

4.6.3 Critical Parameter Traces

The previous section has its main focus on the stability properties of a structure subjected to a one-parametric forcing, which is the most basic engineering setting of a stability problem. This section is considering other forms of multi-parametric settings, and systematic stability investigations in this context.

While many classes of problems can be based on Eq. (4.19) with parameters $\underline{P}$ and selector functions $\underline{R}_x$, the focus is here on critical equilibrium sequences, where one selector function is of the type in Eq. (4.34), or some similar function expressing the critical state[66]. As an increment selector is needed for a sequence, and the forcing parameter is always of interest, the basic critical sequence evaluation allows one more parameter.

The typical setting of a critical sequence is therefore to use one, e.g., geometry parameter in the model, and to solve the relation between this and the critical forcing parameter. As this type of parameter normally affects the internal force vector, the problem setting is of the form in Eq. (3.49), which fits well into the methods discussed in Sect. 4.4. If the added parameter is used for the forcing, the same basic form is still applicable, even if internal force is not affected.

The increment selector can use any—or several—of the variables, and is not necessarily connected to the added parameter, even if this in many cases is natural. The properties of each converged equilibrium state are evaluated with all parameters in $\underline{P}$, as well as all hard-coded ones, frozen.

A variation of this setting is the one shown by graph No. 2 in Fig. 4.6b, where the forcing parameter is hard-coded and two geometry parameters introduced. With the criticality and increment selector functions, parametric combinations are sought, for which the critical state appears at the hard-coded forcing level.

As the sequences discussed here more or less explicitly use the eigenmodes in the formulation of the problem, they trace a sequence where the critical modes are similar between the successive states solved. The solutions thereby must show the same number of negative eigenvalues, which verifies[67] that the intended sequence is traced. If this number has changed for a provisional new state, an isolation of the transition equilibrium state can be performed, according to Sect. 4.5.6. The isolated equilibrium state is then critical of higher degree, i.e., shows a higher number of zero eigenvalues. This happens, for instance, when a limit and bifurcation state merge into a hilltop branching state for a particular parameter combination. The same situation also appears when two buckling modes change the order in which they appear under a parameter variation, e.g., the plate buckling modes in Sect. 1.6, under the variation of the length to width ration a/b in Eq. (1.52).

The solution process for the critical sequence evaluations operates close to states with a singular operative stiffness. It is obvious that the simulation is more sensitive to both mechanical and numerical aspects than the more robust evaluation of sta-

[66] Another form is to use the whole critical eigenvector $\underline{\varphi}_{\text{cr}}$ as parameters, and $\underline{\underline{K}}\,\underline{\varphi}_{\text{cr}}$ as selector functions, adding also a selector equation $\| \underline{\varphi}_{\text{cr}} \| - 1 = 0$.

[67] or at least strongly suggests.

ble primary equilibrium sequences. Specially developed and tested algorithms are thereby needed. Commercial software do not normally offer this type of sequence tracing.

The mentioned sensitivity of the sequence and the states also indicate that knowledge about the problem investigated is valuable for efficient and reliable simulations. For particular problems studied, the alternative formulation of criticality in Eq. (4.35), and the symmetry preservation approach also discussed in Sect. 4.4.1 have proven useful to improve algorithmic performance.

When a critical state with multiple critical eigenvectors is handled, and the secondary branches around it sought, the hyper-circle method briefly discussed in Sect. 4.4.1 can help in finding them. The basic idea is to introduce an additional—well chosen—disturbance force, and a selector function defining a radius from the critical state. Following the resulting sequence shows all outgoing branches through a vanishing disturbing force; this method was denoted as branch-connecting by Eriksson (1998).

The example continued

The example in Sects. 4.6.1 and 4.6.2 is continued. Two symmetry-breaking critical states were found on the primary path for $c = 0$. These can be used as starting states for the evaluation of critical sequences, where the dependence on the parameter c is investigated. A critical selector equation from Sect. 4.4.1 is then replacing the equation fixing c in Eq. (4.53). For numerical stability, an equation fixing the critical state to be on the primary path is also introduced.

In an experiment, the setting was defined by an augmented potential, according to

$$\Pi^+ = \Pi(\text{Eq.}(4.48)) - \mu(d_1 - 0), \tag{4.54}$$

and an augmented parameter set, cf. Eq. (4.49)

$$\underline{P} = \begin{pmatrix} \lambda \\ c \\ \mu \end{pmatrix}. \tag{4.55}$$

The residual then is

$$\underline{R} = \underline{R}(\text{Eq.}(4.50)) + \begin{pmatrix} -\mu \\ 0 \end{pmatrix}, \tag{4.56}$$

while the operative stiffness $\underline{\underline{K}}$ remains, and the parameter derivatives of the residual is expanded into

$$\underline{R}_{,\underline{P}} = \begin{pmatrix} -d_1 & 0 & -1 \\ -1 - 3cd_2^2 & -3\lambda d_2^2 & 0 \end{pmatrix}. \tag{4.57}$$

Using the method from Eq. (4.35), which seeks states with a very low positive eigenvalue, the selector equations were written as

$$\underline{R}_x = \begin{pmatrix} \Sigma_{\mathrm{cr}} - \overline{\Sigma} \\ -(d_1 - 0) \\ c - \overline{\tau} \end{pmatrix}, \tag{4.58}$$

where the final—increment selector—function was step-wise updated; the results show that c cannot be used as sequence parameter for all steps.

The critical—lowest magnitude—eigenvalue Σ_{cr} is easily evaluated for any $\underline{y}$ in this small-size problem[68]. Its derivatives with respect to displacement variables $\underline{D}$ and parameters $\underline{P}$ are obtained analytically or by numerical differentiation[69]. The remaining parts of $\underline{\underline{J}}$ are trivially found from $\underline{R}_x$.

In the numerical tests, a low critical eigenvalue $\overline{\Sigma} = 10^{-5}$ was used.

The tangent space at all solutions in the sequence is two-dimensional, as the critical eigenvector together with zero parameter increments satisfies the tangent conditions. The evaluation of the critical sequence must use the other tangent space basis vector. In the example case, starting from the bifurcation state[70] around $\underline{y} = (0, 1, 2, 0, 0)^{\mathrm{T}}$, the tangent vector has the components $(0, 0.6904, 0.6904, 0.2161, 0)^{\mathrm{T}}$, showing the local dependence of the critical state on the parameter c. Starting instead from the lower symmetry-breaking critical state, the tangent will just be a c increment, as this critical state exists for any c. The two critical equilibrium sequences are shown in Fig. 4.10a. All solutions included $d_1 = 0$ and $\mu = 0$ to machine precision.

The upper critical sequence in subfigure (a) shows a turning state in the c parameter, indicating a change of qualitative response of the model; the turning state is isolated at $c = 0.0833$, and can be analytically verified to appear at $c = 1/12$. The first observation is that this critical situation does not exist for higher c, the second is that two such states exist for (at least a range of) lower c values. The situations can be interpreted from the properties of the equilibria on the critical sequence, but are most clearly shown by performing primary and secondary branch evaluations for values of c around the turning state value. Figure 4.10b–d show the results from sequence simulations with $c = 0.075$ and $c = 0.085$, respectively. The three bifurcation states existing for the lower c, with one closed and one open secondary branch are replaced by just one for the higher c. In addition, subfigures (c)–(d) show that a maximum state for the λ parameter exists on the primary branch; this can also be traced by the same method[71], giving another critical sequence for the parameterized problem.

For this, rather academic, example problem, also other qualitatively different responses exist for other parameter ranges.

---

[68] as the critical eigenvector is $\underline{\varphi}_{\mathrm{cr}} = (1, 0)^{\mathrm{T}}$ for the bifurcation states, and thereby Σ_{cr} equal to the $(1, 1)$ component of $\underline{\underline{K}}$.

[69] In a more complex problem, it is obtained from a numerical evaluation of the directional derivative of the residual, cf. Eriksson (1998).

[70] and including $\mu = 0$ as a fifth variable in $\underline{y}$.

[71] but with a critical eigenvector being just a d_2 component.

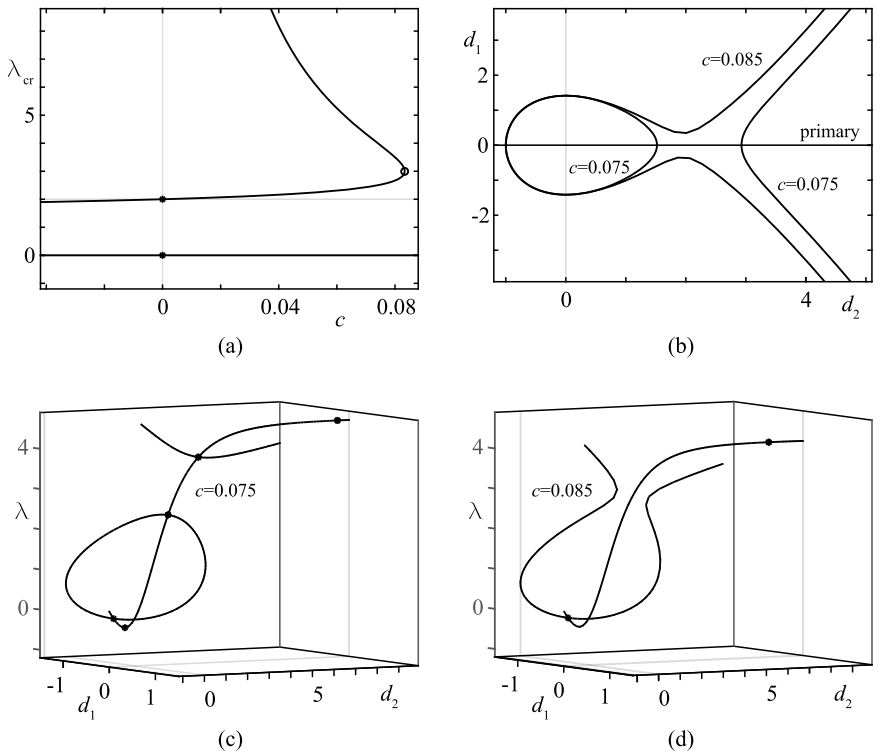

Fig. 4.10 Results from evaluation of critical sequences for example problem. **a** Critical forcing levels as function of parameter c. **b** Primary and secondary equilibrium sequences for two different c. **c**, **d** Projections of sequences for these values

4.6.4 Grazing Contacts

Equilibrium states with grazing contacts in a discretized setting have several similarities with the critical states discussed in the previous section, and they are transition states in the sense of Sect. 4.5.6. Sequences of grazing discretized contacts can thereby be evaluated by similar sequence tracing simulations. As for the critical sequences, a particular grazing state is traced in parametric space, which implies that a specific set of contact conditions are active, while another specified set of grazing contacts are present.

Again, an exterior forcing parameter is often relevant, and is introduced together with the increment selector function. The numbers of additional parameters and other selector functions must therefore match in the problem definition.

Referring to Sect. 4.4.1, a grazing state can be defined by two different settings, introducing constraint and selector functions. As constraint equations bring in an implicit constraint variable, either setting demands one selector function for each grazing contact point. This selector is acting on either the constraint-enforcing vari-

able in $\underline{C}$ or on a displacement component in $\underline{d}$. The problem definition must therefore add a number of parameters equal to the number of points in grazing contact. This does not imply that parameters must have an immediate connection.

An example of a grazing equilibrium sequence is a problem setting according to Sect. 5.4, and described by Fig. 5.10. A simple structure is affected by a pressure p, and constrained by a rigid surface at level H. Assuming that it is obvious which node will first make contact with the surface[72], a setting can be formulated where the pressure needed for first contact is solved as dependent on H.

A more complex setting of grazing contact is also shown for the same example, when a branching from the primary symmetric contact for a pressurized membrane is investigated. This setting illustrates that very good problem knowledge, probably based on several preliminary simulations, is needed for this kind of equilibrium sequence tracing.

4.7 Algorithmic Implementation

A prototype implementation of the solution method for parametric equilibrium problems has been developed, and used in several investigations of structural stability. Based on the descriptions of several algorithmic methods in this Chapter, a very coarse description of the prototype implementation is shown in Fig. 4.11.

The description needs a few comments, in addition to those given already in the Chapter. First, the (re-)start state is not necessarily in equilibrium, and an initial step is performed to ensure starting conditions. For this and coming steps, the choice of increment parameter and its step length is variable between the steps, dependent on the progress and the previous increment[73]. It may also be changed when no convergence is reached in the Newton iterations after a defined number of iterations[74]. Also, the number of re-starts of the iterations after non-convergence in a step is limited by an iteration parameter.

The properties of the evaluated equilibrium states, which are evaluated and monitored in a simulation, are selected dependent on the problem at hand. They may be the signs of parameters and their corresponding components in the tangent vector, the eigenvalue sign spectrum and the contact status. Changes to these may lead to an isolation of the transition state at which the change occurs.

The 'isolation loop' indicated in the figure consists of rather extensive numerical treatment, where a number of new equilibrium states are solved by an almost identical procedure as used for the evaluation of the provisional equilibrium state, i.e., a parameterization of the interval between previous and provisional states[75], Newton iteration and a property evaluation. Based on the properties of the intermediate state,

[72] whichever H is chosen.

[73] even if they are often, as discussed in Sect. 4.4.3, are kept throughout the simulation run.

[74] typically chosen as around 10 for reasonably well-behaved problems.

[75] typically keeping the parameter, and adjusting the increment length, cf. Fig. 4.8.

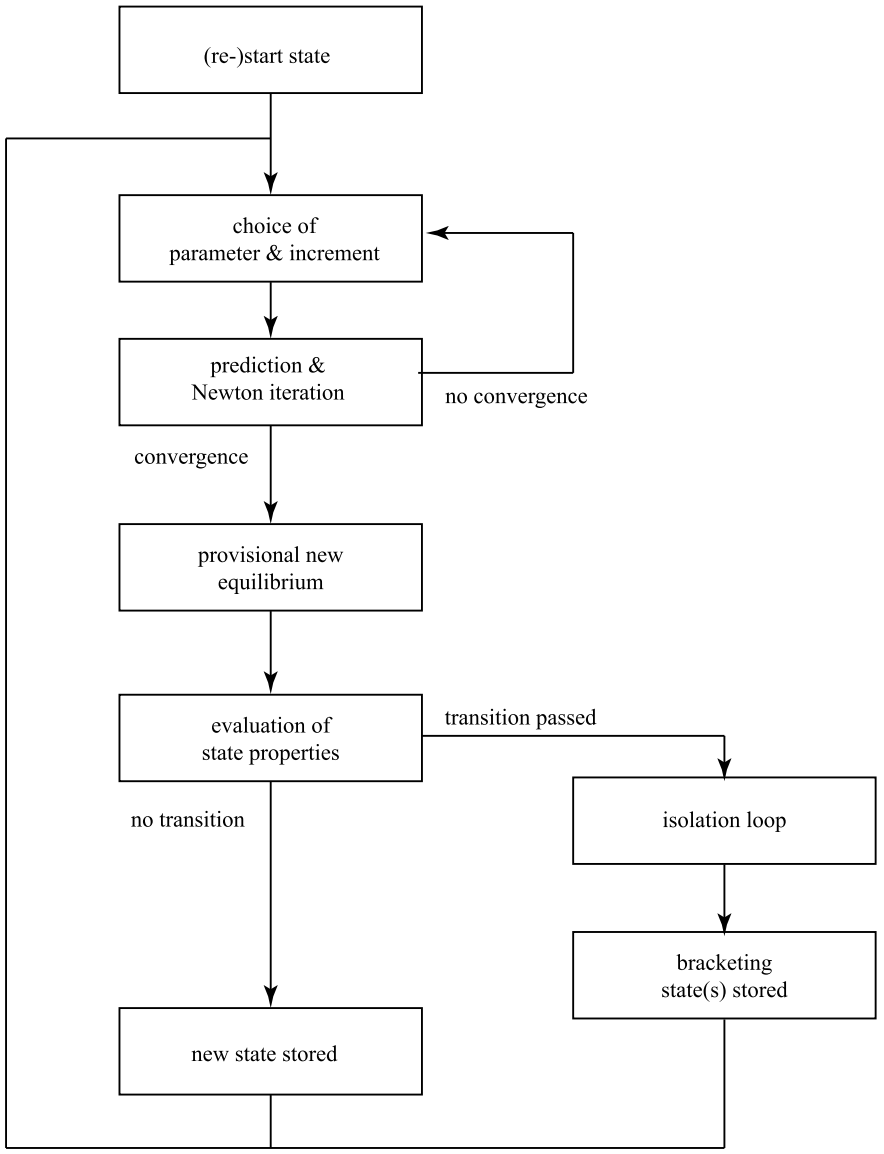

Fig. 4.11 Main steps of algorithm implementation

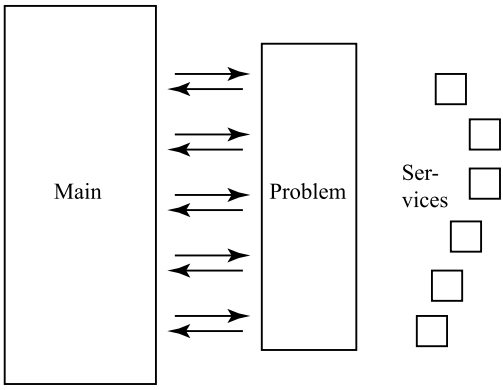

Fig. 4.12 Implementation structure

either of the bracketing states is updated. For accurate isolation and identification of the transition state, the number of bisection states may be high, and the computation demanding; the work is somewhat reduced by the normally very good predictions available for the new states.

After an isolation of a transition state, at least one new state is stored as an equilibrium solution. As further discussed in Sect. 4.5.6, depending on the class of transition identified, also the second bracketing state and the provisional state may be valid equilibria, and are then stored as results. In the cases when they are not valid, they may serve as good predictions for a coming step in the overall process.

As is obvious from the treatment in this Chapter, not least several of the selector functions suggested for particular investigations are rather highly problem specific, and not easily described in the common form of commercial software, where the simulation settings are chosen by keywords and option flags. The structure of the prototype implementation is thereby according to Fig. 4.12, where the main program code is fixed and independent of the specifics of a problem and investigation. Essentially, the code expects evaluations of the residual vector $\underline{R}_y$ and the Jacobian $\underline{\underline{J}}$ as functions of a current approximation to the solution variables $\underline{y}$. Based on this, the main code executes a parametric trace, according to some provided governing algorithmic parameters.

The 'problem' code is developed for a particular investigation, and includes the evaluation of the structural model, but also the selector equations for the investigation at hand; a primary equilibrium branch evaluation does not have the same problem code as, e.g., a critical sequence evaluation for the same structural model[76].

The problem code responds to a set of requests from the main code during different stages of the simulation. This mechanism is used to set the algorithmic parameters, to initiate (a re-start of) the simulation, to evaluate the residual and Jacobian from current solution variables, and to perform different aspects of result presentation. Contact formulations also demand some specialized parts.

[76] but, obviously, with many parts in common.

The problem code is built modularly based on a set of service functions, for, e.g., all element-related quantities and the assembly functions.

Conclusions from this Chapter

The Chapter has discussed how sophisticated solution methods can be used for the simulation of stability aspects in structures. The main issues complicating the simulations are the inherent non-linearity in the formulations, and the need to solve for a sequence of equilibrium states. The sequence is needed in order to fully describe the structural response, and in particular the transitions between stable and unstable equilibria. Although special situations can motivate other approaches, incremental-iterative algorithms based on a selector equation approach together with Newton iteration are proposed for the treatment of these problems. Primarily in order to describe the properties of problems with non-unique responses, a contrasting dynamic relaxation method is discussed in passing. Methods based on secant stiffness forms, but also methods based on so-called linear pre-buckling approaches are shown to be highly unreliable except for limited classes of problems.

The generalized settings allow the investigations of how the stability properties of a structural model depend on a general set of parameters introduced. These can be related to the forcing or to the model itself, and the solution method makes possible parametric traces in any parameter. The parametric view on stability is emphasized, where the stability conclusion for an equilibrium state is a property of the current situation, when all implicit and explicit parameters—and not only a single forcing parameter—are frozen.

The Chapter sets the structural equilibrium problem in a general context, with or without mechanical constraints on the equilibrium solution. This is shown to lead to three different classes of operative stiffness for the model, where a common treatment is described for problems defined by a tangential, incremental or constrained stiffness matrix. A main difference in the treatment relates to the mass matrix in the extraction of the eigenvalues, i.e., the stability coefficients. General methods suggested can be simplified for particular problem settings.

Being of particular interest to engineering simulations, a focus is set on the treatment of critical states of neutral equilibrium, commonly interpreted as the point of loss of stability for an increasing forcing, but here with a more generic meaning. When such an equilibrium state is found in a simulation, the parametric setting allows the investigation of its sensitivity to the parameters considered, and methods are shown for studying properties of secondary equilibrium branches, but also for the parametric dependence of the critical state.

With a focus on one-dimensional parametric equilibrium sequences, an algorithm can be created for automatic tracing of a wide variation of problem settings. For specific problem classes, a fine-tuning of methods and algorithmic parameters can increase efficiency in computations; no algorithmic setting can be assumed to be optimal for all problems. A particular aspect of this is related to problems or states

where the tangent vector is not unique. A method and strategy for re-starts in simulations, including possibilities to choose among sequence segments connected to the state, is an important part of an algorithm.

The Chapter has described the needed algorithm for this generalized sequence-tracing method in rather deep details, facilitating the implementation of similar functions in any general structural simulation software.

Tasks for this Chapter

1. Study the effects from different step choice algorithms, for a scalar problem with $p = 1 - \cos d + 0.05d^2$, $f = \lambda \cdot 1$ in a region roughly delimited by $0 \leq d \leq 8$, $0 \leq \lambda \leq 5$. Test force, displacement and curve stepping, with different choices of increments in fictitious time τ. Then, change the definition of external force to $f = \lambda \cdot 10$, with a correspondingly decreased interval for λ, and perform similar experiments. Document all results, and formulate conclusions; at least one non-trivial observation should be reached
2. Model the plane beam structure in Fig. 4.5 in a general FE software, with forcing described by some relevant formulation. Investigate which solution evolution strategies are available in the software, and test what happens with different choices of strategies and control parameters. Test, in particular, a case where geometric, material and forcing parameters are chosen such that a snap-through response will appear.
3. Consider a thin-walled spherical object, free-floating but subjected to interior over- or under-pressure. In an available software, create a model of this object, for linear or non-linear analysis. Model the whole sphere, but use a mesh with as high symmetry as possible. Use the available methods in the software to introduce necessary—but not more—displacement conditions to allow the analysis. Check the symmetry of the solution, and discuss alternative assumptions and/or methods. **Hint:** If a very thin sphere is modelled, and non-linear effects allowed, then external over-pressure can easily give stability problems in the calculation, which is not the idea of this task (but is, anyhow, interesting).
4. For a toggle frame, similar to Fig. 1.5, introduce hard-coded parameters EA and L, and variable parameters H and F, but also a constraint-enforcing variable C, which ensures that $u = 0$ in a 2 d.o.f. model (u, v). Formulate the constrained total potential, the residual force, the constraint equation and the tangent space. Perform some investigations to demonstrate the meanings of the introduced concepts and quantities.

References

Bathe KJ (2014) Finite element procedures, 2nd edn. KJ Bathe, Waterton, MA, also published by Higher Education Press, China, 2016. First edition published by Prentice-Hall, 1996

Cox BS, Groh RMJ, Avitabile D, Pirrera A (2018) Exploring the design space of nonlinear shallow arches with generalised path-following. Finite Elem Anal Des 143:1–10

Crisfield MA (1981) A fast incremental/iterative solution procedure that handles snap-through. Comput Struct 13:55–62

Dahlquist G, Björk Å (1974) Numerical methods. Prentice-Hall, Engelwood Cliffs

Eriksson A (1991) On the usage of one-step O. D. E. solvers as predictors for structural equilibrium path evaluations. In: Vichnevetsky R, Miller J (eds) IMACS 91, Dublin, pp 339–340

Eriksson A (1989) On linear constraints for Newton-Raphson corrections and critical point searches in structural F. E. problems. Int J Numer Methods Eng 28:1317–1334

Eriksson A (1997) Equilibrium subsets for multi-parametric structural analysis. Comput Methods Appl Mech Eng 140:305–327

Eriksson A (1998) Structural instability analyses based on generalised path-following. Comput Methods Appl Mech Eng 156:45–74

Eriksson A, Kouhia R (1995) On step size adjustments in structural continuation problems. Comput Struct 55:495–506

Eriksson A, Nordmark A (2019) Constrained stability of conservative static equilibrium. Comput Mech 64(4):1199–1219

Eriksson A, Pacoste C (2001) Solution surfaces and generalised paths in non-linear structural mechanics. Int J Struct Stab Dyn 1:1–30

Géradin M, Rixen D (1997) Mechanical vibrations. Theory and application to structural dynamics, 2nd edn. Wiley, Chichester

Groh RMJ, Pirrera A (2018) Generalised path-following for well-behaved nonlinear structures. Comput Meth Appl Mech Eng 331:394–426

Li Q, Healey TJ (2016) Stability boundaries for wrinkling in highly stretched elastic sheets. J Mechan Phys Solids 97:260–274

Nakashino K, Nordmark A, Eriksson A (2020) Geometrically nonlinear isogeometric analysis of a partly wrinkled membrane structure. Comput Struct 239:106302

Noh G, Bathe KJ (2019) The Bathe time integration method with controllable spectral radius: the ρ_∞-Bathe method. Comput Struct 212:299–310

Noh G, Bathe KJ (2023) Imposing displacements in implicit direct time integration and a patch test. Adv Eng Softw 175:103286

Rheinboldt WC (1986) Numerical analysis of parameterized nonlinear equations. Wiley, New York

Riks E (1979) An incremental approach to the solution of snapping and buckling problems. Int J Solids Struct 15:529–551

Strang G (1988) Linear algebra and its applications, 3rd edn. Brooks/Cole, Thomson Learning

Chapter 5
A Wider View

This Chapter discusses a few special aspects related to numerical investigations of structural stability. While the problem settings can be very diverse, dependent on problem class and objective of investigation, a sound understanding of the stability phenomena can guide numerical analyses. While the most basic aspects of structural and forcing modeling are covered in the previous Chapters, three important general aspects are considered here. These are emphasized by illustrative small examples, where the structural modeling through finite elements is straight-forward, but some aspects in the response need special care. The reported examples are verified to show the same types of behaviour also for very finely discretized models.

The problems considered are the interaction of several mechanisms for loss of stability in a hollow column, the effects from symmetries in a problem setting, and the effects from contact conditions, which affect the stability conclusions. In addition to these reported cases, some general comments on material and forcing assumptions are given. Which aspects can be modelled, and how they are specified in a particular software need careful investigations.

Brief Objective of this Chapter

This Chapter shows a set of situations where more advanced methods for stability investigations are needed, illustrating the diversity of stability issues, thereby emphasizing the need for a thorough understanding of the phenomena, but also demonstrating the requirements on sufficiently competent software tools.

A. Eriksson and A. Nordmark, *Structural Stability and Its Computational Modelling*, Computational Methods in Engineering & the Sciences,
https://doi.org/10.1007/978-3-031-36072-5_5

5.1 Special Situations

This Chapter will focus on some particular aspects of stability investigations for structures. While previous Chapters have given the basic theories, discussed the discretization necessary for complex structures, and shown an algorithmic setting for complete stability mappings of parametric structural models, a wide variety of special issues may arise in particular cases. A number of such issues have been dealt with in previous research articles by the authors, and a few will be further elaborated here.

A common denominator of the aspects handled in the present Chapter is that they all relate to aspects which are not always covered even by the general approaches discussed in previous Chapters, and therefore need some special treatment. They are also examples of issues where available commercial software might offer options for their treatment, but where the interpretation needs a very clear view on the meaning of results obtained. This, for instance, relates to some material models, which can lead to unexpected results in certain structural models, but also to discretization models lacking some important parts of needed kinematics. The necessity to correctly introduce the boundary conditions for the model is emphasized.

Most treatises on stability, not least the simplified engineering analysis schemes, tend to focus on one clear-cut stability aspect at the time, but the discussion above has emphasized the parameter dependence in all response aspects, and the present Chapter gives a first example, where parameters for a problem are chosen such that unstable response modes tend to interact.

As also discussed in previous Chapters, one issue of major importance for stability investigations is related to symmetries of a structure. Whereas utilization of symmetry and repetitions is normally problem-free for linear cases—and in earlier computational approaches was often necessary due to limited resources—this is not the case in relation to modern computational treatment of stability. The treatment below focusses on a problem with high symmetry, and shows how lacking consideration of this leads to incorrect, or at least inaccurate, results. The example also emphasizes the sensitivity of results to assumptions concerning, e.g., boundary conditions.

A third aspect where stability conclusions can be strongly affected by the numerical structural modeling is in relation to constraints, and in particular contact conditions in the model. The previous Chapters give basic formulations for the modelling of hard smooth contact conditions, and an example here gives an illustration of how discretized contact conditions in a structural model lead to artifact bifurcations.

The Chapter ends with a short description of some situations where care must be directed towards the choice of models for material, forcing and boundary conditions, when using commercial general simulation software.

5.2 Critical Mode Interaction

Traditional engineering stability investigations focus on individual components, and on specific critical modes, often with picturesque naming. These clear-cut situations do not necessarily exist and appear in more general simulation approaches. This section deals with a simple structure, for which stability can be lost in several ways. An interaction between these phenomena is potentially of relevance, at least for some parametric instances. The problem is the one shown already in Sect. 1.7, where a compressed thin-walled beam is analyzed by two different simple methods for global and local buckling; a geometric relation gave the parametric borderline between the two possibilities.

The problem was here analyzed by the general FE software COMSOL Multiphysics[1], which is a very powerful simulation tool, allowing an extensive flexibility in problem settings. The basic idea of the example was to show what can be expected for a problem, when no initial assumptions are made regarding the results. An objective was also to investigate how the analytical assumptions on, e.g., boundary conditions can be modelled, considering that the analytical assumptions often deviate from what can be believed to be the practical conditions in a structure.

5.2.1 Model Setup

The problem studied is described by Fig. 5.1, and refers to the compression of a prismatic aluminium beam of square thin-walled section, with a central compressive forcing. The beam geometry is defined by length L, outside width B, and wall thickness h. The material is assumed as linearly elastic, cf. Sect. 2.4.2, with material parameters (E_m, ν_m), but also a density ρ_X used in the mass matrix; self-weight was not considered as an exterior forcing. The model was set up as completely parametric. Geometrical non-linearity was considered.

For all experiments shown here, data were defined as $B = 100\,\text{mm}$, $h = 2\,\text{mm}$, $E_m = 70\,\text{GPa}$, $\nu_m = 0.3$, and $\rho_X = 2800\,\text{kg/m}^3$. Length L was varied between cases below. For any length[2], local buckling is calculated by the simple expressions in Sect. 1.7 to occur at a compressive force $F_{\text{loc}} = 82.9\,\text{kN}$ with present data, while global Euler-type buckling appears at $F_{\text{glob}}(L) = 867\,\text{kNm}^2/L^2$. The length of equal buckling loads, when $F_{\text{glob}} = F_{\text{loc}}$ is approximately $L = 3.24\,\text{m}$. Two beam lengths were primarily considered below, and are denoted as: $L = 2.5\,\text{m}$ for case 'S', and $L = 4.0\,\text{m}$ for case 'L'.

The basic model used shell elements with quadratic internal interpolation, where the midsurface widths of all sides were set to $b = B - h$, cf. Figs. 5.1 and 1.17. The models were rather finely meshed, using the built-in meshing method, giving models

[1] version 6.0, Comsol AB, Stockholm, Sweden

[2] which is longer than a few times the section width

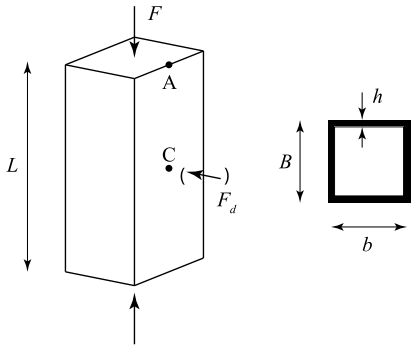

Fig. 5.1 Hollow rectangular compressed column. Geometry, forcing and relevant points. Point C is at the midpoint of the side; a point D was situated opposite to C. Main loading was along the X_3 axis, while disturbance force acts along X_1. b is the width between side-plate midsurfaces

of around 12,000 degrees of freedom. It was noted in experiments that rather fine meshes were needed to resolve the local buckling modes.

In order to avoid severe local deformation effects, and to allow a central compressive force resultant, end plates were added to both ends of the beam. These were, after some initial testing, created to be 5 times thicker than the beam walls, and have a fictitious elastic modulus of $10\,E_m$, with a zero Poisson ratio. The end plates were thereby considerably—but not extremely—more stiff than the structure itself. This choice led to an almost uniformly distributed compressive stress at the end sections, with only small local deformations. An alternative approach—using more elaborate methods available in the software—is possible, but not trivial and not easily reproduced in other software.

The center point of the lower end plate was restrained from all translations, while the center of the top end plate was restrained from horizontal translation, with a compressive force acting in the vertical direction. For equilibrium analyses, a fictitious support against rotation was introduced in point A of Fig. 5.1.

The simulations were imagined to be performed 'ab initio', with no initial knowledge of the response, and in particular the possible modes of lost stability, The created model was affected by an increasing parametric compressive force. One result evaluated for each state in the solution was a prediction of the lowest critical force level, from an LPB approach, cf. Sect. 4.1.3. With respect to an applied force F, the LPB gave a force multiplier $\lambda_{\rm cr}$ leading to an estimate for the critical compressive force as $F_{\rm cr} = \lambda_{\rm cr} F$. The possibility in the software to visualize the predicted critical mode was used to interpret these results.

Table 5.1 Main results from simulations for column case 'L'

F	F_{cr}	Natural frequencies									
1	53.8	19 ∗ 2	77 ∗ 2	165	170 ∗ 2	271	278	288 ∗ 2	290	300	344
10	53.8	18 ∗ 2	76 ∗ 2	165	168 ∗ 2	272	278	286 ∗ 2	290	299	343
20	53.8	16 ∗ 2	74 ∗ 2	165	166 ∗ 2	271	278	284 ∗ 2	290	298	341
30	53.8	13 ∗ 2	72 ∗ 2	164 ∗ 2	165	271	276	282 ∗ 2	290	297	339
40	53.8	9.9 ∗ 2	70 ∗ 2	162 ∗ 2	165	271	276	280 ∗ 2	290	295	337
50	53.8	5.2 ∗ 2	68 ∗ 2	160 ∗ 2	165	270	275	278 ∗ 2	290	295	335
53	53.8	2.4 ∗ 2	67 ∗ 2	160 ∗ 2	165	270	275	278 ∗ 2	290	294	334
kN	kN	Hz	Hz	Hz	Hz	Hz	Hz	Hz	Hz	Hz	Hz

The notation '*2' shows double modes at the same frequency, and an interpretation as global bending modes

For each applied compressive force F, also a set of the lowest natural frequencies of the forced model were calculated. The consistent mass distribution of the software was introduced. Vibration modes corresponding to the frequencies were visualized and interpreted.

Concerning the global buckling, a slight complication in simulations lies in the square section, which will lead to equal buckling force for modes of any transversal direction; coinciding eigenvalues were expected. The appearance of double eigenvalues was interpreted as related to global phenomena.

5.2.2 Basic Results

Results from the simulations for the long column, case 'L', are given in Table 5.1. The applied force levels were chosen manually, starting from (what was assumed to be) a small force F, and then manually choosing a set of steps from the initial LPB prediction of critical force; the aim was to solve equilibrium as close to the critical state as possible.

As the provisional analytical treatment in Sect. 1.7 evaluates the critical force, which is the global buckling force for this case, as $F_{cr} = F_{glob} = 54.2\,\text{kN}$, the LPB prediction here is consistent and very accurate, already from $F = 1\,\text{kN}$. This is common when the deformation of the structure is linear—and very small, compared to structural dimensions—before the critical state.

Vibration frequencies are in most cases double, indicating global 'Euler type' sinus-wave modes, and the first row gives almost exactly the ratios 1:4:9 as expected for these. The frequency at 165 Hz corresponds to a torsional mode, the single one at around 290 Hz an axial mode, while the other frequencies have modes which are visually identified as breathing modes. Only the latter group of modes slightly resemble local buckling modes. It is noted that no modes obtained from these simulations

are exactly corresponding to the analytically derived clear-cut situations, but contain at least small contributions from other modes.

The table shows how the frequencies for all modes tend to be reduced with increased compression, but only the lowest bending mode tended to zero, and this clearly shows the approaching global buckling. A final calculation with $F = 53.7$ kN gave the lowest double frequency at 0.9 Hz, with all other frequencies identical to the final row in the table. No particular convergence or other problems were noted for this case of almost clear-cut global buckling.

Similar results for the short column, case 'S', are given in Table 5.2. The same method was used to find suitable forcing magnitudes. In addition to the double, global buckling modes, and the torsional and axial modes—now with frequencies 261 and 446 Hz, respectively[3]—a large number of local vibration modes were found in this case. An attempt to connect frequencies for the same modes for increasing forcing, and an extrapolation of these to zero frequency was difficult, but tended to show that a local buckling mode will become critical first. The situation with lost stability is, however, very numerically sensitive, and could not be reached.

The results show that the LPB prediction is consistently converging with increased forcing, and rather clearly points to a critical force $F_{cr} \approx 81$ kN; the mode shown for the predicted loss of stability is visually the same for all force levels: a local buckling with around 25 half sine-wave shapes[4], but with amplitudes of the local buckling higher in the middle part of the column: an effect of the bending type global buckling. The double vibration frequency corresponding to a one half-wave bending mode (the first frequency column) is reduced with forcing, but is still rather far from zero at the final reported forcing level. Analyzing the table shows how many frequencies corresponding to local modes are decreasing quickly, and will be decisive for the loss of stability. At the final state in Table 5.2, the frequency 106 Hz is visually identified as a mode, where the beam sides buckle in 24 half-waves, but affected by the global buckling shape. The physical interpretation is that the local buckling reduces the bending stiffness of the beam section, leading to a lower interacting local-global buckling phenomenon.

The two potential sources for loss of stability—of which the local buckling offers several closely neighboring cases, with modes of different numbers of half-waves—obviously interact for moderately long beams. The interaction is difficult to find with the approaches above, but other methods will give clearer results.

5.2.3 *Trigger Force*

For structures where the loss of stability is not easily predicted in initial design consideration, an alternative approach can often be used. The basic ideas is to introduce

[3] agreeing well with the corresponding results for case 'L', as these frequencies should be approximately proportional to $1/L$

[4] Very similar estimates are obtained for a number of modes of approximately the same wavelengths

Table 5.2 Main results from simulations for column case 'S'

F	F_{cr}	Natural frequencies									
1	79.2	50 * 2	192 * 2	261	284	321	394 * 2	418	446	486	488
10	79.2	48 * 2	190 * 2	261	284	320	392 * 2	417	446	486	487
40	79.3	42 * 2	184 * 2	261	283	316	386 * 2	411	445	484	485
60	79.1	37 * 2	180 * 2	261	282	314	381 * 2	406	406	408	410
70	79.1	35 * 2	178 * 2	261	282	301	304	309	310	310	312
80	81.0	28 * 2	106	124	151	166 * 2	176	185	190	212	220
kN	kN	Hz	Hz	Hz	Hz	Hz	Hz	Hz	Hz	Hz	Hz

The notation '*2' shows double modes at the same frequency, and an interpretation as global bending modes

an imperfection to the structural model, which can replace the bifurcation at buckling by something resembling a limit point; one version of the idea is shown already in Fig. 1.3. The imperfection can be introduced in several ways, but for the present case, a disturbance force in point C of Fig. 5.1 is added to the main forcing. The position and direction of the force are chosen such that it can initiate both a global and a local buckling situation.

The disturbance force is either small and constant, while a successively increasing force F is applied, or a small proportion of the applied forcing. With U_c and U_d denoting the displacements at points C and D in the direction of the disturbance force, results can be interpreted, based on a reasoning. Without the disturbance and for small F, the points C and D would move outwards, i.e., get (small) displacements of equal magnitude but opposite signs, due to the Poisson effect in the compressed column. For local buckling, recognizing the synchronous buckling on all four sides, the displacements are also of different signs but of the same magnitude—larger than from just Poisson effects. For a global buckling situation, the column buckles as a whole in the transversal direction, and the displacements of the two points are of very similar magnitudes and of the same sign. When different modes are close to loss of stability, the displacements will be some mixture of these cases.

For case 'L', a constant force of just $F_{\text{disturb}} = 1\,\text{N}$ was applied, the main force F was gradually increased. equilibrium solved, and the displacements U_c and U_d recorded. The results are shown in Fig. 5.2a. The two displacements are indistinguishable in the diagram, increase with the main force magnitude, and go towards very large deflections for $F \approx 53.6\,\text{kN}$, above which level convergence is not reached. The similar deflections show that this is a global buckling situation, where beam bending is clearly dominant. No local buckling is seen, at least not at points C and D.

For case 'S', the alternative approach with $F_{\text{disturb}} = 0.001F$ was used, but otherwise the same method. Results are shown in Fig. 5.2b. The local buckling in this case makes the deflections become initially different, but the reduced bending stiffness from this buckling finally makes the column buckle globally, with the deflections almost equal, at a forcing $F \approx 87.6\,\text{kN}$. Subfigure (c) shows a magnified displacement view of the column at a force close to this case; both the local buckling and the global bending deflection are obvious.

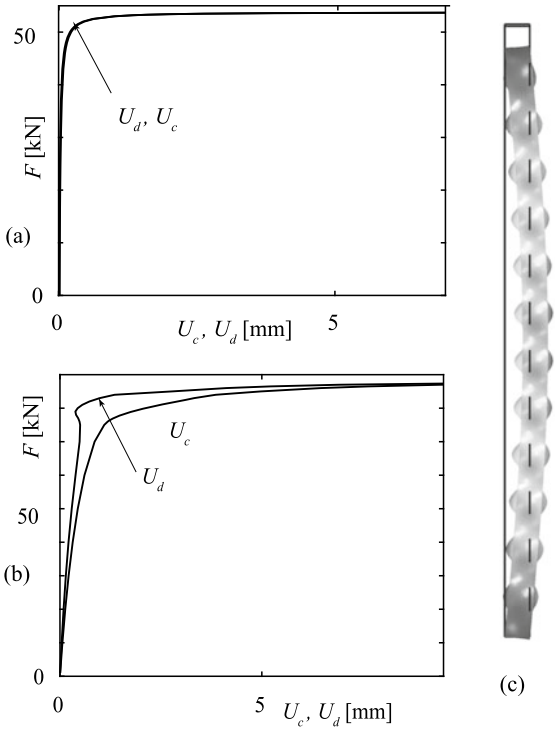

Fig. 5.2 Results from simulation with compressed column, disturbed by transversal force. **a** Deflections of points *C* and *D*, case 'L'. **b** Deflections for case 'S'. **c** Magnified deflection at high compressive force for case 'S'

As the global buckling phenomenon is clearly present in subfigure (c)—for a forcing considerably lower than the $F_{\text{glob}} = 139\,\text{kN}$ evaluated for this length—an interaction takes place between the two modes for loss of stability. This makes the analytical expressions unreliable. The practical semi-analytical handling of this interaction is based on the concepts of effective thickness or width, where the stiffness of plate fields is reduced when affected by the compressive stresses, and thereby also the overall bending stiffness entering the expressions for global buckling. Numerical simulations of the whole structural model, without any assumptions on probable response, give a picture of this interaction.

5.2.4 Comments to the Problem

One conclusion from the performed simulations is that the local buckling modes are of small scale compared to global dimensions. This implies that results are rather strongly affected by the discretization mesh in the simulations. An unexpectedly fine element mesh was needed for the situations where local buckling is of importance for the response.

It is also noted that the square beam section used in the example is a special case. In a general parametric modelling, a rectangular section would rather be defined, and the results obtained for the parameters defining the rectangle. Such cases would not show the double eigenvalues, due to the different bending stiffnesses in the two section axis directions. The parametric equilibrium tracing methods discussed in Chap. 4 could trace either of the critical states[5] in the parametric space, evaluating the critical force as function of the parameters. Such a procedure would find the square section as a special case, where two critical modes meet at a common forcing level.

5.3 Symmetry in Modeling

The importance of symmetry in a structural model and its forcing has been mentioned several times in previous Chapters. The key aspect is that a discretized model must neither add nor remove symmetry aspects in relation to the real physical object. The discussion in Sect. 3.5.1 focusses on two aspects of symmetry: a macro-symmetry inherent in the problem at hand, and a micro-symmetry, which is an effect of its discretization. The present section shows results from experiments with a simple but highly symmetric problem, i.e., a square thin plate which is compressed by uniform edge tractions from all sides, Fig. 5.3. This is a case with high symmetry, as also forcing is symmetric. Although the case is somewhat uncommon, it is phenomenologically related to engineering buckling problems, where a primary equilibrium branch in a reduced dimensional space, cf. Sect. 2.5.6, loses stability through bifurcation with a secondary response out of this space. This is one reason for the need for complete kinematic descriptions in Chap. 3.

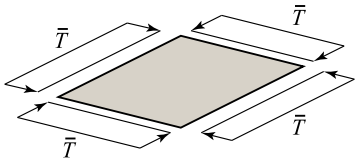

Fig. 5.3 Highly symmetric problem, where forcing gives a primary response in the plane, and secondary branches out of plane

[5] e.g., global buckling in one of the directions

In the figure, and results, compressive edge traction is denoted as positive. In simulations, the plate was assumed as free-flying. As this problem setting is unstable, with three negative eigenvalues for any non-zero compressive traction[6], the displacement boundary conditions needed care. The free-flying condition implies that no setting of these can be considered fully correct, but the chosen setting aimed at minimum constraints on the response. With 'mid' denoting the midpoint of the plate, and Γ its boundary, the displacement boundary conditions were applied as

$$\begin{aligned} U_{1\,\mathrm{mid}} = U_{2\,\mathrm{mid}} = U_{3\,\mathrm{mid}} = 0, \\ \oint_\Gamma X_2 U_3 = \oint_\Gamma -X_1 U_3 = \oint_\Gamma X_1 U_2 - X_2 U_1 = 0, \end{aligned} \tag{5.1}$$

where, according to Chap. 2, the X_i and U_i are components of initial position and current displacement, respectively, and $X_3 \equiv 0$ for all points in the plate. These expressions are in general rather easily formulated and adopted for discretized models.

A somewhat similar problem is described by Eriksson and Nordmark (2016), when stability is studied for a square horizontal membrane affected by a hydro-static pressure from below, leading to bifurcation behavior. An analytical treatment of this case showed the symmetry aspects existing in a set of computational models, and the effects from these on the results from numerical simulations.

Even if the structural models are very similar, the present case is of even higher symmetry, due to its up-down reflection symmetry. While the reference analyzes the C_{4v} symmetry group of a square pyramid, the present case belongs to the group D_{4h} of square prisms. The presentation here uses the Schönflies notation from Cotton (1990), but also other notations for symmetry aspects exist, e.g., the one used in the book by Conway et al. (2008). The two groups have several aspects in common, and the treatment in the reference is useful also for the present problem.

5.3.1 Group-Theoretical Background

The analysis is performed by using group theory concepts, cf. the work by Ikeda et al. (1991) and Zingoni (2014). A symmetry group is a group where each element is an isometric transformation of $3D$ space or fields in the $3D$ space. For a finite sized object, the symmetry group is a point group, where each transformation leaves a common point, e.g., the origin, fixed. The symmetry group is thereby defined by a set of basic distance-preserving operations, which map a field onto itself. The C_{4v} group has eight such operations, while the present D_{4h} group has 16, due to the up-down symmetry. The relevant operations are of four classes: reflections, rotations, inversions and rotary reflections.

[6] and three zero eigenvalues, corresponding to rigid body translations

For a specific problem setting, a well-defined symmetry exists and can be deduced from the operations possible. The symmetry aspects are most easily visualized from finite element meshes, showing an initial geometry of a model. The symmetry can then somewhat loosely be described as the set of operations on the mesh, for which the results are visually identical to the starting mesh. A set of meshes of the full square are given in Fig. 5.6 connected to the numerical simulations. These meshes have varying symmetry properties, as denoted by the labeling of the meshes. The reflection symmetries in planes orthogonal to the plate and rotations around the normal axis are rather obvious, while rotations around in-plane axes, and inversions through the origin are more intricate.

The Schönflies notation gives information about the types and numbers of different distance-preserving operations. For example, in D_{4h} the subscript 4 indicates a main X_3-axis with four-fold (quarter-turn) rotation symmetry, while it together with the D indicates two-fold rotation symmetry along four different axes orthogonal to the main one, including the secondary X_1-axis. Finally, the subscript h indicates a reflection symmetry in a plane orthogonal to the main axis. This implicitly leads to a number of other operations, like reflection in four planes containing the main axis, four-fold rotary reflection symmetry along the main axis, and inversion.

The symmetry group D_{4h} has 13 different kinds of subgroups, with a total of 34 subgroups differing in their axis orientations. Only a few these can appear as secondary equilibrium branches in the present problem, losing just one of the symmetry aspects of the initial group.

A notation is introduced for the orientation of the relevant subgroups. Some of the subgroups of D_{4h} come out in non-standard orientation, where for example the secondary axis could be different from the X_1 -axis. Denoting the X_1- and X_2-axes by σ_1 and σ_2, and the diagonal axes pointing to the right- and left-hand sides of the X_2-axis as δ_1 and δ_2, the following extra suffixes are used to denote non-standard orientations:

Subgroup	Main axis	Secondary axis
$D_{2d}(\delta)$, $C_{2v}(\delta)$, $D_{2h}(\delta)$	X_3	δ_1
$C_{2v}(\sigma_i)$, $C_{2h}(\sigma_i)$, $C_2(\sigma_i)$, $C_s(\sigma_i)$	σ_i	X_3
$C_{2v}(\delta_i)$, $C_{2h}(\delta_i)$, $C_2(\delta_i)$, $C_s(\delta_i)$	δ_i	X_3

For consistency, also the following are used even though the subgroups are in standard orientation: $D_{2d}(\sigma)$, $C_{2v}(\sigma)$, $D_{2h}(\sigma)$.

Solutions to an equilibrium problem can be classified in the same way, essentially by studying the deformed mesh in the same terms. In general, there is no reason to believe that solutions will fulfil the symmetry of the region, and it must be expected that solutions normally do not show the full symmetry. For the present case, where both region and forcing fulfil the D_{4h} symmetry, the primary equilibrium branch can be defined as consisting of the solutions which keep this symmetry. On the other hand, all secondary branches leave the symmetry, and the response may then be characterized by any subgroup, down to the completely unsymmetric C_1.

While the above is valid for the solutions to the equilibrium problem, the analysis of critical states demand some further concepts. The stability of an equilibrium solution is determined by a linearized analysis of deviations from the equilibrium state. The space of linearized deviations is spanned by the set of the $N_d - N_c$ eigenvectors for the discretized model at the equilibrium solution, cf. Sect. 3.7. It is there shown that, for a critical state with vanishing eigenvalues, the corresponding eigenvectors are independent of the way mass is introduced.

Group representation theory is used to conclude that the eigenspace of a problem can be separated into types of eigenmodes sharing the same symmetry properties. This splitting is valid at any equilibrium state: stable, unstable or critical. The practical conclusion is that the $N_d - N_c$ eigenvectors of the fully symmetric equilibrium each shows a particular symmetry, but that many share symmetry properties, as shown by a numerical investigation in Sect. 5.3.4. It is noted that the eigenvectors stay in the same group, but are not constant when following an equilibrium branch. They can therefore never be meaningfully evaluated just at the unforced reference equilibrium state, as in a mode superposition approach.

As more deeply described and discussed in the above reference, although for a different case, the critical eigenspace for a problem with finite symmetry group can be written as a direct sum of finite-dimensional spaces. Finding these representations is a non-trivial task, but the general result is known for the D_{4h} group. This shows that critical modes for a basic problem of D_{4h} symmetry must belong to either of ten types[7]. Two of these mode types are displacement fields based on arbitrary linear combinations of two eigenvectors—which are related—while the other eight are defined by one eigenvector each. The symmetry properties for these eigenvectors are given by the analyses.

For the present case, with primary branch equilibria respecting the full D_{4h} symmetry, the critical modes are most easily described by some numerical results obtained with a fully symmetric mesh denoted m1(512) below. This simulation shows that seven critical states exist for the present case for tractions lower than $\overline{T} = 1\text{MPa}$, but continued simulation towards higher tractions give new critical states. The modes of the seven critical states are visualized in Fig. 5.4, with a gray-scale shading representing the transversal deflection in the mode[8].

In the figure, the critical situation with lowest traction is related to mode 1 of type B_{2u}. The obvious symmetry consists of reflections in two planes containing one of the in-plane axes, and a half-turn rotation around the normal axis, but also other symmetry transformations are fulfilled: half-turn rotations around the diagonal axes, and quarter-turn rotary reflections around the normal axis. For the remaining transformations of D_{4h}, this mode is instead anti-symmetric. While the concept of anti-symmetry can not be meaningfully transferred to an equilibrium branch, the symmetries of the mode are kept for secondary branches created in the bifurcation, which will thus be of symmetry $D_{2d}(\delta)$.

[7] compared to only five for the C_{4v} symmetry group

[8] In-plane displacements in modes are numerically zero, even if in-plane displacement from traction is non-zero

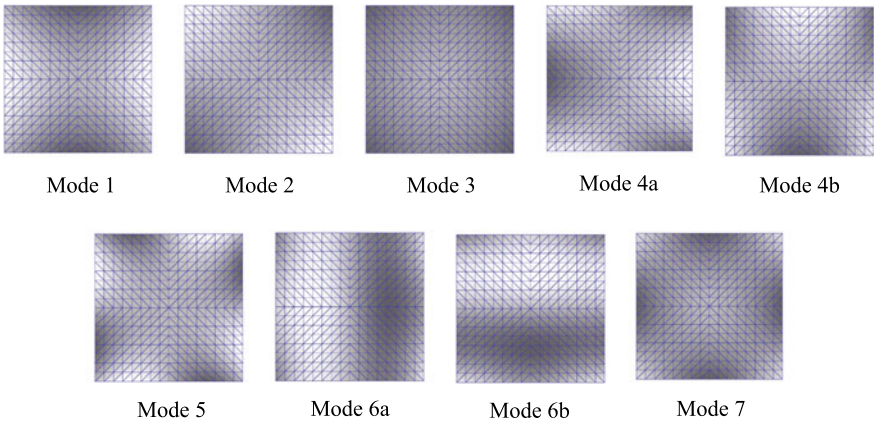

Fig. 5.4 Critical modes at successive bifurcations, in order of increasing traction. Gray-scale indicates transversal deflection in the modes. Traction values at bifurcations are given in Tables below

The second critical state gives mode 2 of type B_{1u}, with an eigenvector belonging to the $D_{2d}(\sigma)$ symmetry group, and (among others) symmetry planes through the in-plane diagonals. Mode 3 is of type A_{2u}, with a 'bubble shape' buckling. As this is no longer up-down symmetric, the symmetry group of the eigenvector is C_{4v}.

The fourth bifurcation is of mode type E_g, with two vanishing eigenvalues; its critical mode space is spanned by two orthogonal eigenvectors, which can be arbitrarily chosen. In the figure, the basis vectors denoted 4a and 4b are chosen to belong to the symmetry groups $C_{2h}(\sigma_i)$ for $(i = 2, 1)$, respectively. These are obviously related through a quarter-turn rotation around the normal axis. The basis vectors could equally well have been chosen to belong to the groups $C_{2h}(\delta_i)$.

Mode 5 is of type A_{1u}, with the obvious symmetry of quarter turns around the normal axis, and belonging to symmetry group D_4. The sixth and seventh modes are new instances of mode types already seen.

Five types of critical modes from the subgroups of D_{4h} are thus represented already at rather low tractions. The other five mode types (E_u, B_{2g}, B_{1g}, A_{1g} and A_{2g}) are in-plane modes and correspond to considerably higher eigenvalues. For the primary branch for the case denoted m1(512) below, an investigation showed that the lowest eigenvalues for the latter modes are at least two orders of magnitude higher than the lowest ones for the former group at low traction levels. They also become critical at much high traction levels.

Increasing traction will successively give critical modes of all types, with increasingly more complex shapes, but still belonging to the ten mode types.

Two further comments are given on the analysis of the critical modes and their symmetry properties. The first is that the symmetry properties discussed above refer to the mode at the critical state, and to the critical eigenvectors at this. The symmetry properties of a branch emanating at a bifurcation state are not these, but analyses of the critical states show the possible symmetries of all branches.

The second comment is that the analysis of modes discussed above is exclusively connected to the case of a branch where equilibrium solutions fulfil the D_{4h} symmetry. For other situations, e.g., a case with lower symmetry, such as the one in Fig. 3.14a with traction on just two sides, the mode analysis must be separately developed. As will be further shown below, this implies that bifurcations on secondary branches need a consideration of the symmetry of the branch.

The outcome of a simulation, and in particular the stability conclusions based on this, depends on to what degree a particular simulation model can represent solutions and eigenmodes of different symmetry properties. With the classification above, a chosen discretization of the displacement field can be immediately evaluated. A lacking capacity of a model implies that a particular critical state is either completely missed or badly represented, as shown by numerical examples below.

5.3.2 Numerical Tests

Numerical tests were performed for the square thin plate under uniform compressive traction. The main test was a parametric trace, where an increasing traction was introduced by a forcing parameter λ, cf. Sect. 4.1.6. All transition states along the primary equilibrium branch—which is linear in this case—were isolated to high accuracy. The critical eigenvectors at these were calculated, and referred to one of the mode types above, based on the symmetry in the discretized critical eigenvectors.

For the numerical tests, measures were arbitrarily chosen as a plane area of $200 \times 200\,\text{mm}^2$, with a thickness of 1 mm. The plate was assumed as linearly elastic, based on plane-stress and the St Venant Kirchhoff material model from Sect. 2.4.2, with $E_m = 10000\,\text{MPa}$, $\nu_m = 0.3$. Simulations were performed with a well tested triangular plane shell element based on the TRIC form, cf. the paper by Eriksson and Pacoste (2002). Uniform traction on all four sides of the square was introduced by equivalent external nodal force components.

Simulations were performed with rather coarse versions[9] of a set of basic meshes, in order to show the effects from the lacking symmetries in the models. Results from a simulation with a refined version of a mesh with high symmetry (the m1(8192) mesh, cf. below) is considered as a converged solution.

Macro-symmetry models

Simulations were performed for a set of macro-symmetry models, an approach assumed to be closely related to common engineering approaches. These simulations gave solutions for a representative subregion, where displacement boundary conditions were introduced to describe the relation of this subregion to the whole. The matching symmetry subgroups can be used to trivially reconstruct a solution on the full region. The reconstructed solution will necessarily show at least the symme-

[9] with a few hundreds of degrees of freedom

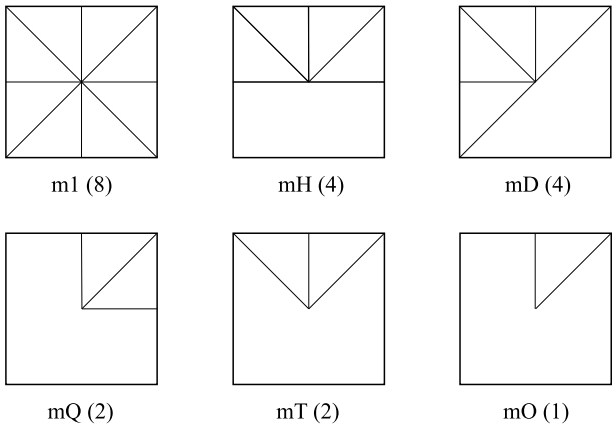

Fig. 5.5 Macro-symmetry basic meshes, based on parts of the full geometry, with mirror reflections assumed for symmetry considerations. Basic meshes were systematically refined to computational meshes. Neither solutions nor modes can be found with symmetry lower than: $C_s(\sigma_2)$ for mH, $C_s(\delta_2)$ for mD, $C_{2v}(\sigma)$ for mQ, $C_{2v}(\delta)$ for mT and C_{4v} for mO

try of the subgroup used in reconstruction, which means that equilibrium solution branches of lower symmetry are unreachable. While this is perfectly valid for a linear equilibrium solution[10], it is in general not sufficient for the stability analyses, with potential symmetry-breaking in critical modes.

A set of macro-symmetry representations are shown in Fig. 5.5, with their symmetry group in the figure caption. These were used together with reflection displacement boundary conditions only, even if other symmetry representations are possible, such as half-turn rotations of the mH mesh around a normal or in-plane axis. The basic meshes were refined systematically by a division of each triangle into four new ones, with nodes on the midpoints of the existing edges. The used meshes are denoted by the 'mX' notation for a particular basic mesh, and a number of triangular elements in the mesh within parentheses[11]; this means that the symmetry introduced by the basic mesh is kept in the refinement. Relevant displacement boundary conditions for the respective meshes are obtained rather easily, even if care is needed in order to avoid over-constraining the model[12].

In these experiments, similar meshes were considered in the sense that models of half the structure used half the number of elements as the full model. Therefore, the solutions for the different meshes are identical as long as a solution or a mode is requested, which fulfills the full symmetry of the basic problem. Less symmetric solutions will possibly be unreachable for some of the meshes.

---

[10] where symmetric forcing of a symmetric structure will give symmetric results

[11] For instance, the mH(256) mesh has undergone three such refinements from the basic mH(4) mesh

[12] which will always tend to increase stiffness and thereby can over-estimate critical forcing

Table 5.3 Number of critical eigenvectors found for set of macro-symmetry models, according to Fig. 5.5

Mesh.	1. (B_{2u})	2. (B_{1u})	3. (A_{2u})	4. (E_g)	5. (A_{1u})	6. (E_g)	7. (A_{2u})
m1 (512)	1	1	1	2	1	2	1
mH (256)	1	-	1	1	-	1	1
mQ (128)	1	-	1	-	-	-	1
mD (256)	-	1	1	1	-	1	1
mO (64)	-	-	1	-	-	-	1
Converged	1	1	1	2	1	2	1

A minus sign indicates that the critical state was not found. Values for the critical states are given in Table 5.4

Results from a few simulations are shown in Table 5.3. The numbers for the different meshes and the seven critical (bifurcation) states show how many critical eigenvectors were found in the experiments. The comparison should be made to the final row, which shows the correct numbers, obtained with the 'Converged' solution of full symmetry, and full capacity to represent eigenvectors of any symmetry property. The numerical results for critical tractions are given for the m1(512) mesh in Table 5.4; identical values were obtained for the other meshes in Table 5.3 if the critical state was at all found.

Minus signs in the table imply that the critical state is not seen at all[13], and cannot be represented by the model. When the mH mesh enforces a reflection symmetry over a plane through the horizontal in-plane axis, it is incapable to show, e.g., mode 2 in Fig. 5.4. For the same reason, it is also incapable to show mode 4b; this reduces this bifurcation to have just one critical eigenvector: mode 4a.

The mO mesh, which is a minimal representation of the linear equilibrium, cannot represent most of the bifurcations for the present problem, when only using reflection symmetry conditions on the edges. When introducing also other types of conditions for the modes, all the bifurcations can be captured by individual treatment of each class of symmetry.

It is also clearly seen from the table, that the capacity of a certain mesh to show the critical states is related to the mode type; the Table columns for modes 3 and 7, but also those for modes 4 and 6 are identical.

[13] and not just inaccurately described

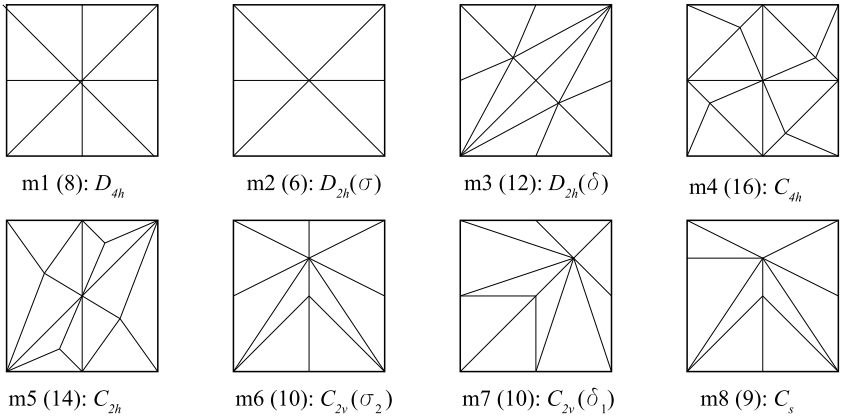

Fig. 5.6 Micro-symmetry basic meshes, based on the full geometry. Meshes represent different symmetry groups, as noted for each mesh. Meshes re-drawn from study by Eriksson and Nordmark (2016)

Micro-symmetry models

Micro-symmetry aspects in the modeling are shown by models of the whole region, where degrees of symmetry are introduced by the element mesh. Eight basic models are given in Fig. 5.6. The symmetry groups of the meshes are given together with the basic mesh names in the figure. It is noted that the meshes in the figure represent all possible classes of mesh symmetry for the present problem, even if some of the meshes have companions created by rotations in the plane; this is obvious for, e.g., the m2 mesh.

Simulations with instances of all the different mesh classes verified that all critical states were found for all meshes, but with very different accuracies. Table 5.4 shows the critical traction values obtained for a set of meshes, where each evaluated critical mode is referred to the converged mode it most resembles[14]. In particular for coarse meshes, bifurcation states were found, where the mode could not be clearly identified in relation to the converged solution, and was a mixture of several basic modes.

One general comment on the results is that the coarse meshes tend to bring out the two first critical situations in the wrong order. This is also the case for the most symmetric m1 meshes[15], emphasizing that both mesh symmetry and mesh refinement are of importance for the accuracy of results. It is also notable that meshes of type m4 are the only ones, in addition to the m1 meshes, which find the double modes in the E_g cases.

[14] which demands a manual, visual, identification of mode shapes for the irregular meshes

[15] for even coarser meshes than the ones in the table

Table 5.4 Critical traction levels for a set of micro-symmetry meshes

Mesh	1.(B_{2u})	2.(B_{1u})	3.(A_{2u})	4.(E_g)		5. (A_{1u})	6.(E_g)		7. (A_{2u})
m1 (128)	0.1691	0.1776	0.2777	0.4191		0.8601	0.9329		0.9426
m1 (512)	0.1675	0.1814	0.2760	0.4229		0.8383	0.9047		0.9780
m2 (96)	0.1704	0.1694	0.2738	0.3895	0.4116	0.8318	0.8941	0.9029	0.8566
m2 (384)	0.1680	0.1784	0.2750	0.4125	0.4214	0.8313	0.8995	0.8978	0.9521
m4 (64)	0.1737	0.1663	0.2735	0.3971		0.8575	0.9318		0.8865
m4 (256)	0.1685	0.1774	0.2750	0.4155		0.8436	0.9071		0.9474
m5 (56)	0.1854	0.1488	0.2662	0.4130	0.3343	0.7549	0.8559	1.1230	0.8453
m5 (224)	0.1723	0.1738	0.2735	0.4245	0.4058	0.8912	0.9062	0.9656	0.9314
m8 (144)	0.1707	0.1744	0.2787	0.4184	0.4265	0.8844	0.9593	0.9324	0.9921
m8 (576)	0.1680	0.1806	0.2762	0.4256	0.4232	0.8478	0.9111	0.9151	0.9882
Converged	0.1670	0.1834	0.2755	0.4258		0.8347	0.8959		0.9937

Modes are visually identified to those of converged solution

Further experiments showed that the shortcomings existing in a basic mesh remain, but are reduced by more refined versions. That all critical states were found for all mesh types is a difference to the macro-symmetry models above, for which some critical states totally disappeared. The result also deviates from the work referenced above, where bifurcations were replaced by limit states for several mesh types.

5.3.3 Secondary Branches

The previous discussion has been concerned with the isolation and identification of critical states on the primary equilibrium branch, and showed that obtained results are strongly dependent on the discretization mesh. For a mesh of sufficient symmetry, all existing equilibrium branches can be traced with the methods from Chap. 4, and classified by their symmetry group.

The existing symmetry in a discretization mesh affects the representation of secondary branches to a higher degree, as these branches belong to lower symmetry groups. The possible critical states, i.e., primarily bifurcation states demand an analysis of the subgroups of the D_{4h} symmetry group.

Critical states can also be identified with respect to their mode types, and solutions with respect to their symmetry groups. The result is a tree structure of equilibrium branches, as shown in Fig. 5.7. The branches were evaluated by tracing sequences of equilibria emanating at the bifurcation states above. All equilibria in all sequences were numerically analyzed with respect to symmetry, and classified as belonging to a particular symmetry group.

This tree is schematic, in the sense that branches are just pointing upwards or downwards, depending on the initial derivative of the traction value along the branch. Only three levels of branches are also shown; most of the outer branches pass through new critical states when following them far enough. In the figure, branches with

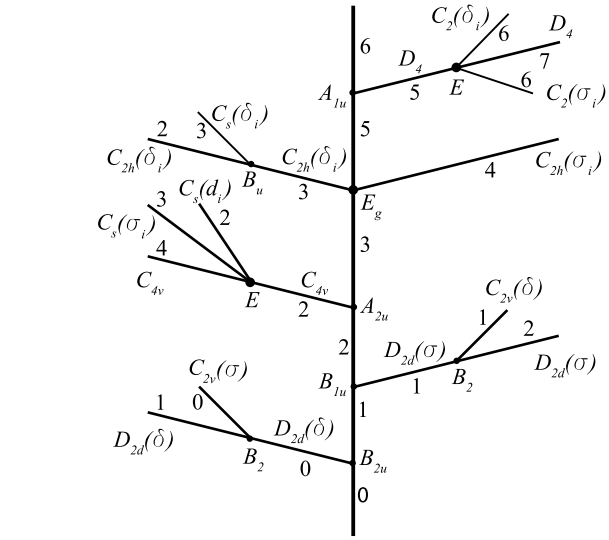

Fig. 5.7 Bifurcation tree for the example. Primary, secondary and ternary equilibrium branches. Branches are marked by their symmetry group, and the number of negative eigenvalues for all states. Bifurcation states are marked by mode type

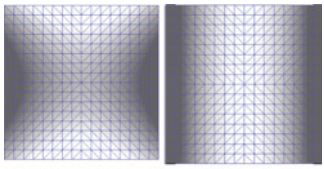

Fig. 5.8 Stable equilibrium solutions, with color shading showing transversal deflection. **a** Situation on $D_{2d}(\delta)$ path at bifurcation of mode B_2. **b** Situation far out on branch $C_{2v}(\sigma)$

symmetry group names including (δ_i) or (σ_i) are representing two cases, each with two directions (i.e., four additional branches emanating at the bifurcation), while all other branches represent one case, with two directions.

The equilibrium branch tree shows that one stable solution sequence—marked by zeroes in the figure—exists for the problem. This sequence passes two bifurcations of mode types B_{2u} (for D_{4h}) and B_2 (for $D_{2d}(\delta)$) to come to a branch where solutions belong to the $C_{2v}(\sigma)$ symmetry group. This solution branch can be followed very far out, without new critical states. Equilibrium states at the B_2 bifurcation state and far out on the $C_{2v}(\sigma)$ branch are shown in Fig. 5.8, with a color shading for the transversal deflection[16].

[16] In-plane displacement is considered in plotting the figure, but is not visible.

Table 5.5 Numbers of modes in different types for m1 meshes

		Mode types									
Mesh	$N_d - N_c$	A_{1g}	A_{2g}	B_{1g}	B_{2g}	E_g	A_{1u}	A_{2u}	B_{1u}	B_{2u}	E_u
m1(128)	$486 - 6 = 480$	26	34	30	30	60	26	34	30	30	60
m1(512)	$1734 - 6 = 1728$	100	116	108	108	216	100	116	108	108	216

Valid at all equilibrium states

The figure shows that the final buckled shape is cylindrical, of symmetry $C_{2v}(\sigma)$, which is mirror symmetric over both axis planes. To reach this stable state from the initial plane configuration, the structure must pass through stable equilibrium states of symmetry $D_{2d}(\delta)$, which have two mirror planes, but also are symmetric for a half-turn rotation around the diagonals.

5.3.4 Comments to the Problem

Mostly out of curiosity, all modes were evaluated for all equilibria found on the primary equilibrium sequence for some of the discretized models above. These evaluations confirmed that a particular discretized model implicitly leads to sets of eigenmodes of the different types. For two of the m1 meshes, results are given in Table 5.5. The distribution on mode types is kept for the whole sequence.

Previous work shows that eigenvalues for mode vectors of different symmetry groups cross independently along a one-parametric forcing sequence, while eigenvalues within the same group never do so; the phenomenon of mode veering appears, in which the modes are smoothly mixed without crossing. When adding the total number of modes, it must be noted that the E_g and E_u mode types contain two eigenvectors each, leading to the correct numbers of free displacement components.

Also out of curiosity, a verification was performed to show that a macro-symmetry meshing of the full region is unable to reproduce all critical states. The bifurcation tree in Fig. 5.9 shows the results obtained by an mH(256) model in the same format as the correct tree in Fig. 5.7.

The symmetry of the problem also suggests other approaches to solving it. While utilization of symmetry in a problem was a necessity in early days of numerical simulations, it can still seem tempting to reduce the computational burden by not reproducing many numbers in a solution. A computational model of any of the forms in Fig. 5.5 can allow this, but needs care in formulation of boundary conditions. All transformations within the symmetry group must be considered, and several models used, equipped with different sets of conditions for modes of different types. A particular aspect of this is that the primary equilibrium solution and the extraction of eigenvectors are not to be performed with the same conditions.

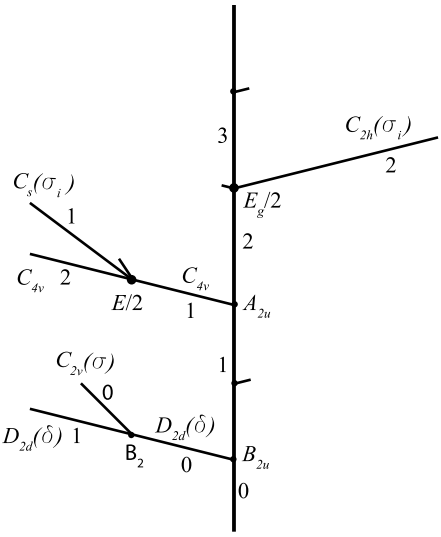

Fig. 5.9 Bifurcation tree for the example, when modelled by an mH(512) mesh, and boundary conditions representing a reflection over a plane parallel to the horizontal in-plane axis of Fig. 5.3. Figure is emphasized as a subset of Fig. 5.7, by leaving small stumps of non-existing branches

5.4 Stability Under Contact

In many relevant structural simulation, the object is affected by some external restriction where contacts will be established during forcing; one example is the buckling of a confined beam under compression; another is related to piles buckling against an elastic foundation. Contact conditions in a discretized mechanical model always lead to complex modelling issues, in particular when frictional contact forces are present, due to history-dependence and non-conservative effects. Even for smooth contacts without friction, the interaction between contact and stability is of interest, and this case will be discussed here; the basic formulation is the constrained equilibrium model in Sect. 3.6.4.

The example shows how the discretized model, regardless of fineness in the representation, creates artifact critical situations in addition to those having a physical meaning. The description, for clarity, discusses a simple $2D$ model which clearly shows this interaction.

The structure is a strip of an infinitely long pressurized membrane, cf. Fig. 5.10a, made of a linearly elastic St Venant-Kirchhoff material defined in Sect. 2.4.2. The membrane is stress-free in a sectorial shape with radius R_0 and a circumference corresponding to an angle $2(\pi - \beta)$. The membrane is expanded towards a rigid friction-less flat surface at a specified height H.

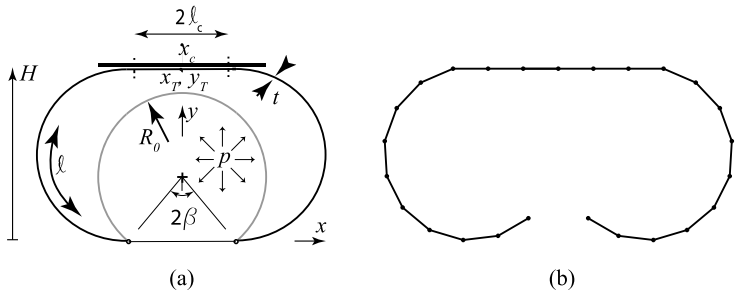

Fig. 5.10 Example problem. Numerical experiments performed with $R_0 = 100\,\text{mm}$, $\beta = 30°$, $t = 0.5\,\text{mm}$, and width 1 mm. Material described by $E^* = \frac{E_m}{1-\nu_m^2} = 1.69\,\text{MPa}$. **a** Model with main parameters. **b** Calculated equilibrium for $p = 50.2\,\text{kPa}$

The structure was computationally modelled by 24 linearly interpolated bar elements, with transversal uniform pressure. Coordinates (x_T, y_T) define current position of the initial top point, (x_c, H) the current mid-contact position[17]. Subfigure (b) shows a relevant solution having seven nodes in contact, revealing that the model was rather coarse[18].

5.4.1 Primary Branch

The primary equilibrium branch for this problem gives an increasing volume for increasing over-pressure, together with an increasing number of nodes in contact; the equilibria are symmetric with respect to the (y, z) plane. The nodes in contact are described as $[n_1, n_2]$, indicating the intervals of nodes in contact, with zero for the initial top point; the solution in Fig. 5.10b is denoted $[-3, 3]$.

Figure 5.11a shows three kinematic result variables for a case with $H = 2.5R_0$; these are rather obvious, as the contact length increases both in jumps when new nodes go into contact and continuously with the expansion. Subfigure (b) shows the lowest eigenvalue of the operative, constrained, stiffness[19], considering the current contact condition. The eigenvalue gradually decreases within each interval of identical contact status, but is immediately increased when a new node comes into contact, as constraints tend to increase stiffness. The dashed graph in (b) shows that the eigenvalue for an unconstrained model is monotonously increasing with pressure; no contact exists, and the primary equilibrium sequence is then always stable.

[17] which, together with the current contact length $2\ell_c$ is the main parameters in an analytical treatment

[18] With a rigid contact surface, the membrane is straight in the contact region.

[19] normalized to the lowest eigenvalue at a solution with a top deflection of 1 mm

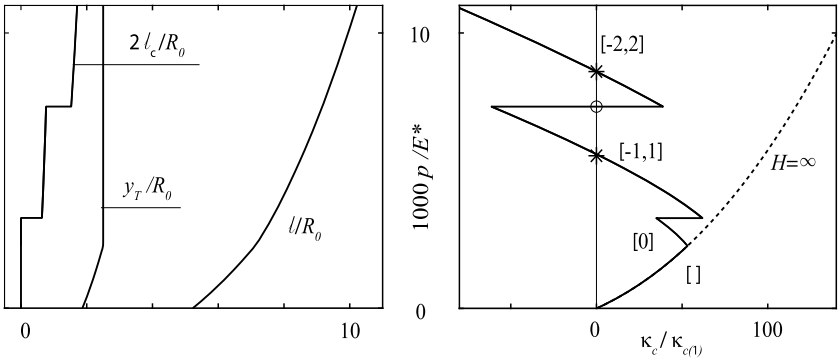

Fig. 5.11 Primary equilibrium sequence for the example with $H = 2.5R_0$. **a** Geometric results. **b** Normalized lowest eigenvalue of operative stiffness

A change of stability, i.e., a changing number of negative eigenvalues, is obtained twice on the continuous branch segments of constant contact status, and once at a discontinuity where a new (symmetric) contact pair appears.

The two continuous zero-crossings are easily isolated with the bracketing methods in Sect. 4.5.6, and are interpreted as bifurcation states, where sideways movement of the structure can be initiated. An analytical treatment of a sideways deflected state[20] shows that the continuous structure has a single bifurcation state. One of the critical states from the discretized model is thereby an artifact.

In general, for most parametric cases, two, but not more, continuous zero-crossings will be recorded in a simulation for increasing forcing, but only one bifurcation occurs for small intervals of H; for the example parameters, this happens for, e.g., $H = 4.2R_0$. These are here denoted 'symmetric bifurcation' states. For all bifurcations, higher order differentials of total energy give positive contributions when tracing the secondary sequence out from the critical state: the bifurcation states are super-critical, i.e., with stable secondary branches emanating from them. In the engineering context, the secondary branches tend to turn upwards in a common force-displacement graph.

[20] which is not too difficult to obtain, as the deformed model always consists of one straight and two circular segments

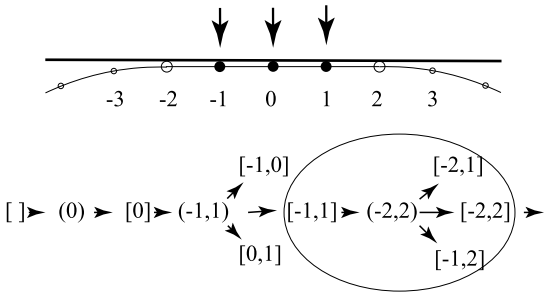

Fig. 5.12 Notation for contact evolution description in the example. Sequence of contact states for a monotonous inflation of the structure against a frictionless rigid surface. The large ellipse implies that all these contact states can be valid immediately neighboring the grazing solution state, and thereby give different stability conclusions

5.4.2 Contact Evolution

The discontinuous crossing of the critical eigenvalue in Fig. 5.11b corresponds to a change of contact status; two new symmetrically placed nodes come into contact, and the stiffness thereby increases. This change of stability is also detected by the bracketing procedure on the primary branch, but not as a critical state in the sense of a singular constrained stiffness. The situation must instead be analyzed by a study of the grazing contact state, cf. Sect. 4.4.

Figure 5.12 shows the development of contact along a primary sequence, with a fixed contact height H. Open circles and curved parentheses indicate a grazing state for a point, where new nodes are in contact, but still without contact force. With the exception of first contact, each grazing state offers three different continuations to the increased expansion, where one keeps the symmetric contact states by adding two contact nodes, while the other two are unsymmetric, and just add a contact node on one side[21]. Due to the discretized setting, this does not imply that any node simultaneously must lose contact, and thus, the new contact will add stiffness. Whether any equilibrium state with this contact state exists close to the state of grazing contact is not certain; if such a state exists, also the mirror contact state exists. These situations can lead to secondary sequences, even if no zero eigenvalue is present, and the grazing states are here denoted 'symmetric branching' states, the term denoting that similar branches exist with the structure moving in either direction.

The algorithm described in Sect. 4.5.6 finds and isolates not just bifurcations, but also the changes of contact status. After an evaluation of the bracketing states, the sequence is then continued with an updated contact status.

[21] This demands a sideways movement

Focussing on the encircled part of Fig. 5.12, with a grazing contact $(-2, 2)$, the four contact states $[-1, 1]$, $[-2, 2]$, $[-2, 1]$ and $[-1, 2]$ are all valid for immediately neighboring situations, but none of them is valid for the state $(2, 2)$.

Each considered hard contact node essentially introduces one extra structural support. The incremental stiffness—which is independent of contacts and identical for all the contact states meeting at the grazing state—as part of the operative stiffness in Eq. (3.92) is thereby extended by, respectively, 3, 5, 4 and 4 constraint rows for the four neighboring situations. These constrained stiffnesses can be evaluated, regardless of whether the unsymmetric cases lead to equilibrium sequences, and give different eigenspectra for the four cases. A systematic investigation of the four cases reveals the properties of this grazing contact state.

Symmetric branching states are in some sense similar to bifurcation states, even if they do not correspond to a vanishing eigenvalue for the operative stiffness. Both situations allow unsymmetric secondary displacement states in either direction. For instance, the contact state $[-1, 2]$ can only exist if all the contacting nodes move to the right in Fig. 5.12. From the numerical viewpoint, the symmetric bifurcation and branching states differ in the sense that the former lead to continuous branches through the critical state, while the latter give two different branches meeting at the grazing state.

The grazing contact states are obviously of major importance in describing structural response. Even if they are singular points on a parametric loading sequence for a particular fixed structure, they can be traced as graphs in multi-parametric formulations, and then delimit different qualitative response regions for a structure, cf. below.

5.4.3 Secondary Branches

Each of the two continuous and one discontinuous zero crossings for the critical eigenvalue of the operative stiffness in Fig. 5.11b can initiate a secondary, unsymmetric equilibrium branch for the model. Once initiated, this displacement can be traced with methods from Sect. 4.1.6. Results are shown for two contact height cases in Fig. 5.13, expressed as the over-pressure related to the horizontal position x_T of the initial top node. Contact states can be deduced for points on the graph segments by noting the discontinuities and their effects. The primary equilibrium branch is shown by the vertical central line. The far-reaching secondary branch clearly shows the changes of contact states as discontinuous slopes, and contains unstable parts, where the pressure is reduced for increasing displacement.

For subfigure (a), the first secondary sequence emanates at a $[-1, 1]$ bifurcation, and can be traced far out for unsymmetric solutions, with continuous subsequences of equilibria with 3 or 4 contact nodes. The equilibrium states on the sequence are unstable for just a short part between $x_T \approx 0.65 R_0$ and $x_T \approx 0.83 R_0$ for contact state $[-2, 0]$, otherwise stable. This is the discrete representation of the analytical case.

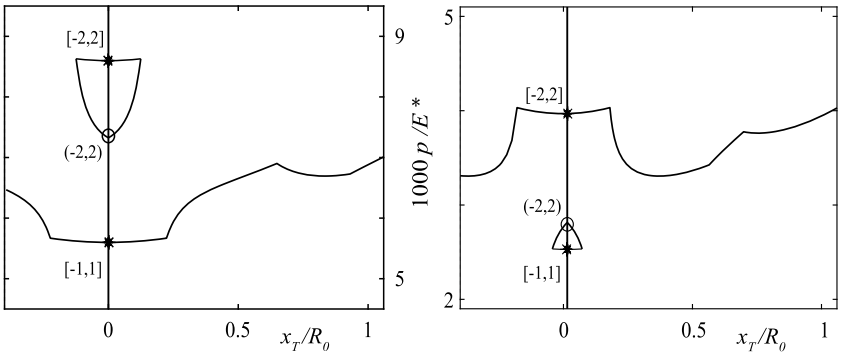

Fig. 5.13 Secondary equilibrium sequences for example, shown as horizontal displacement x_T of initial top node versus over-pressure. **a** $H = 2.5R_0$. **b** $H = 2R_0$. Note the different vertical scales

The upper secondary equilibrium sequence emanates at a $[-2, 2]$ bifurcation, and solutions are all stable. This sequence only exists for a rather short interval, delimited by two branches—$[-2, 1]$ and $[-1, 2]$—which are both connected to the primary equilibrium branch at grazing contact state $(-2, 2)$. Figure 5.13b shows a rather different outcome, even if the same phenomena appear on the primary branch. The symmetric branching state is indirectly connected to the lower bifurcation state, and large parts of the far-reaching secondary branch are unstable.

Comparison of the two cases in Fig. 5.13, shows that the correct and the artifact bifurcations can come in any order on the primary path; the distance—measured in forcing parameter—can also be substantial[22]. Further experiments show that the difference is reduced with finer discretizations, but the phenomenon of artifact situations does not disappear. The precise stability behaviour is very strongly parameter dependent.

5.4.4 Parametric Investigations

The two classes of eigenvalue zero-crossings, discussed in connection with Fig. 5.11, i.e., the symmetric bifurcation and branching states, are further investigated with the generalized equilibrium approaches from Sects. 4.4 and 4.6.3. As one example, the parameters considered are the forcing pressure p and the contact height H, cf. Fig. 5.10.

Critical equilibrium states with symmetric bifurcations were evaluated through parametric critical sequences in the (H, p) space. Two selector functions are needed for this: one criticality selector from Eq. (4.34), and one increment selector function from Sect. 4.4.3, the choice of which is of minor importance here. For reliable convergence along this sequence, a further equation $x_T = 0$ was introduced in order to

[22] even if this partly is due to a not too well refined computational model

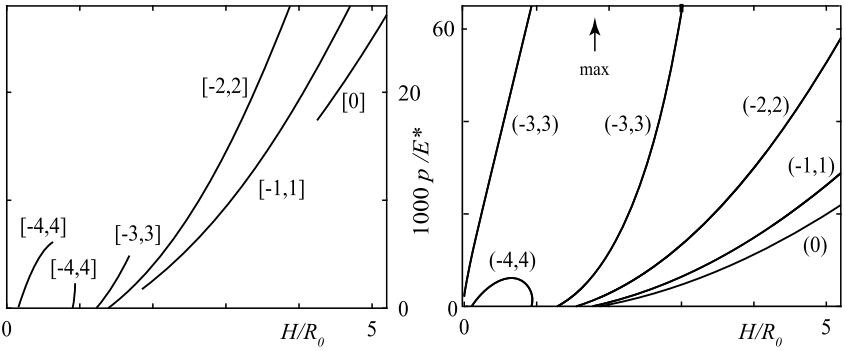

Fig. 5.14 Parametric dependence of eigenvalue zero crossings for example. **a** Symmetric bifurcation states. **b** Symmetric branching states. Note the different vertical scales, and that the $(-3, 3)$ graph in **b** is closed (outside the figure)

ensure only symmetric equilibria[23]. This selector was enforced by a horizontal force f_{x_T}, which vanishes for all solutions; note that the sequence follows bifurcation states on the primary branch.

As each sequence of bifurcation states in the parametric space corresponds to a particular contact state, simulations need be started at a selection of bifurcation states, found for particular primary cases[24]. The end of such a graph is defined by a transition equilibrium state beyond which no legal continuation exists.

Results from such simulations are shown in Fig. 5.14a, one critical equilibrium sequence for each symmetric contact condition. The $[-4, 4]$, $[-3, 3]$ and $[-2, 2]$ critical sequences gave distinct upper end points, while the $[0]$ and $[-1, 1]$ sequences continued to at least $H = 100\, R_0$. At the lower end, all graphs except the $[0]$ and $[-1, 1]$ critical sequences exist down to $p = 0$. It is noted that $H < R_0$ implies that the contact height is lower than the unstretched height of the structure, so equilibrium will imply at least one contact.

Similar simulations were performed for the grazing contact states, where a symmetric branching can be initiated on the primary branch. Parametric equilibrium sequences thereby evaluated combinations of surface height H and over-pressure p, for which a specific grazing contact state exists on a primary equilibrium sequence. The constraints and selectors were set according to Sects. 3.6.4 and 4.4. Results are given in Fig. 5.14b.

Figure 5.14b deserves a special comment. As discussed in Sect. 4.4, and for this particular problem[25], a symmetric grazing state situation on the primary branch can be expressed in two ways. First, the situation may be defined by established contact constraints for nodes $-N_c + 1, \ldots, N_c - 1$ together with displacement conditions

[23] or the sequence will easily deviate a little bit to solutions on the secondary branches

[24] Two of them were found from the primary solution depicted in Fig. 5.11b

[25] In particular, the $1D$ form and the pressure forcing, together with a structure without bending stiffness, does not allow any contact to leave the contact surface when forcing is increased

for the nodes $-N_c$ and N_c. This defines the outer nodes to be touching the contact surface, but without contact forces. While the established contacts give $2N_c - 1$ constraint equations in the operative stiffness, the displacement conditions give two selector equations; the situation is denoted a 'displacement form' below.

Second, the nodes $-N_c, \ldots, N_c$ are defined as constrained, and affecting the operative stiffness. The grazing contact state then corresponds to the contact forces in nodes $-N_c$ and N_c existing, but vanishing. These force conditions are thereby two selector equations added to the $2N_c + 1$ constraint equations included; the situation is denoted a 'force form' below.

The two forms give identical equilibrium solutions but different stability conclusions. As the force form introduces more constraints, it will always give higher stability coefficients. This implies that regions may exist, where the same equilibrium solution is stable in the force form but unstable in the displacement form. Figure 5.14b gives results from both settings, but the stability conclusions were also obtained from simulations. From these, with very accurate isolations, the equilibria on the $(-2, 2)$ graph are stable for $H < 1.85R_0$ based on the displacement condition, and for $H < 4.17R_0$ for the force condition. The $(-1, 1)$ and (0) graphs are always stable with a force condition, whereas both the $(-3, 3)$ and $(-4, 4)$ have regions of stability for the force conditions, while they are always unstable with the displacement conditions.

The three graphs marked (0), $(-1, 1)$ and $(-2, 2)$ seem to continue monotonously even for very high H, while the graphs for $(-3, 3)$ and $(-4, 4)$ indicate that the number of contacting nodes will again decrease with increasing pressure p for low H. This implies that a multi-contact state will be established already for very low pressures. Bringing together all the results from Fig. 5.14 shows that the symmetric bifurcation graphs in (a) connect the states of changing stability on the graphs in (b), but these results are beyond the scope of this treatise.

5.4.5 *Soft Contact Modelling*

As an alternative to the hard contact modeling above, with strict constraints on contact nodes, soft contact modelling was introduced for all nodes where $y_j > H$, according to the third-order penalty form

$$F_j = k_j \, (y_j - H)^3 \quad ,$$

where the penalty constant was chosen in relation to the number of elements along the unstretched circumference. The third-order form avoids a discontinuity in the incremental stiffness.

Results are shown in Fig. 5.15, for two different choices of the penalty coefficient k_j, differing by a factor of 100. Subfigure (a) should be compared to Fig. 5.11b, and subfigure (b) to Fig. 5.13a, which both were evaluated for hard contacts. It is noted

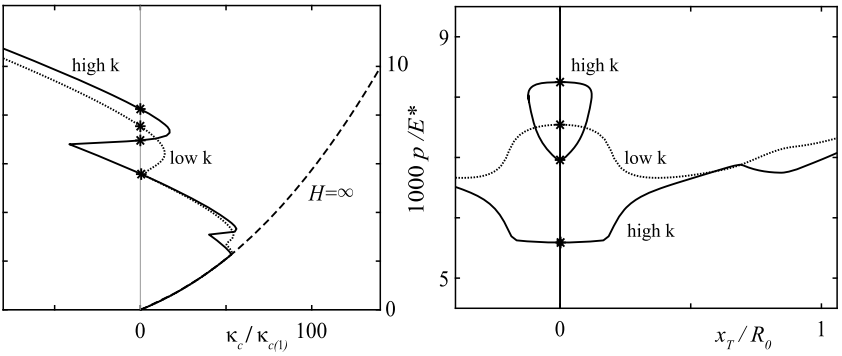

Fig. 5.15 Results from the example, evaluated with soft rather than hard contact formulation, and with two different penalty constants. **a** Eigenvalue variation. **b** Secondary sequences. Note the difference in vertical scale, and that the 'low k' case does not reach the zero line more than once (even if it is very close)

that the 'low' case only shows one zero-crossing for the eigenvalue[26], and thereby only one secondary branch.

Comparing to the hard contact case, the single zero-crossing for the 'low' case appears at a pressure about 30% higher than the analytical value; subfigure (b) shows that the single secondary sequence from this state deviates strongly from all other cases presented. The 'high' case gives three bifurcations, with continuous zero crossings for the lowest eigenvalue, as also the intermediate one is possible to isolate. The secondary sequences are then similar to the hard contact case, but without discontinuities. All simulations with soft contacts give results that more or less significantly penetrate the contact surface.

5.4.6 Comments to the Problem

The simulation model reported above was rather coarse, in order to show the phenomenon of artifact criticalities. Other simulations were also performed with finer meshes for the same problem. Even if the gap between the two appearing bifurcations is reduced with a finer mesh, the phenomenon remains. As one comparison, the model above (24 elements) gave the critical pressures as $p = 5.60$ and 8.60 times $E^*/1000$, respectively, with the physical bifurcation as the first one. For a finer mesh with 192 elements, the multipliers of the critical pressures were obtained as 6.04 and 6.34, respectively, with the artifact bifurcation now as the first one. The bifurcation appeared for the $[-1, 1]$ and $[-2, 2]$ contact conditions for 24 elements, and for $[-10, 10]$ and $[-11, 11]$ contact conditions for 192 elements.

[26] even if it comes very close at a lower pressure

From the algorithmic viewpoint, it is noted that the soft contact modeling gives a somewhat smaller operative stiffness matrix, and that the changes of the number of contacts is only needed for presentation of results. Linear and third-order forms are almost identical in handling. The discontinuity in the operative stiffness appearing for the linear form gives some, but limited, effects on the convergence of equilibrium iterations around states where new nodes start penetrating the contact surface.

The same treatment can be used also for other problem classes, where for instance contact conditions for membranes and shells are a tempting possibility. It is expected that similar problems with artifact critical states will appear also for such problems. Not least the symmetric branching states will be more demanding for these problem classes due to the high numbers of possible changes to contact conditions at a grazing state. When a problem with bending stiffness is analyzed, the contact patterns can also be different, with, e.g., nodes leaving the contact.

5.5 Final Comments

This chapter has to some depth discussed three aspects of computational modelling which can be of importance for the practical numerical treatment of stability-affected structures under exterior forcing. Obviously, these only represent a small subset of the possible settings of the problem class, but they have hopefully given some ideas on suitable treatment of also other types of problems. This final section will very briefly point to a few areas, where a numerical modelling always needs extra care when adopted for an engineering problem.

One important aspect is concerned with the material modelling. Although the majority of stability investigations are probably performed using ideally elastic materials, other material models, such as the Mooney-Rivlin model in Sect. 2.4.2, can be highly relevant. It is also important to consider the limits for elastic behavior in a material. Related to the example in Sect. 5.2, where interaction between global and local buckling was considered under elastic conditions, the possibilities for plastification can be an aspect in the solution and in the stability conclusions. Also, time-dependent material descriptions such as visco-elastic effects can be of relevance, even when only equilibrium is considered.

Some material models can also give rise to stability issues, at least for particular forcing situations. Previous work by the authors has shown how an incompressible Mooney-Rivlin material model can lead to unstable solutions under a specific stress situation. Also other non-linear material models can lead to unstable situations.

Even if not strictly an issue of material modelling, a constitutive model can cause other types of difficult stability issues. One case is in the wrinkling, appearing typically in thin membrane or shell problems. This reduces the carrying capacity of the material in the directions of principal compression. Numerical handling of this phenomenon is often based on so called tension field models, where stiffness is reduced or removed in critical directions. In certain situations, this can lead to local instabilities, which are affecting the whole response, as shown by Patil et al. (2016).

Another main aspect in the analysis of stability-affected structures is related to the description of the exterior forcing, which affects its computational modelling. Several aspects must be considered, when the structure and forcing need be described as non-linear in displacements and deformations. This needs care in describing the positions and directions of the exterior forcing components, as discussed in, e.g., Sect. 2.6.4.

The forcing not least needs special care when representing other classes of forcing than gravity forces from the structure itself or from some supported objects. In this respect, forcing from gas or other fluids need careful description and quantification. So can gas included in a closed structure be modelled as either an over-pressure (acting on a deformable structure) or as a gas amount. This topic was discussed in relation to constrained equilibrium settings above, and the difference in viewpoint was shown to have significant effects on the stability evaluation. Forcing from liquids, in the form of hydro-static pressures, can also be described in different ways, in a parametric context; the parameter used can be of importance for both the problem relevance and diverse computational aspects.

While the forcing is one aspect of boundary conditions for a structural model, and acting on the boundary part Γ_T of a region, the displacement conditions on Γ_U are also of major importance for the outcome of the simulations, and in particular the stability conclusions. As noted already from the analysis of the Euler beam buckling cases in Sect. 1.4, the assumed boundary conditions are fundamental to the calculations, even if the structural models in themselves are identical between cases. At least two aspects of displacement boundary conditions are of major importance, and both were considered in Sect. 5.2.

The first aspect concerns the relation to reality, and in particular to the assumptions used for traditional analytical approaches. In a computational model, it is desirable to describe the physical situation for the modelled structure as accurately as possible: without going into all the smallest details of support (and also forcing) arrangements; important aspects should be considered in the modelling. The key question is often to which degree supports should be seen as points or as distributed—where point conditions are common in most analytical treatments, but non-existing in reality. As noted in connection with the example in Sect. 5.2, the difference between the common analytical conditions and a more realistic representation can be of significance for results: the description of an ideal hinge is not always trivial in a computational model. A basic aim with the numerical models is also always related to model balance, interpreted as equally refined descriptions of all aspects of a model.

In connection with boundary conditions, it is also necessary to introduce these in such a way that both global and local views are represented. Connected to the previous paragraph, point-wise force applications or supports tend to give localized effects due to the singularity in the model, with local phenomena over-shadowing the, perhaps more interesting, macroscopic response. In particular if material non-linearities are considered, local stress concentrations can lead to local instability around the point source, a problem which may be restrained by the real physical conditions. In this context, it is always interesting to consider whether the realistic

support is best modelled as a contact condition, even if this does not affect the stability situation as clearly as in the example in Sect. 5.4.

The final comment is concerned with structural optimization, where stability aspects on a structural model are not trivially included. As has been very briefly mentioned in Sect. 4.4.1, the parametric view on structural modelling promoted in this treatise can be very interesting in the context of mathematical structural optimization. The main idea in this is to easily and clearly define the boundaries of the feasible region coming from stability constraints on the solution. Several other classes of constraints can also be introduced through the parametric solution methods discussed in Chap. 4.

Conclusions from this Chapter

The Chapter has shown a set of special situations, where stability investigations are possible, but when these have to be handled with extra care. The implicit view is that some commercial software is used to evaluate the structural response to forcing. A main message is that, although the software might be competent to set up the desired situation and present its results, these may be difficult to interpret without a deep insight into both the mechanical problem modeled and the exact numerical implementations. The Chapter thereby has had as one objective to show also drawbacks and potential pitfalls when using general software for structural stability investigations.

In addition to pointing to some far from trivial problem areas, where care must be taken in simulations, the Chapter has tried to show how the general approaches from the previous Chapters can be used to fully reveal the stability properties of a parametric structural model. Some of the approaches discussed in Chap. 4 can be utilized for this mapping in general software, but some of the approaches need more elaborate solution methods not commonly available. This not least relates to more integrated design processes, where the structural stability analysis is part of a wider view, for instance when integrated design or mathematical optimization procedures are used.

Task for this Chapter

1. Pick any of the problems discussed in the Chapter, or any interesting variation of it. Analyze it in an available software. First, aim at the closest possible reproduction of the results given here, and discuss similarities and differences. Then, try to improve the modeling in order to approach a relevant representation of (some) reality. Comment on results and interpretation.

References

Conway J, Burgiel H, Goodman-Strauss C (2008) The symmetries of things. CRC Press
Cotton FA (1990) Chemical applications of group theory, 3rd edn. Wiley
Eriksson A, Pacoste C (2002) Element formulation and numerical techniques for stability problems in shells. Comput Meth Appl Mech Eng 191:3775–3810
Eriksson A, Nordmark A (2016) Symmetry aspects in stability investigations for thin membranes. Comput Mech 58:747–767
Ikeda K, Murota K, Fujii H (1991) Bifurcation hierarchy of symmetric structures. Int J Solids Struct 27(12):1551–1573
Patil A, Nordmark A, Eriksson A (2016) Instabilities of wrinkled membranes with pressure loadings. J Mech Phys Solids 94:298–318
Zingoni A (2014) Group-theoretic insights on the vibration of symmetric structures in engineering. Philos Trans Royal Soc A 372:20120037

Notation

General Symbols

Symbols	Explanation
$\mathbf{A}$	Physical vector, represented by its three coordinates
A	Second-order tensor, represented by 3-by-3 matrix
$\mathcal{A}$	Fourth-order tensor
$\underline{A}$	Numerical vector, i.e., a column matrix
$\underline{\underline{A}}$	Numerical matrix
$\underline{\bullet}$	Row matrix of quantities, operated on by numerical vector
$\underline{\underline{\bullet}}$	Matrix of quantities, operated on by two numerical vectors
m-by-n	Dimension of a matrix ($n = 1$ for a numerical vector)
$\mathsf{1}$	Identity tensor in vector space
$\underline{\underline{1}}_{\bullet}$	Identity matrix of indicated order
$(\bullet)^{\mathrm{T}}$	Transpose of a matrix or tensor
$\mathbf{x} \bullet \mathbf{y}$	Scalar product of two physical vectors: sum of component products
$\mathsf{A}{:}\mathsf{B}$	Contraction of two tensors: sum of component products
$\underline{a}^{\mathrm{T}}\underline{b}$	Scalar product of two numerical vectors
$\|\cdot\|$	Euclidean norm of (physical or numerical) vector
$\frac{\partial(\cdot)}{\partial(\cdot)}$	Partial derivative
$\frac{\mathrm{d}(\cdot)}{\mathrm{d}(\cdot)}$	Total derivative
$(\bullet)_{,a}$, $(\bullet)_{,\underline{a}}$	Derivative of quantity w.r.t. scalar and vector
$\dot{(\bullet)}$	Time derivative of quantity
$\mathrm{grad}_{(\bullet)}(\bullet)$	Gradient w.r.t. indexed physical vector
$\mathrm{div}(\bullet)$	Divergence of vector or tensor quantity
$\mathrm{d}(\bullet)$	Differential quantity
$\mathfrak{D}(\bullet)$	Virtual quantity
$\Delta(\bullet)_i$	Forward difference in increments
$\delta(\bullet)^j$	Forward difference in iterations
δ_{ij}	Kronecker delta operator, being $= 1$ for $i = j$, zero otherwise
$\overline{(\bullet)}$	Prescribed quantity
$(\bullet)_{\mathrm{cr}}$	Critical quantity

A. Eriksson and A. Nordmark, *Structural Stability and Its Computational Modelling*, Computational Methods in Engineering & the Sciences,
https://doi.org/10.1007/978-3-031-36072-5

Mechanical Quantities

Symbols	Explanation
$\mathbf{e}_1, \mathbf{e}_2, \mathbf{e}_3$	Base unit vectors for fixed Cartesian system
t	Physical time
τ	Fictitious (non-physical) time
$\Omega, \Gamma, \Gamma_T, \Gamma_U$	Region and its boundary, with parts
$\mathbf{X}$	Reference position of a point
$\mathbf{x}$	Current position of a point
$\mathbf{U}$	Displacement of a point
$\mathbf{N}, \mathbf{n}$	Boundary normal vectors in reference and current configuration
$\mathbf{T}, \mathbf{t}$	Boundary traction in reference and current configuration
$\mathbf{B}, \mathbf{b}$	Body force intensity in reference and current configuration
$\mathbf{R}, \mathbf{r}$	Residual force intensity in reference and current configuration
$(\bullet)_{\text{con}}, (\bullet)_{\text{non}}$	Conservative and non-conservative parts of quantity
$\underline{\Xi}$	Set of parameters for constitutive material model
ρ_X, ρ_x	Material density in relation to reference and current volume
F, F'	Deformation gradient tensors
C	Green deformation tensor
E, E'	Green-Lagrange deformation tensors
$\Lambda_\bullet$	Principal stretch components
S	2nd Piola-Kirchhoff stress tensor
σ	Cauchy stress tensor
$\mathcal{K}$	Tangent constitutive relation (fourth-order tensor)
$\Theta, \underline{\underline{\Theta}}_e$	Orientation or rotation tensor and (element) matrix
$\pi_\bullet$	Energy density quantities of different kinds
$\Pi_\bullet$	Integrated energy quantities of different kinds
$W_\bullet$	Work quantities of different kinds
$P_\bullet$	Power quantities of different kinds
$\underline{d}$	Discretized displacement vector
$\underline{C}$	Discretized vector of constraint-enforcing variables
$\underline{D}$	State variable vector, with $\underline{d}$ and $\underline{C}$
$\underline{\mathbf{N}}$	Displacement basis vectors
$\underline{\mathsf{B}}_\bullet$	Strain basis tensors of different kinds
$\underline{p}, \underline{f}, \underline{r}$	Discretized force vectors: internal, external, residual
$\underline{R}$	Constrained residual vector
$\underline{\underline{K}}^\bullet$	Discretized stiffness matrices of various kinds
$\underline{\underline{M}}^\bullet$	Discretized mass matrices of various kinds
$\underline{\varphi}, \underline{\underline{\Phi}}$	Discrete eigenvector and set of such
$\Sigma_\bullet$	Stability coefficient or eigenvalue
$(\bullet)_e$	Element contribution to quantity
$\mathbb{A}$	Assembly operator for FE models

Engineering Parameters

Symbols	Explanation
L, b, h, R, H	Geometrical parameters, explained in relation to example
E_m, ν_m	Young's modulus and Poisson ratio for ideally elastic material
c_1, c_2	Constitutive constants for Mooney–Rivlin material model
μ	Linearized initial shear modulus
ρ	Material density in reference geometry $= \rho_X$
g	Acceleration from gravity
A	Area for beam section
I	Area moment of inertia for plane beam bending
J_i	Mass moment of inertia around coordinate axis
EA	Axial stiffness for bar or beam
EI	Bending stiffness for beam
D	(Elastic) plate stiffness

Consolidated List of References[1]

Argyris J, Tenek L, Olofsson L (1997) TRIC: a simple but sophisticated triangular element based on 6 rigid-body and 12 straining modes for fast computational simulations of arbitrary isotropic and laminated composite shells. Comput Methods Appl Mech Eng 145:11–85

Ashwear N, Tamadapu G, Eriksson A (2016) Optimization of modular tensegrity structures for high stiffness and frequency separation requirements. Int J Solids Struct 80:297–309

Bathe KJ (2014) Finite element procedures, 2nd edn. KJ Bathe, Waterton, MA, also published by Higher Education Press, China, 2016. First edition published by Prentice-Hall, 1996

Bertoldi K (2017) Harnessing instabilities to design tunable architected cellular materials. Ann Rev Mater Res 47

Bucalem M, Bathe KJ (1993) Higher-order MITC general shell elements. Int J Numer Methods Eng 36(21):3729–3754

Champneys AR, Dodwell TJ, Groh RMJ, Hunt GW, Neville RM, Pirrera A, Sakhaei AH, Schenk M, Wadee MA (2019) Happy catastrophe: recent progress in analysis and exploitation of elastic instability. Frontiers Appl Math Stat 5

Como M, Grimaldi A (1995) Theory of stability of continuous elastic structures. CRC Press, Boca Raton, FL

Conway J, Burgiel H, Goodman-Strauss C (2008) The symmetries of things. CRC Press

Cotton FA (1990) Chemical applications of group theory, 3rd edn. Wiley

Cottrell JA, Hughes TJR, Bazilevs Y (2009) Isogeometric analysis: toward integration of CAD and FEA. Wiley, Singapore

Cox BS, Groh RMJ, Avitabile D, Pirrera A (2018) Exploring the design space of nonlinear shallow arches with generalised path-following. Finite Elem Anal Des 143:1–10

Crespo J, Latorre M, Montáns FJ (2017) WYPIWYG hyperelasticity for isotropic, compressible materials. Comput Mech 59(1):73–92

Crisfield MA (1981) A fast incremental/iterative solution procedure that handles snap-through. Comput Struct 13:55–62

Dahlquist G, Björk Å (1974) Numerical methods. Prentice-Hall, Engelwood Cliffs

[1] A list of relevant literature is given here. The bibliography has not been intended to give complete subject descriptions, but more of general references, which can also point to further, more extensive and detailed information.

A. Eriksson and A. Nordmark, *Structural Stability and Its Computational Modelling*, Computational Methods in Engineering & the Sciences,
https://doi.org/10.1007/978-3-031-36072-5

Eriksson A (1989) On linear constraints for Newton-Raphson corrections and critical point searches in structural F. E. problems. Int J Numer Methods Eng 28:1317–1334
Eriksson A (1991) On the usage of one-step O. D. E. solvers as predictors for structural equilibrium path evaluations. In: Vichnevetsky R, Miller J (eds) IMACS 91, Dublin, pp 339–340
Eriksson A (1997) Equilibrium subsets for multi-parametric structural analysis. Comput Methods Appl Mech Eng 140:305–327
Eriksson A (1998) Structural instability analyses based on generalised path-following. Comput Methods Appl Mech Eng 156:45–74
Eriksson A, Kouhia R (1995) On step size adjustments in structural continuation problems. Comput Struct 55:495–506
Eriksson A, Nordmark A (2014) Non-unique response of Mooney-Rivlin model in bi-axial membrane stress. Comput Struct 144:12–22
Eriksson A, Nordmark A (2016) Symmetry aspects in stability investigations for thin membranes. Comput Mech 58:747–767
Eriksson A, Nordmark A (2019) Constrained stability of conservative static equilibrium. Comput Mech 64(4):1199–1219
Eriksson A, Nordmark A (2020) Computational stability investigations for a highly symmetric system: the pressurized spherical membrane. Comput Mech 66(2):405–430
Eriksson A, Pacoste C (2001) Solution surfaces and generalised paths in non-linear structural mechanics. Int J Struct Stab Dyn 1:1–30
Eriksson A, Pacoste C (2002) Element formulation and numerical techniques for stability problems in shells. Comput Methods Appl Mech Eng 191:3775–3810
Fung YC (1993) Biomechanics: mechanical properties of living tissues, 2nd edn. Springer, New York
Géradin M, Rixen D (1997) Mechanical vibrations. Theory and application to structural dynamics, 2nd edn. Wiley, Chichester
Ghali A, Neville A, Brown T (2003) Structural analysis. A unified classical and matrix approach, 5th edn. Spon Press, London, New York
Gilmore R (1981) Catastrophe theory for scientists and engineers. Wiley, New York
Godoy L (2000) Theory of elastic stability: analysis and sensitivity. Taylor & Francis
Groh RMJ, Pirrera A (2018) Generalised path-following for well-behaved nonlinear structures. Comput Methods Appl Mech Eng 331:394–426
Gurtin ME (1982) An introduction to continuum mechanics. Academic Press, Boston
Holzapfel GA (2000) Nonlinear solid mechanics. A continuum approach for engineering. Wiley, Chichester
Holzapfel GA, Gasser TC, Ogden RW (2000) A new constitutive framework for arterial wall mechanics and a comparative study of material models. J Elast 61(1–3):1–48
Hughes TJR, Cottrell JA, Bazilevs Y (2005) Isogeometric analysis: CAD, finite elements, NURBS, exact geometry and mesh refinement. Comput Methods Appl Mech Eng 194(39–41):4135–4195
Ikeda K, Murota K, Fujii H (1991) Bifurcation hierarchy of symmetric structures. Int J Solids Struct 27(12):1551–1573
Ko Y, Lee P, Bathe KJ (2017) A new MITC4+ shell element. Comput Struct 182:404–418
Koiter W (1970) The stability of elastic equilibrium. Technical report Report AFFDL-TR-70-25, Air Force Flight Dynamics Laboratory, Wright-Patterson Air Force Base, Ohio, a translation of the Dutch original from 1945
Li Q, Healey TJ (2016) Stability boundaries for wrinkling in highly stretched elastic sheets. J Mech Phys Solids 97:260–274
Liapunov AM (1966) Stability of motion. (Mathematics in science and engineering, Volume 30). Academic Press, New York/London (translated from Russian Doctoral dissertation, Univ. Kharkov 1892)
Malvern LE (1969) Introduction to the mechanics of a continuous medium. Prentice-Hall, Englewood Cliffs

Nakashino K, Nordmark A, Eriksson A (2020) Geometrically nonlinear isogeometric analysis of a partly wrinkled membrane structure. Comput Struct 239:106302
Nguyen QS (2000) Stability and nonlinear solid mechanics. Wiley, Chichester
Noh G, Bathe KJ (2019) The Bathe time integration method with controllable spectral radius: the ρ_∞-Bathe method. Comput Struct 212:299–310
Noh G, Bathe KJ (2023) Imposing displacements in implicit direct time integration and a patch test. Adv Eng Softw 175:103286
Patil A, Nordmark A, Eriksson A (2016) Instabilities of wrinkled membranes with pressure loadings. J Mech Phys Solids 94:298–318
Reis PM (2015) A perspective on the revival of structural (in)stability with novel opportunities for function: from Buckliphobia to Buckliphilia. J Appl Mech Trans ASME 82:11
Rheinboldt WC (1986) Numerical analysis of parameterized nonlinear equations. Wiley, New York
Riks E (1979) An incremental approach to the solution of snapping and buckling problems. Int J Solids Struct 15:529–551
Strang G (1988) Linear algebra and its applications, 3rd edn. Brooks/Cole, Thomson Learning
Strogatz SH (2019) Nonlinear dynamics and chaos. With applications to physics, biology, chemistry, and engineering. CRC Press
Thompson JMT, Hunt GW (1973) A general theory of elastic stability. Wiley, Chichester
Thompson JMT, Hunt GW (1984) Elastic instability phenomena. Wiley, Chichester
Timoshenko SP, Gere JM (1961) Theory of elastic stability, 2nd edn. McGraw-Hill, New York
Wilkinson JH (1988) The algebraic eigenvalue problem. Oxford Science Publications, Oxford, New York
Zienkiewicz OC, Taylor RL (2000) The finite element method. Volume 1: the basis, 5th edn. Butterworth-Heinemann, Oxford
Zingoni A (2014) Group-theoretic insights on the vibration of symmetric structures in engineering. Philos Trans Royal Soc A 372:20120037

Index

An extensive index to used terms is given below. Bold page numbers are important definitions of terms.

A. Eriksson and A. Nordmark, *Structural Stability and Its Computational Modelling*, Computational Methods in Engineering & the Sciences,
https://doi.org/10.1007/978-3-031-36072-5